Development and Evaluation of a Hybrid Wind Instrument

Thesis

DEVELOPMENT AND EVALUATION OF A HYBRID WIND INSTRUMENT

KURIJN BUYS

Thesis submitted in accordance with the requirement of The Open University for the degree of Doctor of Philosophy

Supervisors:
Prof. David Sharp
Dr Robin Laney

School of Engineering and Innovation, The Faculty of Science, Technology, Engineering and Mathematics

March 2017

CERTIFICATE OF ORIGINALITY

This is to certify that I am responsible for the work submitted in this dissertation, that the original work is my own except as specified in acknowledgements, footnotes or references, and that neither the dissertation or the original work contained therein has been submitted to this or any other institution for a degree.

Milton Keynes, March 2017

Kurijn Buys

ABSTRACT

A hybrid wind instrument generates self-sustained sounds via a real-time interaction between a computed excitation model (such as the physical model of human lips interacting with a mouthpiece) and a real acoustic resonator. Attempts to produce a hybrid instrument have so far fallen short, in terms of both the accuracy and the variation in the sound produced. The principal reason for the failings of previous hybrid instruments is the actuator which, controlled by the excitation model, introduces a fluctuating component into the air flow injected into the resonator.

In the present thesis, the possibility of using a loudspeaker to supply the calculated excitation signal is evaluated; the loudspeaker is placed at the entrance of the resonator (a clarinet-like tube), along with a microphone. This work focusses particularly on two possibilities: using the instrument as a new musical instrument and using it as a tool to carry out wind instrument research.

First, a theoretical study facilitates the modelling of the loudspeaker-resonator system and the design of a feedback and feedforward filter to successfully compensate for the presence of the loudspeaker.

The prototype is then evaluated using physical models of a single-reed, a lip-reed and a bow-string interaction and using a purely mathematical "polynomial" excitation model. For the design of excitation models, the usefulness of dimensionless and reduced parameter forms is outlined, and a sound prediction theory is presented, enabling the pre-estimation of both amplitude and spectral related features of the self-sustained sounds.

The resulting self-sustained sounds are evaluated by a mapping of their sound descriptors to the input parameters of the excitation models, both for sustained and attack sounds. For all excitation models, the sounds produced by the hybrid instrument are shown to match those predicted by simulation.

However, the hybrid instrument is more easily destabilised for certain extreme parameter states.

PUBLICATIONS AND PRESENTATIONS

Some ideas and figures presented in this dissertation have appeared previously in the following publications:

JOURNAL PAPERS

- K Buys, D Sharp, and R Laney. Developing and evaluating a hybrid wind instrument. *Acta Acust united Ac*, 2017.

CONFERENCE PAPERS

- K Buys, D Sharp, and R Laney. Developing a hybrid wind instrument: using a loudspeaker to couple a theoretical exciter to a real resonator. In: *Proceedings of the International Symposium on Musical Acoustics*, Le Mans, France, pp. 331–336, 2014. URL http://oro.open.ac.uk/id/eprint/40589.
- K Buys, D Sharp, and R Laney. Developing and evaluating a hybrid wind instrument excited by a loudspeaker. In: *Proceedings of the Institute of Acoustics*, Birmingham, UK, pp. 294–303, 2014. URL http://oro.open.ac.uk/id/eprint/41419.
- K Buys, D Sharp, and R Laney. A comparison of single-reed and bowed-string excitations of a hybrid wind instrument. In: *Proceedings of the Third Vienna Talk on Music Acoustics*, University of Music and Performing Arts Vienna, Austria, pp. 290–296, 2015. URL http://oro.open.ac.uk/id/eprint/44711.

- K Buys, D Sharp, and R Laney. Improving the stability of a hybrid wind instrument using two microphones. In: *Proceedings of the International Symposium on Musical and Room Acoustics*, Asociación de Acústicos Argentinos, AdAA, Buenos Aires, Argentina, 2016. URL http://oro.open.ac.uk/id/eprint/47417.

CONFERENCE PRESENTATIONS

- K Buys, D Sharp, and R Laney. Developing a hybrid wind instrument, In: *Journées Jeunes Chercheurs en Acoustique, Audition et Signal audio*, Groupe Spécialisé d'Acoustique Musicale, Lyon, France, 2014.
- K Buys, D Sharp, and R Laney. Developing and evaluating a hybrid wind instrument excited by a loudspeaker, In: *Digital Music Research Network One-day Workshop*, Queen Mary University, London, UK, 2016.
- K Buys, D Sharp, and R Laney. A comparison of single-reed, lip-reed and bowed-string excitations of a hybrid wind instrument, In: *The Galpin Society in association with The Institute of Acoustics: Musical instrument in Science and History*, University of Cambridge, UK, 2015.
- K Buys, D Sharp, and R Laney. Development of a hybrid wind instrument — Electronic excitation of an acoustic resonator, In: *Rotkat Records and LINCH*, Born in Antwerp, Belgium, 2016.
- K Buys, D Sharp, and R Laney. Improving the stability of a hybrid wind instrument using two microphones, In: *The Institute of Acoustics: Current Developments in Musical Acoustics*, London South Bank University, UK, 2016.
- K Buys, D Sharp, and R Laney. Development of a hybrid wind instrument — Electronic excitation of an acoustic resonator, Milton Keynes Gallery, UK, 2016.

- K Buys, D Sharp, and R Laney. Improving the stability of a hybrid wind instrument using two microphones, In: *Journées Jeunes Chercheurs en Acoustique, Audition et Signal audio*, Institut de Recherche et Coordination Acoustique/Musique, Paris, France, 2016.

- K Buys, D Sharp, and R Laney. Development of a hybrid wind instrument — some key findings, In: Batwoman — public meeting: Musical instruments — understanding the old and inventing the new, The University of Edinburgh, UK, 2017.

- K Buys, D Sharp, and R Laney. Development of a hybrid wind instrument — some key findings, In: *Acoustics'17: 173rd Meeting of the Acoustical Society of America and the 8th Forum Acusticum*, Boston, USA, 2017.

ACKNOWLEDGMENTS

Foremost, I would like to express my sincere gratitude to my supervisors Prof. David Sharp and Dr Robin Laney for their very helpful critical yet understanding support and guidance throughout the research and for their patience, motivation and enthusiasm. I am further deeply grateful to my examiners, Maarten van Walstijn and Simon Holland, for having carefully read my dissertation and for providing me with very constructive and important feedback.

My sincere thanks also goes to all colleagues with whom I've been sharing the postgraduate office. Our frequent work interruptions were either a welcome rest from continuous reflection or they were supporting and informative. A special gratitude goes out to all other colleagues in the "Acoustics corridor" and colleagues who guided me or provided me with helpful knowledge. Notably I thank the colleagues and leaders of the Centre for Research in Computing's "postgraduate forum", who helped me a lot in learning and understanding all aspects that come into play in such a research project. I gratefully acknowledge the university staff for their unfailing support and assistance and The Open University for funding my PhD research.

A particular thanks goes to my internship student François Vonthron, who very enthusiastically furthered the research project and offered me important insights through his questioning. Special thanks goes to Simon Benacchio and his team at IRCAM, who devoted their time, effort and space to help setting up the real-time computer, and to Mathieu Barthet, who provided his MATIMBRE toolbox for the sound descriptor calculations.

I would like to extend my deepest gratitude to my family and friends. Their efforts to understand my work, and their appreciation and critical feedback has

been a great encouragement, with a special mention to my girlfriend Isabel Tesfazghi, who particularly heartened and inspired me.

And finally, last but by no means least, I thank the people with whom I've been sharing a house over the last three and a half years, for their support and enthusiasm and for living together in such a great atmosphere.

CONTENTS

LIST OF FIGURES

LIST OF TABLES

Part I

BACKGROUND

The first part of this dissertation provides an appropriate background to the reader so that they can familiarise themselves with the topic with a global introduction (in chapter 1) and with required acoustic theories to understand the functioning of self-sustained wind instruments (in chapter 2).

1 INTRODUCTION

1.1 THE CONCEPT IN BRIEF

The principal concept laid out in this thesis concerns a class of electronically augmented acoustic instruments, referred to as "hybrid instruments". In hybrid instruments, a crucial sound production component of the original instrument is replaced by an electronic equivalent. In the first instance, the physical functioning of an embouchure of a wind instrument (e.g. a clarinet mouthpiece, including the player's mouth) is simulated by a computer, which is then put in interaction with a real acoustic resonator (a clarinet-like tube). The interaction is facilitated with a loudspeaker and a microphone, both positioned at the entrance of the resonator.

At this point, it may be helpful to gain an intuitive understanding of the concept by watching a video of one of the outcomes of this work, where the hybrid wind instrument can be seen in action with a clarinet resonator: `http://dx.doi.org/10.21954/ou.rd.3848115`.

Figure 1 illustrates the concept of the hybrid instrument principle. The pressure $p(t)$ at the resonator entrance is measured with a microphone, which sup-

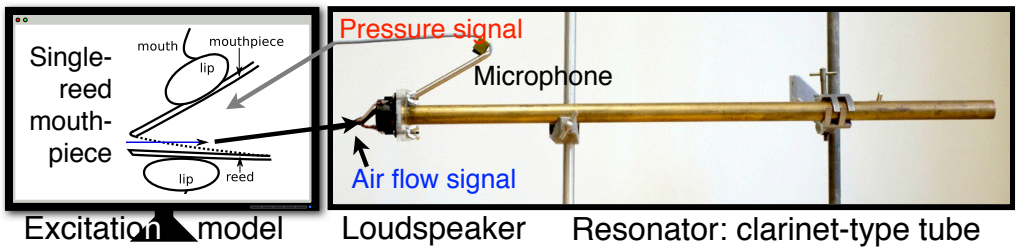

Figure 1: The hybrid wind instrument set-up: a computed mouthpiece in interaction with a physical resonator by means of a loudspeaker.

plies the signal to the embouchure model. The embouchure model then enables the calculation of the associated flow rate signal $q(t)$, which in turn is sent to the loudspeaker that realises a real (fluctuating) flow at the entrance of the tube.

A simple way to understand the hybrid principle is to consider it as a feedback loop generating a feedback squeak. Given that the loudspeaker and microphone are positioned at the entrance of a resonator, the squeak will be automatically tuned according to the length of the resonator. Hence, the pitch can be determined by fingering the resonator, just as with a traditional wind instrument. However, instead of simply amplifying the microphone signal, the signal is modulated using the embouchure physical model. Rather than a simple squeak, the resulting timbre is more like that of a clarinet.

More generally, it is possible to implement any "excitation model" on the computer; the model could be based on the physics of real components or it could be a purely theoretical design. As far as the acoustic resonator is concerned, the bore of any wind instrument with a near-to-closed entrance condition can be used.

As a loudspeaker is incapable of producing a mean (DC) air flow, it could be questioned as to how it can be used to simulate a wind instrument's air flow signal. However, the mean flow component is known to be of secondary importance for proper self-sustained functioning, to the extent that it can actually be removed. This paradox is, for instance, revealed by an experiment where a membrane is introduced between the mouthpiece and the resonator of a brass instrument; when the mean flow is diverted through a small hole in the mouthpiece, the instrument can still be played normally, the fluctuating air in the resonator is enough to self-sustain the oscillation.

An important aspect to note is that the entire hybrid operation has to occur in "real-time". This imposes tight requirements on the computing system, as the process sequence must be much faster than the oscillations produced by the hybrid instrument, and the input-to output latency must be much shorter

than the oscillation's period, which is generally not the case for general purpose computing systems.

Compared with fully simulated or fully physical wind instruments, the hybrid approach differs in its sound generation possibilities and its accessibility, so that one can imagine several applications in different contexts; for instance: as a new musical instrument, as a wind instrument research tool, as an educational aid for musicians or as an aid for instrument makers.

1.2 MOTIVATION

The diversity of the possible applications can be considered in terms of different research perspectives from which several related research questions arise. (These research questions are presented in subsection 1.4.3, after a literature review and a description of the limitations of the hybrid instrument.)

In the first instance, two branches are considered — the "musical" and "research tool" perspectives — each have clear possibilities with respect to our early prototypes. In addition to these possible uses, other perspectives can be imagined for the hybrid instrument. For example, if using a hybrid instrument as an educational aid for musicians, it would be useful to perform additional research on a suitable mouth controller that takes into account the learning strategies of the student. Alternatively, the player's mouth could be left out so that the the fingering techniques can be independently mastered. Meanwhile, if used as an instrument maker's aid, as well as a similar mouth controller, an electronic mouthpiece would be required. This mouthpiece would need to be so precise that the mouthpiece parameters quantitatively correspond to physical parameters of a real mouthpiece. Finally, in contrast to a real embouchure, the hybrid instrument does not introduce (humid) air into the instrument. Therefore it has a clear potential usage in the testing and playing of historical instruments that are no longer allowed to be played by human musicians.

1.2.1 *Musical perspective*

THE INFLUENCE OF THE EXCITATION MODEL ON THE SOUND From the musical perspective, it is important to consider what influence the excitation source has on the characteristics of the sound produced by an instrument. This requires a minimum understanding of the functioning of the instrument. In general, the excitation source can be understood as a component that acts nonlinearly with regard to the amplitude. The resonator behaves in a mainly linear manner, but introduces an important time delay. It is the coupled interaction between these components that makes self-sustained sounds possible.

Slawson (1985) makes an interesting distinction between two types of functioning, depending on the strength of this coupling. When the coupling between the nonlinear and linear element is weak, the resonator's response is not strong enough to achieve a self-sustained state, so that either no sound or a sound created by the independent excitation source is produced. In the strongly coupled case, the resonator and excitation source supply energy to each other, resulting in a looped system where the characteristic time period of the resonator will mainly determine the pitch of the self-sustained sound that appears. This is the typical functioning of most wind instruments, but bowed strings and other self-sustaining acoustic mechanisms also belong to this category.

In this study, the strongly coupled scenario is the main focus of interest, as it allows the pitch to be controlled by fingering. Both the resonator and the excitation source have an influence on the features of the sound produced. The latter particularly influences the timbre, but its exact role is not straightforward and also depends on the resonator type and the note that is being played. However, it is known that the excitation allows for parameter modulations that are valid for the whole note range of the instrument (by varying the mouth pressure for example, a roughly similar change in timbre can be expected, independent of the played note).

The influence of several features in the excitation-sound relation are discussed in the literature. Early works demonstrated the characteristics in the vibration signals as a function of the nonlinear element (McIntyre et al., 1983) and mentioned the role of the dynamic aspects of this element on the sound's spectrum (Thompson, 1979). Next, attempts were made to quantify this relation by defining so called "timbre spaces" (Deutsch, 1999), where the hard to quantify notion of timbre is spread over a number of dimensions by using a set of "sound descriptors". More recent studies demonstrated the effect on the timbre (spaces) of specific excitation types such as single and double reeds (Giordano and McAdams, 2010), the clarinet (Almeida et al., 2013; Barthet et al., 2011) and the saxophone (Guillemain et al., 2010). In particular, the case of the clarinet has been thoroughly investigated. A clarinet-specific, close to orthogonal, three dimensional timbre space was found (Barthet et al., 2011) and the role of the player's vocal tract and tongue was evidenced (Wolfe and Tarnopolsky, 2003). Although the fingering ultimately determines the played note, it is known and it has been theoretically shown that it is still possible to vary the pitch by up to several tones by changing embouchure properties (Almeida et al., 2013). Meanwhile, the sound level and the phenomenon of multiphonics are known to be partly governed by the excitation source (Backus, 1977). A specific class of multiphonics, known as "subharmonic behaviour" or "period doubling", has been identified as appearing to be a simple mathematical solution of a theoretical wind instrument approach (Maganza et al., 1986; Gibiat and Castellengo, 2000). For instance, some special playing techniques on the violin and singing techniques lead to a physical realisation of "period doubling"; however, it remains a rare phenomenon in practice (Taillard et al., 2010).

This opens up the possibility of programming a nonlinear element, in a manner that doesn't represent a real physical situation, so that subharmonics (and most likely other types of sound features) become easily achievable and controllable. It has also been shown that purely theoretical nonlinear functions can res-

ult in sound oscillations when put into interaction with a resonator (Maganza, 1985).

Throughout this dissertation both physical and non-physical models are considered. It should be understood that a non-physical model is not based on an existing physical system, but only on a mathematical formulation that, in this context of the hybrid instrument, is designed to allow for similar operations as a physical model, i.e. to enable the production of self-sustained oscillations. This distinction is worth considering with regard to the musical perspective. It is known that our perception is particularly strong at identifying the physical (based) origin of a sound source (see e.g. (De Poli and Rocchesso, 1998) for an example of where this property is exploited for multimedia purposes). Since physical sound sources have always surrounded us, our perception is shaped towards this identification, creating the potential for a fully immersive experience with these sound sources. Hence, it may be supposed that physical sound sources offer a broad playing ground for musical expression. On the other hand, sound synthesis not based on physical processes is directly inspired by perception, which is an approach that also offers appealing musical expression possibilities to players and composers. Hence, it is estimated that the hybrid integration of a non-physical model in a physical system may well imply new interesting "hybrid" musical potential.

To conclude, it can be expected that specially designed excitation sources, together with a suitable mapping of the input parameters, could allow (more) independent control over the sound features.

WHY NOT SIMULATE THE RESONATOR AS WELL? As there are reasonably good resonator models available, the importance of a hybrid instrument might be called into question, given that an entirely simulated physical model might offer the same musical potential.

One argument favouring hybrid over simulated instrument designs is that (real-time computable) resonator models still don't capture the full physical

reality. Human perception is extraordinarily well trained in tracking physical variations of the sound source, which can lie in extremely detailed aspects, such as transient sounds for example. Therefore, any small non-physical irregularity in the simulation can be perceived as less natural compared with the behaviour of real acoustical components. While those non-physicalities could be musically relevant (as explained in the previous paragraph), the point here is that the original physical situation is also valuable and is difficult to simulate.

In addition, the presence of artefacts resulting from the transducers (i.e. the microphone and the loudspeaker) used in the hybrid wind instrument could also have particular qualities that add an identifiable and musically appreciable touch to the instrument.

Furthermore, it is well known that when the sound originates from the instrument itself, the player experiences a greater feeling of "immersion" with their performance, compared with the case where the sound originates from an external loudspeaker.

Finally, while a simulated resonator offers much wider control possibilities, it can be preferable to embrace the constraints that come with classical fingering possibilities, as these limitations can provide musical inspiration. When playing an instrument, the maximum expressive instrument control is limited by the capabilities of the player. As a consequence, a greater amount of control possibilities has to be reduced by the player or the designer beforehand, which is a separate task that is usually not welcomed by musicians (Cook, 2001). This is, for example, one reason why the enormous amount of design and control possibilities that electronic systems offer also result in a lack of standardised instruments.

In an interview with Michel Waisvisz, developer and virtuoso of several live systems and late former director of the Studio for Electro-Instrumental Music (STEIM, Amsterdam, The Netherlands), Waisviszs formulates his vision for the future of electronic instruments as follows (Krefeld and Waisvisz, 1990):

"Apart from frequent sentimental revivals of ancient acoustic instruments, I think electronics will integrate fully with acoustical instruments and vice versa. I'm hoping to witness the time when we will be able to manipulate matter electronically. Then one will be able to combine all the qualities of electronic control with the superior timbral qualities of acoustically generated sound. It basically would redeem us from the use of loudspeakers."

Considering the work that has been done so far, and the potential of this current research, we might possibly be not so far away from a fully merged electro-acoustic wind instrument design.

Finally it should be noted that with the proposed hybrid instruments, the aim is not to come up with "better" alternatives to existing instruments. Instead, an alternative approach is sought, with a different accessibility to sound generation.

1.2.2 *Perspective as a tool for wind instrument research*

IN THE EXTENSION OF BLOWING MACHINES As the mouthpiece and its parameters are programmed, the hybrid device provides similar and extended capabilities to the nowadays commonly used mechanical "blowing machines" or "artificial mouths" for wind instruments (see e.g. (McGinnis and Gallagher, 1941; Wilson and Beavers, 1974; Ferrand and Vergez, 2010)). Such artificial excitation enables a repeatable and more controlled sound production, so that more objective research can be performed, for example to verify physical wind instrument hypotheses and to compare different instruments.

The successful implementation of a hybrid instrument would enable the same research applications as blowing machines, but with the additional precise knowledge and control over the mouthpiece parameters. Furthermore, a hybrid system also has the advantage that both the pressure and flow rate signals are known.

PRECISION Given that the transducers that are employed in a hybrid instrument will inevitably introduce small errors in the signals, it is difficult to determine what precision hybrid results will have. However, additional parallel measurements on the actuator can be performed and transducer models can be taken into account, which can enable a precision estimation. Also, even a hybrid set-up that is not precisely equivalent to a real instrument can be useful. For example, such a set-up would still allow investigation of phenomena that can be shown to be independent of the transducer artefacts (see next paragraph). Finally, it may be expected that future technological improvements will result in more precise transducers and/or possibilities for the design of filters that compensate for all of their artefacts.

POSSIBLE APPLICATIONS As mentioned before, hybrid instruments would be useful for studies where different resonators are compared through the self-sustained sound they produce, which is the focus of works such as (Sharp et al., 2003; Kowal et al., 2014). In addition, specific wind instrument theories can be verified, especially with respect to resonator characteristics that are not yet experimentally confirmed. For instance, it would be interesting to test the hypothesis that the mean flow component that propagates through a wind instrument essentially has negligible influence on the produced sound (Rienstra and Hirschberg, 2013). This could be done by injecting a constant air flow near the entrance of the resonator. (To minimise the acoustic effect of the parasitic presence of this additional air channel, a capillary tube could be used.) Furthermore, nonlinear effects of the resonator (Campbell, 1999), the effect of lateral valve holes (Dalmont et al., 2002) and the nature of attack transients (including those occurring in complex resonator geometries and due to fingering transitions) (Dalmont et al., 2005; Almeida et al., 2010) can be studied experimentally. In addition, mouthpiece models (McIntyre et al., 1983; Facchinetti et al., 2003; Avanzini and Van Walstijn, 2004) can also be studied by evaluating the sound obtained with the same resonator.

1.3 STATE OF THE ART

Among the earliest man made musical instruments were rattles, stampers and various drums, dating back to prehistoric times (Blades, 1992). The oldest discovered instrument was a flute, found in Slovenia in 1995 and estimated to be about 50,000 years old (Slovenian Academy of Sciences, 1997). The flute was constructed from a carved bone and at least four tone holes could be noticed.

Other than that discovery, only evidence of relatively much younger wind instruments has been found, dating from over twenty thousand years ago. These wind instruments were constructed from hollow cane or dried up fruit shells and, similar to today's flutes, could be sounded by blowing an opening in a certain way.

With the introduction of musical acoustic research starting with Pythagoras in the 6th century BC, little by little the underlying operational principles of musical instruments were revealed. Much later this resulted in the identification of generalised models of these traditional musical instruments. Such a basic model is briefly introduced in section 1.3.1.

With the advent of electronics in the late nineteenth century, electronic musical instruments quickly made their introduction. Initially the focus was on the electronic components providing a complementary new sound generation mechanism, leading to instruments such as the Telharmonium, the Theremin and electronic organs. It was mainly during the digital synthesis revolution, starting in the 1980s, that the idea of simulating acoustic instruments came about. Section 1.3.2 focusses on a particular simulation technique known as "physical modelling".

From the moment that real-time simulation of physical models became feasible, attempts have been made to merge physical and electronic components, through the use of electro-acoustic "transducers". A literature review on these new "hybrid" instrument classes is presented in section 1.3.4, starting with studies of the hybrid principle as applied to wind instruments. These are described

in depth, discussing their motivations and results, and providing personal critical opinions. The discussion concludes with reviews on hybrid string instruments (section 1.3.5) and "active control" of musical instruments (section 1.3.6). The latter concerns the interaction of an electronic controller with an acoustic resonator.

Specific information related to the technical limitations highlighted by the literature will be addressed in section 1.4 and information about the electronic systems (both those described in the literature and the system used in this study) can be found in appendix B.

1.3.1 *Models of acoustic musical instruments*

There is a vast amount of literature on the acoustical functioning of musical instruments (see for example (Fletcher and Rossing, 2012; Chaigne and Kergomard, 2013)). A key publication by McIntyre, Schumacher and Woodhouse in 1983 (McIntyre et al., 1983) beautifully summarises how oscillations in (self-sustaining) musical instruments emerge and how they can be described by a common block diagram, consisting of a nonlinear element (the excitation) and a linear element (the resonator), which are in physical interaction. Figure 2 shows a block diagram of this type, representing the modular composition of an arbitrary acoustic musical instrument. The double-headed arrows indicate those blocks that are in bi-directional interaction, thus designating interactive components. The physical feedback from the instrument to the control block is marked by an open arrow, this type of interaction is referred to as "haptic" feedback (see e.g. (Berdahl et al., 2009)).

Such an acoustic instrument consists of some means of providing a physical excitation (e.g. an embouchure for wind instruments, a finger plucking a string, a stick hitting a membrane, a bow-string interaction,...) and a resonator (e.g. an air-column, a string, a membrane,...), both of which are controlled by human gestures (e.g. by blowing, bowing, plucking, fingering,...). It should be noted

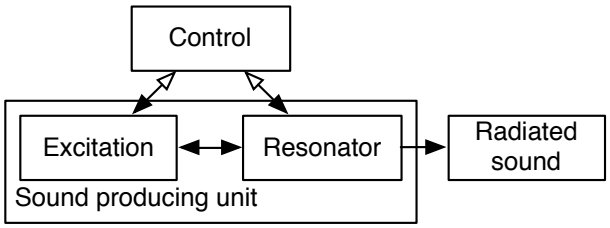

Figure 2: Block diagram representing the physically relevant components of an acoustic musical instrument with their interactions. Arrows indicate the direction(s) of physical interchange.

that certain (continuous) excitation types, such as those for winds or bowed strings, lead to "self-sustained sounds"; i.e. they can sound continuously until the energy of the excitation is stopped. Meanwhile other excitations, such as plucked strings or hit membranes, result in a directly decayed sound.

This block diagram is a somewhat simplified representation of real instruments. For instance, it is not clear where a piano soundboard would sit within the diagram (it could be interpreted as a part of the "resonator" block). Also, for some sounding principles the excitation and oscillation-driving resonator are actually the same physical element (for instance vocal chords, freely buzzing lips or an accordion reed).

1.3.2 *Electronic musical synthesis*

The knowledge of these models of acoustic instruments has informed an electronic synthesis technique that implements the governing mathematical equations. This synthesis technique is known as physical modelling, and nowadays forms a discipline in its own right. Apart from implementing physical models for the imitation of real musical instruments, the theoretical nature of this approach also enables new musical possibilities via the synthesis of virtual physical situations. Therefore De Poli and Rocchesso speak about "Physically-based Sound Modelling" (De Poli and Rocchesso, 1998), which is a convenient notion to capture the whole range of possibilities.

The first physical model implementation was carried out by Hiller and Ruiz in 1971, who used finite difference approximations of the wave equation (Hiller and Ruiz, 1971). However, it took another decade before the computational efficiency of the physical model's algorithm and of the computers themselves became ready for real-time synthesis applications, thereby allowing a direct interaction with a musician. In 1983, Karplus and Strong proposed a very computationally efficient algorithm to simulate a plucked string by approximating the string by a delay with filtered feedback. This technique is widely used and referred to as the "Karplus-Strong" algorithm (Karplus and Strong, 1983). Subsequently, the algorithm was refined and generalised (implementing other musical instruments) into the highly efficient technique of digital waveguide synthesis by Julius O. Smith III (Smith III, 2006) and others. Together with the increase in Digital Signal Processing power in the late 1980s, commercial implementations became feasible. Yamaha signed a contract with Stanford University (where Smith is based) in 1989 to jointly develop digital waveguide synthesis, and as such most patents related to the technology are owned by Stanford or Yamaha. A hardware example is the Yamaha VL1, the first physical modelling synthesiser.

Alongside physically-based sound modelling, there are a vast number of alternative electronic methods of synthesising sounds (for an overview, see for example (Russ, 2004)). These can often be computationally more efficient and easier to implement, but the character of the sound (and the control over it) is typically less "physical" in nature (see section 1.2.1 for the related discussion regarding the musical perspectives around physicality). As the hybrid instrument concept is based on the physical modelling approach, a detailed development on these alternative synthesis techniques is beyond the scope of this dissertation.

In order to trigger and manipulate sounds from electronic musical instruments, either programmed directives are given (which can be understood as an "electronic score"), or physical "controllers" can be used. The latter allows

for the transformation of gestures into electronic signals. Simple buttons and knobs fall in this category, and the electronic piano keyboard is probably the most well known example. The situation where a synthesised physical model is piloted via a controller is represented by the block diagram in figure 3. The

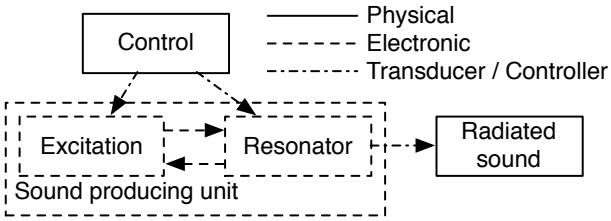

Figure 3: Block diagram with the components of a synthesised physical model of a musical instrument piloted via a controller. Arrows indicate the direction(s) of (electro-) physical interchange.

dashed blocks represent electronic components and the dash-dotted arrows imply the presence of transducers or controllers. At the present time, there is an increased interest in more advanced controllers to allow for optimal transfer of the player's expressions. Many more controllers can be imagined, and there are still many that haven't reached the market yet (Cook, 2004). Of relevance to this study, one could consider the Yamaha WX-series (Onozawa and Fujita, 2006) and AKAI EWI-series wind instrument controllers for example, and similarly, "The pipe", by Scavone (Scavone, 2003), all of which capture both fingering and mouth gestures.

1.3.3 *Sound transformations*

Another possibility provided by electronics is the transformation of an incoming sound signal, typically originating from a microphone or from other acoustic sensors, such as the pickups of an electric guitar. Such operations are generally named "sound effects". Filters, flangers, distortions and numerous electronic transformation units fall in this category. Figure 4 depicts a block diagram of a musical instrument that is transformed by a sound effect.

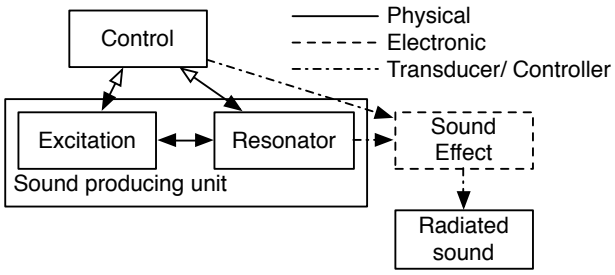

Figure 4: Block diagram with the components of a musical instrument transformed by an effect. Arrows indicate the direction(s) of (electro-) physical interchange.

Effects are electronic contributions that are not in bi-directional interaction with the physical component; hence, the influence on the sound tends to be manifested as an independent layer on top of the original sound rather than being part of the sounding mechanism itself. Note that, as the block diagram suggests, the effect itself can also be manipulated while performing, by means of controllers.

1.3.4 *Electronic excitation of acoustic resonators*

From the moment real-time electronic synthesis of physical models became possible, there have been experiments to design hybrid musical instruments, consisting of a combination of physical and electronic components. Various goals were targeted, principally corresponding to the motivations for the present study. To allow for the electro-acoustic interchange, "transducers" (sensors and actuators, such as a microphone and a loudspeaker) are used. The hybrid principle that is studied in this thesis concerns the situation where the excitation block is electronic and the resonator is an acoustic wind resonator. The corresponding block diagram is presented in figure 5 (although this diagram is not limited to wind instruments).

Only a handful of studies have been reported on this hybrid wind instrument principle.

In the context of the "chaos and period-doubling bifurcations" phenomenon, which was an extensively investigated topic in the early 1980s, a first basic hy-

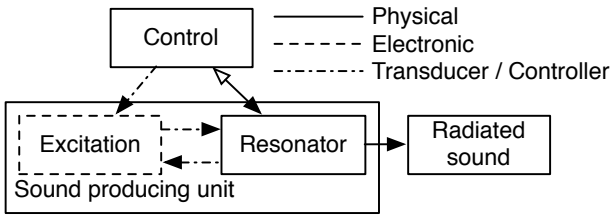

Figure 5: Block diagram with the components of a hybrid musical instrument consisting of an electronic excitation and a physical resonator. Arrows indicate the direction(s) of (electro-) physical interchange.

brid instrument experiment was performed by Kitano in 1983 (Kitano et al., 1983). The period-doubling theory describes how it is possible to obtain chaotic behaviour out of a deterministic system with feedback. This scenario applies in many different physical systems and Kitano briefly demonstrated its validity on a simple acoustic system. His set-up didn't include a resonator; instead a physical delay was implemented, by placing a microphone at a certain distance from a loudspeaker. The microphone signal was applied to a nonlinear static function that determined the signal sent back to the loudspeaker. This function was chosen such that the resulting looped operation resulted in an oscillation (with the delay as the period), based on the "iterative maps" theory that describes the dynamical path when iteratively evaluating the nonlinear function on its own outcome (see for example (Collet and Eckmann, 1980)). It was shown that, depending on the parameters of the system, a range of typical oscillatory behaviours could be obtained where the so-called "bifurcation diagram" indicated when the oscillation consecutively doubles in period. Signals with periods of length two, four and eight were observed to eventually turn into chaos.

It is remarkable that such an apposite behaviour was observed, given that the loudspeaker's characteristics were ignored in that study. Indeed, the loudspeaker's dynamics have an important effect on its response and it will be shown later that a careful loudspeaker choice and the application of compensation techniques leads to superior performances. Kitano's study (which is only reported in a "Physical review letter") also doesn't provide an acoustical or mechanical interpretation of the results. While Kitano didn't consider a potential musical interest, he did mention that several oscillatory behaviours were

obtained. Apart from the expected period doublings, oscillations with (much) smaller periods, oscillations modulated with long period (of about 10 ms) and intermittent chaotic oscillations were also observed, potentially opening up an enriched musical sound palette.

Other research that informs the set-up developed in the current work, was performed by Maganza in 1985, and is documented in his PhD thesis (Maganza, 1985) and a subsequent paper (Maganza et al., 1986). Building on the work of Kitano (whose work he first repeated and confirmed), Maganza replaced the loudspeaker-microphone delay by a loudspeaker and microphone that were placed at the entrance of an acoustic resonator (first a simple pipe, then a real clarinet resonator). This system can also be interpreted as a delay, not between the simple microphone and loudspeaker input and output signals, but between the separate up- and downwards propagating pressure waves that can be derived from them. First, Maganza used several polynomial nonlinear excitation functions that were known to result in self-sustained oscillations with bifurcating behaviour. He then empirically confirmed some period-doubling scenarios (again up to three bifurcations). Finally, he implemented a clarinet embouchure model (an early model, proposed by Schumacher (Schumacher, 1979)) for the nonlinear function; and, as such, demonstrated a hybrid self-sustained functioning of the clarinet. Like Kitano, Maganza wanted to contribute to the understanding of the bifurcation phenomenon from an acoustic point of view. However, he also summarised a number of motivations that are similar to those of the present work:

- To improve our understanding of the functioning of the clarinet's excitation mechanism (the acoustic functioning of the embouchure).
- Given that the artificial excitation of the instrument represents a stable sound source, to study radiation of sound from the instrument (there is also reference to other "research tool" type motivations, similar to those mentioned in section 1.2).

- To improve sound synthesis by deduction.
- To act as an instrument maker's aid, e.g. deducing desired reed and mouthpiece features.
- To become a new — hybrid — instrument, whose body remains the clarinet's but whose excitation — being both electronic and mechanical — would allow increased possibilities to musicians and composers.

There are several points to be considered regarding Maganza's work. Generally, many components are kept as "black boxes" (i.e. theoretical systems without any knowledge of their internal working) and an empirical methodology is followed. Like Kitano, Maganza assumes that the loudspeaker outputs a pressure signal that is equivalent to the supplied electric signal. Not only is this not the case for a standalone speaker, when it is mounted on an acoustic resonator, the strong pressures generated in front of the membrane will impose a non-negligible coupling between those components. Finally, upon interpretation of the empirical results, Maganza acknowledges that there are some "parasitic delays" which might result from the electronic system or the loudspeaker. In the present thesis, these issues are taken into account and compensated for (see chapter 3). While the loudspeaker's characteristics are not provided by Maganza (it is only said that a "Beyer" headphone loudspeaker with a 200 Ω impedance was used), some assumptions can be made from the description of the set-up. For example, by comparing the loudspeaker and resonator size, it is most likely that the loudspeaker's resonant frequency lay above the played note's fundamental frequency. From the study in chapter 3 in this dissertation, it is clear that this results in significant phase and gain deviations; however, the implications are not further considered in this introduction. Another inconsistency in Maganza's work is related to the interpretation and the use of physical quantities; this is further discussed in subsection 1.4.1.

Despite these shortcomings, Maganza's preliminary investigation showed that the hybrid self-sustained operation and bifurcation conditions are surpris-

ingly consistent with theory, which suggests that there is a certain robustness for dynamic perturbation of the system.

A little later, in 1994, as part of his doctoral thesis on the study of the oscillation threshold in nonlinear systems, Grand built a set-up that used an electrodynamic shaker to regulate a valve between a pipe entrance and an external pressurised chamber (equivalent to the mouth pressure) (Grand, 1994; Grand et al., 1997). Grand also used Schumacher's single-reed mouthpiece model and also placed a microphone at the pipe entrance. His aim was to experimentally explore the influence of the mouthpiece parameters and to study how separate resonator modes affect the playing frequency and the bifurcation behaviour. Again, some basic coherent phenomena were demonstrated even though the valve's response (in particular its dynamics) wasn't taken into consideration. In Grand's study, the shaker's resonant frequency most likely fell below the note's fundamental frequency (there is no mention of these characteristics). Interestingly if the electrical signal sent to the shaker were inverted in phase, the whole set-up would become equivalent to an instrument driven by a lip-valve model (see 4.3 for details on this model). On the other hand, if the phase weren't inverted, the condition for oscillation would be false. This suggests that Grand might have unknowingly applied a phase inversion (for example by switching an electrical polarity).

More recently, in 2010, in a very brief study on attack transients in wind instruments, Almeida adopted the same physical implementation as Maganza (Almeida et al., 2010). To avoid complex computing systems or electronic circuits, the excitation was modelled by a simple linear gain feedback. This was considered to sufficiently approximate the mouthpiece model during the first oscillations of a note onset (given that the typical nonlinearity doesn't come into play for such low amplitude oscillations). However, while the physical implications of the presence of the loudspeaker in the system were studied in depth, no actions were taken to account for its side-effects and only minor usefulness was reported. The author further draws an interesting conclusion: "Some com-

plications were identified in this study, in particular the fact that the oscillation frequencies are affected by the characteristics of the loudspeaker. A complete emulation of the musical instrument will require, other than the shaping of a nonlinear relation between the input and output pressures, a circuit to balance the effect of the microphone / loudspeaker configuration." This consideration is further developed in section 3.2.3.

Finally, in 2012, with the aim of creating a device that can serve for wind-instrument research as well as considering musical potential, Vergez and the current author explored a hybrid prototype that resembled the one of Grand, but with an electronic control valve for the actuator and with a very high input pressure compared to the mouth pressure (Buys and Vergez, 2012). With this set-up, the control and the function of the valve are not analogous to the reed movement. Instead the valve movement is proportional to the air flow rate signal that enters the pipe, which allows the mouth pressure value to be electronically simulated. By choosing a pipe that is long enough, a playing frequency that lies far below the resonance frequencies of the valve could be achieved. In this way the response of the valve was roughly flat in amplitude and phase for the first resonant modes of the pipe and no additional correcting filters were needed. As such, specific (limited) parameter ranges of the embouchure model resulted in self-sustained oscillations and comparison with entirely numerical simulations of the set-up demonstrated that the hybrid instrument behaved coherently to some extent. For instance, a correct pitch was obtained, and for an increasing mouth pressure parameter a typical sound level evolution was established. However, the valve wasn't designed for rapid precise oscillations; in particular its friction characteristics imposed substantial limitations on the system. The result was a restricted amplitude and timbre range and a significant hysteresis factor.

1.3.5 *Hybrid string instruments*

Just like wind instruments, bowed strings can be described by an interaction between a linear resonator (the string) and a nonlinear excitation source (the bow-string interaction). Therefore, in a similar manner, hybrid versions of string instruments can be designed.

In the late nineteenth century, in 1893, a patent was filed by Eisenmann for an electronically enhanced piano ("elektronisches Klavier") where microphones and electromagnets were added to an acoustic piano in order to sustain the string vibrations (Eisenmann, 1893). This principle was adopted much later on the electric guitar, with tools like the Ebow (1978, (Heet, 1978)) and the Sustainiac (1999, (Osborne and Hoover, 1999)); however, here the strings were both measured and excited by the electromagnets.

From 1986, in order to study the stability of the bowed string motion, Weinreich and Caussé (Weinreich and Caussé, 1986, 1991) and later Müller (Müller and Lauterborn, 1996), worked on a similar system but with a more precise and theoretically known excitation control. This was achieved by optical string displacement sensing and an electromagnetic actuation principle. A simplified bow-string excitation model was implemented on the electronic system, which allowed for self-sustained sounds to appear. Their devices have proven useful to attest some basic properties of the bowed string model.

On string instruments, more work has been done on the inverse hybrid principle. That is, putting a physical excitation in interaction with an electronic resonator simulation. This synthesis approach is represented by the block diagram in figure 6.

Guérard and Boutillon investigated such an inverse hybrid principle by bowing a "virtual string" (Boutillon and Guérard, 1995; Guerard and Boutillon, 1996; Guérard, 1998): a co-located force sensor and electrodynamic shaker that are interconnected with a simplified string model programmed on a DSP interface. Some characteristics of the physical elements were taken into account to

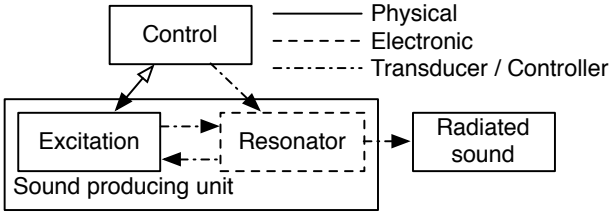

Figure 6: Block diagram with the components of a hybrid musical instrument consisting of an physical excitation and an electronic resonator. Arrows indicate the direction(s) of (electro-) physical interchange.

achieve an operation comparable to a real bowed string and the typical Helmholtz movement was observed.

Although the main purpose of their work was verification of the theoretical string model, Guérard and Boutillon also briefly discussed musical perspectives with the motivation of achieving a more realistic gestural bowing control of partly synthesised sounds.

1.3.6 *Active control applied on musical instruments*

Another electro-acoustic principle employs "active control" to provide linear electro-acoustic feedback to the resonator, allowing alternative tonal control possibilities. The functioning of this principle is represented by the block diagram in figure 7.

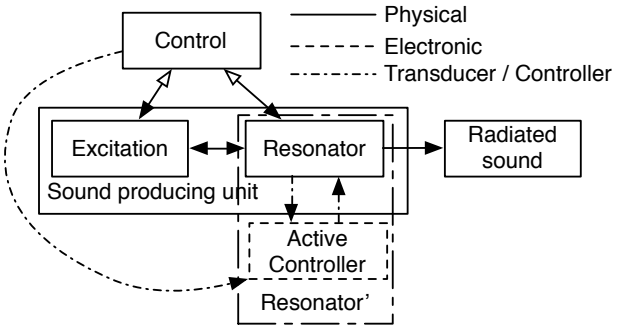

Figure 7: Block diagram with the components of a actively controlled musical instrument. Arrows indicate the direction(s) of (electro-) physical interchange.

Active control can be thought of as an electro-acoustic "parasite" on a physically vibrating system; and, as opposed to the hybrid concept, the system is still

capable of performing its initial function when the active control is switched off. In contrast to hybrid instruments, active control on musical instruments has been more extensively investigated. While the actual principle of sound control is substantially different from the hybrid approach, both concepts share similarities in their physical implementation and their technical requirements, which enables these research areas to mutually benefit from each other. The following literature review is mainly focused on wind instrument applications, which also often use a microphone-loudspeaker pair to facilitate the electro-acoustic interaction. Note that, just like any electronic component, the "active controller" can be manipulated while playing, for instance by using controllers. As a matter of fact, for most active control applications it is even required that the active controller is aware of what note is being played in order to apply appropriate operations to that state of the resonator.

The active control principle was first studied for the purpose of removing undesired sounds. As such, it is commonly referred to as "active noise control" (ANC); which explains why it has been investigated in much more depth. In 1936, Lueg initially proposed a feedforward system to reject pure tones in ducts by measuring the pressure with a microphone and re-inserting a signal with the opposite phase (Lueg, 1936). Such a system works as long as the pressure waves can be assumed planar. Their frequency should be sufficiently low so that the transversal waves in the duct can be neglected.

It was not until 1953 that the first applications appeared: a similar system allowed reduction of the sound level in a small volume (Olson and May, 1953). Unlike Lueg's, this device was effective in open spaces. However, it was only capable of absorbing the acoustic wave locally, close to the microphone.

After that, many others explored the technology (see for example (Nelson and Elliott, 1991)); and, by using an extra sensor to measure and minimise the error signal, an improved broadband feedforward ANC was found (Elliott and Nelson, 1985). Various filters were designed to guarantee stability and also

a related improved feedback control was possible, which solely required the error microphone (Elliott and Nelson, 1985).

In 1995, with the motivation of producing instruments with new timbres for musical expression, Besnainou started to experiment with applications on musical resonators (Besnainou, 1995). Later, he applied this technique on prototypes equipped with piezoelectric transducers using an analogue circuit to perform the control (Besnainou, 1999).

Meanwhile, in 1996, Chen and Weinreich published a paper where a "feedback enabled adjustable Helmholtz resonator" was employed (Chen and Weinreich, 1996). Using a "microphone - phase/gain active controller - loudspeaker system", the resonant frequency of the resonator could be changed while it was synchronously driven by a brass excitation type (i.e. buzzing lips). This enabled an experimental study of whether the brass player's lips behave either as in- or outward striking (i.e. to observe the phase relation between the mouthpiece pressure and the lip movement at the played note's fundamental frequency). However, the simplicity of the approach was neither intended nor appropriate for further developed studies or musical purposes.

Two years later, Pickett pursued his Master thesis on an active control implementation applied to the trumpet (Pickett and Saunders, 1998). The main purpose was to reduce the sound level as an alternative to a physical mute, but also timbre modification was an aim. His set-up included a microphone and a loudspeaker (a compression driver with a capillary tube), closely mounted to the instrument's embouchure.

In the same period, Guérard pursued his doctoral thesis on a hybrid concept that was presented as the inverse principle of the set-up proposed in the current work (Guérard and Boutillon, 1998; Guérard, 1998). A (flute-type) mouthpiece was maintained and a target resonator response was simulated using an array of five microphones in a pipe and a loudspeaker at the end of the pipe. First, an analogue circuit enabled separation of the upward and downward travelling acoustic pressure waves in the pipe using the five microphone signals. Then,

the loudspeaker was used to absorb the downstream pressure waves and to produce an upstream pressure wave, synthesised according to the imaginary resonator model. In other words, the set-up involved the coupling of an acoustic wave-separation system to the wind instrument's model and so-called ARMA filters were used to simulate acoustic resonances (with the AR-part) and anti-resonances (with the MA-part). It was possible to play an entire octave on this instrument. While Guérard didn't describe his method as an active control application in the first place, it can be seen as a form of it, as it concerns a linear feedback loop applied to a pipe which represents a real resonator.

Given that the system identification is performed on the complete system, between the electrical input from the microphone to the electrical output to the loudspeaker, the responses of the transducers (most importantly of the loudspeaker) are inherently included whilst the system performs its resonator simulation. This is a significant improvement in comparison with the previously discussed hybrid instruments (with simulated excitation), where the transducers were not considered. Also in contrast to those instruments, Guérard's study much more explicitly expressed the musical interests: "to explore existent and non-existent virtual resonators for the purpose of artistic expression". However, his chapter on "hybrid synthesis of the flute" concludes by stating that the instrument hasn't proved to be of great quality. The author then laid the focus on its use as a reflectometry and echo-cancellation instrument.

In 2009, using a co-located sensor/actuator pair, Berdahl managed to modify the damping and the amplitude of an electric guitar string (Berdahl, 2009).

Two years later, Boutin submitted his doctoral thesis, directed by Besnainou, where he explored how the resonant properties of a xylophone bar and the violin bridge's twisting mode could be changed using a proportional-integral-derivative (PID) controller (Boutin, 2011).

An example where the control loop is interpreted more crudely, but which has proven to be a practically advanced and musically applied implementation, is the "Magnetic Resonator Piano" of McPherson (McPherson, 2010), which op-

erates similarly to Eisenmann's electronically enhanced piano or to the ebow, but is much more technically enhanced. Given that the electronic component primarily linearly interferes with the strings, it is categorised with the active control approach here. However, this example demonstrates that this categorisation can become blurry, as the electronics can be driven more strongly so that it becomes an excitation component, which would suggest categorising the instrument as a hybrid instrument. In the same regard, the feedback generated from a guitar amplifier back to the guitar strings may considered to be a form of (arbitrary) active control or hybrid instrumentation.

A specific branch of active control, known as "modal control", employs a modal representation of the structure that is being controlled (see for example (Preumont, 2011) for an overview on the general principle). This is a form of feedback control that allows operation with a minimum of sensor/actuator pairs. When control in a limited frequency band is targeted, a single sensor and actuator can be sufficient. First a modal identification of the physical system is performed (this includes the transducers so that their response is considered). Then, independent features of each mode (the frequency, amplitude and quality-factor) can be controlled, which is valid as long as the physical limitations of all components are respected. Furthermore, it should be noted that the required dynamic range is related to the positions of the transducers relative to the modal vibration shape (e.g. a loudspeaker positioned at a given mode's pressure minimum (a pressure node) would require high amplitudes to influence that mode and as such, its control will be limited by the loudspeaker's power rating).

Using two piezoelectric transducers and applying modal control, Hanagud and Griffin created so-called "smart materials" in the sound board of string instruments (Hanagud and Griffin, 1998). They managed to control the damping factor of the first (low frequency) modes.

A multi-modal control concept has been recently investigated at IRCAM, in the "IMAREV" project led by Mamou-Mani. Two PhD projects have been

carried out; one on soundboards, by Benacchio (Benacchio et al., 2015, 2016; Benacchio, 2015), and one on wind instruments, by Meurisse (Meurisse et al., 2014; Meurisse, 2014; Meurisse et al., 2016). Also aiming for musical sound transformations, they managed to develop applications that have been used by IRCAM-based composers.

Another recent example of an actively controlled string instrument is the work carried out by Donovan, who investigated the control of the string itself (Donovan and McPherson, 2015).

1.3.7 *Terminology*

In order to avoid confusions with earlier writings it is convenient to introduce some of the terminology used by the authors of the most related topics. The term "hybrid" was, for example, used by Boutillon and Guérard, who spoke about "hybrid synthesis" (Boutillon and Guérard, 1995; Guérard and Boutillon, 1998). Maganza, working on an early version of the same concept as that developed in the current thesis, didn't name his device but rather used expressions such as "nonlinear excitations of an acoustical duct" for instance. However, in the conclusion of Maganza's PhD dissertation, the expression "hybrid instrument" was also used to describe musical perspectives (Maganza, 1985). This explanatory approach was also employed by Weinreich and Grand (Weinreich and Caussé, 1986; Grand, 1994). In earlier works by the present author and Vergez, the term "hybrid" was used to refer to the same concept as used in the current dissertation (Buys and Vergez, 2012). However, Mamou-Mani, Meurisse and Benacchio also used the expression "hybrid instrument" to describe a greater class of instruments, including their musical active control applications, which they further specified as "modal active control" applications (Meurisse, 2014; Benacchio, 2015). Benacchio interchangeably used the term "smart instruments" (Benacchio et al., 2015), which he most likely adopted

from Hanagud's work on "smart structures" (designating actively controlled soundboards) (Hanagud and Griffin, 1998).

The term "hybrid" is also used for non-interactive electro-acoustic examples, e.g. the conventional use of "hybrid guitar", which refers to a traditional guitar equipped with an electric pickup system. In contrast, Michon and Smith's hybrid guitar is an advanced guitar controller, piloting a computed physical model (Michon and Smith, 2014). Another understanding of "hybrid" was proposed by Yamaha, who own a patent on a "hybrid wind instrument", which is a traditional acoustic wind instrument that can also be used as a controller for electronic sound generation (Onozawa and Fujita, 2006).

Meanwhile, in a wide variety of literature, the term "augmented" is used for the more general concept of modified versions of a traditional musical instrument. In this view, hybrid and actively controlled instruments could be seen as sub-categories of "electronically augmented" instruments.

Another general and ambiguously used expression is "electro-acoustic", which is mostly used for non-interactive combinations of electronic and acoustic systems, but given the appropriate wording, Almeida preferred to use this term for his (early) similarly loudspeaker-driven wind instrument (Almeida et al., 2010).

Recently, the Belgian composer, performer and instrument maker Godfried-Willem Raes, as part of his wide collection of automated musical robots, built a loudspeaker driven pipe organ which he named <hybr> (referring to "hybrid") (Raes, 2015). The organ is also electro-acoustic in nature, but there is no feedback mechanism involved. Rather, for each pipe, a pre-tuned signal is sent to the associated loudspeaker.

1.4 LIMITATIONS AND REQUIREMENTS

In contrast to electronic synthesis and effects, hybrid and actively controlled musical instruments both imply an electronic bi-directional interaction with

an acoustic component, within the sound frequency domain. Those properties contribute to respectively an adaptable, dynamic and physical character (see the related paragraph discussing physical and non-physical systems in section 1.2.1). While this is a trump card for musical expression possibilities with those electro-acoustic applications, in turn, their functionality is limited by several conditions. An important question to be asked is: what functionality limitations does a given hybrid instrument set-up imply?

In line with good research practice, another question, which takes an opposite view should also be considered: what is required in terms of "set-up architecture", calculation methods, technologies and component specifications with regard to the desired aims of a hybrid wind instrument? This question describes the requirements for the instrument design, which informs practical design strategies. The requirements should derive from more fundamental questions, i.e. the research questions. These research questions, in turn, formalise the motivations of the research project.

It is interesting to consider this distinction between limitations and requirements. The limitations view is bottom-up in nature, i.e. by asking "what is (not) possible with a given device?" The requirements point of view is top-down in nature, i.e. by asking "how can a tool be designed that can realise a target application?". While the former question allows estimation of the practical potential of a concept, the latter question enables verification of the realisability of ideas.

For the case of the current research project, given that the hybrid instrument concept is already chosen, the limitations approach is more appropriate in the first instance. However, there are further layers of development where the requirements point of view returns, for example when asking more specific questions such as "how can a certain timbre be obtained?". This dual questioning is a constant throughout the research study, but it is important not to lose the focus on the underlying research questions and motivations.

The next two subsections will address the limitations of the hybrid instrument set-up studied in this thesis and some references are made to the earlier cited literature. Then, the following subsection stipulates appropriately related research questions, which in turn result in the definition of requirements, which represent the direct goals of this work.

1.4.1 *Limitations imposed by the synthesis approach*

First some limitations that are imposed by the synthesis concept are considered. The synthesis component used for the proposed hybrid instrument consists of a computed excitation, with a pressure measurement at the input and a flow rate signal at the output, which should generate sounds when coupled to a resonator. This concept already imposes important limitations on the operational possibilities of the hybrid instrument. Indeed, a freely designed excitation model in feedback-interaction with a resonator does not allow for the simulation of any imagined sound. In addition, the numerical implementation of such models also introduces limitations. These two limitation categories will be discussed in more detail in the next paragraphs.

Another limitation, that typically applies to the general case of many synthesised musical applications, is the lack of haptic feedback, which plays an important role with respect to the player's "immersion" with their performance. New efforts have been made over the past few decades to equip electronic instruments with haptic actuators (see e.g. (Berdahl et al., 2009)), which could be useful in later stages of the hybrid instrument's development.

MUSICAL LIMITATIONS IMPOSED BY EXCITATION MODELS AND BY PHYSICALLY-BASED MODELLING While some musical possibilities of excitation models have already been discussed in the motivation in subsection 1.2.1, it is appropriate now to consider their limitations.

The design of excitation models with the purpose of favouring musical possibilities, and the related case of "physically-based modelling" (introduced by De Poli and Rocchesso (1998), as noted earlier) is relatively poorly developed in the literature, which forms a first limitation in this regard. Regarding the real-instrument-based case of physical modelling, a broad range of algorithms for simulating musical instruments exists (developed by for example the recent NESS project and by various other groups such as IRCAM, McGill, CCRMA SARC). However, a detailed physical understanding of many musical instrument aspects important to obtaining a realistic and natural sound is still missing.

Alternatively, new excitation models could be designed, however this is far more complicated than any other sound synthesis technique. In that quest, it should be minded that the functionality of both physically-based and non-physically based (as explained in section1.2.1) excitation models is limited by particular oscillation conditions. Moreover, even within these oscillation conditions the relation between the excitation model and the produced sound is not straightforward. These design limitations are due to the instant and bi-directional interaction between the excitation model and the resonator, which will be further considered in chapter 2.

Another limitation exists for the particular case of musical active control applications. As mentioned earlier, the active controller should be "aware" of the exact state of the resonator to be able to coherently interfere with it. The control of a manipulatable resonator imposes musical limitations, given that resonator transition information is usually not available "on the fly" (i.e. while playing). Therefore, in order to track the resonator's status, it may be necessary to either introduce a pitch tracking mechanism or to capture the musician's actions. However, since such measurements usually disregard subtle physical variations that can be substantial to the oscillatory behaviour, these methods may be prone to undesirable sound glitches.

NUMERICAL CONSIDERATIONS Even when an excitation model (or similarly, a physically-based model) is known, its numerical implementation on the computing system introduces new limitations. This can be inferred from Avanzini's PhD dissertation for instance, which is tellingly entitled: "Computational issues in physically-based sound models" (Avanzini, 2001).

Many of the implementations presented in the state of the art section disregard an important issue, which is related to the instantaneous influence of the entering air flow on the pressure at the resonator entrance. While the real physical functioning is an instantaneous bi-directional interaction between physical Kirchhoff variables (the pressure and flow rate in the case of wind instruments), a computing system can only function sequentially. Or, in mathematical terms, the Kirchhoff variables are often related by an implicit equation (an expression that depends on itself), while a computing system can only calculate explicit expressions. The issue is further detailed in section 4.1, where a number of workarounds are reviewed. It should be mentioned that this issue only arises when there is an inherently instantaneous (or "stiff") relationship between the Kirchhoff variables, which is the case for most physical excitation models. Hence, the issue is of particular concern for the chosen hybrid set-up.

In his first experiments, Maganza ignored the implicit equation issue (calculating the equations as if they were explicit). This still resulted in oscillatory states, but with a poorer relation to the real physical model. In a second experimental part, he partly compensated for the issue by transforming the Kirchhoff variables to wave variables, using a digital wave-table implementation (Maganza, 1985), but the wave variables were not correctly derived.

Conversely, since the resonator can be usually considered as a linear dynamic system, the issue does not apply to active control applications and the simulation of resonators (e.g. for the inverse hybrid principle, such as the one investigated by Guérard and Boutillon (Boutillon and Guérard, 1995; Guerard and Boutillon, 1996; Guérard, 1998)).

1.4.2 *Limitations imposed by physical components specific to the hybrid instrument*

The effects of physical components in a feedback system such as the proposed hybrid instrument can be various and are not always straightforward to predict. These components (i.e. transducers, amplifiers and the computing system) do not necessarily have a flat magnitude and zero phase response and their linear dynamic range is also limited by noise and saturation. While each of these deviations can often be compensated for with corresponding "inverse" filters (provided the inverse system is causal, the component's model is implicitly known and/or the required measurements are performed), the compensation will never be complete in practice, as it can only work over a limited amplitude and/or frequency range. Hence, it is important to consider such deviations. The next two paragraphs separately discuss these nonlinear and time-related deviations, but it should be mentioned that (the combination of) both deviations can lead to the appearance of undesired instabilities during the playing performance of the instrument.

Another effect of physical components, which particularly applies to transducers, is that even their passive presence interferes with the surrounding acoustics, which is generally not desired. The active control literature often stresses the importance of actuator and sensor placement and dynamics. For instance Preumont states: "If the dynamics of the actuators and sensors may significantly affect the behaviour of the system, they must be included in the model before the controller design" (Preumont, 2011). For this interference, additional compensation filters can be introduced, but their effect is also conditioned by the limitations of the transducers; moreover, they can lead to instabilities.

A generalised rule of thumb (derived from conclusions by Berdahl (2009), Boutin (2011) and Meurisse (2014) for instance) is that the greater the difference between the desired situation and the passive state, the greater the risk of instabilities occurring and the more the limitations of the transducers become apparent. In other words, while in theory many targeted operations would be

possible, it is the performance and presence of the physical components which limits those possibilities.

For the hybrid instrument studied in this thesis, it is the loudspeaker that introduces the most significant deviations. An example of a theoretically extreme case could be a hybrid instrument that is programmed to simulate an acoustically open pipe at the loudspeaker's position. However, given that the passive role of a loudspeaker-terminated pipe approaches a rigidly closed pipe, this application would probably require a loudspeaker performance with an unrealistically high amplitude and precision.

LINEARITY DEVIATIONS Linearity or amplitude deviations occur when the dynamic range of a component is exceeded.

For example, the realistic performance of Weinreich and Caussé's "electronically bowed string" was limited to relatively small force amplitudes (Weinreich and Caussé, 1986, 1991). Indeed, the maximum achievable electromagnetic force of the solenoid coil (e.g. due to string heating (Weinreich and Caussé, 1991)) lies below the static friction forces that can occur during the "sticking phase" of a bow-string interaction when playing mezzo-piano on a violin for instance. Louder sounds could be obtained, but these would have unrealistically slow transients and restricted brightness.

As a first precaution, Guérard (who developed inverse hybrid instruments combining real physical excitations with a partly simulated resonator) limited the amplitude range by focussing on bowed string and flute instruments, which both can operate at low dynamic levels (taking into account the mentioned small amplitude condition as used by Weinreich and Caussé). However, the transducer linearity is still of particular concern, given that simulation of various resonator lengths requires quite different situations from the electronically passive case. In addition, Guérard's wind resonator simulation is realised by a small pipe that is terminated by a loudspeaker. This complicates the evaluation of excitation types that inject a constant air flow in the resonator, such as reed

excitations. To enable such excitation models, a small vent hole could be introduced, as in the experimental setup in (Van Walstijn and Sanctis, 2014), but this may also introduce acoustic effects that are difficult to compensate for.

Due to similar dynamic range limitations, Picket could only attenuate low amplitude excitations with his actively controlled trumpet (Pickett and Saunders, 1998) (i.e. real mouth-driven excitations were too strong, but softer excitation signals could be produced by an additional loudspeaker mounted on the embouchure). This is indeed what can be expected, given that the compression driver used had a low acoustic power compared with the typical acoustic pressures inside the instrument (in particular at relatively low frequencies and with the resistive effect of the capillary tube used).

On the matter of transducer placement, it is claimed in both the noise control and musical active control related literature that systems with collocated actuator and sensor display very interesting properties (see e.g. (Preumont, 2011; Berdahl, 2009)). This is related to the appearance of vibration modes in the controlled body, which can amplify or attenuate certain frequencies depending on the location. Hence, this eventually also relates to the dynamic constraints of the transducers. The influence of resonance modes is for instance evidenced by Meurisse's modal active control application for wind instrument resonators. Given the strong acoustic field, Meurisse placed both the microphone and loudspeaker near the open end of the resonator, i.e. near a pressure node (Meurisse, 2014). While this choice is favourable with respect to the loudspeaker's dynamic possibilities, it also reduces the possibilities of electronically modifying the resonator's response.

These shortcomings only apply to a small extent in the case of the hybrid wind instrument studied in this thesis. This is so, given that on one hand both the loudspeaker and microphone are located at the resonator entrance, where a rigid acoustic termination is required and all pressure anti-nodes take place; while on the other hand, the excitation is simulated, so that the mean air flow signal can be removed. However, it should be mentioned that this set-up only

enables the simulation of excitation types that are compatible with a closed-entrance resonator. Again, theoretically speaking an open-entrance could be simulated with the loudspeaker, but this probably requires unrealistic loudspeaker performance.

DYNAMICS AND TIME-RELATED DEVIATIONS Another physical components feature relates to the presence of dynamics and time-related deviations. Examples are the friction and inertia in the transducers and delays caused by a realistic computing system. Those deviations can also be understood as a non-flat frequency response, i.e. a certain filtering effect.

While the linearity deviations can be simply avoided by using small amplitudes, the dynamics and time-related deviations can only be corrected by using appropriate inverse filters. To the author's knowledge, there have been no studies of electronically excited wind instruments that compensate for these deviations. Therefore this aspect is given careful attention in this thesis, by selecting a suitable loudspeaker (further described in 3.3.2) and computing system (see appendix B), and then taking the necessary compensation measures (worked out in subsection 3.2.3 for the loudspeaker and in chapter 6 for the computing system).

The advantage of active control applications with respect to this issue is that it is usually applied on linear components (e.g. the resonator). This allows for a direct integration of the transducer's response in the control system.

The virtual string set-up by Guérard and Boutillon also has this advantage (Guerard and Boutillon, 1996; Guérard, 1998). One way to understand this is by imagining that the delay caused by the actuator response (an electrodynamic shaker) and its correction filter can be interpreted as a part of the string response that consists of delayed pulses coming back from the string ends.

This solution is not applicable to the case of electronic excitation of acoustic resonators, which therefore imposes more important limitations to the sound possibilities.

1.4.3 *From research questions to requirements*

Now that the motivation, state of the art and limitations have been discussed, it is possible to consider what long term research questions are appropriate and, in turn, what requirements this imposes on the design of the hybrid instrument.

The research questions formalise the underlying motivations, they define the work to be done and set priorities. Hence, they represent the fundaments of the research project, which will be the starting point for putting the research into operation. They represent a base of reference at any point during the research project.

The questions are formulated by considering the study in terms of the underlying theory and possible methods; thus potentially providing clear, well-defined answers and filling an important gap in knowledge.

The first research focus is on the musical perspectives of the hybrid instrument, which first requires some consideration of today's new music scene. Over the last few decades, there has been a clear increasing interest in the musical exploration of timbre. This can be seen as emerging within all contemporary music scenes: one is the classical music scene (generally referred to as contemporary classical music, see e.g. (Paddison and Deliège, 2010)) another is in the avant-garde jazz scene (usually referred to as free-jazz, with "free improvisation" as an often occurring element, see e.g. (Jenkins, 2004)). While both of these scenes comprise electronic and/or computed music approaches, these approaches appear in many other musical scenes and they can also be interpreted as a scene in its own right (see e.g. (Wishart, 1996)). In all of these scenes, traditional and new musical instruments are used in alternative ways to come up with novel sonorities, extending the musical sound palette. Hence, these musical directions are referred to in what follows when speaking about "musical expression", allowing the first research question to be formulated as:

Research question 1. *What factors in the design of loudspeaker-driven hybrid wind instruments with computed excitation models influence the perceptible sound palette with respect to favouring musical expression?*

It should be noted that this question draws on the subjective notion of musical preference, which indicates that eventually an evaluation with human participants will be required. This was not envisaged to be within the scope of this thesis, given that the entire thesis period was needed for the development and quantitative evaluation.

With regard to the perspective of using the hybrid instrument as a tool to carry out subsequent wind instrument research, as mentioned in the motivation section earlier on, the hybrid instrument can be used in a similar way to blowing machines for wind instruments. The foremost advantages of using a blowing machine over a human player are: more controlled and objective measurements as the embouchure parameters can be regulated independently, easier measurement of embouchure parameters and good repeatability (Ferrand and Vergez, 2010). It is notable that the advantages regarding all of these aspects are even greater when using a hybrid wind instrument. Indeed, the embouchure parameters are programmable quantities and the equipment is barely influenced by e.g. set-up, mounting manipulations, general ageing or the inevitable blowing pressure perturbations in the case of blowing machines (Ferrand and Vergez, 2010). Nevertheless, it should be said that for many applications a blowing machine would be a better choice, given that that set-up is closer to a real blown instrument and hence the approximation error associated with simulated excitation models is avoided. Another concern may be the physical limitations of hybrid wind instruments, e.g. the dynamic level may not be high enough to investigate nonlinear sound propagation in resonators. Furthermore, the fact that a hybrid wind instrument only introduces the fluctuating component of the air vibration, and that the flow is introduced by a membrane instead of through a narrow air channel as in the case of a reed-instrument, certainly results in a different detailed fluid-dynamic behaviour.

Some possible scenarios that would particularly benefit from evaluation with a hybrid wind instrument can be summarised. For instance, wind instrument theories on self-sustained oscillations could be verified (e.g. as in (Wilson and Beavers, 1974) with a blowing machine), but with an even more quantified approach than is possible with a blowing machine. Also, it would be straightforward to reproduce certain rapid pressure changes (e.g. caused by fast tonguing) recorded in the mouth of actual musicians, which would be a challenging task with blowing machines (Ferrand and Vergez, 2010). Using a hybrid instrument may also make it easier to keep track of the flow velocity signal; it can be easily recorded with a hybrid instrument, but is hard to measure in a physical set-up. The comparison of real and hybrid instruments could also be particularly useful to study self-sustained operations in resonators, and notably during fingering transitions, as these are difficult to simulate; which was a motivation for the construction of Almeida's hybrid wind instrument (Almeida et al., 2010). Furthermore, just like blowing machines, the hybrid instrument can be useful to play historical musical instruments that are no longer permitted to be played by human players, with the advantage of even lower intrusiveness given the absence of the mean air flow and the possibility of playing at very low amplitudes.

With these perspectives in mind, it is important that the hybrid instrument's operation is objective and well-calibrated, leading to the following research question:

Research question 2. *What factors in the design of hybrid instruments with computed excitation models lead to a precisely quantified excitation of resonators and allow for an optimal evaluation of existing physical theories on wind instruments?*

As mentioned earlier, more possibilities can be imagined, such as in an educational context, as an instrument maker's aid, to make historical instruments sound,... However, these purposes all depend on the positive outcome of the two stipulated research questions.

These two questions alone still define long-term goals of the hybrid instrument. For the current thesis, a number of provisional requirements are stipulated, which guided the research project in the direction of both research questions and support the initial development steps that are taken in this work.

Requirement 1. *Diversity (in terms of the perceptible variety of the sound).*

In musical instrument and musical controller design, a large control bandwidth is often aimed for. While, for instance, Cook advertises that this feature is not necessarily in favour of musical expression, due to the inspiration-decreasing effect of the excess in control freedom (Cook, 2001), it should be realised that Cook's rule applies to an instrument in the state made available to a performer. A musical system with a wide variety of sounds can still be limited to a specific application and this bandwidth therefore represents a measure of possible sub-implementations. In other words, the hybrid instrument shouldn't necessarily be seen as a single instrument, but rather as a platform for musical instrument implementations.

Requirement 2. *Precision, in terms of:*

- *the sound control (regardless of parameter mapping strategies).*
- *the accuracy of the sound (control) in relation to predictions and simulations.*

While an important factor with regard to the former feature is (quantisation) noise, the latter feature is of particular importance from the research tool perspective, which has the aim of obtaining a situation that is close to an "ideal hybrid instrument", i.e. without the earlier stated limitations of the physical components. However, given that the ideal hybrid instrument's properties are the closest to the original acoustic instrument, it is also favourable from the musical perspective. The predictability is also desirable to enable guidance in the design of sub-implementations.

Requirement 3. *Repeatability, i.e. repeated progressions of the excitation model's input parameters should result in repeated sound features (if hysteresis effects are avoided before the repetition).*

Note that hysteresis is not necessarily a problem in this regard, it could even represent a desirable feature (see e.g. (Mudd et al., 2015)).

Requirement 4. *Musically relevant atypical behaviour, typical to the hybrid operation.*

While in the first instance, a hybrid operation close to that of an ideal hybrid instrument is aimed for (as stipulated by the accuracy requirement), the sounds obtained with the simulations is very close to those of an ideal hybrid instrument. From the musical perspective, as pointed out earlier, in the musical motivation in subsection 1.2.1, it would be interesting if the hybrid instrument's character were distinct from both the original acoustic instrument and the simulated sounds. Therefore, the atypical behaviour is at odds with the accuracy requirement. It should be understood that in this work, the primary focus is on the accuracy requirement, but in parallel, an eye is kept open to musically interesting atypical behaviour. Indeed, such atypical behaviour is actually likely to occur, given that the real hybrid wind instrument contains (uncompensated) physical elements that are not found in an acoustic instrument, and which are also complicated to simulate. Particular electronic or mechanical saturation effects could be thought of for instance, and also future adaptations can be envisaged in this direction.

1.4.4 *Conclusions*

In the first instance, the choice of the electro-acoustic synthesis approach and of which components to use determines the musical and research tool possibilities and to what extent a stable and accurate operation is guaranteed. Therefore, the limitations imposed by the physical components should be carefully considered. Considering the current state of the art, there are many aspects that require a thorough investigation in order to obtain a functional hybrid set-up. An important focus for the current thesis is the choice of suitable components and the design of appropriate loudspeaker-compensating filters. However, in order to achieve a wide range of possibilities, the functionality obtained

without transducer-compensating filters should not diverge too much from the intended operation (as explained in the introduction of subsection 1.4.2). Meanwhile, it should be borne in mind that some limitations or deviations could also introduce desirable musical values.

Secondly, in order to answer fundamental research questions that relate to the possibilities of the hybrid instrument, a number of initial requirements for a desired operation can help in directing the first development and early evaluations steps to be taken in this work. The chosen requirements are focussed on broad and precise control possibilities to obtain a large perceptible sound range, resulting in a platform with a wide variety of musical possibilities.

Finally, from a research expertise point of view, the interdisciplinary character of the work can be identified as a challenge for the researcher, which could be interpreted as a so far unmentioned, "limitation". The following disciplines are mainly involved: informatics, electronic and mechanical engineering, musical acoustics, signal processing, and music. This forms a limitation in the sense that a single person carrying out all tasks cannot be an expert in all disciplines, which therefore slows down the design process.

It can be concluded that there are good reasons to continue the research and development of this intriguing hybrid concept.

1.5 OUTLINE AND CONTRIBUTIONS OF THE DISSERTATION

1.5.1 *Outline of the dissertation*

Figure 8 shows a schematic diagram summarising the entire thesis, with indication of each of the chapters in the dissertation.

The yellow box in the diagram refers to chapter 2, where the basic functioning of wind instruments (with a cylindrical resonator) is laid out. The green box refers to the development of the loudspeaker-tube system and the associated filters, which is discussed in chapter 3. The blue part of the diagram refers

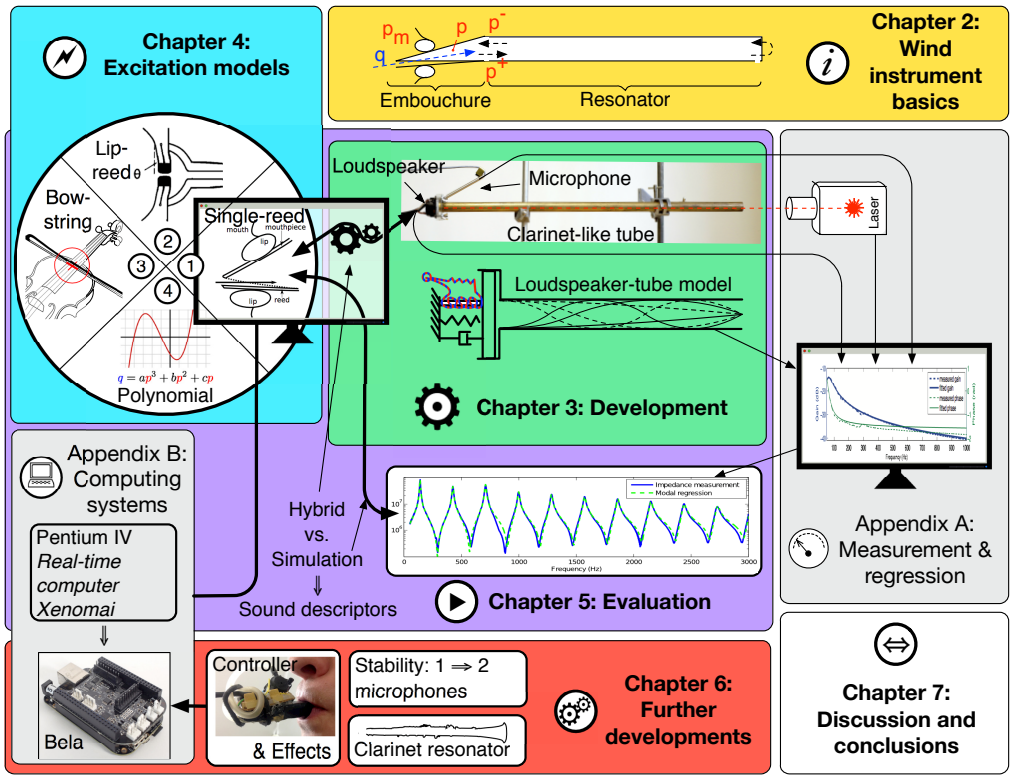

Figure 8: Schematic diagram of all work carried out in this thesis, with indication of the chapters and some key notions.

to chapter 4 where the excitation models are introduced. Next, the combination of the loudspeaker-tube system, the computing system and the excitation models, indicated by the purple box, leads to the evaluation of the hybrid functionality, discussed in chapter 5. The red box combines a number of further developments on the hybrid instrument, discussed in chapter 6. In that chapter, a stability issue is addressed and compensated for, a brief evaluation with a real clarinet resonator is discussed and some control and effect possibilities are presented. The white box refers to chapter 7, where conclusions and discussions are provided on the wider outcomes of the work.

Finally, there are two appendixes, which are referred to by the two grey boxes. Appendix A contains details regarding the measurement equipment and procedures and the regression techniques, which are informed by physical models obtained in earlier chapters. Appendix B provides details of the employed

real-time computing systems and presents a few examples of source code and programs developed for the hybrid instrument.

1.5.2 *Main contribution to the relevant fields*

Many of the theoretical frameworks and practical approaches discussed in this dissertation draw on existing work in various fields. Whereas references to the relevant literature are made in the text, it is appropriate to summarise the main contributions here.

Most of the introductory theory presented in chapter 2 is pre-existing wind instruments acoustics theory. However, mainly original contributions are made in section 2.3.2, particularly on the mean power approach to estimate the influence of frequency dependent acoustic losses on the sound.

The principal contribution of this thesis is captured in chapter 3. Whereas the general concept to combine an acoustic resonator with a theoretically simulated excitation by means of a loudspeaker was already introduced by for instance Maganza (Maganza, 1985), the chapter quickly builds further on newly introduced more specific implementation strategies such as the design choices and the idea of employing loudspeaker compensation filters. That being said, the theoretical models used for all components, including the filters and their digital implementation, and the use of equivalent circuit analysis of the mechano-acoustic components are adopted from existing sources, as indicated accordingly. Furthermore in this chapter, while there are evidently previous studies that reported on mathematical descriptions of coupled single-degree-of-freedom systems, the employed original representation for the loudspeaker-coupled tube, e.g. by defining a "coupling frequency", turns out to be particularly useful for the comparison of the coupled and uncoupled systems. Also the criteria in section 3.3.2, for the choice of a suitable loudspeaker are originally proposed here. And finally, most of the noted shortcomings and compensation

measures discussed in section 3.4 have not been reported before (apart from for a few aspects, for which a reference is provided).

Most of the excitation models and numerical calculation methods discussed in chapter 4 are adopted from well established literature, but a few noteworthy contributions have been made to allow for a coherent representation and use in the context of the present thesis. Notably the theory to predict the influence on the sound (presented in chapter 2) is an original contribution that is applied to each excitation model. The employed lip-reed model (discussed in section 4.3) draws on a combination of established theories, but the non-dimensionalised representation and also the discrete and explicit development has not been explicitly reported before to the author's knowledge. Furthermore, the use of a quasistatic interpretation of this dynamical excitation model is new and the usefulness attested in the reported results in this thesis support the value of this introduced concept. Meanwhile, the small signal approximation for the lip-reed's analysis is adopted from the literature, but the graphical representation, shown in figure 45, to directly identify oscillation features is a newly proposed approach. Similar originality conclusions apply to the bow-string interaction model (section 4.4). The similarity to the single-reed excitation model has been mentioned before, and the hyperbolic model is well-known, but the dimensionless and reduced parameter form, originally proposed in this thesis, reveals a much clearer insight of the similarities and differences of those models and it further allows for a simplified evaluation. Finally, Maganza already broached the idea of employing a polynomial formula for the production of self-sustained oscillations by putting it into interaction with a resonator, but the generic third order formula employed here, and its useful sound-influence focussed representation is novel, as is its analytically discrete and explicit development.

All evaluation methods described in chapter 5 draw on existing theory. However, the interpretation of the results via comparison with the earlier mentioned sound feature estimations for each excitation model is a newly proposed tech-

nique (apart from the amplitude). Evidently, the final results and the associated discussion and conclusions reported in section 5.5 provide original findings.

Chapter 6 contains additional new development propositions and outcomes. Just like chapter 3, most of the precise ideas and the implementations are original but the employed methods are adopted from basic mathematical and other existing theories.

In chapter 7, the overall contributions with regard to the hybrid instrument's performance are discussed and compared with the literature. Also the perspectives and recommendations discussed in section 7.2, are mainly original ideas, but some perspectives also refer to earlier writings.

Finally, the appendix is mostly based on existing theory and previously built systems, but the particular measurement set-up and method used to characterise the entire loudspeaker-tube system is a new approach.

1.6 SUMMARY

This introductory chapter outlined the background of the hybrid wind instrument concept discussed in this thesis.

To provide a basic understanding, the first section briefly explained the concept, which can be understood by imagining the interaction between a computed (clarinet) embouchure with an acoustic resonator (e.g. a clarinet-like tube), by means of a loudspeaker and a microphone.

In a next section, two motivations of primary interest for the realisation of the hybrid instrument were discussed. The first motivation focussed on musical possibilities, using the hybrid instrument as a new musical instrument. The second motivation was with regard to its usage as a research tool, where the hybrid instrument could be used to carry out wind instrument research.

A subsequent section provided a detailed overview of the state of the art, explaining similar and related fields with reference to the existing literature. Models of acoustic musical instruments were introduced, along with concepts

in electronic musical synthesis (with a focus on synthesis by physically-based modelling). Next, electronic excitation of acoustic resonators was discussed (which is the category of the hybrid instrument discussed in this thesis). Furthermore, the related concepts of hybrid string instruments and active control applied in musical instruments were briefly reviewed. Finally, attention was given to the terminology, reviewing the use of the term "hybrid" in the literature, while also referring to related terms.

A further section was focussed on limitations and requirements. The limitations of hybrid and related musical instruments were discussed, focussing on limitations imposed by the synthesis approach (such as musical limitations imposed by physically-based modelling and numerical considerations) and limitations imposed by physical components specific to the hybrid instrument (introducing linearity and time related deviations). Then, the musical and "research tool" oriented research questions were formulated and a number of requirements were derived from them to provide a focus for the current work. Some general reflections were provided as a conclusion. The limitations informed the importance of choosing suitable components and designing appropriate loudspeaker-compensating filters and the main requirements were found to be focussed on broad and precise control possibilities to obtain a large perceptible sound range.

Finally, in the last section, the outline of the dissertation was presented, along with a schematic representation of the content.

2

ON THE OPERATION OF WIND INSTRUMENTS WITH A CLARINET-TYPE RESONATOR

This chapter provides the reader with the basic acoustic theory that is required to understand the development and evaluation of the hybrid wind instrument, which will follow in the succeeding chapters. First the clarinet is discussed, as the acoustic operation of this instrument can be reduced to a relatively simple theory in the time domain. The clarinet theory includes excitation of the resonator via a single-reed model. Then, some alternative possibilities for exciting an acoustic resonator are presented. Further, some theories are laid out that allow pre-estimation of a few perceptually important sound features, as a function of an excitation model and its parameters. Finally, a frequency domain description of acoustic resonators is presented, which will be useful later when implementing an entirely computed simulation of the instrument. Throughout this chapter, various theorems are expressed. They will be applied to the individual excitation models, discussed in chapter 4.

2.1 BASIC FUNCTIONING OF THE CLARINET

In this section, the fundamental operation of the clarinet will be laid out as an example of the functioning of wind instruments in general (some differences will be discussed in the following sections). The detailed understanding of the clarinet involves both frequency dependent behaviour and amplitude nonlinearities. While frequency dependency is best studied in the frequency domain, the nonlinear behaviour is much better understood in the time domain. Since these domains are difficult to combine (simple operations in the time domain

can be very complicated in the frequency domain and vice versa), a thorough understanding of the clarinet acoustics can become fairly elaborate.

Nevertheless, given that the frequency dependency in wind instruments can be reduced to a simple delay component (which is obviously straightforward to express in the time domain), it is possible to describe the emergence of oscillations solely in the time domain. While characteristics such as the timbre are poorly represented after this simplification, the oscillation conditions and amplitudes remain in good accordance with the case of a real clarinet (see for example (McIntyre et al., 1983; Atig et al., 2004)).

In addition to providing a global understanding, this theory will be used in section 2.3, where the physical properties of the instrument are linked to a few more of its sound features.

Figure 9 shows a schematic diagram of a clarinet including a player's mouth. Two components can be distinguished, the embouchure and the resonator, which each have a distinct functioning. Their combination is the key to the typical "self-sustained" sounds produced by wind instruments, i.e. the oscillation is maintained by the interaction. These components and the pressure and flow rate signals (respectively in red and blue in the diagram) are discussed in the next section.

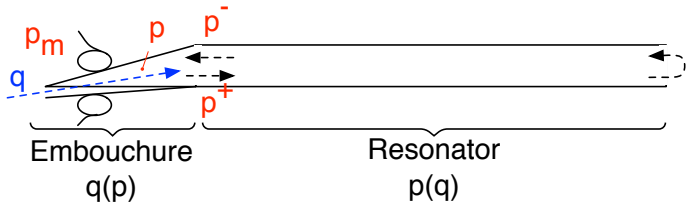

Figure 9: Schematic diagram showing a clarinet's basic acoustic functioning, distinguishing the embouchure (the mouthpiece and the player's mouth) and the resonator.

2.1.1 *Acoustics of separate clarinet components*

THE RESONATOR When speaking about "the resonator", what is being referred to is: the section of the bore from the mouthpiece to the first open key (which is somewhat of a simplification of a real clarinet bore). In order to give a simple explanation of the functioning of the instrument, a number of assumptions will be made in this section. (For later use, a more pertinent - frequency domain - model of the resonator is discussed in section 2.4.)

First, the atmospheric pressure can be interpreted as a global offset pressure relative to all other involved pressures, so that it can be ignored (or theoretically it can be set equal to zero). Second, as the wavelengths of the oscillations that will appear are greater than the diameter of the inner section of the bore, it is reasonable to assume that the waves are planar in form and the pressure waves can be described in a one dimensional space, i.e. on the axis along the length of the resonator (see e.g. (Bernoulli, 1764)).

Another mostly valid assumption is the resonator's "linearity" with respect to the amplitude. This property can be understood by imagining that the resonator entrance is closed by hitting it with a hand. A short response can be heard, and by hitting harder or softer the same response will appear, but its amplitude will be in linear relation to the impact of the hit.

Finally, it is assumed that at all frequencies the wave velocity is constant and the same amount of acoustic losses is experienced, i.e. the dispersion and the frequency dependent component of the acoustic losses (further referred to as the "frequency dependent losses") inside the resonator and at its ends is ignored so that the propagation can be characterised with a real constant $\lambda \lesssim 1$, the acoustic transmission factor. In other words, a pressure burst travelling from the bore entrance will maintain it's "burst shape", it will only be slightly reduced in amplitude when it arrives at the end. Then, the open end will return a pressure wave that is inverted in amplitude. It should be noted that in practice the dispersion and frequency dependent losses are not insignificant, but

neglecting them results in a mathematical simplicity which still has properties that are surprisingly coherent with the real functioning of the instrument. (In fact, it is even possible to demonstrate the basic functioning principles when the frequency independent component of the acoustic losses (further referred to as the "frequency independent losses") is neglected too.)

As depicted in figure 9, the pressure at the entrance of the resonator (at the mouthpiece side) can be subdivided into forward and backward travelling pressure waves, respectively $p^+$and p^-:

$$p(t) = p^+(t) + p^-(t). \tag{1}$$

This pressure is further referred to as either the "mouthpiece pressure" or the pressure at the resonator entrance.

The embouchure introduces an air flow $q(t)$ which instantaneously produces a forward travelling pressure contribution $q(t)Z_c$, where Z_c is the "characteristic impedance" of the resonator, which is a real constant, inversely proportional to the internal cross-sectional area of the resonator (see section 2.4 for a detailed explanation).

Given that the mouthpiece side of the resonator can be assumed perfectly reflecting, the incoming pressure $p^-(t)$ is reflected back with the same amplitude and sign; hence, the up-going pressure wave can be rewritten as the sum of the flow-related pressure and $p^-(t)$:

$$p^+(t) = q(t)Z_c + p^-(t), \tag{2}$$

so that $q(t)$ can be expressed as:

$$q(t) = \frac{p^+(t) - p^-(t)}{Z_c}. \tag{3}$$

At the same time, the forward travelling pressure can be related to the backward travelling pressure, as the latter will be reflected back (with an inverted sign)

after having travelled down and up the length of the resonator l at the speed of sound c, which gives:

$$p^-(t) = -\lambda p^+(t - 2l/c), \tag{4}$$

where typically $\lambda \approx 0.9$ (Taillard et al., 2010). It expresses the amplitude of a pressure pulse with an initial unity gain, after it has travelled down the resonator, from the embouchure towards the bell, and back up. Based on this definition, λ, then represents the frequency independent losses. For a cylindrical open tube, with no radiation at the open end, where losses only occur inside the bore: $\lambda = \exp(-2\alpha l)$, with α, the absorption coefficient. Of course this is an approximation: real losses are frequency dependent and radiation occurs from the open end. However, as the frequency dependence of the losses is a relatively small correction in musical instruments, this is sufficient for our initial purposes.

Altogether, by combining equations (1), (2) and (4) , it can be shown that the resulting overall pressure can be expressed as a function of the flow rate introduced by the mouth and the delayed forward travelling pressure:

$$p(t) = q(t)Z_c - 2\lambda p^+(t - 2l/c). \tag{5}$$

The last term can be replaced by using equation (2) again, so expressing it in terms of the previous set of incoming pressure waves. This replacement can be repeated again and again until the initial moment is reached where the incoming pressure wave is zero, i.e. just before the oscillation is initiated by the mouth of a player. As this term only depends on the past, it is also referred to as the *historical pressure*: $p_h(t) = 2p^-(t) = -2\lambda p^+(t - 2l/c)$ (initially introduced by McIntyre et al. (1983)), so that:

$$p(t) = q(t)Z_c + p_h(t). \tag{6}$$

In the next steps, for simplicity and universality, a normalised (or "dimensionless") form is introduced. This involves the replacement of the variables by new variables that are normalised using characteristic values (with dimensions that correspond to the old variables) of the instrument's model. The dimensionless pressure and flow rate are defined as: $\bar{p}=\frac{p}{P_M}$ and $\bar{q}=\frac{qZ_c}{P_M}$, where P_M is a characteristic pressure that will be explained later. All other pressures and flow rate signals are made dimensionless with these characteristic values. Also for simplicity, in what follows, the time notation is left out for variables with argument t. Hence, equation (6) becomes:

$$\bar{p} = \bar{q} + \bar{p}_h, \tag{7}$$

with $\bar{p}_h = \frac{p_h}{P_M}$. Furthermore, using equation (4), equations (1) and (3) can be rewritten as:

$$\begin{cases} \bar{p} &= \bar{p}^+ + \bar{p}^- = \bar{p}^+ - \lambda\bar{p}^+(t-2l/c) \\ \bar{q} &= \bar{p}^+ - \bar{p}^- = \bar{p}^+ + \lambda\bar{p}^+(t-2l/c) \end{cases}. \tag{8}$$

Or, alternatively:

$$\begin{cases} \bar{p}^-(t) = -\lambda\bar{p}^+(t-2l/c) &= \frac{\bar{p}(t)-\bar{q}(t)}{2} \\ \bar{p}^+(t) &= \frac{\bar{p}(t)+\bar{q}(t)}{2} \end{cases}, \tag{9}$$

which introduces a coordinate system $(\bar{p}^-, \bar{p}^+)$ that is rotated by 45° from the original $(\bar{p}, \bar{q})$ coordinate system. This will be further developed and used in section 2.1.2.

In order to generate oscillations with the resonator, it has to be acoustically excited. One way to do this, is to introduce an energy burst. Just like the plucking of a string, a duct-type resonator can be hit on the open entrance to produce a tone. However, in contrast to a typical string resonator, the acoustic losses in a wind instrument are much higher so that the produced tone is very short,

which explains why this type of excitation is rarely applied in a musical context. A more appropriate type of excitation is a continuous interaction, where energy is introduced in (nonlinear) relation to the pressure signal in the resonator, as such resulting in "self-sustained oscillations". For wind instruments this excitation is performed by the embouchure; that is, the ensemble of the musician's mouth and the reed mechanism.

THE EMBOUCHURE In contrast to the resonator, the combination of the mouth and mouthpiece, from now on referred to as "the embouchure" (or more generally for any musical instrument: the excitation mechanism), does not operate linearly with respect to the amplitude. Detailed physical models of the clarinet embouchure and other excitation mechanisms will be discussed in section 4.2. Here it is sufficient to note that the excitation model can be represented by a characteristic function that expresses the air flow as a function of the pressure difference across the reed. Hence, for a constant mouth pressure p_{m}, this becomes a function of the mouthpiece pressure only: $q(p)$. This, together with equation (6) for the resonator, forms a set of equations whose solution describes the oscillatory physical interaction between embouchure and resonator.

The reed of the clarinet mouthpiece is "inward striking" (a concept introduced by Fletcher (Fletcher, 1979b)), which means that it tends to close the air channel when the pressure in the mouth is greater than the pressure inside the instrument. This property enables self-sustained oscillations to appear when the reed's resonance frequency lies far above the frequency of the played note (see e.g. (Chaigne and Kergomard, 2013)). Hence, it is a reasonable approximation to ignore the inertia of the reed, freeing the characteristic function of time-dependent terms, and thus making it "quasistatic".

A characteristic occurrence for this model is the moment where the reed starts hitting the lay (the curved cut-off surface onto which the reed is fixed) of the mouthpiece. This occurs at the so-called "beating pressure" p_{M}, which is therefore chosen as the characteristic value used to define the dimensionless

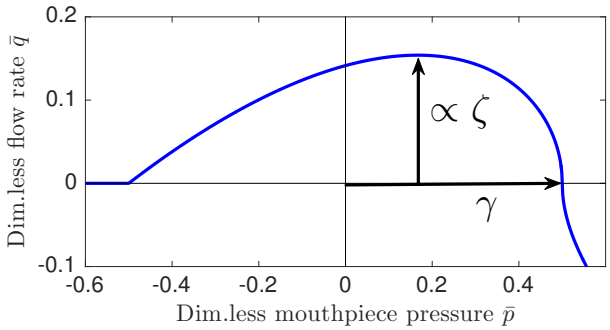

Figure 10: Characteristic nonlinear curve of the static single-reed model for a dimensionless mouth pressure of $\gamma = 0.5$ and an embouchure parameter $\zeta = 0.4$.

characteristic function $\bar{q}(\bar{p}) = q(\frac{p}{p_M})\frac{Z_c}{p_M}$. The dimensionless mouth pressure is denoted $\gamma = \frac{p_m}{P_M}$, so that for a dimensionless pressure difference across the reed of $\gamma - \bar{p} \geq 1$, the reed hits the lay. In addition, several properties of the embouchure are lumped together and represented by the parameter ζ; which is inversely proportional to the reed opening at rest (Kergomard, 1995). This parameter will be explained in more detail in chapter 4. Figure 10 depicts this characteristic function for $\gamma = 0.5$. As can be seen, with increasing γ the nonlinear curve is shifted along the $\bar{p}$ axis and ζ proportionally defines the height of the curve.

For this case, when $\bar{p} \leq -0.5$, the dimensionless pressure difference across the reed is greater than unity, the reed is beating and no flow will occur. For a dimensionless mouthpiece pressure of $\bar{p} = 0.5$, the pressure difference is 0, which again results in no air flow. It is between these states that a nonlinearly variable flow amplitude occurs.

2.1.2 *Self-sustained oscillations*

OSCILLATION AND STABILITY CONDITIONS An intuitive understanding of self-sustained oscillations can be gained by thinking of the excitation in terms of a parent pushing a child on a swing (the resonator). The parent can either make a negative or positive energy contribution: when the child approaches (i.e. when the pressure burst wave is reflected back up the resonator and ap-

proaches the mouthpiece), a positive contribution would be to pull and push respectively with the child's arrival and departure (or: a positive pressure burst is supplemented with some extra pressure from the mouth). The supplied energy will then enable a continuous oscillation, as it compensates for the lost energy in the swing (/resonator).

Returning to the presented theory on the clarinet, the energy supplied by the embouchure is represented by the slope of the nonlinear function (i.e. its derivative) and thus varies with $\bar{p}$. If this slope or "local amplification factor" is positively increasing, it represents a "negative resistance" (Schelleng, 1973) to the resonator. Therefore, if the slope at $\bar{p} \approx 0$ is greater than the acoustic losses, an oscillation can occur, which is expressed in a first theorem:

Theorem 1. *Condition of oscillation: Instability. An oscillation can appear from the moment that the characteristic function furnishes sufficiently positive energy around* $\bar{p} \approx 0$*, i.e. when the derivative at that point is greater than* $1 - \lambda$*.*

This understanding also explains the importance of the nonlinear character of the excitation. If the added energy were only linearly related to the amplitude of the swing, the oscillation would either die out or (theoretically) wouldn't stop growing. Therefore an amplitude-dependent (i.e. nonlinear) relation is required: for small pressure amplitudes the contribution should be greater than the losses, but at higher amplitudes the derivative should become less than the losses so that the oscillation will stop growing and settle at a certain amplitude.

ITERATIVE MAPS THEORY The simplifying assumptions with respect to the resonator and the quasistatic property of the excitation provide a convenient way of studying the self-sustained oscillations. First, the original nonlinear curve in the $(\bar{p}, \bar{q})$ coordinate system, as represented in figure 10, can be plotted in the $(\bar{p}^-, \bar{p}^+)$ system; which results in a 45° rotation, as can be understood from equation (9). By then introducing the index n for the time instance $t = n(2l/c)$, and noting that $p^+_{n-1} = \frac{p^-_n}{-\lambda}$, the characteristic curve of the embouchure model can be represented in the new Cartesian coordinate system

$(\bar{p}^+_{n-1}, \bar{p}^+_n)$; which mirrors and slightly stretches the nonlinear curve towards the $\bar{p}^+_n$ axis, as can be seen in figure 11. Indeed, while the diagonals of the $(\bar{p}^-, \bar{p}^+)$ system were the $(\bar{p}, \bar{q})$ axes (shown as dashed axes), the rescaling of the horizontal axis results in a shift of the $(\bar{p}, \bar{q})$ axes, away from the new diagonals. The new diagonals (shown as solid axes) will be later referred to as the $(\tilde{\bar{p}}, \tilde{\bar{q}})$ system. This representation in the $(-\bar{p}^-_n/\lambda, \bar{p}^+_n)$ system can be interpreted as an alternative, "hypothetical" oscillating system that operates with a hypothetical internal pressure $\tilde{\bar{p}}(t)$ and flow rate $\tilde{\bar{q}}(t)$, and comprises a hypothetical excitation $\tilde{\bar{q}}(\tilde{\bar{p}})$ and resonator $\tilde{\bar{p}}(\tilde{\bar{q}})$. In other words, the hypothetical resonator has the same characteristics as the original resonator, but with no frequency independent losses. These losses are, so to speak, "transferred" from the resonator model to the excitation model. It should be noted that the equation of the nonlinear curve in the $(\tilde{\bar{p}}, \tilde{\bar{q}})$ system becomes implicit and greatly complicates the mathematical study of the oscillations; this coordinate system is therefore purely of interest in terms of facilitating easy graphical interpretations of the oscillatory operation, as will be shown shortly.

As demonstrated by McIntyre et al. (1983), the representation in the $(\bar{p}^+_{n-1}, \bar{p}^+_n)$ coordinate system and later by Taillard et al. (2010) in the $(\tilde{\bar{p}}^+_{n-1}, \tilde{\bar{p}}^+_n)$ system, allows reconstruction of the emergence of self-sustained oscillations from the initial moment when the resonator is in a static state (the pressure being at atmospheric pressure throughout), and the excitation is set such that it satisfies the oscillation condition, which results in an "iterative map".

Initially, the resonator entrance is at atmospheric pressure so that $\bar{p}^+_{0-1} = 0$. By setting this as the abscissa in the coordinate system, the nonlinear function indicates the subsequent downstream pressure value as the ordinate: $\bar{p}^+_0$ (which will be the result of a first puff of air entering through the mouthpiece); and in its turn, this will be the next abscissa for $\bar{p}^+_{n-1}$. Hence, this lookup procedure can be repeated for consecutive values of n, i.e. for every time jump of $2l/c$, which can be represented by an iterative progression on the nonlinear curve, as

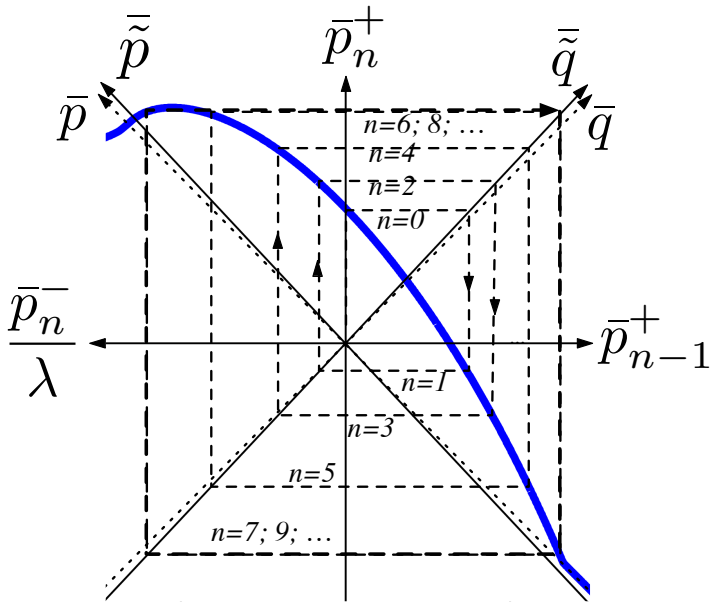

Figure 11: The single-reed curve in the $(\bar{p}_{n-1}^+, \bar{p}_n^+)$ coordinate system, for $\gamma = 0.5$ and $\zeta = 0.4$. The $(\bar{p}, \bar{q})$ coordinate system is indicated as well, these axes slightly diverge from the 45° diagonals (the $(\tilde{\bar{p}}, \tilde{\bar{q}})$ system) due to the fact that $\lambda \lessapprox 1$. This allows for the representation of an iterated map (in dashed), illustrating the emergence of a self-sustained operation. Note that after a few steps the iteration remains inside an "iteration square".

shown in figure 11. This can also be represented as a temporal progression of the mouthpiece pressure, as shown in figure 12.

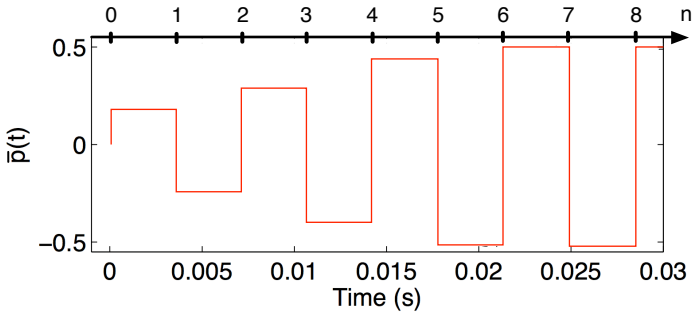

Figure 12: Dimensionless mouthpiece pressure progression over time from an initial static state to the steady state regime, for $\gamma = 0.5$ and $\zeta = 0.4$.

Given that the oscillation repeats every two time jumps, the period of oscillation is $2n = 4l/c$.

Such a "two-step" oscillation with block-shaped pressure waves is also observed for the case of an idealised bowed-string operation, referred to as the "Helmholz motion"; which was thoroughly studied by Raman (Raman, 1918),

who also took into account the frequency independent losses in his model. It has since been shown that the discussed simplified wind instrument theory operates in an analogous manner to the string instrument model (McIntyre et al., 1983; Ollivier et al., 2004).

After a few iterations, the pressure $\bar{p}$ will alternatively jump between exactly opposite values, i.e. a stable amplitude is reached, which will be further referred to as "the steady state regime". On the nonlinear curve, the iteration stagnates between two opposite points, forming a maximum "iteration square" (see e.g. (Taillard et al., 2010)). An important property of this steady state oscillation is that it always represents a perfectly harmonic signal, i.e. the frequency components are perfect multiples of a fundamental frequency. This is a consequence of the coupling of the excitation model and the resonator. While a real resonator (with frequency dependent losses) usually stimulates an inharmonic relation, which induces a difference in phase among the frequency components after an oscillation period, the excitation model removes this phase difference again when the steady state regime is reached. Therefore, the temporal wave signals in this regime are perfectly repeating cycles.

When not in a steady state regime, the oscillation is in the so-called "transient" regime, where it changes each cycle. This happens when the excitation model undergoes any changes such as an increase in mouth or lip pressure, and continues until the excitation-resonator combination has reached oscillatory "agreement" i.e. the steady state regime. It is worth noting that the initial transient at the onset of the sound, as seen in figure 11, is called the "attack" of the sound.

It should be mentioned that in theory some nonlinear curves can result in two or more alternating squares, which is known as period doubling (introducing sub-harmonics). This has been theoretically studied for single-reed instruments (e.g. (Taillard et al., 2010)) and also in previous hybrid instrument set-ups (Maganza et al., 1986). However, the phenomenon rarely occurs in practice and only the single square regime is considered for now.

2.2 OTHER EXCITATION MODELS

It is possible to excite a clarinet with other types of embouchures, which opens up the possibility of generating different sounds. While other designs of single-reed embouchures can be thought of, embouchures that follow a completely different excitation principle can also be introduced. This is particularly interesting for the hybrid wind instrument, in terms of creating new timbres, as the computer allows any type of excitation to be freely programmed. A number of excitation models are discussed in detail in chapter 4, but it is worth mentioning here how excitation models can be different from the single reed model. This is also of relevance for section 2.3, which discusses the influence of an arbitrary excitation model on the produced sound.

2.2.1 *Quasistatic excitation*

Any excitation model whose functioning can be approximately described by leaving out any time derivatives is quasistatic in nature. This property implies that the model can be represented by a static curve; its shape does not depend on the input's history. As shown, the property greatly simplifies the understanding of self-sustained oscillations.

As well as the discussed single reed model, the double reed falls in this category. In addition, models that are not explicitly based on pressures and flow rates can be considered, for instance models for the "bow-string interaction", which is the excitation for bowed string instruments. The presented theory and the derived theorems can be simply extended by replacing the nonlinear curve of the single reed by the curve of any quasistatic excitation model. However, certain quasistatic excitation types can also be categorised as dynamic excitations, as will be explained.

2.2.2 *Dynamic excitation*

In this thesis, the focus lies on quasistatic excitations, and the next section is initially based on this assumption. However a dynamic model (the lip-reed model) is also employed (in section 4.3) and, in that section, an adapted theory is proposed to approximately suit this dynamic case.

An excitation can be considered dynamic if there is any time dependency involved in the excitation's interaction with the resonator, so that the nonlinear $q(p)$ curve is composed of varying paths.

There are a few possible ways that such excitations can emerge.

One is due to the presence of time derivatives, for example to model friction or inertia; this is necessary when modelling brass-playing lips (the "lip reed") for instance. The complexity of such systems is reflected in the literature; a good overview is given by Campbell (2004). To explain the self-sustained operation, the derived theorems are mostly valid, but they impose different conditions. For the lip-reed model for instance, the lip resonance frequency should be around or below the frequency of the played note, so as to enable the occurrence of a "negative resistance", which is required for the initial instability, as stipulated in theorem 1.

An interesting feature of excitation models that are themselves vibrating systems, is that they can also contribute to maintaining the self-sustained oscillation, therefore becoming more independent from the resonator. This allows this component to have a greater influence on the signals, i.e. on how the instrument will sound.

Another type of dynamic excitation is one where the characteristic function is a multivalued function in the $(\bar{p}_{n-1}^{+}, \bar{p}_{n}^{+})$ coordinate system (and not necessarily in the $(\bar{p}, \bar{q})$ system). This can be understood as a state where a change in pressure would lead to a bigger change in pressure induced by the entering air flow, or: $\partial p < Z_c \partial q(p) \Rightarrow \frac{\partial q(p)}{\partial p} > \frac{1}{Z_c}$ (partial derivatives are used as the condition should not take into account the implicit dependency of p by q). This

causes the oscillation to stick to the branch of the curve that it was following, and jump to the other branch when a certain threshold is exceeded. This hysteresis effect only occurs when there is a multivalued zone within the domain of the oscillation (i.e. for $|p| \leq p_\mathrm{a}$, where p_a is the amplitude of the oscillation) and repeats for each oscillation cycle. The following theorem summarises the condition for the appearance of hysteresis for the dimensionless case:

Theorem 2. *Condition of hysteretic excitation. An excitation model with dimensionless implicit equation $\bar{q}(\bar{p})$ is hysteretic when its explicit equation is multivalued in the domain where the oscillation occurs, i.e. when $\exists \bar{p} \in [-\bar{p}_a, \bar{p}_a] | \frac{\partial \bar{q}(\bar{p})}{\partial \bar{p}} > 1$.*

This phenomenon occurs, for example, for the bow-string interaction model when high bowing forces are applied (see 4.4). In this way, it is demonstrated that a quasistatic model can also be dynamic in its operation.

2.3 HOW THE EXCITATION INFLUENCES THE SOUND

In this section, the issue of how the interaction of the excitation model and the resonator determines the sound produced is discussed. This study is interesting with regard to discovering the sound potential of a given excitation model. Also, understanding the excitation-sound relationship enables pre-estimation of the sound features, ideally providing a tool for selecting excitation models and/or parameters to deliver a desired sound output. Hence, this theory provides some general guidelines in the "quest" for musically interesting excitation models (note however that this quest can also be undertaken in different ways).

Many sound features are generally difficult to accurately predict, either due to the complexity of the excitation model and/or the requirement of a more complex resonator model. This also explains why these sound features are generally not precisely and independently controllable by the player. That is, while some sound features can be directly related to a single factor of the characteristic nonlinear equation, it is usually not the case that this factor is also related

to a property of the physical model that is independently controllable; mostly the physical properties relate to several sound features at the same time. Nevertheless, it may be possible to find a new (reduced) dimensionless parameter set for an excitation model (such as for the presented single-reed model) with a more direct connection to the sound features, a point which will also be clarified in the next subsections.

The first subsection discusses amplitude-related features of the oscillation, revealed by the simplified model of the resonator with only frequency independent losses and no dispersion considered. Then the second subsection extends the resonator model to include frequency dependent losses, revealing certain spectral features of the oscillation. It should be mentioned that this subdivision of the acoustic losses is purely of practical use and has no physical meaning.

2.3.1 *Amplitude-related features*

Amplitude of oscillation

From the iterative maps theory - more precisely, from the iteration square - a new theorem can be derived that will enable direct estimation of the amplitude of the oscillation in the steady state regime by solely considering the excitation model's characteristic curve:

Theorem 3. *Amplitude of oscillation. The dimensionless amplitude of the oscillation in the steady state regime, $\bar{\tilde{p}}_a$, is determined by the intersection of the dimensionless nonlinear curve with its $\tilde{\bar{q}}$ axis mirrored curve, i.e. the peaks are indicated by the non-zero solutions of $\tilde{\bar{q}}(\tilde{\bar{p}}) = \tilde{\bar{q}}(-\tilde{\bar{p}})$. Hence, the domain occupied by the oscillation is $\tilde{\bar{p}} \in [-\bar{\tilde{p}}_a, \bar{\tilde{p}}_a]$.*

As discussed earlier, these solutions will not be mathematically derived here, given the enormous complexity and the fact that the detail is not important for our study (the solutions can be found in (Taillard et al., 2010)); instead, the theorem is used here to graphically identify the solutions. In this way it can be

easily understood that, for instance, the mouth pressure, shifting the nonlinear curve along the $\bar{p}$ axis, has an important influence on the amplitude of the oscillation. Figure 13 shows the case for $\gamma = 0.8$. The outer intersections of the dashed curves indicate the amplitude in the steady state regime. It can be seen that the beating reed threshold is greatly exceeded for this case and the outer intersections reveal a steady state amplitude of $\tilde{\bar{p}}_a \lesssim 0.8$.

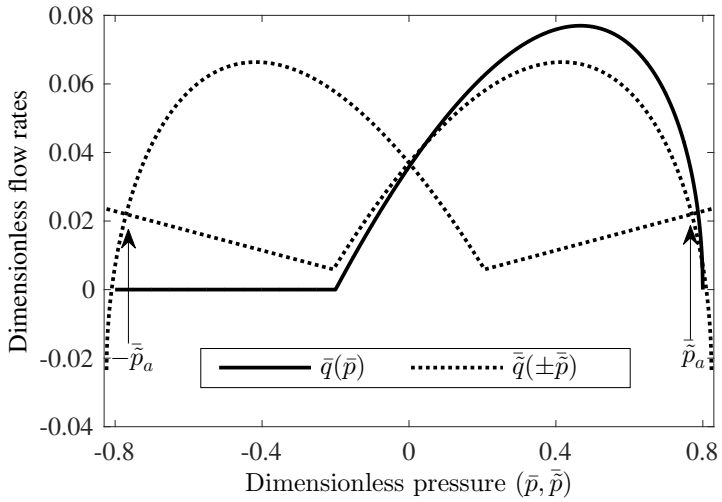

Figure 13: Characteristic single-reed curves for $\gamma = 0.8$ and $\zeta = 0.2$; in the $(\bar{p}, \bar{q})$ and $(\tilde{\bar{p}}, \tilde{\bar{q}})$ coordinate system, resp. in solid and dotted lines. The mirrored curve is also plotted in the latter system, which reveals $\tilde{\bar{p}}_a$, the amplitude of the oscillation in the steady state regime.

It should be noted that the total, dimensional, amplitude is then obtained by multiplying by the global scaling factor P_M. While P_M cannot be separately controlled with a real embouchure, this is possible in the case of the dimensionless model, so that the global amplitude can be controlled independently of any other sound feature.

In contrast to P_M, altering γ changes the shape of the characteristic excitation curve, which therefore also influences other sound features.

Extinction of the oscillation

It is interesting to note that the representation in the $(\tilde{\bar{p}}, \tilde{\bar{q}})$ coordinate system reveals an important property of the clarinet: when the mouth pressure is increasing, the amplitude will grow, but at the same time the injected flow signal

becomes a smaller fraction of the oscillation period so that the excitation becomes weaker and at a certain point, the oscillation extinguishes; this is when the outer intersections of the nonlinear curve with its mirrored curve disappear.

Amplitude of excitation

The "excitation amplitude" $\tilde{\bar{q}}_a$ is defined as the peak-to-peak amplitude of the flow rate signal $\tilde{\bar{q}}$ or, in other words, the vertical reach of the part of the excitation function that is used in the oscillation . Note that contrary to the pressure, the presence of a mean flow component requires the use of a peak-to-peak flow rate amplitude. While a given excitation model does not necessarily provide a parameter that directly controls this amplitude, it is mathematically straightforward to control it with a global factor in the characteristic function, for which the parameter name ζ is chosen, in convention with the literature on the single-reed model (Kergomard, 1995).

The iterative maps theory directly demonstrates the influence of this amplitude on the onset of the oscillation. Whereas figure 11, the embouchure parameter was $\zeta = 0.4$, for the nonlinear curve in figure 14, $\zeta = 0.2$. Given that for both cases $\gamma = 0.5$, the amplitude of oscillation is nearly equal and, as such, ζ only controls the excitation amplitude. As can be seen, many more iterations are needed (about 30) before the steady state regime is reached. This suggests that ζ is inversely related to the attack time, which is also in agreement with existing theories on the single-reed model (Kergomard, 1995), but this interpretation generalises the idea for any quasistatic excitation model.

Another way to understand this is to interpret the resonator as a reservoir of energy, which will be charged during the attack time. As such, when the steady state is reached, the reservoir is full and the energy supplied by the mouth equals the energy outputted by the resonator. In that regard, it can also be understood that when the excitation is of higher amplitude, a shorter attack time is needed to fill up the reservoir.

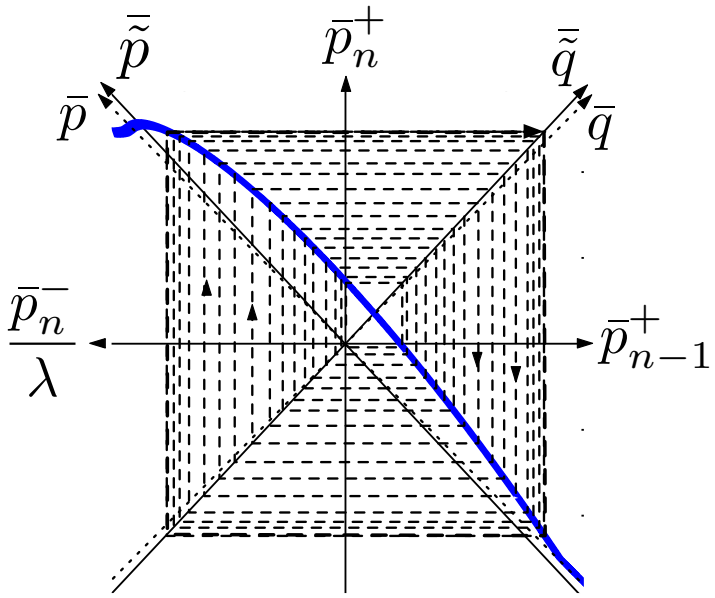

Figure 14: Iterative map on the single-reed curve, for $\gamma = 0.5$ and $\zeta = 0.2$. The number of iterations to reach the iteration square increases for a decreased embouchure parameter.

The excitation amplitude also has an effect on the spectral richness, or the "brightness" of the sound during the steady state regime. However, in order to study spectral variations, the frequency dependent losses component and/or the dispersion has to be taken into account; in their absence, only square waves are obtained, which have a rich but constant spectrum. Taking into account those effects complicates the study greatly; without it everything can be fairly easily presented in the time domain. The impact of those losses and the dispersion would be more easily understood in the frequency domain, but this domain is not suited for the study of the nonlinearities of the excitation. Here a simplified — yet somewhat empirical — technique is proposed to study the influence of the frequency dependent losses.

2.3.2 *Effect of the frequency dependent losses*

Many theories exist that discuss the relationship of the excitation with the steady state spectrum of self-sustained sounds using frequency-domain-based methods, first investigated by Worman, then by Benade (Worman, 1971; Ben-

ade, 1988). Later, the numerical "harmonic balance method" (e.g. (Schumacher, 1978; Gilbert et al., 1989; Karkar et al., 2012)) and analytical "variable truncation method" (Kergomard et al., 2000) were introduced, which operate in the frequency domain by seeking for pressure and flow rate spectra that both match the excitation model (and its parameter status) and the resonator's impedance and thereby reveal the steady-state oscillation. However, the early theories are too case specific for our purpose (only small oscillations, for the clarinet only,...) and the harmonic balance and variable truncation methods tend to overshadow the intuitive link between a given excitation model and the resulting spectrum. Nevertheless, it will be shown that there is a method that approximately relates the characteristic nonlinear curves to some characteristic sound features. This will be achieved by deriving some generalised rules, relying on the case of the quasistatic single-reed excitation; their detailed application to the specific excitation models employed in this thesis is further investigated in chapter 4.

Remaining in the time domain, it is interesting to consider how a pressure impulse would look after it has travelled down and back up the resonator. This introduces the notion of "reflection function" (see e.g. (Chaigne and Kergomard, 2013)). A lossless cylindrical resonator with an open ending has the reflection function $r(t) = -\delta(t - 2l/c)$, where δ is the Dirac delta function, with l the resonator length and c the speed of sound. This will result in an inverted equal amplitude impulse returning after a time $2l/c$. The reflection function for a dissipative resonator is shown in figure 15 (c). It is calculated using a theoretical model (Polack, 1987), with geometrical parameters corresponding to the tube resonator that is employed throughout this thesis.

As can be seen, it is close to a delayed, inverted impulse, but when examined closely, the impulse appears smeared out in time, particularly in its decay.

The temporal procedure to calculate the backward travelling pressure response for an arbitrary injected forward travelling pressure signal is by convolution of the forward travelling signal with this reflection function. Given that it is not the intention to demonstrate the self-sustained oscillation mathem-

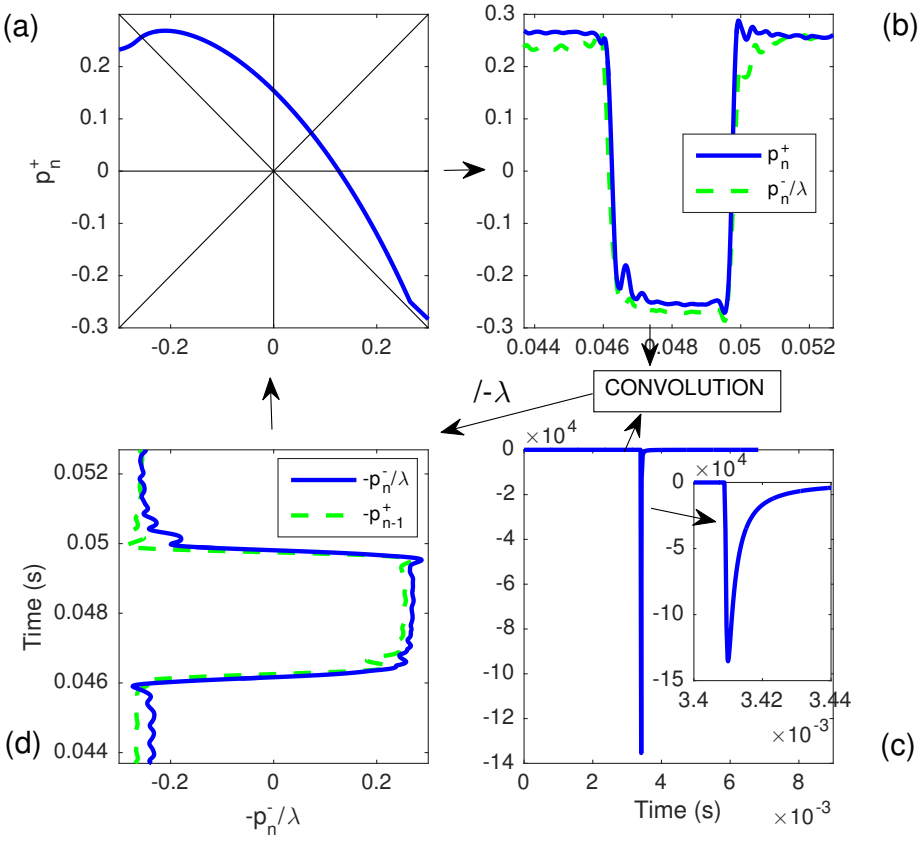

Figure 15: Flow diagram of the clarinet's operation, consisting of the nonlinear characteristic curve in the $(-\bar{p}_n^- / \lambda, \bar{p}_n^+)$ system, for $\gamma = 0.5$ and $\zeta = 0.4$ (up, left), the downstream pressure signal $\bar{p}^+(t)$ (up, right), the resonator's theoretical reflection function $r(t)$ (down, right), and the upstream pressure signal $-\bar{p}^-(t)/\lambda$ (down, left).

atically here (which would be very complicated), the impact of this convolution is simply interpreted as a "smearing out" effect, which can be observed when comparing both down- and upstream pressure signals. Figure 15 is set up in such a way that one cycle through the curves in a clockwise direction (e.g. from (a) to (d)) represents half a period of an oscillation (i.e. one iteration). As earlier, the single-reed model with parameters $\gamma = 0.5$ and $\zeta = 0.4$ is used. The effect of the frequency independent losses component (i.e dictated by the acoustic transmission factor) is better understood by using the equivalent — hypothetical — oscillating system, where λ is integrated into the excitation model. Thus, by dividing the outcome of the convolution by $-\lambda$, the effect of the remaining losses component and the dispersion can be separately studied. As such, the ho-

rizontal axes of the two graphs on the left side of figure 15 are represented by $-\bar{p}_n^- / \lambda$; however, due to the extra losses and dispersion, this no longer exactly corresponds to $\bar{p}_{n-1}^+$. Therefore, the separate downstream (b) and upstream (d) pressure signals are not simply identical, delayed signals. Their axes in figure 15 are scaled and orientated so as to correspond to the axes of the nonlinear curve and of the reflection function. The displayed pressure signals are chosen for an arbitrary time for one oscillation cycle during the steady state regime.

While the effect of the frequency dependent losses and the dispersion is small, it can be generally seen by the fact that the pressure waves are not perfectly block-shaped anymore (i.e. high frequencies are reduced in amplitude). When observing for example graph (d), the forward travelling pressure $-\bar{p}_{n-1}^+$ (dashed line) convolved with the reflection function (and divided by $-\lambda$), results in the backward travelling pressure one iteration later $-\bar{p}_n^- / \lambda$ (solid line). This reveals that the influence of the effect is a slight rounding of the wave shape. Hence, the upstream pressure jump is no longer instantaneous (as it was for the model with only frequency independent losses) so that the whole characteristic curve is evaluated during the iteration. As such, when observing graph (b), after evaluating the backward travelling pressure signal $\bar{p}_n^- / \lambda$ (dashed line) with the nonlinear function (which applies instantaneously), it can be noted that the corners are sharpened again in the downstream pressure $\bar{p}_n^+$ (solid line). Hence, it can be concluded that an increase in the "amount of nonlinearity" will positively compensate for the rounding effect of the frequency dependent losses and the dispersion and pull the equilibrium back towards the block-shaped case, i.e. towards a richer, brighter sound spectrum and a decreased attack time. Nevertheless, it is not straightforward to quantify this compensation effect and to measure its impact on the spectral richness, but the theory in the next subsection proposes a slightly more detailed approach by distinguishing two components of the nonlinear curve.

Excitation of odd and even harmonics

Given that a cylindrical resonator, open at one end and closed at the other, only stimulates the odd harmonics (i.e. its impedance has antiresonances on even multiples of the first resonant frequency), the pressure signal at the resonator entrance almost solely consists of these frequencies. Considering now the case of the hypothetical resonator, the (hypothetical) absence of the frequency independent losses component results in an accentuation of the resonances and antiresonances, so that the hypothetical pressure $\bar{\tilde{p}}(t)$ contains even fewer even harmonics. By also neglecting the insignificant influence of the mean flow (provided that $Z(\omega = 0) \approx 0$) (see section 2.4), it can first be assumed that the spectrum of this pressure signal only contains odd harmonics, i.e. it is anti-symmetrical in shape.

It is easy to verify that the evaluation of an odd function (whose graph is known to have rotational symmetry with respect to the origin) on an anti-symmetrical signal results in a new anti-symmetrical signal. Alternatively, the application of an even function (a symmetrical graph) on that signal generates a purely symmetrical signal. Furthermore, given that any function can be written as the sum of an odd and an even function, the excitation curve can be written as: $\bar{\tilde{q}}(\bar{\tilde{p}}) = \bar{\tilde{q}}_o(\bar{\tilde{p}}) + \bar{\tilde{q}}_e(\bar{\tilde{p}})$. In summary, the even and odd components of the flow signal can be simply derived from the odd and even function definitions applied on $\bar{\tilde{q}}(\bar{\tilde{p}})$:

$$\begin{cases} \bar{\tilde{q}}_e(\bar{\tilde{p}}(t)) & = \frac{\bar{\tilde{q}}(\bar{\tilde{p}}) + \bar{\tilde{q}}(-\bar{\tilde{p}})}{2} \\ \bar{\tilde{q}}_o(\bar{\tilde{p}}(t)) & = \frac{\bar{\tilde{q}}(\bar{\tilde{p}}) - \bar{\tilde{q}}(-\bar{\tilde{p}})}{2} \end{cases}. \tag{10}$$

This demonstrates that, after evaluation of the pressure with the nonlinear function, the generated flow signal $\bar{\tilde{q}}(t)$ can contain even harmonics, thus they will also be present in the sound waves radiated from the open end of the tube (albeit not so loud). Indeed, using a monopole radiation model (which is a reasonable approximation of the reality), the radiated pressure wave can be

estimated as $p_{ext} \propto \frac{\mathrm{d}\bar{p}^+}{\mathrm{d}t} \propto \frac{\mathrm{d}(\bar{p}+\bar{q})}{\mathrm{d}t}$ (see e.g. (Jacobsen, 2011)), showing that the emitted sound is proportional to the derivative of both the pressure and the flow rate. It is interesting to note that in the lossless resonator case, all signals are square waves, which only contain odd harmonics. Thus, it is as a result of the frequency dependent losses and the dispersion that a clarinet also outputs even harmonics (this can also be thought of in terms of non-zero values of the impedance at even harmonic frequencies (Barthet et al., 2005)).

The fact that a closed-open cylindrical tube only stimulates the odd harmonics ensures that the odd component is actually maintaining the oscillation. Therefore, the influence of $\tilde{\bar{q}}_{\mathrm{o}}(\tilde{\bar{p}})$ is essentially responsible for the spectral richness of the sound. While the even component also contributes to the spectral richness, because of the absence of resonator feedback, its effect is much smaller (note that, for example a purely even excitation curve cannot generate self-sustained oscillations). Hence, instead of the "amount of nonlinearity" of the entire curve (as hypothesised in the previous section), the "amount of nonlinearity" of the odd part is considered to be a more representative indicator of the brightness and attack time of the sound. This amount of nonlinearity is related to the vertical range of the part of the curve between the outer excursion points, i.e. in the domain $[-\tilde{\bar{p}}_{\mathrm{a}}, \tilde{\bar{p}}_{\mathrm{a}}]$.

An appropriate calculation should take into account the pressure wave, which is still close to block shaped, and thus should evaluate the nonlinear curve mainly close to $-\tilde{\bar{p}}_{\mathrm{a}}$ and $\tilde{\bar{p}}_{\mathrm{a}}$. However, the pressure wave is unknown a priori, and although the odd curve component will only generate odd harmonics, it cannot easily be verified by how much each of the harmonics will be excited.

Mean power

In order to provide a solution to this interdependency of the pressure and flow rate, an assumption is made, based on empirical observations of the self-sustained pressure waves produced by the hybrid instrument and simulations. These observations (see e.g. figure 15 (d) and figure 60 in chapter 5 for examples

of pressure waves obtained with the evaluated excitation models and a selection of arbitrary parameters) reveal that, for any quasistatic excitation of a closed-open resonator, the pressure wave is noted to be approximately "trapezoidal" in shape, with a variable "flank steepness", as shown in figure 16.

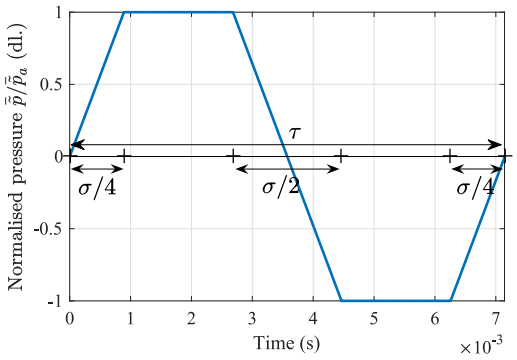

Figure 16: Empirical "trapezoidal" model of the pressure wave shapes.

The flank steepness in this model is determined by the fraction $\frac{\sigma}{\tau}$, where τ is the period of the oscillation and σ is the time during which the pressure is linearly increasing and decreasing. Note that a normalisation by $\bar{\tilde{p}}_a$ is performed to reduce the number of parameters. As such, this model can be used to calculate a corresponding flow rate signal for both the case of the excitation model (by applying its characteristic nonlinear function) and the resonator (by deconvolution of the resonator's impulse response). By varying the excitation parameters, the flow rate signals can be matched, which in turn enables the estimation of $\frac{\sigma}{\tau}$ as a function of the excitation parameters. However, it is more convenient to reduce this fitting operation to a comparison of the mean power dissipated over one oscillation cycle in the steady state regime, as calculated for the excitation model and the resonator. This quantity is typically deployed for such purposes; for example, McIntyre et al. used the similar notion of "mean rate of working" to demonstrate the self-sustained oscillation requirements (McIntyre et al., 1983). Moreover, it will be shown that the mean power calculation for this particular wave form can be interestingly reduced, resulting in a surprisingly intuitive excitation-sound relationship.

First of all, a few preliminary points are noted:

- The calculations are carried out on the dimensionless parameters, but they can be easily transformed to a dimensional case.
- The hypothetical excitation and resonator (i.e. the tilde-signals) are used, so that the power is entirely related to the dispersion and not partly to the frequency independent losses, which only affect the amplitude of the oscillation.
- The linear expression for the flank that crosses the origin is: $\forall\, t \in [-\sigma, \sigma]$, $\bar{\tilde{p}}/\bar{\tilde{p}}_\mathrm{a} = \frac{4t}{\sigma}$.
- The proposed assumed pressure wave is anti-symmetric, implying that it only contains odd harmonics.

The general expression to calculate the dimensionless mean power over one oscillation cycle is (Chaigne and Kergomard, 2013):

$$\bar{\tilde{\mathcal{P}}}_\mathrm{m} = \frac{1}{\tau}\int_{-\tau/2}^{\tau/2} \bar{\tilde{q}}(t)\bar{\tilde{p}}(t)\,dt \tag{11}$$

CALCULATED FOR THE CASE OF THE EXCITATION MODEL For the case of the excitation model, $\bar{\tilde{q}}(t)$ in equation (11) can be replaced by using its characteristic equation $\bar{\tilde{q}}(\tilde{p}(t))$.

$$\bar{\tilde{\mathcal{P}}}_\mathrm{me} = \frac{1}{\tau}\int_{-\tau/2}^{\tau/2} \bar{\tilde{q}}(\tilde{p}(t))\bar{\tilde{p}}(t)\,dt \tag{12}$$

Given that $\bar{\tilde{p}}(t)$ is anti-symmetric and $\bar{\tilde{q}}(\bar{\tilde{p}}_\mathrm{a}) = \bar{\tilde{q}}(-\bar{\tilde{p}}_\mathrm{a})$, the power generated at these pressure extrema is opposite and cancels itself out, so that the mean power integral can be reduced to the domain $[-\sigma/4, \sigma/4]$:

$$\bar{\tilde{\mathcal{P}}}_\mathrm{me} = \frac{2}{\tau}\int_{-\sigma/4}^{\sigma/4} \bar{\tilde{q}}(\tilde{p}(t))\bar{\tilde{p}}(t)\,dt \tag{13}$$

By substituting the pressure signal with its assumed wave shape in this domain $\bar{\tilde{p}}(t \in [-\frac{\sigma}{4}, \frac{\sigma}{4}]) = \bar{\tilde{p}}_\mathrm{a}\hat{\tilde{p}}(t) = \bar{\tilde{p}}_\mathrm{a}\frac{4t}{\sigma}$, so that $\frac{\mathrm{d}\hat{\tilde{p}}}{\mathrm{d}t} = \frac{4}{\sigma}$, and defining $\hat{\tilde{q}} = \bar{\tilde{q}}/\bar{\tilde{p}}_\mathrm{a}$, the mean power expression can be calculated as:

$$\bar{\hat{\mathcal{P}}}_{\mathrm{me}} = \hat{\mathcal{P}}\,\bar{\hat{p}}_{\mathrm{a}}^{2} = \frac{\sigma}{\tau}\frac{\bar{\hat{p}}_{\mathrm{a}}^{2}}{2}\int_{-1}^{1}\hat{\hat{q}}(\hat{\hat{p}})\hat{\hat{p}}\,d\hat{\hat{p}} \tag{14}$$

Hence, the value $\hat{\hat{\mathcal{P}}}_{\mathrm{m}}/\frac{\sigma}{\tau}$ can be calculated by only relying on the excitation model's characteristic curve. This is done numerically and it can also be graphically represented, as shown in figure 17.

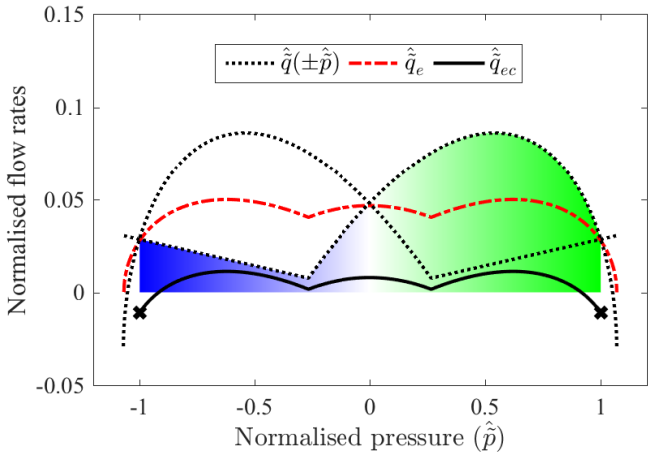

Figure 17: Single reed excitation curves for $\gamma = 0.8$ and $\zeta = 0.2$; in the normalised $(\hat{p},\hat{q})$ and $(\hat{\hat{p}},\hat{\hat{q}})$ coordinate systems; with indication of a gradient, which graphically represents the mean power calculation by the excitation model. The red dash-dotted curve is the even component of the nonlinear curve and the solid curve is that component after subtraction of the mean flow; providing an indication of a part of the even harmonics RMS calculation.

In this figure, the $\hat{\hat{q}}(\hat{\hat{p}})$ curve is filled with a gradient which demonstrates the calculation of $\hat{\hat{\mathcal{P}}}_{\mathrm{m}}/\frac{\sigma}{\tau}$ by subtracting the amount of blue (related to the negative normalised power contribution during one cycle) from the amount of green (related to the positive normalised power contribution).

CALCULATED FOR THE RESONATOR MODEL While the flow rate signal in equation (11) could be simply replaced by a deconvolution of the pressure signal with a theoretical estimation of the resonator's impulse response, there are a few things that complicate this reasoning. The fundamental frequency of the oscillation is also an unknown and as such, the pressure wave is not exactly known a priori. This issue can be resolved by making the assumption that the imaginary part of the impedance only introduces a constant delay, which can

be interpreted as a length correction to the resonator. In other words, the dispersion of the resonator is neglected and thereby also the inharmonicity, which is a reasonable approximation, especially given the fact that this feature is typically aimed for in the design of wind instruments. Hence, all harmonics exactly fall on the entrance impedance peaks and the phase at the harmonic frequencies can be considered zero. The fundamental frequency can be calculated from the tube's length (including the length correction) and the deconvolution can be performed using a frequency domain expression of the maximum impedance peaks of $\bar{\bar{Z}}_t$ (the dimensionless entrance impedance of the hypothetical resonator), which takes into account the acoustic radiation losses (Chaigne and Kergomard, 2013):

$$|\bar{\bar{Z}}_t|_{max} \approx \frac{1}{tanh\left(\alpha L + \frac{1}{4}(kR)^2\right)}, \tag{15}$$

where $\alpha = 1.044$ for air, $k = \frac{\omega}{c}$ is the wave number and L and R are the length and internal radius of the cylindrical resonator. So that the deconvolution in the frequency domain using the (circular) Fourier transform $\mathscr{F}$; and the succeeding inverse transform to the time domain using $\mathscr{F}^{-1}$ is performed giving:

$$\bar{\bar{q}}(t) \approx \mathscr{F}^{-1}\left(\frac{\mathscr{F}(\bar{\bar{p}}(t))}{|\bar{\bar{Z}}_t|_{max}}\right). \tag{16}$$

Finally, the dimensionless mean power for trapezoid pressure signals - as calculated via the resonator - is found as:

$$\bar{\bar{\mathcal{P}}}_{mr}(\sigma) = \hat{\bar{\mathcal{P}}}_{mr}(\sigma)\,\bar{\bar{p}}_a^2 = \frac{\bar{\bar{p}}_a^2}{\tau}\int_{-\tau/2}^{\tau/2} \mathscr{F}^{-1}\left(\frac{\mathscr{F}(\hat{\bar{p}}(\sigma,t))}{|\bar{\bar{Z}}_t|_{max}}\right)\hat{\bar{p}}(\sigma,t)\,dt \tag{17}$$

For geometrical parameters corresponding to the tube resonator used throughout this thesis (see subsection 3.3.1), the numerical calculation of the normalised mean power $\hat{\bar{\mathcal{P}}}_{mr}(\sigma)$ is obtained for $\frac{\sigma}{\tau} \in [0,1]$, which is presented in figure 18.

As can be seen in that figure, a first order approximation of this curve can be obtained by a linear regression, so that:

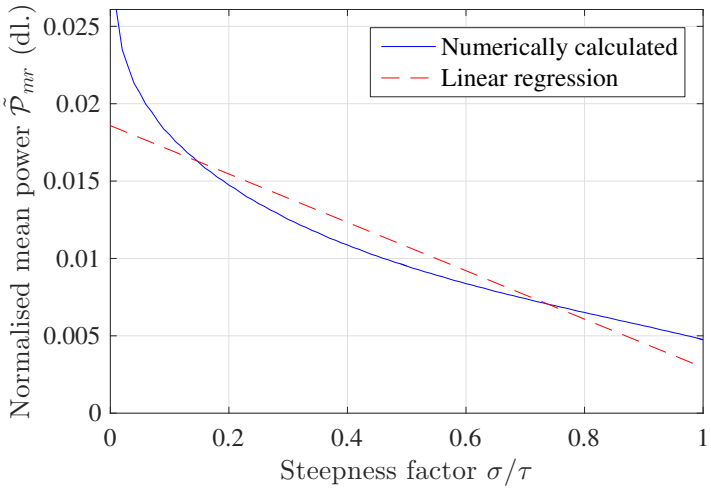

Figure 18: Normalised mean cyclic power dissipated in a tube resonator for a trapezoidal pressure wave, as a function of the trapezoid flank steepness factor $\frac{\sigma}{\tau}$. The solid curve shows the numerical calculation for a harmonic resonator without frequency independent losses, whose maximum impedance peaks are indicated by $|\bar{\bar{Z}}_t|_{max}$. The dashed curve shows a numerical linear regression.

$$\hat{\bar{\bar{\mathcal{P}}}}_{mr}(\sigma) \approx k_0 + k_1 \frac{\sigma}{\tau}, \tag{18}$$

introducing the regression constants k_0 and k_1, which can be found numerically (for the used resonator $k_0 = 0.0186$ and $k_1 = -0.0156$). This crude approximation is sufficient for the purpose of the approximate steepness estimation (which has been confirmed by numerical comparison); very low steepness factors have an increased error, but they are unlikely to occur in practice. The first order expression enables the rearrangement of the power comparison equation so that the estimated steepness factor can be revealed, as will be shown in the next section.

MATCHING THE POWER CALCULATIONS Since the mean powers, calculated with the excitation model and with the resonator, are equal during the steady state regime (i.e. $\bar{\bar{\mathcal{P}}}_{me} = \bar{\bar{\mathcal{P}}}_{mr}$), equations (14) and (18) can be combined:

$$\frac{\sigma}{\tau}\frac{1}{2}\int_{-1}^{1} \hat{\bar{q}}(\hat{p})\hat{p}\, d\hat{p} \approx k_0 + k_1 \frac{\sigma}{\tau}. \tag{19}$$

Hence, after rearrangement, the steepness factor of the trapezoidal wave shape for a given excitation curve can be found as:

$$\frac{\sigma}{\tau} \approx \frac{k_0}{\frac{1}{2}\int_{-1}^{1} \hat{\bar{q}}(\hat{\bar{p}})\hat{\bar{p}}\, d\hat{\bar{p}} - k_1}. \tag{20}$$

Finally, it is possible to relate the steepness factor to the RMS of the normalised pressure. Given that a pure normalised square wave (i.e. for $\frac{\sigma}{\tau} = 0$) has an RMS pressure value of 1, and a triangular normalised wave (i.e. for $\frac{\sigma}{\tau} = 1$) has $\hat{\bar{p}}_{\mathrm{RMS}} = \frac{1}{\sqrt{3}}$, the RMS value as a function of $\frac{\sigma}{\tau}$ can be found as:

$$\hat{\bar{p}}_{\mathrm{RMS}} = 1 - \frac{\sigma}{\tau}\frac{\sqrt{3}-1}{\sqrt{3}}. \tag{21}$$

In conclusion, the following theorem can be formulated:

Theorem 4. *Spectral richness vs. normalised power. To a good approximation, the normalised RMS pressure of the resulting trapezoidal-shaped pressure wave, which indicate the spectral richness, is linearly related to the normalised power calculation over the domain of the excitation curve, which can be directly estimated via a graphical method using a negative and positive gradient under the hypothetical excitation curve, or it can be numerically obtained using that curve.*

For the parameter values $\gamma = 0.8$ and $\zeta = 0.2$, used in figure 17, the results are $\frac{\sigma}{\tau} = 0.66$ and $\hat{\bar{p}}_{\mathrm{RMS}} = 0.72$. This theory can also be applied to other excitation models, which is further developed in chapter 4. For all excitation models, the evaluation for a wide range of parameter values and a comparison with experiments is discussed in chapter 5.

EVEN HARMONICS CONTRIBUTION It can be noted that, due to the absence of even harmonics in the trapezoidal pressure signal, the power calculation only relies on the odd flow rate component. While the even harmonics do not dissipate any power in the hypothetical instrument, $\bar{\tilde{q}}$ does produce even harmonics, which contribute to the radiated pressure. Therefore, the RMS amplitude of these even harmonics can serve as a measure of this feature. This

amplitude, for consistency also normalised by the pressure amplitude $\bar{\tilde{p}}_a$, is given by:

$$\hat{\tilde{q}}_{eRMS} = \sqrt{\frac{1}{\tau}\int_{-\tau/2}^{\tau/2} (\hat{\tilde{q}}_{ec}(t))^2\, dt}, \tag{22}$$

where $\hat{\tilde{q}}_{ec}(t) = \left(\bar{\tilde{q}}_e(t) - < \bar{\tilde{q}} >\right) / \bar{\tilde{p}}_a$ and $< \bar{\tilde{q}} >$ is the mean flow, which is not audible and therefore it is excluded from the even harmonics RMS calculation. The mean flow can be calculated by summing the weighted mean values of $\bar{\tilde{q}}_e$ during the flank and during the time the pressure is at its extremum: $< \bar{\tilde{q}} >= \frac{\sigma}{\tau} < \bar{\tilde{q}}_e\left(\right] - \bar{\tilde{p}}_a, \bar{\tilde{p}}_a[\right) > + (1 - \frac{\sigma}{\tau})\bar{\tilde{q}}_e(\bar{\tilde{p}}_a)$.

Unlike the mean power, the even RMS calculation at the pressure extrema doesn't cancel itself out, so that the formula cannot be reduced to the $[-\frac{\sigma}{4}, \frac{\sigma}{4}]$ domain, which also applies to the mean flow calculation. However, as the pressure signal is already known (after matching the mean powers), $\bar{\tilde{q}}_e$ can be directly calculated using eq. (10). For example, for the parameter values used in figure 17, the determined factor $\frac{\sigma}{\tau} = 0.66$ enables calculation of the mean flow and $\hat{\tilde{q}}_{ec}(\hat{\tilde{p}} = [-1, 1])$, which is plotted out in solid black in figure 17, while the extrema $\hat{\tilde{q}}_{ec}(\hat{\tilde{p}} = -1) = \hat{\tilde{q}}_{ec}(\hat{\tilde{p}} = 1)$ are indicated with black crosses.

Finally, the RMS of the even flow component can be calculated by:

$$\hat{\tilde{q}}_{eRMS} = \sqrt{\frac{\sigma}{\tau}\left(\frac{1}{2}\int_{-1}^{1} (\hat{\tilde{q}}_{ec}(\hat{\tilde{p}}))^2 d\hat{\tilde{p}}\right) + (1 - \frac{\sigma}{\tau})\,(\hat{\tilde{q}}_{ec}(1))^2}, \tag{23}$$

Thus, for the estimation using the graphical representation, the following theorem can be used:

Theorem 5. *Presence of even harmonics. The estimation of the even component's RMS pressure can be carried out in three steps:*

1) The mean flow $< \bar{\tilde{q}} >$ is found using the steepness factor $\frac{\sigma}{\tau}$.

2) $\hat{\tilde{q}}_{ec}$, the normalised even characteristic function component minus the mean flow is drawn out.

3) The even RMS pressure is the square root of the weighted sum of the mean squares of $\hat{\tilde{q}}_{ec}([-1, 1])$ and the mean square of a constant flow $\hat{\tilde{q}}_{ec}(1)$ (the values found at each

of the extremities of $\hat{\tilde{q}}_{ec}$); the former is weighted by the fraction $\frac{\sigma}{\tau}$, and the latter by the fraction $(1 - \frac{\sigma}{\tau})$.

For the parameter values used in the figure, the result is $\hat{\tilde{q}}_{\text{eRMS}} = 0.0092$. This is a very low amplitude, due to the fact that the amount of symmetry of the characteristic curve is particularly low for this excitation parameters. It is shown in chapter 4 that much higher even harmonics RMS values are obtained with other parameters and other excitation models.

Fundamental frequency

While constant excitation parameters result in a sound with a fixed playing frequency, the resonator's inharmonic modal distribution together with the variation of the mouthpiece pressure spectrum causes the oscillation frequency to diverge (see for instance (Coyle et al., 2014)). Given that the greatest instability is obtained at the resonant peaks, the higher harmonics tend to pull the frequency in the direction of the nearby resonant peak. Therefore, a richer spectrum, containing stronger higher harmonics, will either cause a frequency up- or down-shift for respectively a positive or negative inharmonic resonator.

On the other hand, dynamical excitation models also can influence the oscillation frequency substantially. A rough idea of the order of divergence can be obtained by noting the amount of phase lag introduced by the excitation's dynamics around this frequency. Adding this to the phase of the resonator, a new zero-crossing phase can be found, which reveals the fundamental frequency near the oscillation threshold with this excitation.

It should be mentioned that, the change in fundamental frequency alters the spectrum in turn, so that an equilibrium is sought during transient oscillation states. However, such a refined timbre study exceeds the scope of this dissertation.

2.4 A MODAL CYLINDRICAL DUCT MODEL

The previously discussed cylindrical resonator model is useful for explaining the basic functioning of the clarinet in the time domain, however far more precise models do exist. Although a theoretical resonator model is not strictly necessary for the implementation of a real hybrid instrument, this discussion is included to enable the impact of the coupling with the loudspeaker to be analysed (in subsection 3.2.2) and enable comparison of the sounds produced by a real hybrid instrument with "entirely simulated" sounds, i.e. where the resonator is also simulated (see subsection 5.1.3).

Here, only resonators whose entrance can be acoustically approximated as being "closed" (such as reed-instruments) and with a cylindrical bore and an open far end are considered (however, for most other resonators similar simplicity and properties can be obtained). Moreover, it is assumed that the resonator is a linear system; to a good approximation this is the case for the clarinet.

The analytically complete expression of the dimensionless bore impedance is written in the frequency domain as (see e.g. (Chaigne and Kergomard, 2013)):

$$\frac{Z(\omega)}{Z_c} = j \tan\left(\frac{\omega l}{c} - j\alpha(\omega)l\right), \tag{24}$$

where $s = j\omega = j2\pi f$ is the complex frequency (neglecting the real part), $\alpha(\omega)$ is a term that introduces all air propagation losses and $Z_c = \frac{\rho c}{S_t}$ is the characteristic impedance, with ρ the density of air, c the speed of sound and S_t the cross-sectional area of the duct.

It is worth noting that for $\omega = 0$, this expression goes to a minimum, which leads to the formulation of the following theorem, which will turn out to be of particular importance to the hybrid instrument:

Theorem 6. *Insignificance of the mean flow. For a closed-open cylindrical resonator, it may be assumed that* $Z(\omega = 0) \approx 0$[1]*, which explains that, to a good approximation, the influence of the mean flow on the self-sustained operation can be neglected.*

Moreover, for a homogeneous tube of this type with relatively widely spaced modes and with ends that approach the Neumann and Dirichlet conditions, each impedance peak can be described as a second order transfer function with real coefficients (Silva et al., 2008). The impedance can thus be written as a sum of these transfer functions:

$$\frac{Z_t(s)}{Z_c} \approx \sum_{n=1}^{N} \frac{a_n s}{\omega_n^2 + \frac{\omega_n}{Q_n} s + s^2}, \tag{25}$$

where $\{a_n, \omega_n, Q_n\}$ are the real modal coefficients (the amplitude, resonance frequency and quality factor of mode n). They can be deduced using a fitting method applied on either a measured input impedance (see appendix A) or on the analytical expression (24), assuming $\alpha(\omega)$ to be a slowly varying function of the frequency.

Hence, the pressure at the tube entrance can be decomposed into N components as follows : $p(t) = \sum_{n=1}^{N} p_n(t)$, where each p_n satisfies the following equation:

$$\frac{\mathrm{d}^2 p_n}{\mathrm{d}t^2} + \frac{\omega_n}{Q_n} \frac{\mathrm{d}p_n}{\mathrm{d}t} + \omega_n^2 p_n(t) = Z_c \, a_n \frac{\mathrm{d}q}{\mathrm{d}t}, \tag{26}$$

with $q(t)$ the temporal flow rate signal at the tube entrance.

This technique allows for a good approximation of a finite number of N modes of the measured impedance. Sufficiently high frequencies can be taken into account by choosing a great enough number of modes, and the calculation cost is relatively low. In subsection 5.1.3 the practical implementation and the choice for the number of modes is discussed further.

1 While this assumption is sufficiently valid for the current study, it should be said that the mean flow can introduce effects like convection, refraction in shear, coupling with vorticity, scattering by turbulence, and many others (Rienstra and Hirschberg, 2013).

2.5 SUMMARY

This chapter provided a theoretical understanding of the functioning of a clarinet and its excitation by arbitrary quasistatic models. It was shown that the resonator can be interpreted as a simple "delay" and the excitation mechanism as a nonlinear curve, which both relate up- and down-going pressure waves. The frequency independent losses of the resonator could be interpreted as a feature of a "hypothetical excitation curve". As such, a graphical "iterative map" demonstrated how the oscillation is established.

Also some aspects of other excitation models (quasistatic and dynamic) were briefly discussed.

Then, a theory relating the properties of a given nonlinear curve to the features of the generated sound was presented. This theory represents a helpful tool for the design of excitation models as a function of a desired sound output, which can be of use for computed sound generation as well as hybrid instruments where a theoretical excitation interacts with a real resonator.

It was shown that the amplitude of the oscillation can be determined by identifying the outer intersections of the nonlinear excitation curve with its $\tilde{\tilde{q}}$-axis mirrored curve. By focusing on the influence of excitation parameters, the amplitude appeared to be mainly controlled by the mouth pressure, for the case of the clarinet embouchure, while the "excitation amplitude" (mainly controlled by the lip force for the case of the single-reed embouchure) appeared to inversely relate to the the attack time.

For the study of spectral features, the remaining — frequency dependent — losses were taken into account. Remaining in the time domain, it was explained how those losses cause the excitation and the resonator to jointly converge to steady-state pressure and flow rate signals that match to both components. It was concluded that an increase in the "amount of nonlinearity" positively compensates for the rounding effect of the frequency dependent losses, pulling

the equilibrium back towards a block-shaped pressure wave case, i.e. towards a richer, brighter sound spectrum.

By then subdividing the excitation curve into an odd and even function, it was shown that the odd part, in combination with an odd harmonic resonator, is of importance to the oscillation condition and the brightness, while the even part gives an indication of the amount of even harmonics in the sound.

By assuming the pressure to be trapezoidal in shape, with a $\frac{\sigma}{\tau}$ flank steepness factor, the mean cyclic power during the steady state regime, as calculated for the case of the excitation model and for the case of the resonator could be matched. This resulted in an approximated expression, revealing a linear relation between $\hat{\bar{\mathcal{P}}}_{\mathrm{me}}/\frac{\sigma}{\tau}$, the fraction of the mean power generated during the pressure flank (which can be intuitively derived from a graphical presentation using a gradient), and the steepness factor $\frac{\sigma}{\tau}$. This factor turned out to be also linearly related to the normalised RMS pressure amplitude, which is related to the spectral richness.

The determined steepness factor then enabled the mean flow offset to be found, which in turn allowed determination of $\hat{\tilde{q}}_{\mathrm{ec}}$, the mean-flow excluded even component of the excitation curve, whose RMS amplitude can be estimated from a graphical representation.

Finally, a frequency-domain model of a cylindrical resonator was presented, providing theoretical expressions reserved for implementations in later chapters.

Part II

DESIGN OF THE HYBRID WIND INSTRUMENT

This part of the dissertation presents the entire design process of the hybrid wind instrument, consisting of a development chapter, a chapter where several excitation models are presented, a chapter where these models are evaluated with the hybrid instrument, a chapter on some further developments, and a discussion chapter.

3

DEVELOPING THE HYBRID WIND INSTRUMENT

This chapter describes the development of the coupled loudspeaker-tube system that forms the heart of the hybrid instrument; that is, the resonator, the microphone, the loudspeaker and a set of filters (implemented by the computing system) to account for the loudspeaker. The computing system also executes the excitation models, with more detail in the next chapter. The actual functionality of the hybrid instrument is discussed in the evaluation in chapter 5.

As stipulated by the requirements determined in subsection 1.4.3, the first aim is to obtain a situation close to an ideal hybrid instrument, i.e. where the transducers do not introduce any side-effects. Therefore, the chapter starts by describing the idealised hybrid instrument before then going on to address some of the practical constraints associated with a real hybrid instrument. In section 3.2, the theory underpinning the loudspeaker and resonator components is studied and loudspeaker-compensating filters are derived. Next, in section 3.3, the practical implementation of the hybrid wind instrument developed during this study is discussed.

Another way to view this development is to see it as the design of an electro-acoustic "transformer" between a computed excitation and an acoustic resonator. If the instrument were able to function in an "ideal" way, the ratio of the Fourier transform of the pressure signal measured by the computing system and the Fourier transform of the calculated flow rate signal sent towards the resonator, would exactly match the entrance impedance of the acoustic resonator. It should be noted that these pressure and flow-rate signals are measured synchronously, which implies that the "computed impedance" exists in real-time. The coupled loudspeaker-tube system could be interpreted as a "hybrid

resonator", or a "hybrid impedance". However, these expressions are somewhat ambiguous so won't be used.

3.1 IDEAL AND REAL HYBRID WIND INSTRUMENTS

3.1.1 *Ideal hybrid wind instrument*

In order to provide a better understanding of how a hybrid wind instrument can be developed, first an idealised situation is described in which the actuator is considered to be a rigid massless moving piston placed at the entrance of the tube. The massless property ensures that the piston velocity is not affected by inertia so that it moves proportionally with the electrical input signal. Meanwhile, the rigid property ensures that this occurs regardless of the surrounding acoustic situation, i.e. the piston presents an infinite acoustic impedance to its surroundings.

In the same regard, the microphone is assumed to be an ideal transducer, outputting an electrical signal that is directly proportional to the pressure, while the acoustic situation is invariant to its presence.

Finally, the computing system is assumed to be a delay-less system, which also provides perfect proportionality between the (input and output) voltages and the corresponding theoretical pressure and flow rate signals that are calculated on it.

If such "ideal" components could be used, the resonator would preserve its acoustic entrance impedance and the real pressure and flow rate at the resonator entrance would exactly match the theoretical pressure and flow rate signals used by the embouchure model on the computer. Hence, the entire set-up would operate as an "ideal hybrid wind instrument".

3.1.2 *Real hybrid wind instrument*

Moving on to study the use of real transducers and a real computer, there are a number of important implications to be considered. In the remainder of this section, these implications and the actions taken to resolve them are briefly described. Section 3.2 then considers the issues in more detail before section 3.3 moves on to discuss the particular configuration of hybrid instrument that has been designed for use in this study.

While a microphone operates almost like an ideal pressure sensor, a loudspeaker is far more distinct from an ideal actuator. Its suspended membrane can be described as a dynamic, mass-spring-damper system, excited by an electrodynamic voice-coil, which in its turn, is connected to a power amplifier. As such, the loudspeaker is not massless, and its dynamics cause the input-to-output response to be filtered. In order to correct for this and to create a flat frequency response like the ideal piston, it is possible to place a preceding "inverse filter" before the loudspeaker (this inverse filter is based on a theoretical model of the loudspeaker).

In addition, the loudspeaker diaphragm is not infinitely stiff, and therefore doesn't present a rigid termination to the tube. In other words, the loudspeaker is in an acousto-mechanically coupled interaction with the tube. Following Newton's third law, the action force on the loudspeaker diaphragm due to the pressure in front of it can be compensated for by using a simple proportional gain feedback controller, to instruct the voice coil to generate an opposite reaction force. Altogether, this makes the membrane robust to external pressure variations.

Figure 19 shows a block diagram explaining the functioning of a real hybrid instrument in terms of transfer functions. This diagram is referred to throughout this chapter (to help with the signposting, the bracketed numbers on the diagram correspond to different subsections both within this chapter and the thesis more generally).

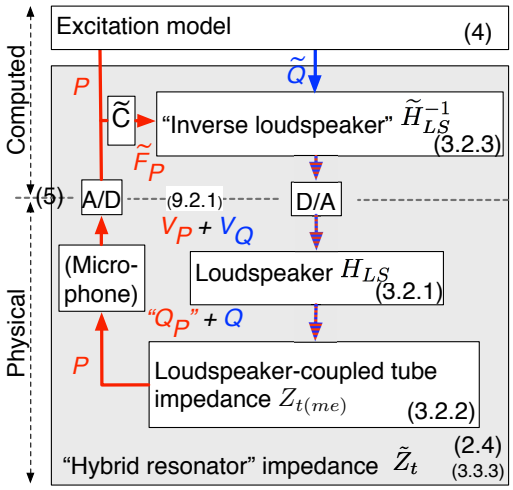

Figure 19: Block diagram of the hybrid instrument's computed and physical parts. The bracketed numbers correspond to different (sub)sections and chapters within the thesis.

For consistency, all signals and systems are expressed in the frequency domain in this diagram (hence their notation in capital letters).

The "physical" part that makes up the lower half of the diagram contains the transfer functions of the real physical components: the loudspeaker transfer function H_{LS} and the (loudspeaker-coupled) tube impedance $Z_{\text{t(me)}}$.[1] The "computed" part that comprises the upper half of the diagram contains two filters to cancel the loudspeaker's presence: a feedback controller $\widetilde{C}$ and a feedforward controller, represented by an "inverse loudspeaker transfer function" $\widetilde{H}_{\text{LS}}^{-1}$. The inclusion of a tilde sign for some of the transfer functions in the block diagram indicates that they are "estimated", having been derived from theory using measured parameters. This also applies to some of the signals included in the block diagram.

Stepping through the block diagram, the operation of the hybrid instrument is as follows. A flow rate $\widetilde{Q}$ (generated by the mouthpiece model) is sent to the "inverse loudspeaker" transfer function. The output is then sent through a

1 In the notation employed in this dissertation, the subscript of the impedance Z can refer to the acoustic tube (by t) and the mechanical and electrical loudspeaker components (by respectively m and e). For coupled impedances, the leading symbol of the subscript indicates the type of impedance, while the subscripts entered between brackets indicate the elements it is coupled to. For instance, $Z_{\text{t(me)}}$ is an acoustic tube impedance for the case of a tube coupled to a loudspeaker, taking into account both the loudspeaker's mechanical and electrical components.

digital-to-analogue converter (D/A) (see section B.2). This results in V_Q, a component of the total voltage signal that is provided to the loudspeaker. The latter, in response, generates a flow rate Q which is applied to the tube-resonator. In turn, the resonator reacts with a pressure P at its entrance. This pressure is captured by a microphone and acquired by the computer via an analogue-to-digital converter (A/D). The feedback controller $\widetilde{C}$ uses this signal to generate a feedback force signal $\widetilde{F}_P$, which results in an additional voltage V_P being provided to the loudspeaker. This component of the total voltage signal ensures that the signal produced by the loudspeaker compensates for the acoustical coupling with the tube (see 3.2.3).

It should be noted that the coupling is interpreted in terms of an altered tube impedance, as this allows the impact on the original tube impedance to be studied. However, this is not a physically realistic representation (in reality the loudspeaker's response is affected by the coupling); hence, the feedback flow rate Q_P is only a theoretical concept.

As the feedback filter compensates for the coupling, when combined with the coupled impedance $Z_{t(me)}$, an approximation of Z_t is obtained. Meanwhile, the feedforward filter $\widetilde{H}_{LS}^{-1}$ corrects for the loudspeaker response H_{LS}, so that all together an uncoupled (or, "hybrid") tube impedance $\widetilde{Z}_t$ is obtained (represented by the large grey coloured frame in the block diagram). This impedance can also be understood in terms of the ratio of the measured pressure P over the calculated flow rate $\widetilde{Q}$. It is then available for interaction with an excitation model, such as the model of a wind instrument embouchure, so that hybrid self-sustained sounds can be produced.

3.2 LOUDSPEAKER-RESONATOR SYSTEM AND FILTERS

This section provides detailed theoretical descriptions of the loudspeaker, the interaction with the resonator in the form of a coupled system (as represented in figure 20, explained later) and the design of filters to compensate for

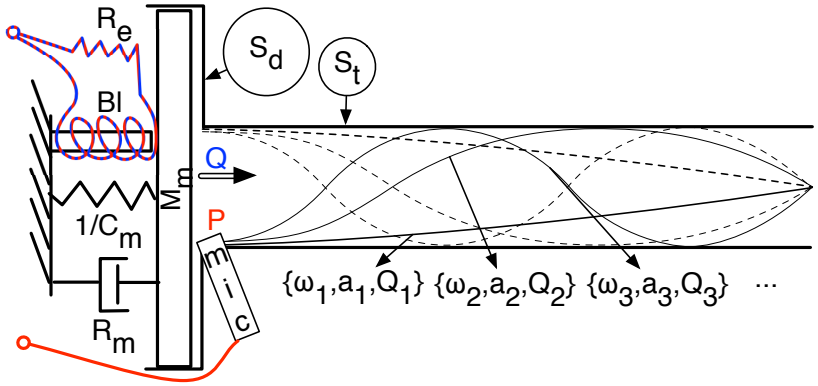

Figure 20: Schematic of the assembled loudspeaker and tube models. The variables R_e, Bl, C_m, R_m and M_m refer to loudspeaker parameters. S_d and S_t refer to respectively the loudspeaker diaphragm area and the tube cross-sectional area.

the loudspeaker. The discussions are spread over three subsections, which also relate to the components of the block diagram in figure 19.

In the theoretical development, the sound is assumed to propagate in the form of plane waves, which is valid as long as the wavelength is much greater than the cross-sectional diameter of the tube and loudspeaker (Hirschberg, 1995). Also, provided that the volume between the loudspeaker diaphragm and the tube is small, the change in cross-sectional area between the loudspeaker (with diaphragm area S_d) and the tube (with area S_t) is assumed to have negligible influence on both the "volume flow rate" Q and the pressure P, so that they can be considered as equal in and between both places.

Throughout what follows, time domain signals are denoted in lower case. Frequency domain signals, denoted in upper case, are expressed in the complex s-plane (for continuous time) by using the Laplace Transform with imaginary argument, with $s = j\omega$, $\omega = 2\pi f$ and f the frequency in Hz. Discrete spectra are expressed in the z-plane by applying the Z-transform with $z = e^{sT}$, with T the sample time. However, for simplicity the s and z function arguments are not repeated after the introduction of a variable.

3.2.1 *The loudspeaker*

Several existing loudspeaker driver designs and technologies have been considered, including piezoelectric, magnetostatic, magnetostrictive electrostatic, ribbon, bending wave, distributed mode, and plasma arc loudspeakers. However, considering the purpose of the hybrid instrument, all of these technologies fall short in comparison with traditional dynamic "moving cone" loudspeakers. They either feature a nonlinear frequency or dynamic response, or they are not suitable due to their physical dimensions or acousto-mechanical impedance of the diaphragm. Therefore, in what follows, only the driver design of dynamic loudspeakers is considered.

To be able to employ a dynamic loudspeaker as the "flow generating" device in a hybrid instrument, it is important to have a detailed understanding of its behaviour in terms of its input-to-output response. The classical small-signal model that was initially proposed by Small is adopted (Small, 1972). To aid understanding, and as typically used in loudspeaker theory (Beranek, 1954) (and also often in mechanics and acoustics (Pierce, 1989)), this model can be represented using the analogous electronic circuit theory to obtain an equivalent circuit as depicted in figure 21. While the left part of this circuit corresponds to a model of the real electric circuit of the loudspeaker, the right part is a circuit that functions analogously to the mechanical components of the loudspeaker. The voltages in this circuit (indicated as orange-coloured variables in the top part of the diagram) represent either real electric voltages (V and V_{m}) or mechanical forces (F and F_{P}). Similarly, the currents in the circuit (indicated by the arrows in the bottom part of the diagram) are related to the real electric current in the voice coil (I) or to the mechanical velocity of the loudspeaker membrane ($\dot{X}$).

The equivalent circuit includes an electrical part with R_{e}, the DC resistance of the voice coil, with voltage $V(s)$ at the input (the voice coil inductance is not taken into account here, as empirical findings showed that it is of negligible im-

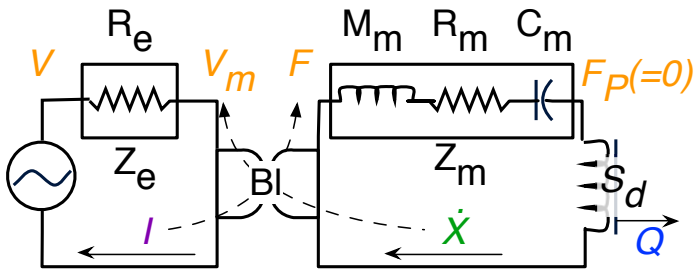

Figure 21: Equivalent electronic circuit representing the loudspeaker's electronic part (the impedance Z_e on the left, consisting of a resistive component R_e) and its mechanical part (the impedance Z_m on the right, consisting of inertia M_m, resistive R_m and compliance C_m components).

portance in our study). It also includes a mechanical part which is modelled by a 1-DOF mass-spring-damper system (with the Thiele/Small electromechanical parameters M_m, C_m and R_m respectively the mass, inverse spring stiffness and damping coefficient), and receives a force $F(s)$ from the voice-coil. The electrical and mechanical parts are coupled by the electro-mechanical functioning of the voice coil so that the force generated by the current $I(s)$ in the coil is $F = Bl\ I$ (with Bl, the voice-coil's "force factor") and the velocity $\dot{X}(s)$ of the coil results in a feedback voltage $V_m(s) = Bl\ \dot{X}$. The configuration for the electrical and mechanical impedances chosen here, requires the coupling to be modelled by a "transconductance transformer", which transforms voltages into currents and vice versa, in both directions multiplying by the force-factor Bl. It should be noted that the amplifier can be considered as a close-to-ideal voltage source and that its output impedance is virtually zero.

The uncoupled electrical and mechanical impedances can be obtained by applying Ohm's law and Kirchhoff's circuit laws to give:

$$Z_e(s) = \frac{V - V_m}{I} = R_e \tag{27}$$

and:

$$Z_{\mathrm{m}}(s) = \frac{F}{\dot{X}} = \frac{C_{\mathrm{m}}^{-1} + R_{\mathrm{m}}\, s + M_{\mathrm{m}}\, s^2}{s} = \frac{M_{\mathrm{m}}(\omega_{\mathrm{LS}}^2 + \frac{\omega_{\mathrm{LS}}}{Q_{\mathrm{m}}}\, s + s^2)}{s}, \tag{28}$$

with $\omega_{\mathrm{LS}} = \sqrt{M_{\mathrm{m}}^{-1}\, C_{\mathrm{m}}^{-1}}$ the speaker's resonance frequency and $Q_{\mathrm{m}} = \frac{1}{R_{\mathrm{m}}} \sqrt{\frac{M_{\mathrm{m}}}{C_{\mathrm{m}}}}$, its Q- (quality) factor.

By defining a virtual force signal $F_{\mathrm{e}}(s)$ as the sum of the real mechanical force with the force generated from the coupling with the electrical part: $F_{\mathrm{e}} = F + Bl\ V_{\mathrm{m}}/Z_{\mathrm{e}} = Bl\ V/Z_{\mathrm{e}}$, a coupled mechanical impedance can be derived, which takes into consideration the interaction between both parts (Small, 1972):

$$Z_{\mathrm{m(e)}}(s) = \frac{F_{\mathrm{e}}}{\dot{X}} = Z_{\mathrm{m}} + \frac{(Bl)^2}{Z_{\mathrm{e}}}. \tag{29}$$

It can be verified that, in terms of the loudspeaker parameter values, the coupling only has a significant effect on the Q-factor of the system (Small, 1972). Therefore, this equation can be simplified:

$$Z_{\widetilde{\mathrm{m(e)}}}(s) = \frac{M_{\mathrm{m}}(\omega_{\mathrm{LS}}^2 + \frac{\omega_{\mathrm{LS}}}{Q_{\mathrm{ts}}}\, s + s^2)}{s}, \tag{30}$$

with $Q_{\mathrm{ts}} = \frac{\sqrt{M_{\mathrm{m}}/C_{\mathrm{m}}}}{R_{\mathrm{ts}}(R_{\mathrm{m}},R_{\mathrm{e}})}$ the coupled or "total" quality factor and R_{ts} the total damping coefficient.

Using equations (27) to (30) and the transformer relationships, the complete loudspeaker system can then be represented by an overall transfer function that expresses the volume flow rate per input voltage:

$$H_{\mathrm{LS}}(s) = \frac{Q(s)}{V(s)} = \frac{Bl}{Z_{\mathrm{e}}} \frac{S_{\mathrm{d}}}{Z_{\widetilde{\mathrm{m(e)}}}}, \tag{31}$$

where $Q(s) = S_{\mathrm{d}}\ \dot{X}$ is the volume flow rate generated by the loudspeaker.

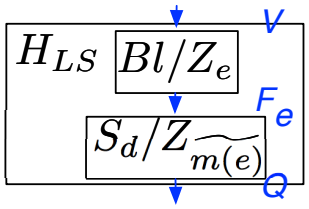

Figure 22: Block diagram of the loudspeaker's transfer function H_{LS}, consisting of the electrical part Bl/Z_{e} and the (electrical-coupled) mechanical part $S_{\mathrm{d}}/Z_{\widetilde{\mathrm{m(e)}}}$.

The total loudspeaker transfer function H_{LS} as represented in the block diagram in figure 19 can thus be decomposed into Bl/Z_{e} and $S_{\mathrm{d}}/Z_{\widetilde{\mathrm{m(e)}}}$ (see figure 22).

3.2.2 *Coupled loudspeaker and resonator*

When mounting the loudspeaker on a tube, a coupled system is formed. This coupled system comprises the resonances of both the loudspeaker and the tube, but altered in frequency and amplitude, particularly where their respective resonance frequencies lie close to each other. In this subsection the modelling of this coupling is investigated, contributing to the choice of suitable components for a practical implementation of a hybrid instrument.

To model a loudspeaker that is coupled to a tube, the analogous loudspeaker circuit of figure 21 can be simply combined with an analogous circuit for the tube based on the modal decomposition of its entrance impedance (the latter is detailed in section 2.4), which results in the circuit represented in figure 23.

Note that figure 23 uses the simplified representation of the loudspeaker mechanics (see equation (30)), where the coupling with the electrical part is fully integrated in the R_{ts} damping coefficient i.e. in the Q_{ts} factor.

Following the analogy of voltage representing pressure, the coupling between the loudspeaker and the tube is represented by a transformer, relating the force $F_{\mathrm{P}}(s)$ and velocity $\dot{X}(s)$ of the loudspeaker membrane respectively to the pressure $P(s)$ and the flow rate $Q(s)$ at the instrument entrance by: $F_{\mathrm{P}} = S_{\mathrm{d}}\ P$ and $\dot{X}\ S_{\mathrm{d}} = Q$.

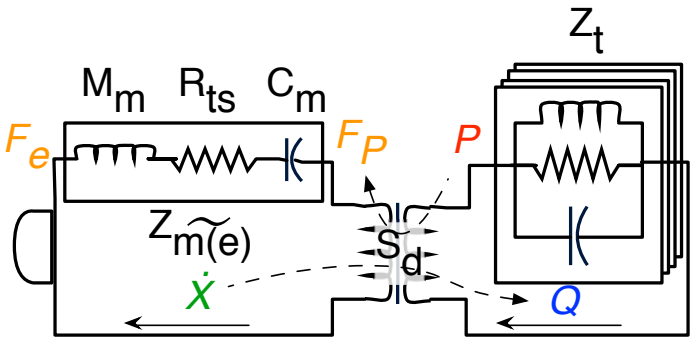

Figure 23: Equivalent electronic circuit representing the loudspeaker's mechanical part (including its coupling with the electronic part) coupled with the modal tube impedance.

INTERPRETING THE COUPLING AS AN ALTERED TUBE IMPEDANCE A convenient representation to enable the impact of the coupling on the loudspeaker-tube's resonance frequencies and amplitudes to be studied, is to interpret the coupling as an altered tube impedance. The transformer in figure 23 makes the left side of the figure appear as a parallel circuit of S_d^2 times lower impedance to the right side of the figure. Hence, the loudspeaker-coupled tube impedance can be calculated by:

$$Z_{\mathrm{t(me)}}(s) = \left(\frac{1}{Z_\mathrm{t}} + \frac{S_\mathrm{d}^2}{Z_{\widetilde{\mathrm{m(e)}}}} \right)^{-1}, \tag{32}$$

which is represented in the global block diagram in figure 19.

If the tube modes are relatively widely spaced in frequency, the coupling with the loudspeaker may be assumed independent for each mode n. This assumption is only valid when the frequency separation between the coupled and uncoupled modes is small. The new coupled resonance frequency $\omega_{n(\mathrm{me})}$ for mode n is found from the roots of the imaginary part of $Z_{\mathrm{t(me)}}$. Considering equations (32), (30) and (25) for a single mode, it can be shown that this results in:

$$-(\omega_n^2 + s^2)(\omega_{\mathrm{LS}}^2 + s^2) = \omega_{cn}^2\, s^2, \tag{33}$$

with $\omega_{cn} = \sqrt{\frac{Z_c S_d^2 a_n}{M_m}}$, the "coupling frequency" (note that the variation between the a_n is small). First this expression can be interpreted as a second order function of (s^2). Then, the loudspeaker-coupled tube mode's resonance frequency $j\omega_{n(me)}$ is found as one of the solutions for s.

For the case where the loudspeaker resonance frequency is far below the tube resonances (i.e. $\omega_{LS} \ll \omega_n$), the solution reduces to:

$$\omega_{n(me)} = \omega_n \sqrt{1 + \frac{\omega_{cn}^2}{\omega_n^2}}, \tag{34}$$

which shows that the strongest coupling occurs for the first mode.

To study the change in amplitude, a similar development can be followed. At $s = j\,\omega_{n(me)}$, the magnitude of the coupled tube impedance can also be derived from eq. (32):

$$\mid Z_{t(me)} \mid = \Re\left(Z_{t(me)}\right) = \frac{1}{\Re\left(\frac{1}{Z_t}\right) + \Re\left(\frac{S_d^2}{Z_{\widetilde{m(e)}}}\right)}. \tag{35}$$

By dropping the zero order term of $Z_{\widetilde{m(e)}}$ and applying basic complex theory, a simplified expression can be found for $Z_{t(me)}(s = j\,\omega_{n(me)})$ from which a loudspeaker-coupled Q-factor can be derived:

$$\frac{1}{\widetilde{Q}_{n(me)}} = \frac{1}{Q_n}\left(1 + \frac{\omega_{cn}^2 \omega_{LS} Q_n}{\omega_{n(me)}^2 \omega_n Q_{ts}}\right). \tag{36}$$

Here, ω_{cn} has a significantly stronger influence than for the amplitude.

Hence, given that the coupling frequency ω_{cn} is proportional to the the diaphragm area S_d and inversely proportional to the square root of M_m, it can be concluded that, for a real hybrid instrument, the choice of a small diaphragm loudspeaker with a heavy membrane would ensure a low coupling with the tube, which is a desirable initial situation. This is important, because, as will be formulated in the next subsection, even though the coupling can be compensated for by electronic means, the size of the deviations caused by approx-

imation errors in the real system will be higher the more the initial coupled system differs from the targeted "uncoupled" system.

In a similar manner, it can be shown that for the case where the loudspeaker resonance frequency is close to or above the first tube resonance, there is a high risk of a strong coupling with one of the resonator modes. Given that the resonance frequencies of a wind instrument can be located at virtually any frequency above the fundamental frequency of the lowest note, this situation should be avoided.

INTERPRETING THE COUPLING AS ALTERED ELECTRIC OR MECHANICAL IMPEDANCES Later, the coupled loudspeaker-tube model will be used to obtain the loudspeaker parameters with measured data (see section A.4). In order to derive useful expressions that are compatible with those measurements, the coupling can also be interpreted as an altered electrical loudspeaker input impedance, which can be obtained from the signals in the circuit in figure 21:

$$Z_{\mathrm{e(mt)}}(s) = \frac{V}{I} = \frac{Z_\mathrm{e}\, V}{V - V_\mathrm{m}} = \frac{Z_\mathrm{e}\, V}{V - Bl\, \dot{X}}. \tag{37}$$

Similarly, considering both circuits in figures 21 and 23, the coupled mechanical impedance can be written as:

$$\begin{aligned} Z_{\mathrm{m(et)}}(s) &= Z_{\widetilde{\mathrm{m(e)}}} + S_\mathrm{d}^2\, Z_\mathrm{t} = Z_{\widetilde{\mathrm{m(e)}}} + S_\mathrm{d}\, \frac{P}{\dot{X}} \\ &= \frac{F_\mathrm{e} - F_\mathrm{P}}{\dot{X}} + S_\mathrm{d}\, \frac{P}{\dot{X}} = \frac{F_\mathrm{e}}{\dot{X}} = \frac{V\, Bl}{Z_\mathrm{e}\, \dot{X}}. \end{aligned} \tag{38}$$

3.2.3 *Compensating for the loudspeaker*

In order for the functioning of a real hybrid instrument to approach that of the idealised situation, the air flow Q acoustically reproduced by the loudspeaker should be as close as possible to the flow rate signal $\widetilde{Q}$ calculated by the mouthpiece model. Therefore, two filters are required: one to flatten the loudspeaker

response and another to compensate for the coupling with the tube. These filters are executed by a real-time computing system, whose analogue-to-digital (A/D) and digital-to-analogue (D/A) converters are assumed to be free of any aliasing and quantisation errors and whose response (including the latency) is represented by $H_{\text{cptr}}(z)$. It is further assumed that the responses of the chosen microphone and amplifier (required to power the loudspeaker) are flat, so that they don't have to be taken into account in this study.

Correcting for the loudspeaker response

DESIGNING AN INVERSE LOUDSPEAKER FILTER An uncoupled system can be compensated for by placing its inverse transfer function as a feedforward filter, in front. This technique was for instance applied by Guérard to compensate for both an actuator and a resonator (Guérard, 1998). If the loudspeaker is not coupled with the tube, the feedforward filter to undo its response is simply the inverse of the loudspeaker transfer function (31):

$$H_{\text{LS}}^{-1}(s) = \frac{Z_{\text{e}}}{Bl} \frac{Z_{\widetilde{\text{m(e)}}}}{S_{\text{d}}}. \tag{39}$$

While the inverse of the electronic part of the loudspeaker's transfer function is simply $\frac{Z_{\text{e}}}{Bl} = \frac{R_{\text{e}}}{Bl}$, the mechanical part is not that easy to correct for and there are several reasons to opt for a loudspeaker that has a resonance frequency much lower than the tube resonance frequencies.

One reason is that the response around the loudspeaker's resonance frequency can be nonlinear in practice. Another reason, as demonstrated earlier for the situation where the loudspeaker is coupled to the tube, is that a heavier membrane minimises the coupling. Finally, this choice enables an inverse filter to be used, which has the additional advantage of allowing the mean flow component to be removed from the signal sent to the loudspeaker (as stipulated by theorem 6 in chapter 2, the ignorance of this flow component still allows for a coherent wind instrument simulation).

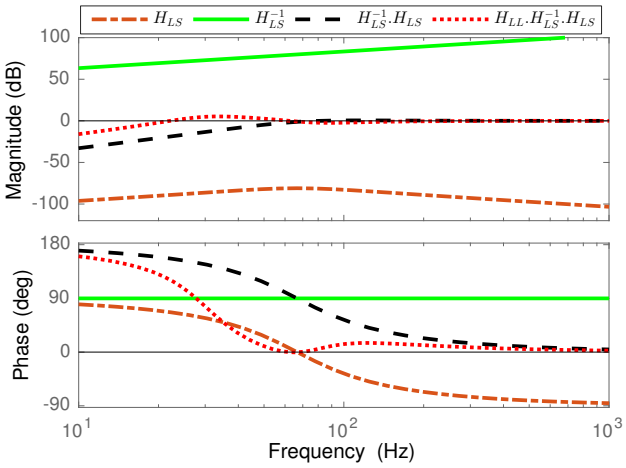

Figure 24: Transfer functions of the loudspeaker $H_{\mathrm{LS}}(s)$ (in dot-dashed brown), the approximate inverse filter H_{LS}^{-1} (in solid green), the combination of both (in dashed black) and combined with the additional "lead-lag compensator" H_{LL}.

This inverse filter can be derived in two steps. First, by considering eq. (30), at high frequencies the impedance approaches the inertia term, which is a pure derivative:

$$Z_{\widetilde{\mathrm{m(e)}}} \approx M_{\mathrm{m}}\, s, \;\; (\text{if } s \gg j\omega_{\mathrm{LS}}). \tag{40}$$

Figure 24 shows the transfer functions of an arbitrary loudspeaker $H_{\mathrm{LS}}(s)$ (in dot-dashed brown), its approximate inverse filter H_{LS}^{-1} (in solid green) given by equation (39), and the combination of both (in dashed black). It can be seen that the loudspeaker is compensated for at high frequencies, but near to the loudspeaker resonance frequency, the influence of the damping and the stiffness increases both the amplitude and phase. While these deviations may seem not substantial, the phase response introduces an inharmonicity to the resonance modes in this frequency region, which can significantly detune the lower notes produced with the hybrid instrument.

The addition of a filter H_{LL}, known as a "lead-lag compensator" (a filter to improve an undesirable frequency response in a feedback system) can compensate for this effect down to $s = 2\, j\omega_{\mathrm{LS}}$, so that:

$$Z_{\widetilde{\mathrm{m(e)}}} \approx H_{\mathrm{LL}}\; M_{\mathrm{m}}\, s, \;\; (\text{if } s \geq 2\, j\omega_{\mathrm{LS}}). \tag{41}$$

A desirable lead-lag filter response can be obtained using a biquadratic second order transfer function with complex poles and zeros (Messner et al., 2007):

$$H_{\mathrm{LL}} = \frac{s^2 + \frac{\omega_{\mathrm{LLn}}}{Q_{\mathrm{LL}}} s + \omega_{\mathrm{LLn}}^2}{s^2 + \frac{\omega_{\mathrm{LLd}}}{Q_{\mathrm{LL}}} s + \omega_{\mathrm{LLd}}^2}, \tag{42}$$

which provides the unique combination of zeros that decrease the amplitude and phase responses towards ω_{LS}, while the poles (situated at lower frequency) reset the gain from increasing to constant in the sub-ω_{LS} zone (and as such the removal of the mean-flow component is maintained). The numerator and denominator are modelled with resonance frequencies ω_{LLn} and ω_{LLd} and they share a common quality factor Q_{LL}, which is a convenient parametrisation that guarantees a converging curve regression to find optimal parameter values.

The transfer function of the combined system $H_{\mathrm{LL}}.M_{\mathrm{m}}s.H_{\mathrm{LS}}$ is also shown in figure 24 (in dotted red). It can be seen that mainly the phase response shows an improved compensation for the loudspeaker for $\omega \gtrsim \omega_{\mathrm{LS}}$, while the magnitude remains reasonably close to 0 dB.

DISCRETISATION AND IMPLEMENTATION For numerical simulation, the derivative term can be approximated by a discrete transfer function, using the "Euler backward method" (also known as the causal first order "Finite Difference Approximation"):

$$M_{\mathrm{m}}\, s \approx \frac{M_{\mathrm{m}}\, (z-1)}{T\, z}, \tag{43}$$

with T, the sample time. While this discretisation introduces an extra delay of half a sample, the scheme ensures a causal and stable implementation. The more advanced bilinear discretisation results in an infinite gain at the Nyquist frequency and, even though an additional pole, placed close to $-\infty$ can stabilise the filter, the gain at the Nyquist frequency remains high and can cause instabilities when the excitation model is included. Therefore, the Euler backward discretisation remains the best choice.

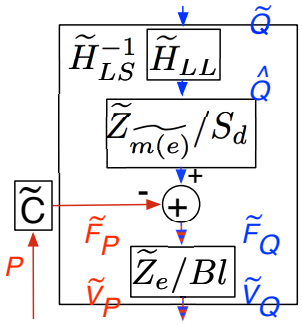

Figure 25: Block diagram of the transfer functions of the feedback filter $\widetilde{C}$ and the feedforward filter H_{LS}^{-1}, consisting of the approximated electrical part $\widetilde{Z}_{\mathrm{e}}/Bl$, the (electrical-coupled) mechanical part $\widetilde{Z}_{\widetilde{\mathrm{m(e)}}}/S_{\mathrm{d}}$ and the lead-lag filter $\widetilde{H}_{\mathrm{LL}}$.

The Euler backward scheme also results in a well-approximated digital equivalent of the lead-lag filter, given that its poles and zeros are small:

$$\widetilde{H}_{\mathrm{LL}}(z) = H_{\mathrm{LL}}(s \rightarrow \frac{z-1}{T\,z}). \tag{44}$$

Hence, the feedforward filter's transfer function, as represented in the block diagram in figure 19, can be written as:

$$\widetilde{H}_{\mathrm{LS}}^{-1}(z) = \widetilde{H}_{\mathrm{LL}} \frac{M_{\mathrm{m}}\,(z-1)}{S_{\mathrm{d}}\,T\,z} \frac{R_{\mathrm{e}}}{Bl}, \tag{45}$$

and its composition is depicted in figure 25.

Compensating for the loudspeaker-tube coupling

As mentioned earlier, the principle behind the feedback filter that compensates for the coupling between the loudspeaker and tube is very simple: in order to undo the force on the loudspeaker diaphragm due to the pressure in front of it ($F_{\mathrm{P}} = S_{\mathrm{d}}\,P$), it is necessary to generate an opposite force with the voice coil. As P is directly measured by the microphone and the voice coil force can be obtained by using $\frac{\widetilde{Z}_{\mathrm{e}}}{Bl}$, the ideal feedback controller (without taking into account the computing system's response) is simply $\widetilde{C} = -S_{\mathrm{d}}$.

This proportional controller solution can also be found by applying basic feedback control theory. The open-loop transfer function of the coupled loudspeaker-tube system, including the real-time computer, can be expressed as:

$$H_{\mathrm{c}}(z) = \frac{P}{\widetilde{F}_{\mathrm{P}}} = \frac{Z_{\mathrm{e}}}{Bl}\, H_{\mathrm{cptr}}(z)\; H_{\mathrm{LS}}(z)\; Z_{\mathrm{t(me)}}(z), \tag{46}$$

where the $H_{\mathrm{cptr}}(z)$ term represents the response of the real-time computing system, and the continuous time transfer function of the loudspeaker and the coupled tube impedance are expressed in the z-plane (using the relation $z = e^{sT}$).

The general expression of a closed loop response is:

$$\frac{H_{\mathrm{c}}}{1 + H_{\mathrm{c}}\, C} \tag{47}$$

where $C(z)$ is the transfer function of a controller, placed between the output and input of the open-loop.

Meanwhile, the transfer function of the desired uncoupled situation is defined by the concatenation of the uncoupled transfer functions of the computer, the loudspeaker, and the tube:

$$H_{\mathrm{u}}(z) = \frac{Z_{\mathrm{e}}}{Bl}\, H_{\mathrm{cptr}}(z)\; H_{\mathrm{LS}}(z)\; Z_{\mathrm{t}}(z), \tag{48}$$

For the design of a controller that will guarantee a closed loop expression that matches the uncoupled situation, equations (47) and (48) should be equal. After re-arrangement of that equality (using equation (46)) and applying some simplifications, the expression of the ideally required controller is found, which only depends on the computing system's transfer function and the loudspeaker membrane area:

$$C(z) = \frac{H_{\mathrm{c}} - H_{\mathrm{u}}}{H_{\mathrm{c}}\; H_{\mathrm{u}}} = H_{\mathrm{cptr}}(z)^{-1}(-S_{\mathrm{d}}). \tag{49}$$

However, this is a non-causal transfer function, as the computing system always contains delay. A causal version can be found by dropping the inverse response of $H_{\text{cptr}}(z)$:

$$\widetilde{C}(z) = -S_{\text{d}}. \tag{50}$$

Provided that the loudspeaker resonance frequency (where the coupling with the tube, and thus the filter's effect, is strong) falls far below the Nyquist frequency and that the computing system introduces minimal delay, the approximation is sufficiently valid. Nevertheless, it is important to mention that any approximation error can perturb the compensatory effect of the feedback filter, leading to an unstable situation. Hence, the stability of the closed loop is to be verified for a given loudspeaker-tube system.

The implementation of the control loop is depicted in the block diagrams in figures 19 and 25.

3.3 PRACTICAL DESIGN OF A HYBRID SET-UP

Sections 3.1 and 3.2 discussed a theoretical framework for a real hybrid instrument. In this section, the practical implementation of a prototype hybrid instrument is described. This prototype has been built to enable the hybrid wind principle to be studied in practice.

First, the different components of the prototype instrument are introduced, including a discussion on the choice of loudspeaker. Then measurements designed to characterise the system are presented.

3.3.1 *The resonator and associated hardware*

For the resonator of the prototype hybrid instrument, a cylindrical tube has been chosen with dimensions (length 58 cm, inner diameter 14.2 mm) that ap-

proximately match those of a soprano clarinet playing its lowest note. Its input impedance is obtained in section A.4 and further discussed in subsection 3.3.3.

A Cambridge Audio type A1 power amplifier and a B&K microphone type 4187 are used (for technical details see section A.1). The microphone is mounted at the entrance of the resonator, just in front of the loudspeaker diaphragm. As reported in section A.1, the responses of the amplifier and the microphone can be considered flat for the purpose of this study, the magnitude and phase deviations being much smaller than those that can be expected from the loudspeaker's response.

Details on the computing system used for the current prototype are given in subsection B.2.1. Its response is found to be reasonably flat and the total input-to-output latency is 25 µs.

3.3.2 *Choice of an optimal loudspeaker*

There are various criteria when it comes to identifying a loudspeaker suitable for use in a hybrid instrument.

Acoustic considerations

Considering the previously discussed theoretical models, $\widetilde{H}_{\mathrm{LS}}^{-1}$ tends towards H_{LS}^{-1} when ω_{LS} is much lower than the tube resonance frequencies. However, it should be noted that this scenario usually corresponds to a loudspeaker with a larger diaphragm or, by adding mass to the diaphragm, a reduction of the acoustic power, i.e. the sensitivity of the loudspeaker.

While the theory presented in section 3.2 implies that for any given loudspeaker, the loudspeaker-tube coupling can be undone by the feedback loop, there are reasons to opt for a weak physical coupling. If one considers an erroneous signal P_{err} that accompanies the pressure measurement, it will be manifested as a false surplus flow rate $Q_{\mathrm{err}} \approx P_{\mathrm{err}} \frac{S_{\mathrm{d}}^2}{M_{\mathrm{m}}\, s}$, which indicates that light and especially large diaphragms are a likely source of instability in practice.

Another reason for choosing S_d to be small, is that the inevitable additional acoustic volume between the diaphragm and the tube entrance will be smaller. In this way the total entrance impedance is closer to the independent tube impedance and the "plane wave assumption" is valid to higher frequencies.

Dynamic range

That said, the dynamic range of the system is determined by the power rating of the loudspeaker. More precisely, it is the RMS current through the loudspeaker coil that roughly indicates its temperature and therefore its maximum rating (Chapman, 1998) (the maximum diaphragm excursion also can be of importance at low frequencies). As the flow rate related signal and the signal related to the feedback filter produce electrical currents in the coil, they should both be taken into account when estimating the electrical power. Whereas the former is inversely related to S_d (specifically $I_{\widetilde{Q}} \approx \widetilde{Q}\ \frac{M_m\, s}{S_d\, Bl}$), the latter is proportional to S_d (specifically $I_P \approx P\ \frac{S_d}{Bl}$) and does not depend on the frequency. For optimal efficiency, these currents should be minimised by considering the loudspeaker parameters. However, this is not a straightforward procedure, as the correlation between the flow rate and pressure signals depends on the tube losses and the applied excitation model. An approximation can be obtained by stating that generally for a single-reed excitation $\mid Q\ Z_c \mid \approx \mid \zeta\ P \mid$ (see section 4.2), with $0.1 \lesssim \zeta \lesssim 0.4$ (Chaigne and Kergomard, 2013).

Choosing the loudspeaker

Given that there is no straightforward mathematical relationship between the loudspeaker properties of interest (the membrane size and mass, the general frequency response, the power rating and the sensitivity), it can be concluded that there is no systematic means of finding the most suitable loudspeaker. However, it is possible to obtain good indications for the choice by following the theoretically determined guidelines.

Interestingly, it seems that the most suitable configuration of loudspeaker is not available as an off-the-shelf product, as its design is not appropriate for a standard audio application. For instance, it would be desirable in our context to have a small-diaphragm loudspeaker (usually only available as low-power units) with a thick-wire voice-coil, to enable high power ratings. Although the heavy coil would decrease the loudspeaker's sensitivity, it would ensure that the loudspeaker's resonance frequency remains much lower than the tube resonance frequencies.

For the prototype hybrid wind instrument, therefore, the idea of adding mass to a commercially available loudspeaker was explored. By applying the theoretical guidelines, a 1″ Tang Band W1-1070SE loudspeaker was chosen. The datasheet specifies a large frequency bandwidth and a resonance frequency of $f_{\mathrm{LS}} = 170\,\mathrm{Hz}$ that, by attaching a mass of 8.1 g to the membrane, was lowered to half the value of the first tube resonance frequency.

This modified loudspeaker is hermetically mounted on the resonator by means of an adaptor. While still allowing for the loudspeaker diaphragm's full range of movement, this adaptor is designed as small as possible in order to minimise the additional volume, and thus its effect on the resonator impedance.

Coupling to the tube

When this loudspeaker is coupled to the tube, the coupling frequency is $\omega_{\mathrm{c1}} = 2\pi\times 73.6\,\mathrm{rad\,s^{-1}}$, so that the first tube resonance $\omega_1 = 2\pi\times 139.7\,\mathrm{rad\,s^{-1}}$ shifts to $\omega_{1\mathrm{me}} = 2\pi\times 157.8\,\mathrm{rad\,s^{-1}}$ and the ratio of quality-factor shifting is $\frac{Q_{n(\mathrm{me})}}{Q_n} = 0.33$.

(It is worth noting that the frequency shift would be much larger for a loudspeaker with a greater $\frac{S_{\mathrm{d}}^2}{M_{\mathrm{m}}}$ factor, coupled to the same tube. Also, for a loudspeaker with a 2″ diaphragm, the $\frac{Q_{n(\mathrm{me})}}{Q_n}$ ratio would become ten times smaller. This illustrates and explains the choice of a loudspeaker with a 1″ diaphragm.)

Stability considerations when accounting for the coupling

In order to verify the stability of the closed-loop situation, with this loudspeaker and tube, the Bode plot stability criterion can be applied. That criterion states that, if at the phase crossover frequency (where the phase is equal to $\pm 180°$), the corresponding magnitude of the open loop (given by equation (46)), including the controller (equation (50)), is less than 0 dB, then the feedback system is stable.

Figure 26 shows the Bode diagram for the chosen loudspeaker and tube, with indication of the magnitudes at the crossover frequencies, whose inverse values represent the "gain margins". As can be seen, there are two crossover frequencies with associated negative magnitudes, corresponding to positive gain margins of 2.1 dB and 33.3 dB, which confirms the stability of the system.

Note that the stability could be expected, as the controller is designed to restore the uncoupled loudspeaker-tube system, which is a stable system. However, that is provided the loudspeaker model used in equation (46) is reliable. In practice, the loudspeaker introduces deviations that are not taken into account by the model, which explains that the gain margins should be reasonably high.

There is a positive open-loop magnitude zone near the first crossover frequency, which could lead to an unstable system in the presence of non-modelled deviations with a phase-upshifting effect in that frequency range; but most deviations introduce a decrease in phase. It should be mentioned that the use of a larger diaphragm loudspeaker would increase the overall magnitude substantially, leading to an increased stability vulnerability.

Maximum amplitude

Considering the power efficiency of this loudspeaker, with a close to sinusoidal self-sustained operation (so with $\zeta \approx 0.1$) at 140 Hz, the amplitudes of the flow rate related and feedback related coil currents are $|I_{\tilde{Q}}| = \{1.13\ 10^{-2} \times |P|\}$A and $|I_P| = \{2.39\ 10^{-2} \times |P|\}$A. These are of the same order and thus result in a good power efficiency (as other S_d values result in an increase of either $I_{\tilde{Q}}$ or

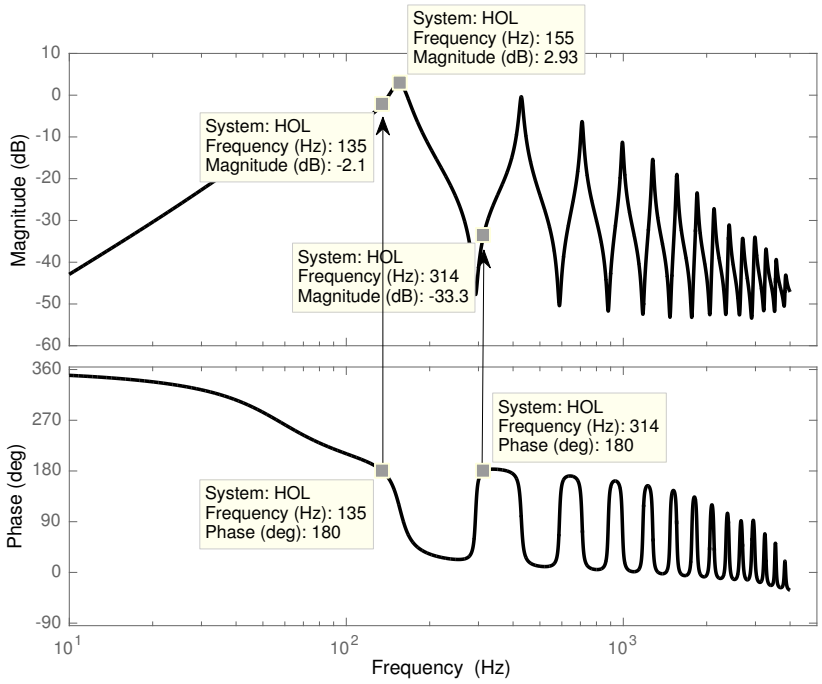

Figure 26: Bode plot of the open-loop system including the controller: $H_c\widetilde{C}$, with indication of the gain margins.

I_P). Nevertheless, it should be borne in mind that additional harmonics and/or playing of higher pitched notes would rapidly increase $|I_{\widetilde{Q}}|$, such that a greater S_d would be more convenient in this regard.

Given that the selected loudspeaker allows for a maximum power input of 8 W, and has an average input impedance of about 6 Ω, maximum currents up to $I_{max} \approx \sqrt{\frac{8}{6}} = 1.15$ A can be used. While $I_{max} = |I_{\widetilde{Q}} + I_P|_{max}$, the correlation between the currents depends on the applied excitation. In the most extreme case, they would be positively correlated, so that $I_{max} \lesssim (1.13 + 2.39)\ 10^{-2}|P|_{max}$ and hence $|P|_{max} \gtrsim \frac{1.15}{(1.13+2.39)\ 10^{-2}}$ Pa=33 Pa. This is a fairly small amplitude, in particular in comparison with real wind instrument amplitudes which typically lie between 1 kPa to 8 kPa (Fuks and Sundberg, 1996). However, empirical findings with the hybrid instrument showed satisfactory and linear results for pressure amplitudes up to 800 Pa. The much higher rating might be due to the fact that $I_{\widetilde{Q}}$ and I_P are less or even negatively correlated, or it could be that the maximum power rating provided by the manufacturer is mainly determined by a maximum membrane excursion, while I_P does not contribute to any mem-

Table 1: The estimated loudspeaker and lead-lag filter parameters.

R_s	$6.32\,\Omega$	S_d	$6.95 \times 10^{-4}\,\mathrm{m}^2$
R_e	$6.08\,\Omega$	ω_{LS}	$2\pi \times 67.4\,\mathrm{rad\,s}^{-1}$
Bl	$3.08\,\mathrm{T\,m}$	M_m	$8.52 \times 10^{-3}\,\mathrm{kg}$
Q_{ts}	1.48	ω_{LLn}	$2\pi \times 82.9\,\mathrm{rad\,s}^{-1}$
Q_{LL}	1.73	ω_{LLd}	$2\pi \times 46.2\,\mathrm{rad\,s}^{-1}$

brane movement. Nevertheless, while the pressure range still lies below the realistic range, it is possible to simulate a wind instrument whose operation is "downscaled" in amplitude.

3.3.3 *Loudspeaker and tube characteristics*

Measurements and parameter identification

To obtain all parameters of the coupled loudspeaker-tube system at the heart of the prototype hybrid instrument, a protocol involving two measurements and four least square linear regressions was applied. The details can be found in section A.4 and the resulting loudspeaker and lead-lag filter parameters are presented in table 1.

Comparing measured and theoretical impedances

In order to establish how well the filters compensate for the loudspeaker, the impedance $\widetilde{Z}_t^* = P^*/\widetilde{Q}^*$ (the asterisks refer to measured quantities) can be compared with the measured tube input impedance $Z_t^* = P^*/Q^*$ (obtained in section A.4). Ideally, these two impedances should match, but there are several theoretical and practical approximations that may prevent them from doing so. To study the impact of particular approximations, it is useful to consider the transition between intermediate states of the impedance, where only a few approximations at a time are taken into account.

The focus of the comparison can be narrowed further. As the intended application of the hybrid wind instrument is the production of self-sustained sounds,

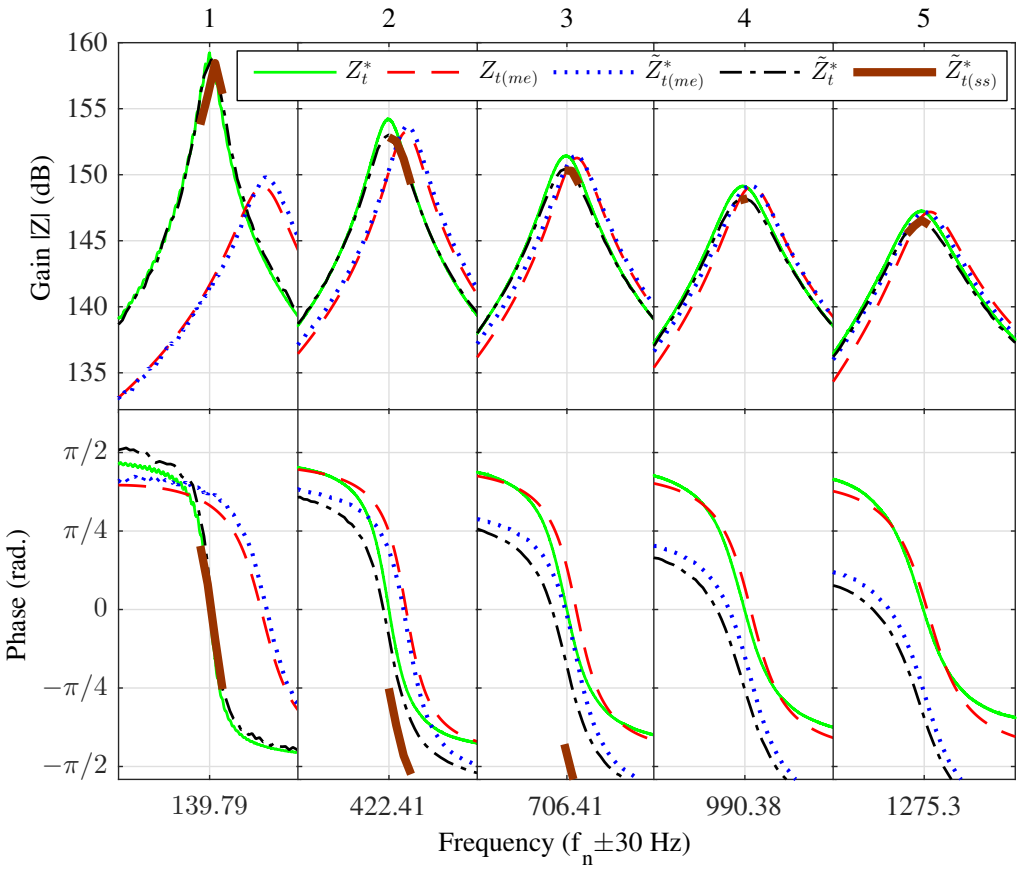

Figure 27: Originally measured (Z_t^*), analytic coupled ($Z_{t(me)}$), measured coupled ($Z^*_{t(me)}$) and measured uncoupled ($\tilde{Z}^*_t$) tube impedance curves ± 30 Hz around the five first modes. The latter is also shown for a measurement using self-sustained oscillation signals ($\tilde{Z}^*_{t(ss)}$) (instead of a sine sweep used for the other measurements). Note that the phase of the fourth and fifth modes of $\tilde{Z}^*_{t(ss)}$ falls below $-\pi/2$.

the principal frequency components are harmonics that lie close to the positive impedance peaks of the resonator's input impedance. Moreover, given that only the first few modes are of importance to maintain the self-sustained operation, the amplitude and phase of only the first five modes are studied.

Following this approach, the measured tube impedance Z_t^* is depicted in figure 27 (in solid green) along with the loudspeaker-coupled tube impedance $Z_{t(me)}$, as theoretically calculated using equation (32) (represented in dashed red).

A modal calculation using the coupled tube parameters $a_{n(me)}$ and $Q_{n(me)}$ in equation (25) resulted in a close match (not plotted). It can be seen that the

modes of $Z_{t(me)}$ lying near to the loudspeaker's resonance are shifted upwards in frequency in comparison with Z_t^*. At higher frequencies, both the amplitude and phase are in much closer agreement.

Figure 27 also shows an impedance measurement of the loudspeaker-coupled tube: $Z_{t(me)}^*$ (in dotted blue), which was measured by applying the feedforward filter but not the feedback filter. The curves are close to the analytically calculated equivalent $Z_{t(me)}$, which also emphasises that the lead-lag compensator satisfactorily corrects the amplitude and phase response. The increasing phase shift at higher frequencies is explained by the phase-lag problem, further discussed in subsection 3.4.1.

Furthermore, the addition of the feedback filter results in the impedance measurement $\widetilde{Z}_t^*$, which is also depicted in figure 27 (in black dash-dotted). The same deviations as were observed for the measured $Z_{t(me)}^*$ are still visible, but the result is fairly close to the original measured tube impedance Z_t^*. The zero-crossings, which are an important indicator for potential self-sustained playing frequencies, are reasonably close to the original resonance frequencies.

In contrast to the measurements reported until now, which were performed with a sine-swept signal (further referred to as sine measurements), it is also possible to obtain impedances and transfer functions from the self-sustained signals that appear during hybrid operation (further referred to as self-sustained measurements), however such measurements only cover the frequency range that was present in the self-sustained signal.

When the tube's input impedance is obtained from a self-sustained measurement: $\widetilde{Z}_{t(ss)}^* = P_{ss}/Q_{ss}$ (the solid thick brown curve in figure 27), an important phase lag is noted, which increases with frequency. This could be a result of the synchronously phased harmonics, a signature of the air flow signal of a self-sustained wind instrument (which arises due to "mode locking"), which demands substantial physical effort from the actuator.

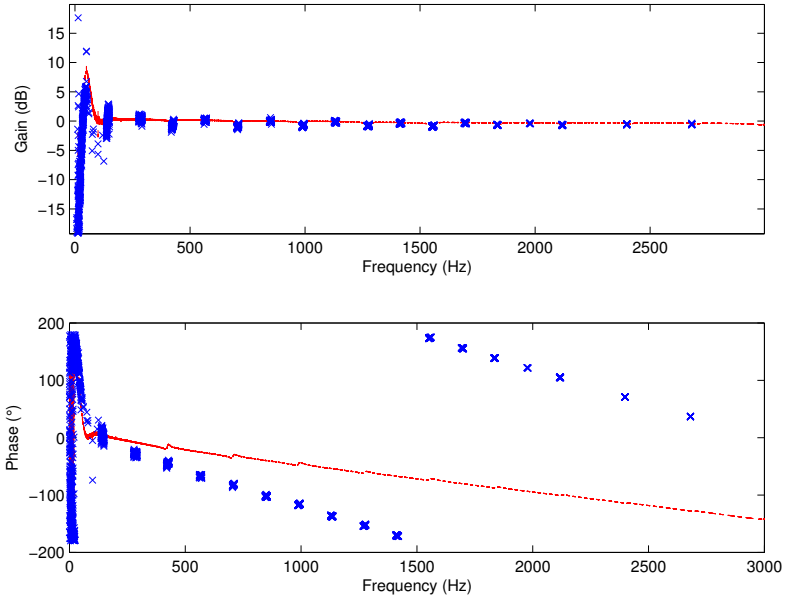

Figure 28: Transfer function $\tilde{Q}/Q$, between the calculated air flow signal and the physical flow rate signal. The red dashed curve is obtained using a sinusoidal swept signal and the transfer function around a series of harmonic frequencies indicated with blue crosses is obtained from self-sustained oscillation signals.

Transfer function for the uncompensated loudspeaker effects

Another way to study the uncompensated loudspeaker deviations is by observing $Q/\tilde{Q}$, the transfer function between the calculated air flow signal and the physical flow rate signal obtained from the measured loudspeaker velocity. If the feedforward and feedback filters were effectively compensating for the loudspeaker, this transfer function would be flat and zero for both the magnitude (in dB) and phase response.

Figure 28 shows two versions of this transfer function, derived from the signals that were obtained during the measurements of $\widetilde{Z}^*_t$ and $\widetilde{Z}^*_{t(ss)}$, i.e. obtained from a sine measurement (in dashed red) and a self-sustained measurement (indicated with blue crosses). Meanwhile, figure 29 shows the phase delay between the calculated air flow signal and the physical flow rate signal, defined as $-\frac{\phi(\omega)}{\omega}$, with $\phi(\omega)$ the unwrapped phase response of the $\tilde{Q}/Q$ transfer function (see e.g. (Papoulis, 1977)). These figures confirm the accuracy of the magnitude response

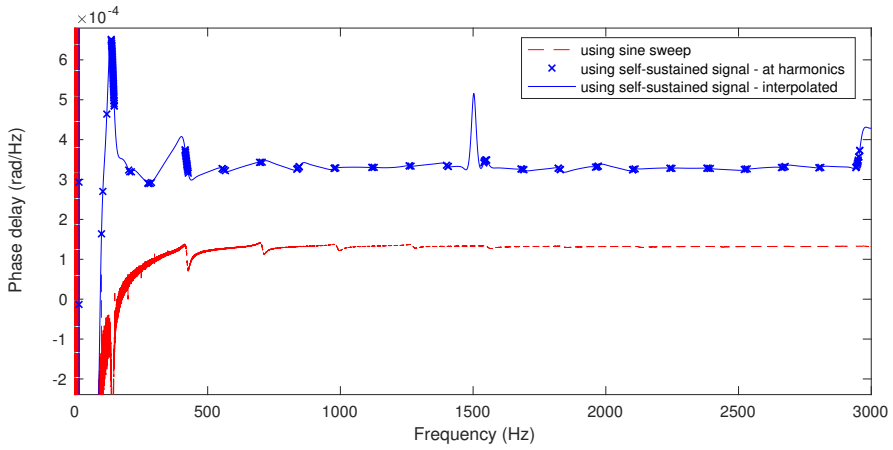

Figure 29: Phase delay between the calculated air flow signal and the physical flow rate signal. The red dashed curve is obtained using a sinusoidal swept signal and the transfer function around a series of harmonic frequencies indicated with blue crosses is obtained from self-sustained oscillation signals.

and the decreasing phase lag found in figure 27, but the resonator-independent representation of figures 28 and 29 give a clearer insight regarding the uncompensated loudspeaker effect. The phase of both measured transfer functions appears to decrease linearly with frequency in the manner of a constant delay (i.e. the phase response appears to be linear with frequency), which can be verified in figure 29 where a constant phase delay is found for a broad frequency range. However, as can be seen, there is no (mean) phase lag around 100 Hz in either of the measurements, which means that the phase delay is zero around the loudspeaker resonance frequency and then tends towards a constant value. The phase delay of the transfer function obtained from self-sustained flow rate signals is around 2.5 times higher than that obtained from the sine-swept measurement case.

3.4 SHORTCOMINGS AND COMPENSATION MEASURES

This section reports some of the known deviations in behaviour of the hybrid instrument prototype from that of the ideal hybrid wind instrument. Certain shortcomings are responsible for undesirable instabilities noted during the self-

sustained evaluation of the hybrid instrument, which are further reported and discussed in chapter 5.

3.4.1 *Increasing phase-lag issue*

As mentioned in subsection 3.3.3, the loudspeaker introduces a phase lag that is not predicted by the loudspeaker model used in this study.

POSSIBLE CAUSES While there is no mention of a delay effects in the literature on loudspeaker modelling, this expression is more frequently used in literature focussed on perception. For instance Blauert states: "Common loudspeakers and earphones are not necessarily minimum-phase systems but show additional all-pass characteristics. The additional group delays caused by these characteristics are on the order of 400 µs." (Blauert and Laws, 1978). For comparison, the group delay derived from the phase responses in figure 29 is approximately 125 µs for the sine measurement and 300 µs for the self-sustained measurement.

When considering the time response of the loudspeaker including the compensating filters, it was noted that steep impulses at the input were somewhat smeared out in the membrane displacement response. Even when the theory states that a steep transition in the input signal should be preserved in the output, it is understandable that a real physical system cannot reproduce such steep transitions in practice. Hence, it could be assumed that the loudspeaker mechanics include nonlinearities such as hysteresis which introduce the phase lag. The computing system's latency also makes part of the total delay, but the computing system of the current prototype only has a latency of 25 µs.

COMPENSATION This side-effect cannot be compensated for with an inverse filter, given that such a filter would be non-causal. Nevertheless, it should be emphasised that self-sustained measurements with higher pitched oscilla-

tions revealed that the phase at the fundamental frequency always coincides with the phase obtained with the sine-swept measurement. This ensures that higher notes can still be played, and have a reasonable pitch relation to the acoustic instrument.

PREVENTION It was hypothesised that a minor cause of the phase lag was related to the (currently unconsidered) voice coil induction. However, preliminary measurements, where this feature was measured and included in the inverse loudspeaker filter, did not result in an improved phase response.

Another way to cope with elements that introduce a phase difference between the loudspeaker's voltage and current, is to use a "current-drive" amplifier; e.g. Mills and Hawksford (1989) investigated the use of current-drive technology with the aim of reducing thermal heat and electric nonlinearities in loudspeakers.

Also taking into account the mechanical loudspeaker part, it may be worth investigating more advanced (nonlinear) loudspeaker models and consequently finding their inverse transfer function for the design of a more accurate inverse filter (if causal).

Finally, it should be mentioned that it is possible to predict the pressure signal in front of the loudspeaker by using a second microphone located further from the loudspeaker down the resonator. In subsection 6.1.2, an initial investigation of this concept demonstrates the possibility of compensating for the computing system's latency. However, the technique could also be used to enable the implementation of non-causal filters, as the pressure prediction enables the introduction of a time shift, which can make the filter causal.

3.4.2 *Loudspeaker non-piston modes*

Another loudspeaker issue appears at relatively high frequencies. As can be noted from the measured transfer functions shown in figure 30 (determined

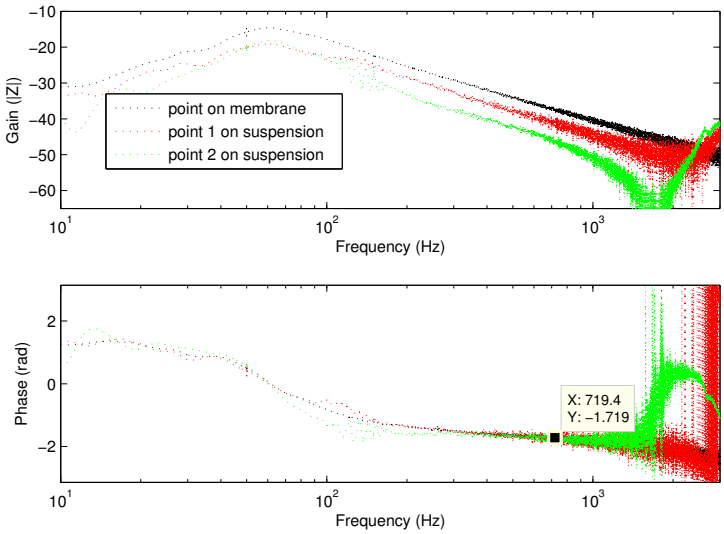

Figure 30: Measured loudspeaker transfer functions, using a laser doppler vibrometer measurement of a point on the loudspeaker membrane (in black) and two points on the suspension (in red and green).

using a laser Doppler vibrometer measurement (see section A.1 for details on that equipment) of a point on the loudspeaker membrane and two points on the suspension), one of the suspension points shows a magnitude dip around 2 kHz, with a corresponding phase deviation. These measurements support the hypothesis that the vibrational modes of the rubber suspension surrounding the membrane come into play. It should be noted that the measurement of other points on the membrane (measured up to 9 kHz) resulted in equal responses, which indicates that the membrane itself (equipped with an additional glued metal layer to add mass) is sufficiently rigid and is not influenced by "tilting modes", and that this component acts as an ideal piston. While the influence of the suspension is reasonably small, its effect on the total radiated pressure wave can be noticeable, as is also stressed by Sagers for instance, who proposed a more extended loudspeaker model in this regard (Sagers et al., 2013).

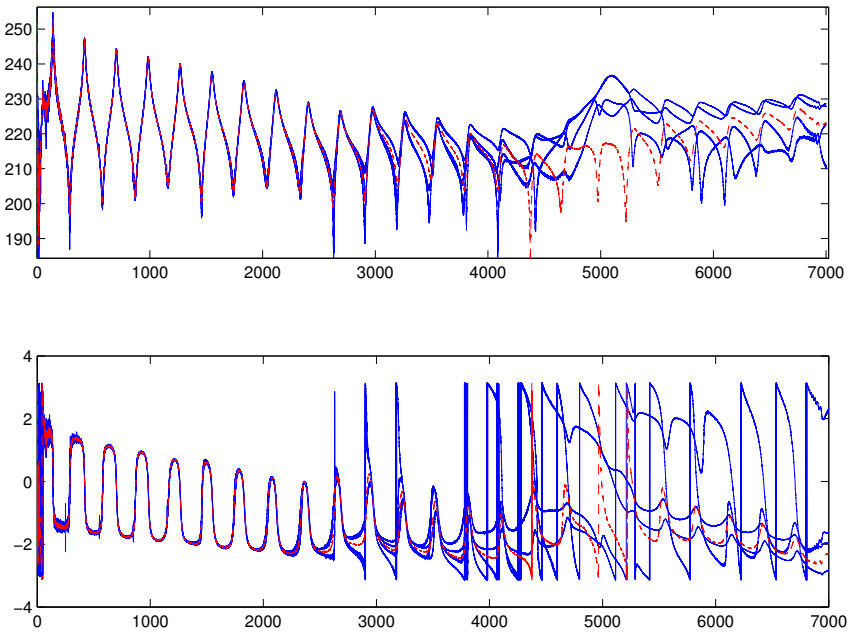

Figure 31: Four tube input impedance measurements (in blue) obtained with the loudspeaker and microphone mounted on the tube. The pressure is obtained for four different microphone positions at different angular positions in front of the loudspeaker membrane. The red dashed curve represents the mean impedance of the four measurements.

3.4.3 *Loudspeaker front-cavity modes*

The tube's input impedance obtained from the loudspeaker membrane velocity and the microphone measurements revealed notable deviations from a normal tube impedance, starting from about 4 kHz. Empirical findings have indicated that the deviations depend on the angular position of the microphone with respect to an axis along the middle of the tube. This can be noted from the impedance measurements shown in figure 31, carried out with four different microphone positions (the solid blue curves).

POSSIBLE CAUSES It is a reasonable hypothesis that the dependence on microphone orientation is due to non-planar vibration modes in the loudspeaker cavity. Indeed, the lowest transverse mode in a disc-shaped cavity (notated as

(+,-)) corresponds to the first standing pressure wave over the cavity's diameter (of length D), with pressure anti-nodes at the extremities and a pressure node in the middle. Hence, the resonance frequency of that mode is roughly found to be $\frac{c}{2D} = \frac{340m/s}{2(37.5\,10^{-3}m)} \approx 4.5\,\text{kHz}$, which corresponds to the onset of the observed impedance deviations. The hypothesis is also supported by the fact that the impedance derived from the mean response of the four pressure measurements (shown in dashed red in figure 31) is much closer to a typical tube impedance.

COMPENSATION Just as with the phase lag issue it is most likely not possible to compensate for these deviations by means of additional filters. Alternatively, the idea of introducing a low-pass filter with its cut-off frequency below the high frequency magnitude peaks may be appealing, but this inevitably introduces a phase lag that is noticeable below the cut-off frequency. Indeed, empirical evaluations showed that the introduction of a low-pass filter caused unstable self-sustained hybrid behaviour at lower frequencies.

PREVENTION As demonstrated in figure 31, using an average signal of several microphones could be an effective workaround. In this scenario, it would be preferable to use an odd number of microphones, to avoid higher transverse modes in the cavity. However, this concept is cumbersome and the technical means were not present.

Instead, for the case of the current prototype it was noted that one of the microphone positions turned out to provide a fairly stable response; this is the solution applied for the evaluations discussed in chapter 5.

Another technique to avoid the non-planar modes is to place the microphone at the centre of the loudspeaker. The successful implementation of this idea is described as a further development in section 6.1.2.

Finally, it should be mentioned that the idea of introducing a "phase plug" in the loudspeaker cavity (as used in the design of "compression drivers", i.e. the driver of a horn loudspeaker, also with the purpose of avoiding cavity modes)

sounds appealing but is probably not realisable, given that the loudspeaker cavity is needed for the membrane displacement (which is much larger than in the case of a compression driver).

3.4.4 *Other shortcomings*

As already mentioned in section 3.3.2, if realistic wind instrument sounds are what is being aimed for, there is also a shortcoming in dynamic range, which is further discussed in subsection 7.1.1. For this issue there are no compensation measures, the only way to improve the situation is to consider other actuator options. Some ideas are provided in section 7.2.1.

Finally, a particular issue was noted with the computing system. It turned out that the timing of the data acquisition was not always precise, which introduced so called "jitter" noise. Further details are given in subsection B.2.1.

3.5 SUMMARY

This chapter described the development of the hybrid wind instrument excluding its excitation, i.e. a real-time computing system connected to a loudspeaker and a microphone, which are placed at the entrance of a clarinet-like "tube" resonator.

First, the functioning of an ideal hybrid wind instrument was described, considering the loudspeaker to be a rigid piston, not influenced by the pressure surrounding it. Then, the case of a realistic hybrid instrument was considered, where the effect of real transducers and a real computer was taken into account. To ensure that the operation was equivalent to that of the ideal hybrid instrument, a feedforward and a feedback filter were introduced to compensate for the loudspeaker.

Next, a thorough theoretical investigation of the loudspeaker-resonator system was carried out. A linear loudspeaker model was adopted and described in detail using analogous electronic circuit theory. The modal resonator representation (given in chapter 2) was used to study its acousto-mechanical coupling with the loudspeaker. Expressions were derived describing how the resonance frequencies and quality factors of the resonator modes are affected by the loudspeaker.

Following this, strategies were laid out to compensate for the side-effects of the loudspeaker. On one hand this involved the design of a feedforward, inverse loudspeaker filter, consisting of a derivative and a "lead-lag" filter. On the other hand, a feedback filter was introduced to compensate for the coupling between the loudspeaker and the resonator.

Subsequently, the practical design of a hybrid set-up was described. After presenting the basic properties of the chosen resonator and computing system, the choice of an optimal loudspeaker was made, which turned out to be a small and heavy membrane loudspeaker. The loudspeaker and tube were characterised with a parameter identification on a series of measurements (provided in appendix A). Theoretical and measured impedances were compared and it was concluded that the filters compensated well for the loudspeaker, particularly in amplitude. However, an increasing phase lag was noted, which was also (more clearly) observed in a transfer function that enabled a focussed view on the uncompensated loudspeaker effects.

Finally, a number of shortcomings and according compensation measures have been listed, addressing the observed increasing phase lag, the appearance of non-piston modes due to the loudspeaker suspension, transversal air-vibration modes in the loudspeaker's front cavity, and dynamic range and "jitter" issues. For some of these issues, compensation and prevention measures have been proposed.

4 EXCITATION MODELS

When a wind instrument is played, the mouth and mouthpiece act as an "excitation mechanism" to the resonator. For the underlying understanding of this concept, the reader is referred to chapter 2. In this chapter, four excitation models are presented, from their theoretical development to their implementation and the sound they are expected to produce with the clarinet-type resonator.

First, the woodwind single-reed mouthpiece physical model is discussed, before then moving on to the "lip-reed" physical model, which is typically used for brass instruments. With the hybrid wind instrument, the excitation is performed on a real-time computer. Although this introduces some computational issues (which are discussed in an initial section 4.1), the freedom offered by this numerical medium enables the implementation of unusual physical and even non-physical models (the motivation for which is discussed in section 1.2.1), such as a "bow-string interaction model" and a mathematical (polynomial) formulation.

As the aim is to explore the various operations that can be achieved with the hybrid instrument, it is of interest to unambiguously evaluate a range of parameters for each excitation model. However, the original physical models often contain numerous parameters, many of which have a similar effect. Therefore, it is often preferable to use a reduced set of "independent" variables, obtained by rearranging the model's equations.

Also related to this simplification is the "non-dimensionalisation" of the models and the physical quantities, in order to obtain dimensionless signals and parameters. This ensures that the models are independent of a particular dimensional situation, which is not relevant when exploring the timbre possibilities. Furthermore, a dimensionless model can be seen as a blueprint of a

physical model, which provides a generalised result and parameter values that are independent of the particular resonator used.

4.1 COMPUTED SIMULATION OF EXCITATION MODELS

4.1.1 *Methods to computationally simulate physically interacting systems*

Before focussing on each separate excitation model, it is useful to lay out the general implications that arise when physical models are numerically simulated. These implications are due to the difference in nature of computational and physical processes. The former operate in discrete steps, calculating output signals with formulas supplied with known variables and input signals. Physical processes, however, relate physical components by a pair of potential and flow variables (pressure and volume flow in the case of acoustics), whose interdependence is governed by Kirchhoff laws (see e.g. (Bilbao, 2003)). Hence, the interaction of these variables is direct and bi-directional, which is fundamentally different from the computational approach. Several approaches to computationally simulate a physical model exist and a detailed development of these can be found for example in (Rabenstein et al., 2007; Bilbao, 2009b). It is possible to formulate finite-difference approximations incorporating detailed components of the entire physical situation, which favours realistic sound production and also doesn't require the formulation of any further physical approximations. Recently, related time domain finite-difference methods have been proposed (see e.g. (Bilbao, 2009a) for a "direct simulation" of reed wind instruments and (Harrison et al., 2015) for brass instruments). Moreover, a globally energy balanced scheme can be used, which takes into account energy conservation laws so that numerical stability is guaranteed, also under highly nonlinear conditions (Bilbao, 2009b; Desvages and Bilbao, 2016). This has been further formalised as Port Hamiltonian Systems for instance (Falaize et al., 2015; Lopes and Hélie, 2016).

The physical models of the excitation mechanisms (i.e. the excitation models) employed in this thesis are formulated as a set of analytic equations and there is no spacial domain involved. While the time derivatives can be approximated via numerical differentiation using a finite difference method, there is a particular issue that occurs when the physical model is a so-called "stiff system"[1], which is the case for many excitation mechanisms. Stiff elements are components which induce an (almost) instantaneous reaction between the Kirchhoff variables and, hence, the equations describing this situation "depend on themselves" or are "implicit". This issue is also referred to as a "delay-free loop" in the system and conflicts with the explicit functional approach of the computing system.

There are several ways of coping with this issue. The simplest idea is to naively introduce a sample delay, making the interdependency indirect. While in some cases, this approaches the continuous system when the time step becomes small enough, there are situations where the numerical system remains unstable, regardless of the used sampling frequency. This is the case for the excitation models used in this thesis (for certain parameter ranges).

Other methods involve transforming the physical Kirchhoff variables into so-called "wave variables" (see e.g. (Rabenstein et al., 2007)). The two wave variables related to the Kirchhoff pressure and flow rate variables are the up- and down-stream pressure waves, as introduced earlier in section 2.1.1. These variables are expressed in a coordinate system that is rotated by 45° from the Kirchhoff variables coordinate system, and they are in an explicit relation with each other, facilitating a computational implementation. Nevertheless, this rotation does not directly provide a set of explicit equations; to achieve this, a number of possible methods can be applied.

The preferable method is to simply re-arrange the equations, in order to analytically obtain equivalent explicit equations. This results in a theoretically correct and easily programmable implementation with light computational de-

1 A "stiff system" is a known concept, designating the presence of (almost) instantaneous physical interactions.

mand, while maintaining the flexibility to alter parameters of the original physical model during the computation. However, it is not always straightforward (and often not even possible) to analytically find the explicit equations, so that another method may be necessary.

While it has been possible to apply the analytical solution to all of the excitation models evaluated in this thesis, it is worth mentioning some other methods that can be useful for the implementation of more complex excitation models.

One possibility is preparation of a lookup table to replace the analytical formulas. The lookup data can be calculated beforehand, for example by discretising the implicit equation and applying a transformation from the implicit to the explicit coordinate system. This technique is relatively simple for non-time-dependent equations (i.e. quasistatic systems), and has for example been applied by Smith (Smith, 1986), who carried out pioneering work on digital simulations of many musical instruments. Meanwhile, excitation models that involve time derivatives can also be simulated using lookup tables, as has been demonstrated by Borin et al. who introduced the "K-method" (Borin et al., 2000). A drawback of using lookup tables is that each controllable parameter of the physical model adds a dimension to the table, increasing the amount of data exponentially, so that the number of control-assignable parameters is very limited.

Finally, it is possible to approximatively solve the implicit excitation equations by means of an iterative method (e.g. by the "Newton–Raphson method", see e.g. (Atkinson, 1991)). This approach involves repeated evaluations of the equation for a given time instance, using the previous evaluation's error (i.e. the difference between both sides of the equation) to improve the approximation at each iteration. While this approach can be applied to any system and is relatively easy to implement, it is usually computationally heavy for sophisticated models.

4.1.2 *Implementation on the hybrid wind instrument*

The computational issue discussed in the previous subsection is focussed on an entirely numerical implementation of a physical model. However, with the first implementation of the hybrid instrument (with a single microphone), only the excitation model is computed and the resonator prepared for hybrid synthesis (discussed in chapter 3) only operates with the Kirchhoff variables p and q. In addition, there is an inevitable small latency introduced by the computational processing time, so that a theoretically coherent implementation is impossible in practice for this implementation.

Nevertheless, it is possible to achieve a partial implementation, resulting in a good approximation where the foremost risk of instabilities is compensated for. Provided that an explicit expression is found of an (arbitrary) excitation model coupled to an infinitely long tube (i.e. with a real constant input impedance, matching the characteristic impedance of the resonator being used), the direct loop in the excitation model is removed and the remaining work involves the conversion from the Kirchhoff variables $\{p, q\}$ to the wave variables $\{p^+, p^-\}$. Taking into account the single sample latency on the measured pressure signal, p_{n-1}, and using the flow rate value of the previous sample time, $\tilde{q}_{n-1}$, the delayed upstream pressure can be used $p^-_{n-1} = \frac{p_{n-1}}{-}\tilde{q}_{n-1}2$ instead of p^-_n. (Note that the discretisation of the excitation models is expressed in terms of the "historical pressure" $p_\mathrm{h} = 2p^-$.) The remaining sample delay in the upstream pressure introduces a minor phase lag, which only becomes of importance at high frequencies. Given that these high frequencies are only poorly reflected at the open end of the resonator, the high frequency content of p_h is low, so that the risk of undesirable instabilities is small.

Alternatively, it is possible to introduce a second microphone, a distance $c\Delta t$ from the resonator entrance (with c the speed of sound and Δt the latency), which enables the calculation of p^-_n. This implementation is of particular in-

terest for systems with higher latencies; an implementation and brief evaluation of such a system is discussed in section 6.1.

4.2 SINGLE-REED MODEL

The single-reed mouthpiece is employed by woodwind instruments such as the clarinet and the saxophone. The basic functioning of this mouthpiece, in combination with the embouchure, has been briefly introduced in chapter 2. Here, a detailed explanation is provided and the model is extended by taking into account some dynamical behaviour. While the latter has little influence on its operation (as the reed resonance frequency is kept high), the inclusion of this feature is mainly for computational reasons, as will be discussed.

Figure 32 depicts a schematic diagram of a transverse intersection of a mouthpiece with a player's mouth. Displacement, pressure and flow rate signals are indicated as a reference to the theoretical model that is discussed next.

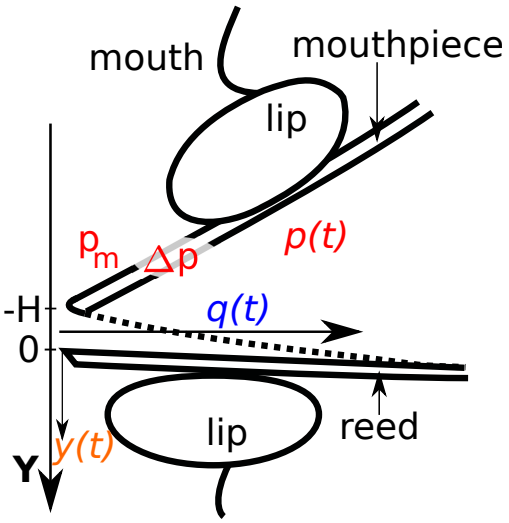

Figure 32: Schematic diagram of a single-reed mouthpiece with a player's mouth, with indications of the reed displacement, the pressure and the flow rate signals.

4.2.1 *Physical model*

To intuitively understand the embouchure's functioning, it can be thought of as a valve mechanism that is controlled by the pressure difference across the reed. As such, one can distinguish two physical phenomena occurring. First, the pressure difference acting on the reed surface is translated in a force, which will cause the reed to bend. Second, that same pressure difference is also responsible for the stream of air flow that is generated through the opening between the reed and the lay of the mouthpiece. Each of these physical model components have been individually researched and it is also appropriate to discuss them separately here.

The single degree of freedom classical model used in this study is depicted in figure 33, which will be referred to in the next paragraphs.

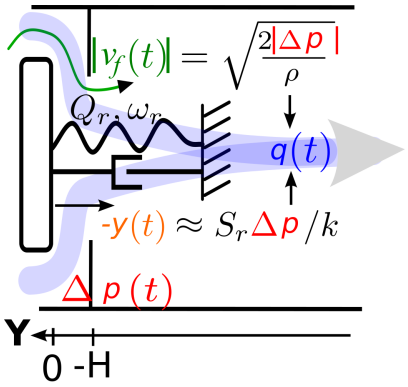

Figure 33: Dynamical, SDOF model of a single-reed embouchure, with indications of the reed displacement, the pressure, the flow velocity and the flow rate signals.

It should be noted that much more developed models exist than the model used in the current study. For instance, Avanzini and van Walstijn have proposed a more realistic mechanical response of the embouchure (Avanzini and Van Walstijn, 2004). Also the "reed induced flow", which is an acoustic flow component that is produced by the movement of the reed surface (see e.g. (Hirschberg, 1995)) is not taken into account here; nor the noise introduced by the flow turbulence (see e.g. (Chafe, 1990)). While the basic model employed in this study is widely accepted (Wilson and Beavers, 1974; Fletcher, 1979a, 1993;

Kergomard, 1995; Kergomard et al., 2000; Ollivier, 2002; Dalmont et al., 2003) and sufficient for the initial investigations on the hybrid wind instrument, an interesting future possibility would be to implement a more realistic single-reed model, allowing a more accurate comparison to real clarinet sounds.

REED DISPLACEMENT The reed (including the player's lower lip) is modelled as a single-degree-of-freedom (SDOF) mass-spring-damper system (as can be seen in figure 33), which is driven by the pressure difference across the reed $\Delta p = p_m - p$ (with $p_m(t)$ the mouth pressure and $p(t)$ the pressure inside the mouthpiece), acting on part of the reed surface S_r. Hence, the reed's dynamics are described by (see e.g. (Wilson and Beavers, 1974)):

$$\frac{1}{\omega_r^2}\frac{d^2 y}{dt^2} + \frac{1}{Q_r\,\omega_r}\frac{d y}{dt} + y = \frac{-S_r(p_m - p)}{k}, \tag{51}$$

with $y(t)$, the displacement of the tip of the reed and k, ω_r and Q_r corresponding to respectively the stiffness, resonance frequency and quality factor of the elementary lip-reed combination. Further, the reed displacement is proportional to the effective reed opening section S_f (also referred to as the reed "channel"):

$$S_f = \mathcal{H}(y + H)(y + H)w, \tag{52}$$

where w is the effective reed width and the Heaviside function $\mathcal{H}$ is introduced to hold a zero flow rate when the reed hits the lay at position $y = -H$, which occurs above the "beating pressure" P_M . It should be noted that, while the effect on the flow control of the reed beating is indeed realised by the Heaviside function, the effect on the reed's dynamics is not included in this model. For a high resonance frequency and a small Q_r-factor this effect is weak, but for a more precise implementation, either a "conditional filter" (such as implemented for the lip-reed model in section 4.3) or a more advanced mechanical reed model (such as (Van Walstijn and Avanzini, 2007; Chatziioannou and Van Walstijn,

2012; Muñoz Arancón et al., 2016)) can be considered. More recent single-reed models describe the reed collision in much more detail (see e.g. (Bilbao, 2009a; Chatziioannou and Van Walstijn, 2012; Muñoz Arancón et al., 2016)).

ENTERING AIR FLOW RATE There have been various assumptions regarding the aerodynamic behaviour of the air flow that enters the bore from the mouth through the reed channel. Wilson and Beavers (Wilson and Beavers, 1974) hypothesised that Bernoulli's equation would be applicable to calculate the flow velocity in the air channel between the reed tip and the mouthpiece. Hirschberg adopted and developed this idea into the form that usually appears in the current literature (Hirschberg, 1995).

This hypothesis arises from the implication that the turbulence created in the mouthpiece at the reed channel's exit results in a negligible pressure recovery. That is, contrary to the case of a steady flow, where the cross-sectional area is inversely proportional to the pressure, in a turbulent air jet leaving a small orifice the kinematic energy is dissipated so that the pressure (almost) remains at the state it was at the end of the orifice.

The flow velocity in the reed channel, which is just before the turbulent air regime, can be calculated from Bernoulli's equation applied to the mentioned pressure difference:

$$v_\mathrm{f} = \operatorname{sgn}(p_\mathrm{m} - p)\sqrt{\frac{2|p_\mathrm{m} - p|}{\rho}}, \tag{53}$$

where ρ is the density of air and the sgn operator is introduced to make the calculation of negative flows possible.

Hence, the air volume flow rate that enters the instrument can be expressed as the product of the effective reed opening area S_f (eq. (52)) and the flow velocity $v_\mathrm{f}(t)$ (eq. (53)):

$$q = S_\mathrm{f} v_\mathrm{f}. \tag{54}$$

The injection of this flow rate into the instrument induces an immediate pressure contribution qZ_c, where Z_c is the characteristic impedance of the resonator. However, it is typically assumed that the flow escaping from the mouth has a negligible influence on the mouth pressure.

NON-DIMENSIONALISING AND PARAMETER VALUES A dimensionless form of the single-reed model initially proposed by Wilson and Beavers (Wilson and Beavers, 1974) has been developed, which has been simplified later by Kergomard (Kergomard, 1995), to the form often used nowadays.

By defining $\bar{y} = \frac{y}{H}$, $\gamma = \frac{p_m}{P_M}$, $\bar{p} = \frac{p}{P_M}$ and $\bar{q} = \frac{q\,Z_c}{P_M}$, the equation for the reed dynamics (eq. (51)) can be written as:

$$\frac{1}{\omega_r^2}\frac{d^2\,\bar{y}}{dt^2} + \frac{1}{Q_r\,\omega_r}\frac{d\,\bar{y}}{dt} + \bar{y} = \bar{p} - \gamma, \tag{55}$$

and the equation for the flow rate (eq. (54)) becomes:

$$\bar{q} = \underbrace{\operatorname{sgn}(\gamma - \bar{p})\sqrt{|\gamma - \bar{p}|}}_{\bar{v}_f}\,\underbrace{\zeta\,\mathcal{H}(\bar{y}+1)(\bar{y}+1)}_{\bar{S}_f}, \tag{56}$$

made up of a dimensionless air velocity component $\bar{v}_f$ and a reed section opening component $\bar{S}_f$.

There are three important remaining independent parameters: P_M, which determines the signal amplitude without timbre variation (within the linear dynamic range of a resonator), the mouth pressure γ and the "global embouchure parameter" ζ, which both have an effect on the signal shape and transients, and thus the timbre of the sound. The global embouchure parameter $\zeta = Z_c w \sqrt{\frac{2H}{\rho k}}$ lumps all remaining embouchure parameters together. For constant resonator and mouthpiece parameters (ρ, Z_c, w and k), ζ is proportional to the square root of the the reed opening at rest, which is related to the lip force.

In this study, the dynamic parameters, of importance to the brightness and in selecting the desired register (Wilson and Beavers, 1974; Silva et al., 2008), are held fixed to the values used in (Guillemain et al., 2005): $\omega_r = 2\pi \times 2500\,\mathrm{rad\,s^{-1}}$

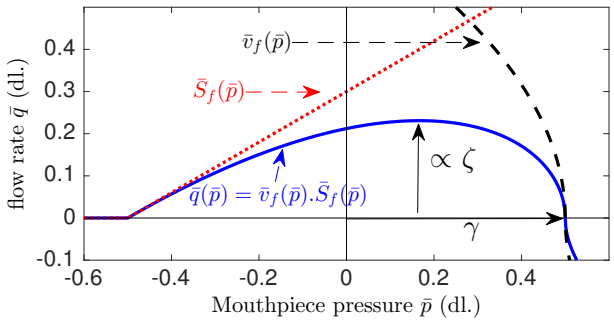

Figure 34: Dimensionless curves of the velocity, the reed opening area and the resulting volume flow rate, as a function of the pressure in the mouthpiece, for a quasistatic single-reed model with a dimensionless mouth pressure of $\gamma = 0.5$ and an embouchure parameter $\zeta = 0.4$.

and $Q_r = 5$. While this resonance frequency is relatively high compared to a real instrument (see e.g. (Dalmont et al., 2003)), this close-to quasistatic implementation is sufficient as a first investigation. Figure 34 depicts the dimensionless curves of the velocity, the quasistatic reed opening area and the resulting volume flow rate, as a function of the pressure in the mouthpiece $\bar{p}$.

It is worth noting that, when the reed dynamics come into play, there will be an increasing phase lag between the pressure oscillation and the reed displacement, so that the curves of $\bar{S}_f$ and $\bar{q}$ become hysteretic, i.e. the curves become dependent on the direction of $\bar{p}$. While it is known that for real reed instruments the quasistatic hysteretic condition (see theorem 2 in chapter 2) does not occur, it is worth considering the theoretical threshold parameters. The second derivative of the quasistatic expression of the single reed model (i.e. considering $\bar{y} = \bar{p} - \gamma$), shows that the maximum positive gradient lies at $\gamma - \bar{p} = 1$. Evaluating the condition $\frac{\partial \bar{q}}{\partial \bar{p}} > 1$ at $\bar{p} = \gamma - 1$ then reveals the hysteretic condition: $\zeta < 1$. This condition only applies when the oscillation domain reaches the beating threshold, otherwise non-hysteretic cases with higher ζ can be obtained (the lower the mouth pressure).

4.2.2 *Making discrete and explicit*

In this subsection, the conversion of the physical single-reed model from implicit equations to computable explicit equations is discussed. While initially the computation of this model was performed using iterative or lookup-table methods (see e.g. (Borin et al., 2000) or the more recently proposed iteratively reweighted least squares method using the standard Nelder-Mead simplex optimisation (Chatziioannou and Van Walstijn, 2012)); Guillemain et al. demonstrated that this model can be made entirely explicit in an analytical fashion (Guillemain et al., 2005). A key concept in Guillemain's paper, adopted from van Walstijn (van Walstijn, 2002), concerns the fact that the reed's dynamic equation can be discretised using a classical central difference scheme that relies only on previous samples, and is therefore causal, while stability is preserved (for the system concerned). Hence, the direct loop is only present in the flow velocity component of the calculation, which is a simple second order equation that can be analytically transformed into an explicit equation. For the detailed development the reader is referred to (van Walstijn, 2002; Guillemain et al., 2005); here only the most important steps are repeated.

First, using the Laplace transform, equation (55) can be expressed in the frequency domain to provide the transfer function of the reed's dynamics:

$$\frac{\bar{Y}(s)}{\Delta\bar{P}(s)} = \frac{\omega_r^2}{s^2 + \frac{\omega_r}{Q_r}s + \omega_r^2}, \tag{57}$$

where $\Delta\bar{P} = \mathcal{L}(\bar{p} - \gamma)$ and $\bar{Y} = \mathcal{L}(\bar{y})$. To discretise this, the following central difference scheme is applied:

$$\begin{cases} s & \approx \frac{1}{T(z-z^{-1})} \\ s^2 & \approx \frac{1}{T^2(z-2+z^{-1})} \end{cases} \tag{58}$$

In order to obtain a computable expression, the discrete transfer function should be causal, which can be achieved by multiplying the numerator and denomin-

ator by combinations of $\frac{z^{-1}}{z^{-1}}$ until all positive powers of z (representing future samples) have disappeared. Given that this transfer function concerns a low-pass filter, all poles remain in the unit circle, and thus stability is maintained. After re-arrangement by negative orders of z, the resulting discrete transfer function is:

$$\frac{\bar{Y}(z)}{\bar{\Delta P}(z)} = \frac{T^2\omega_r^2 z^{-1}}{(1+\frac{T\omega_r}{2Q_r}) - (2-T^2\omega_r^2)z^{-1} - (\frac{T\omega_r}{2Q_r}-1)z^{-2}}, \tag{59}$$

so that an inverse Z-transform yields the time domain difference equation:

$$\bar{y}_n = 0 \times \bar{\Delta p}_n + b_1 \bar{\Delta p}_{n-1} + a_1 \bar{y}_{n-1} + a_2 \bar{y}_{n-2}, \tag{60}$$

with coefficients:

$$\begin{cases} a_0 &= 1 + \frac{T\omega_r}{2Q_r} \\ b_1 &= \frac{T^2\omega_r^2}{a_0} \\ a_1 &= \frac{2-T^2\omega_r^2}{a_0} \\ a_2 &= \frac{\frac{T\omega_r}{2Q_r}-1}{a_0} \end{cases} \tag{61}$$

Hence, it can be verified that the output $\bar{y}_n$ only depends on previous instances of the pressure and therefore this is also true for the $\bar{S}_{fn}$ term in equation (56):

$$\bar{S}_{fn} = \zeta \mathcal{H}(\bar{y}_n + 1)(\bar{y}_n + 1). \tag{62}$$

The dimensionless mouthpiece pressure in equation (56) is replaced by the sum of the historical pressure and the entering flow rate (see equation (7)): $\bar{p} = \bar{p}_h + \bar{q}$. Considering the case where $\bar{q} \geq 0$, this leads to the following implicit equation for time instance n:

$$\bar{q}_n = \underbrace{\sqrt{|\gamma - \bar{p}_{hn} - \bar{q}_n|}}_{\bar{v}_{fn}} \bar{S}_{fn}. \tag{63}$$

By taking the square of $\bar{q}_n$, a second order polynomial is obtained, whose roots:

$$\bar{q}_n = \frac{1}{2}\left(-\bar{S}_{fn}^2 \pm \bar{S}_{fn}\sqrt{\bar{S}_{fn}^2 + 4(\gamma - \bar{p}_{hn})}\right),$$

lead to the explicit solution, which is the $(+)$ case, for which $\bar{q}_n$ is real and positive (note that $\gamma - \bar{p}_{hn} > 0$ since $\bar{q} \geq 0$ and $\gamma - \bar{p}_n > 0$). For the case where $\bar{q} < 0$, a similar solution is found, so that a general expression can be composed of both cases, by re-introducing the absolute value and sgn operator:

$$\bar{q}_n = \frac{1}{2}\operatorname{sgn}(\gamma - \bar{p}_{hn})\bar{S}_{fn}^2\left(\sqrt{1 + \frac{4|\gamma - \bar{p}_{hn}|}{\bar{S}_{fn}^2}} - 1\right). \tag{64}$$

Hence, the entire computational process consists of the sequential evaluation of equations (60), (62) and (64). And, as mentioned in subsection 4.1.2, due to the inevitable delay of the computing system, $\bar{p}_{hn-1} = \bar{p}_{n-1} - \bar{q}_{n-1}$ is used instead of $\bar{p}_{hn}$ in equation (64).

It should be noted that the parameters γ and ζ, and the dynamic reed parameters ω_r and Q_r, can also vary over time. However, this lies well below the variation rate of the pressure and flow rate signals, so that the parameters appear as constants in the above equations.

4.2.3 *Predicting the influence on the sound*

In a continuation of the theory presented in chapter 2, where a number of rules were obtained to estimate the influence on certain sound features, the case of the single-reed embouchure model is now studied in depth.

While the estimation theory is only designed for quasistatic excitation models, the dynamics involved in this single-reed model are almost negligible, as the resonance frequency of the reed is kept fairly high, at 2.5 kHz (moreover, empirical tests with a resonance frequency at 10 kHz produced almost the same sound spectrum). As stated by theorem 1 (see chapter 2), a self-sustained oscillation can only appear when the derivative of the nonlinear excitation curve

around $\bar{p} \approx 0$ is greater than a small value $1 - \lambda$. This introduces the notion of an "oscillation threshold", which is the set of minimum excitation model parameter values that satisfies this condition. The oscillation threshold has been extensively studied for the case of single-reed instruments (e.g. (Grand et al., 1997; Dalmont et al., 2005)). An approximate formula has been derived for the minimum dimensionless mouth pressure, by considering a resonator with a single resonance mode and $Z(\omega = 0) = 0$ (Dalmont et al., 2005):

$$\gamma_{\text{th}} \approx \frac{1}{3} - \frac{\ln(\lambda)}{\zeta 3\sqrt{3}}. \tag{65}$$

Theorem 3 in section 2.3 states that the amplitude of the sustained mouthpiece pressure, $\tilde{\bar{p}}_{\text{a}}$, is found from the intersection of the characteristic curve with its $\tilde{\bar{q}}$-axis mirrored curve: $\tilde{\bar{q}}_{\text{a}}(\tilde{\bar{p}}_{\text{a}}) = \tilde{\bar{q}}_{\text{a}}(-\tilde{\bar{p}}_{\text{a}})$. While the calculation of an analytical solution is complicated when resonator losses are taken into account, an approximate formula for a lossless resonator case is fairly easy to obtain, resulting in (Chaigne and Kergomard, 2013):

$$\begin{cases} \bar{p}_{\text{a}} = \sqrt{(3\gamma - 1)(1 - \gamma)} & \text{for } \gamma < 1/2 \\ \bar{p}_{\text{a}} = \gamma & \text{for } \gamma \geq 1/2 \end{cases} \tag{66}$$

For the case where frequency independent losses are included, the amplitude of oscillation can be found graphically, by studying the progression of the outer intersections, which is illustrated in figure 35.

Meanwhile, theorem 4 in section 2.3 states that the "spectral richness" in the steady-state regime is proportional to the RMS of the normalised mouthpiece pressure wave and therefore to the integration of the gradient under the excitation curve; and theorem 5 provides a protocol for the estimation of the even harmonics content of the steady state sound, which is related to the even (symmetric) component of the excitation curve.

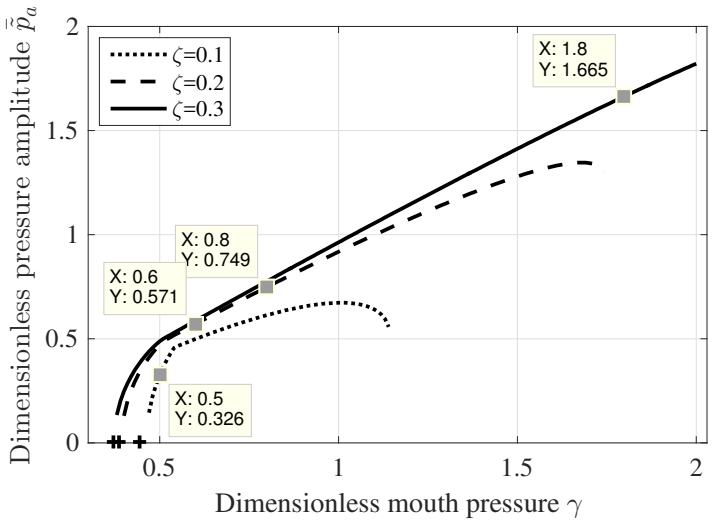

Figure 35: Evolutions of the estimated dimensionless pressure amplitude for three ζ values and γ ranging from the oscillation threshold (indicated with a + symbol) until the extinction threshold.

These curves were originally presented in section 2.3, for a single-reed excitation with parameters $\gamma = 0.8$ and $\zeta = 0.2$, but for convenience are repeated here, in figure 36 (c).

Other values of the mouth pressure and global embouchure parameter result in different nonlinear curve shapes, enabling the estimation of the spectral richness and the even harmonics content as a function of the excitation parameters. Figures 36 (a) to (d) depict four arbitrary parameter states which demonstrate the variety of sound features this excitation model is expected to produce. In (a), a low $\zeta = 0.1$ and $\gamma = 0.5$ are applied; it can be seen that this results in a mainly symmetrical curve. The estimation of $\hat{\tilde{p}}_{\mathrm{RMS}}$ is obtained by integrating the gradient, i.e. by subtracting the amount of blue from the amount of green, resulting in the small amount of green that is captured in the upper right intersection of the dotted curves, thereby predicting a relatively low spectral richness. In (b), representing the state $\zeta = 0.2$, $\gamma = 0.6$, a much higher spectral richness is predicted and also the even component has significantly increased in amplitude, which is mainly due to the increased amplitude $\tilde{\tilde{p}}_{\mathrm{a}}$. However, in (c), with the same ζ and a slight increase of the mouth pressure to $\gamma = 0.8$, the gradient integration does not change significantly but the even component becomes par-

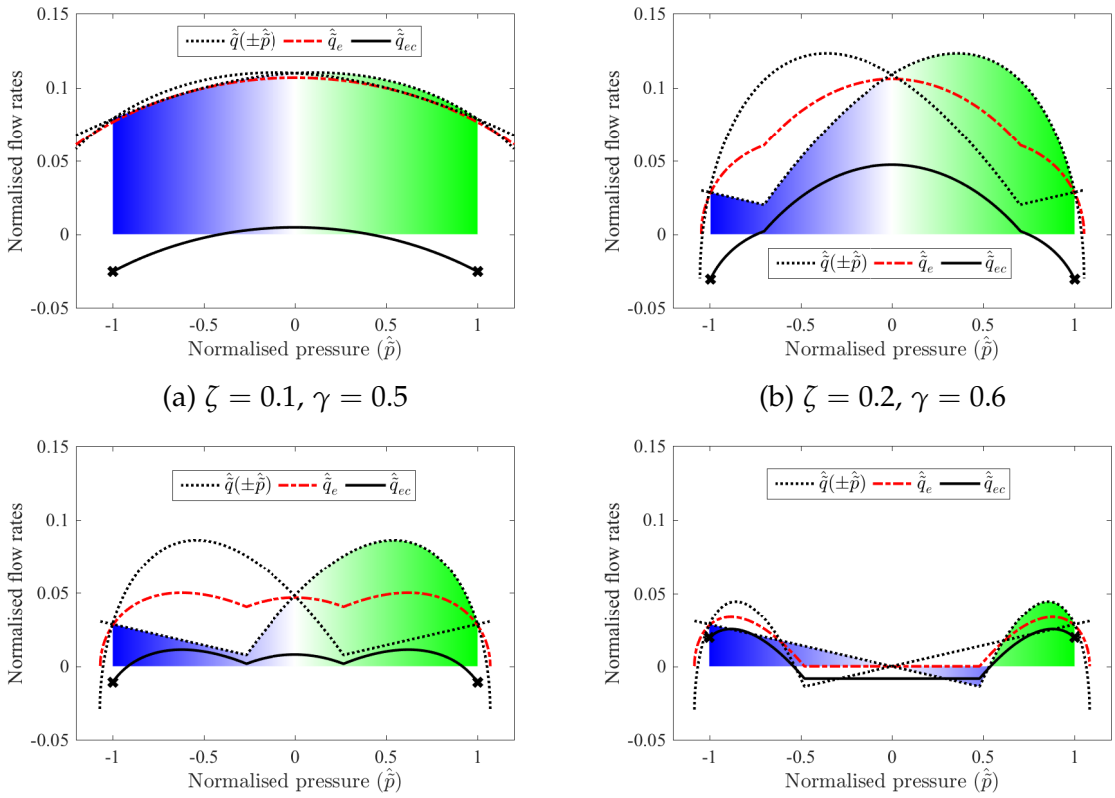

(a) $\zeta = 0.1$, $\gamma = 0.5$

(b) $\zeta = 0.2$, $\gamma = 0.6$

(c) $\zeta = 0.2$, $\gamma = 0.8$

(d) $\zeta = 0.3$, $\gamma = 1.8$

Figure 36: Nonlinear curves of the single-reed excitation model for four sets of parameters γ and ζ, with indication of the mean acoustic power estimation with a gradient (the amount of blue is to be subtracted from the amount of green); and the even component before and after the subtraction of the mean flow (respectively in dot-dashed red and solid black lines).

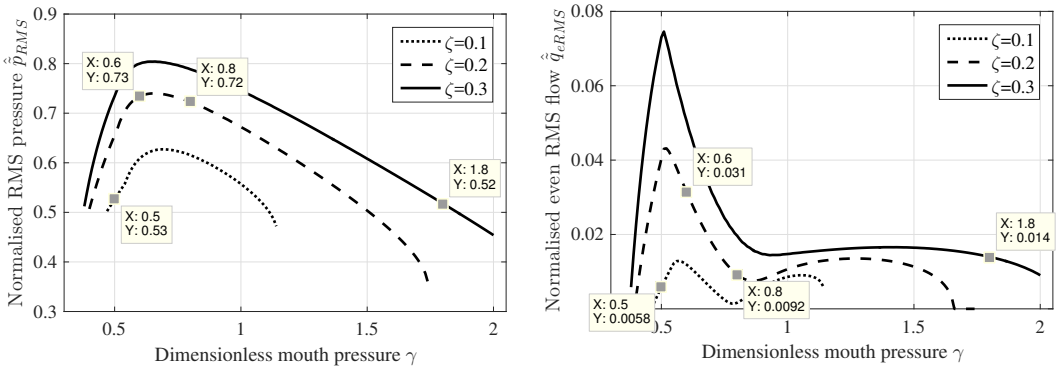

(a) (b)

Figure 37: Evolutions of the RMS of the normalised pressure wave $\hat{\tilde{p}}_{\text{RMS}}$ (a), and the RMS of the even harmonics normalised flow component $\hat{\tilde{q}}_{\text{eRMS}}$ (b), for three ζ values and γ ranging from the oscillation until the extinction threshold. The four parameter sets presented in figure 36 are marked as data points.

ticularly small for this γ. (It is interesting to note that the acoustic losses play an important role, as otherwise the outer intersections would lead to the introduction of far more even harmonics.) Finally, in (d), the embouchure parameter and mouth pressure are increased to $\zeta = 0.3$ and $\gamma = 1.8$, which results in a high oscillation amplitude, but as can be seen, the negative part of the gradient almost equals the positive part, which again leads to a particularly low spectral richness.

In figure 37, the RMS of the normalised pressure $\hat{\tilde{p}}_{\text{RMS}}$ and of the normalised even flow rate component $\hat{\tilde{q}}_{\text{eRMS}}$ (obtained using respectively equations (21) and (22)), are plotted for three ζ values and γ ranging from the oscillation to the extinction threshold. The four discussed parameter states are indicated and the curves will be referred to in chapter 5, where the experimental evaluation of the hybrid instrument is discussed.

It is interesting to note that, around $\gamma = 0.8$, $\hat{\tilde{p}}_{\text{RMS}}$ attains a maximum while $\hat{\tilde{q}}_{\text{eRMS}}$ goes to a minimum, which reflects the previous discussion concerning figure 36(c). It can be expected that this will be reflected in the evaluation by a rich timbre of mostly odd harmonics. Another general observation that might be expected is that the influence of ζ is mainly reflected in the amplitude of both curves; however, a low embouchure parameter also brings the oscillation

and extinction thresholds closer to each other, this can also be explained by the acoustic losses in the resonator.

4.3 LIP-REED MODEL

Another class of wind instruments uses the lips themselves as a "pressure-controlled valve system". This is the case for brass instruments (also called "labrosones", literally meaning "lip-vibrated instruments" (Baines, 1993)). In the acoustics literature the excitation type of brass instruments is also referred to as the "lip-reed". The acoustical functioning of the lip-reed shares similarities with the single-reed model, but there are differences which are of particular importance in explaining the appearance of oscillations when coupled to a resonator. Moreover, in contrast to the single-reed embouchure, small variations of the lips can have a large impact on the lip-reed behaviour, which makes its physical description more challenging (Campbell, 1999). Therefore, unlike the single-reed model, there is far less consensus on an established lip-reed model. While it is generally accepted that at least a second degree of freedom model is required, perceptually convincing simulations have still been obtained with single-degree of freedom (SDOF) models (see e.g. (Adachi and Sato, 1995; Vergez and Rodet, 2000)). Given the easier implementation and the less complex relation to the sound produced, as a first step, it is opted to employ a SDOF model in this thesis.

It should be mentioned that brass instruments have a typical timbre feature known as "brassiness", which is caused by the nonlinear propagation of high pressure waves in the resonator (Campbell, 1999). This feature is not conserved when the lip-reed is evaluated at a lower dynamic range when coupled to a clarinet resonator, which is generally the case for the hybrid wind instrument.

4.3.1 *Physical model*

Figure 38 shows a cross-section of the lips under playing conditions on a brass instrument's mouthpiece.

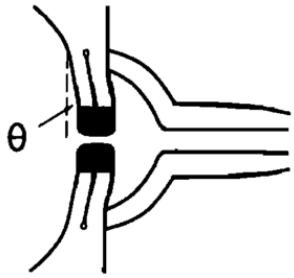

Figure 38: Schematic diagram showing the cross-section of lips in playing position on a brass mouthpiece. (Source: (Adachi and Sato, 1995))

GENERAL CONSIDERATIONS An important distinction is made between two main types of functioning of the lip-reed, which has been thoroughly studied by Fletcher (Fletcher, 1979b).

From a first viewpoint, the lips are considered to displace rotationally (as indicated in the schematic diagram of figure 38), with their movement controlled by the pressure difference acting across the lips. This model is referred to as the "swinging door" mechanism. As can be deduced from the schematic diagram, contrary to the single-reed model, where the reed closes in response to an increasing mouth pressure (i.e. it is "inward striking"), this reed type behaves in an opposite fashion (and is therefore said to be "outward striking"). This imposes important conditions on the reed's dynamic parameter values in order to obtain a functional instrument. This was already predicted by Helmholtz in 1877 (Helmholtz, 1877), who stipulated that an outward striking valve model requires its resonance frequency to be lower than the playing frequency, while the inward striking reed (such as the single-reed) requires the opposite condition. This is demonstrated in figure 39, where the lip displacement $y(p)$ for a high lip resonance frequency $\omega_r >> \omega_0$ does not result in the "negative resistance" (i.e. a positive-sloping curve in the $\{p, q\}$ coordinate system) that is required to

obtain the instability which can result in self-sustained oscillations. Instead, a negative resistance is obtained with a low lip resonance frequency, $\omega_r \lesssim \omega_0$, as the phase is turned towards $-180°$. It is worth noting that the lip resonance frequency should remain relatively close to the fundamental frequency, to enable sufficiently large lip displacements.

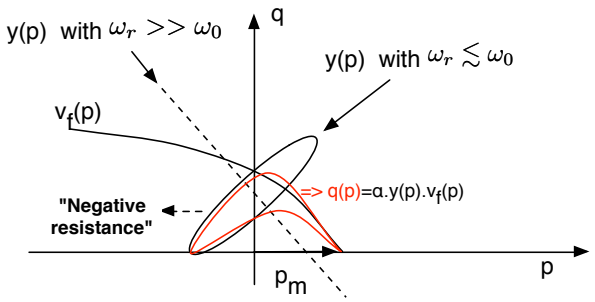

Figure 39: Curves in the $\{p, q\}$ coordinate system, related to the lip-reed's flow velocity $v(p)$ and the lip displacement $y(p)$, the latter is drawn for both high and low lip resonance frequencies. For $\omega_r \lesssim \omega_0$ the appearance of a negative resistance in the total $q(p)$ curve (in red) is demonstrated.

Another interpretation of the lip-reed's functioning is still supported by a considerable number of authors, who stress that the Bernoulli-force causes the lip-reed to move longitudinally. This is referred to as the "sliding door" principle (see e.g. (Adachi and Sato, 1995)), which leads to an operation that is equivalent to the inward striking reed. It is interesting to note that this model enables "lipping up", which is a technique achievable with a real brass embouchure, and occurs when the lip resonance frequency is above the frequency of the played note.

While most authors seem to agree on the swinging door model, it may be assumed that a real lip-reed is governed by both the sliding and swinging door mechanisms (which would require a higher dimensional model), and that the principally active mechanism depends on the applied embouchure. Interestingly, this hypothesis is experimentally supported by the findings of Chen and Weinreich (Chen and Weinreich, 1996), who constructed a simple hybrid wind instrument set-up for this research purpose. From the viewpoint of perception, both swinging and sliding door lip-reed models have resulted in satisfactory

results (Campbell, 1999). Vergez evaluated a model comprising both swinging and sliding door components and noted that the perceptual influence of the Bernoulli-force on synthesised sounds was small (Vergez and Rodet, 2000).

Finally, it has been concluded that for the evaluation of the hybrid wind instrument studied in this thesis, the swinging door model is an appropriate choice.

SIMILARITIES AND DIFFERENCES WITH THE SINGLE-REED MODEL Similar to the single-reed model, a SDOF mass-spring-damper system is set up as a valve mechanism. In addition, a few more refinements, related to the lip vibrations and valve functioning, have been adopted from different authors in order to obtain more realistic brass sounds. The employed model mainly draws on the one proposed by Vergez (Vergez and Rodet, 2000), but it also features a smoothened transition of the air-channel opening, as observed and implemented using a power function (Bromage et al., 2010). A schematic diagram of this model is presented in figure 40.

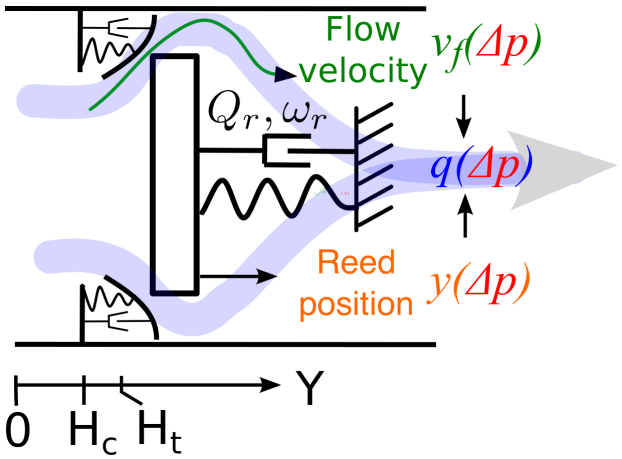

Figure 40: Schematic diagram of the employed lip-reed model.

The lips are assumed to displace with small rotations with an angle θ, so that the distance y between both lips is proportional to θ. Similar to the single-reed model, the pressure difference across the lips $\Delta p = p_m - p$ (with $p_m(t)$ the mouth pressure and $p(t)$ the pressure inside the mouthpiece) acts on an "effective" part of the lip surface S_r. Hence, for freely vibrating lips, apart from

an inverted pressure difference, the dynamic equation is the same as equation (51) for the single-reed model. Furthermore, the equation for the flow velocity is equal to equation (53) of the single-reed model.

INTRODUCING A LIP-COLLISION MODEL An important additional feature of the lip-reed model is when the lips start colliding. In contrast to the single-reed model, the much lower resonance frequency and the progressively introduced collision requires more precise modelling. Vergez assumes that the lip collision can be modelled by an increased stiffness k_c and damping coefficient r_c (while the mass remains equal) (Vergez and Rodet, 2000). Meanwhile, to model the smooth transition between the free and collided lip states, the parameters are gradually changed over a small transition range, which introduces displacement-dependent nonlinear reed parameters. Given that the dynamics are modelled in terms of the frequency ω_r and Q_r factor, the nonlinear stiffness is expressed by $\alpha_\omega(y)\omega_r$ and the nonlinear Q factor by $\alpha_Q(y)Q_r$. Thus, the dynamic equation becomes:

$$\frac{1}{(\alpha_\omega(y)\,\omega_r)^2}\frac{d^2\,y}{dt^2} + \frac{1}{\alpha_Q(y)Q_r\,\alpha_\omega(y)\omega_r}\frac{d\,y}{dt} + y = \frac{S_r(p_m - p)}{\alpha_\omega(y)k}. \tag{67}$$

At rest, without any pressures involved, i.e. when $p_m = p = 0$, the lips are assumed to be slightly pressed against each other. It should be noted that Vergez also assumes a closed lip position at rest but doesn't assume there to be any lip-stiffness stresses in this condition, whereas most authors do (see e.g. (Adachi and Sato, 1995)). The full collision-stiffness is thus defined to occur from $y \leq H_c$, while the collision starts happening at the threshold value H_t with a gradually increasing collision-stiffness (as can also be seen in figure 40).

THE LIP'S OPENING SECTION The lip displacement enables calculation of the opening area between both lips, which functions as a channel for the entering air flow. Msallam et al. (2000) found that the more realistically smooth transition from open to closed lips, plays an important role for the sound syn-

thesis, avoiding unrealistically harsh sounds. In order to understand this behaviour and propose a coherent model, Bromage et al. (2010) and Copley and Strong (1996) observed the lip vibrations with a high-speed camera, filming the lips through a transparent mouthpiece. They concluded that, depending on the played note and the used embouchure, the shape of the lip opening area could vary from almost rectangular to diamond-shaped. Bromage proposed an approximate formula, relating the lip displacement extrema to the opening area by a power function (Bromage et al., 2010), which can be adapted to the notation used for the comparable single-reed equation (eq. (52)):

$$S_f = \mathcal{H}(y - H_c)\left(\frac{y - H_c}{H_c}\right)^{\epsilon} H_c w, \tag{68}$$

where w is the effective lip opening width and ϵ is an arbitrary exponent that is found by regression on measured lip-opening area-variations.

NON-DIMENSIONALISING AND PARAMETER VALUES Since the additional features of the proposed lip-reed model are all expressed as factored versions of the parameters of the single-reed model, and given the general similarity with that model, a set of dimensionless equations can be obtained in a similar fashion. Hence, by defining $\bar{y} = \frac{y}{H_c}$, $\gamma = \frac{p_m}{P_M}$, $\bar{p} = \frac{p}{P_M}$ and $\bar{q} = \frac{q\, Z_c}{P_M}$, the dimensionless equation for the lip-reed dynamics becomes:

$$\frac{1}{(\alpha_\omega(\bar{y})\,\omega_r)^2}\frac{d^2\,\bar{y}}{dt^2} + \frac{1}{\alpha_Q(\bar{y})Q_r\,\alpha_\omega(\bar{y})\omega_r}\frac{d\,\bar{y}}{dt} + y = \frac{\gamma - \bar{p}}{\alpha_\omega^2(\bar{y})}. \tag{69}$$

As Vergez's lip collision parameter values are expressed relative to the "free" lip stiffness and damping, by respectively $k_c = 4k$ (as proposed by e.g. Strong (1990)) and $r_c = 5r$ (proposed by e.g. Rodet and Depalle (1990)), the nonlinear lip resonance frequency and quality factors are provided in the following table:

	$\bar{y} < 1$	$1 \leq \bar{y} < 1.2$	$1.2 \leq \bar{y}$
$\alpha_\omega(\bar{y})$	$\sqrt{k_c/k} = 2$	$-5\bar{y} + 7$	1
$\alpha_Q(\bar{y})$	$\frac{\sqrt{k_c/k}}{r_c/r} = \frac{2}{5}$	$3\bar{y} - 2.6$	1

Meanwhile, the dimensionless equation for the lip opening section is expressed as follows:

$$\bar{S}_f = \zeta \mathcal{H}(\bar{y} - 1)(\bar{y} - 1)^\epsilon. \tag{70}$$

For a playing frequency around 140 Hz, the exponent is found to be around $\epsilon \approx 1.5$ to 1.8, based on regressions on data from two players (Bromage et al., 2010). For the evaluation of the hybrid wind instrument, ϵ is kept constant at 1.5, which resulted in the most realistic sounds.

It can be noted that the lip-reed model contains many more independent control parameters than the single-reed model, which is a consequence of the greater complexity of this embouchure type. Some parameters are common to the embouchure models and play the same role, such as P_M, which determines the signal amplitude without timbre variation (within the linear dynamic range of a resonator). However others have a different influence, which will be further discussed in subsection 4.3.3.

Just as for the single-reed model, the global embouchure parameter $\zeta = Z_c w \sqrt{\frac{2H_c}{\rho k}}$ lumps a number of embouchure parameters together. For constant resonator and mouthpiece parameters (ρ, Z_c, w and k), ζ is proportional to the square root of the the lip opening area at rest, which is related to the force used to squeeze the lips together. Given that many aspects of a real lip embouchure are difficult to measure, the parameters w, H_c, k and therefore ζ are unknown. Consequently, the range of ζ values is chosen in accordance with a realistic sound output.

Meanwhile, the lip resonance frequency is of great importance for selecting the desired register and when "lipping" the playing frequency down or up. While for a real lip-reed, the lip resonance frequency is also mainly controlled

by the lip force, the resonance frequency is independently evaluated in this thesis, so that the independent influence of this feature can be revealed.

4.3.2 *Making discrete and explicit*

An entirely correct discretisation of the dynamic equation (eq. (69)) is not straightforward, as the equation contains nonlinearities that depend on the output, i.e. the α coefficients vary with the reed position $\bar{y}$. In other words, the equation is implicit in itself and there is no analytic explicit solution. Nevertheless, it is possible to simply introduce a sample-delay for the calculation of the α coefficients, i.e. using $\bar{y}_{n-1}$. This is empirically found to lead to a stable approximation, which may be due to the fact that the variations of the resonance frequency and the Q-factor are relatively small. Hence, the procedure to make the lip-reed model's equations implicit becomes entirely analogous to that used for the single-reed. The dynamic equation is discretised by using the classical central difference scheme, so that a different equation of the same form as eq. (60) is obtained:

$$\bar{y}_n = 0 \times \bar{\Delta p}_n + b_1 \bar{\Delta p}_{n-1} + a_1 \bar{y}_{n-1} + a_2 \bar{y}_{n-2}. \tag{71}$$

Here, the coefficients are:

$$\begin{cases} a_0 &= 1 + \frac{T\alpha_\omega(\bar{y}_{n-1}}{)}\,\omega_r 2\alpha_Q(\bar{y}_{n-1})\,Q_r \\ b_1 &= \left(-T^2\omega_r^2\right) / \left(\alpha_\omega(\bar{y}_{n-1})\,a_0\right) \\ a_1 &= \left(2 - T^2(\alpha_\omega(\bar{y}_{n-1})\,\omega_r)^2\right) / a_0 \\ a_2 &= \left(\frac{T\alpha_\omega(\bar{y}_{n-1}}{)}\,\omega_r 2\alpha_Q(\bar{y}_{n-1})\,Q_r - 1\right) / a_0 \end{cases} \tag{72}$$

which are all equal to the coefficients of the single-reed case, except for the inclusion of the $\alpha_\omega(\bar{y}_{n-1})$ and $\alpha_Q(\bar{y}_{n-1})$ coefficients and the inversion of the b_1 coefficient, which is due to the outward striking reed behaviour.

The subsequent discretisation steps are also similar to those used for the single-reed model. The $\bar{S}_{\mathrm{f}n}$ term, provided by equation (70), is written discretely as:

$$\bar{S}_{\mathrm{f}n} = \zeta \mathcal{H}(\bar{y}_n - 1)(\bar{y}_n - 1)^{\epsilon}. \tag{73}$$

Finally, the entire development to analytically obtain the explicit expression for the square root component resulting from the Bernoulli equation is identical to the development for the single-reed, resulting in the explicit solution:

$$\bar{q}_n = \frac{1}{2}\,\mathrm{sgn}\,(\gamma - \bar{p}_{\mathrm{h}n})\bar{S}_{\mathrm{f}n}^2 \left(\sqrt{1 + \frac{4|\gamma - \bar{p}_{\mathrm{h}n}|}{\bar{S}_{\mathrm{f}n}^2}} - 1 \right). \tag{74}$$

For the lip-reed, the computational process consists of the sequential evaluation of equations (71), (73) and (74). And also just as for the single-reed model, and as mentioned in subsection 4.1.2, due to the inevitable delay of the computing system $\bar{p}_{\mathrm{h}n-1} = \bar{p}_{n-1} - \bar{q}_{n-1}$ is used instead of $\bar{p}_{\mathrm{h}n}$ in equation (74).

For future work, it is interesting to note that more advanced lip-reed models (e.g. multidimensional models) can also be analytically made explicit by following van Walstijn's filter implementation (van Walstijn, 2002).

4.3.3 *Predicting the influence on the sound*

As mentioned in subsection 2.2.2, dynamic excitation models have properties that make the estimation of sound features cumbersome. One way to understand this is to realise that an excitation mechanism of this type can store energy using its dynamic properties, which allows for a weaker coupling between the excitation and the resonator, resulting in a stronger influence of the excitation properties on the sound. While more complex, the low lip-resonance frequency imposes a strong low-pass filter effect, which results in displacement, pressure and flow rate signals that are much closer to sinusoidal than for the case of the quasistatic single-reed. Therefore, this sinusoidal approximation is taken as a

first general assumption in this sound features prediction study. Furthermore, the lip collision model also complicates the intuitive understanding. Given its relatively small influence, this feature is left out as a second general simplification.

The end result is that two approximated cases are considered here, each of which result in useful indications for isolated parameter cases.

Quasistatic approximation

One solution is to consider a quasistatic approximation of the dynamical model, which enables the application of the theorems derived in section 2.3. However, it is important to realise that the quasistatic condition is easily violated, which results in both systematic and random error. For instance, important features that are characteristic to the lip-reed model, such as the variation of the playing frequency, cannot be explained with the quasistatic assumption. Furthermore, the playing frequency is much more shifted from the resonator's resonance frequencies, compared to real quasistatic models, which in turn affects the calculation of dissipated power in the resonator (see subsection 2.3.2). This somewhat invalidates the calculation of the normalised RMS pressures and flow rates, so that only the trends of those results should be considered.

The quasistatic assumption made for the lip-reed relies on the fact that the lip resonance frequency must be smaller than the playing frequency, in order to become a "negative resistance", as demonstrated in figure 39. The (close to sinusoidal) lip displacement signal becomes in phase with the pressure signal, i.e. $\bar{y} \propto \bar{p}$. This can be understood by first considering the mean component of all oscillations. Neglecting all time varying signals in equation (69), it can be concluded that $< \bar{y} >= \gamma$. Then, focussing on only the time varying components and considering the case where ω_r is low, only the inertial term on the left side of equation (69) remains and only the dimensionless mouthpiece pressure remains on the right side, so that the equation reduces to $\frac{1}{\omega_r^2} \frac{d^2 \bar{y}}{dt^2} \approx -\bar{p}$. Integration (considering $\bar{p} \approx |\bar{p}|.\sin(\omega_0 t)$) and addition of the the mean value

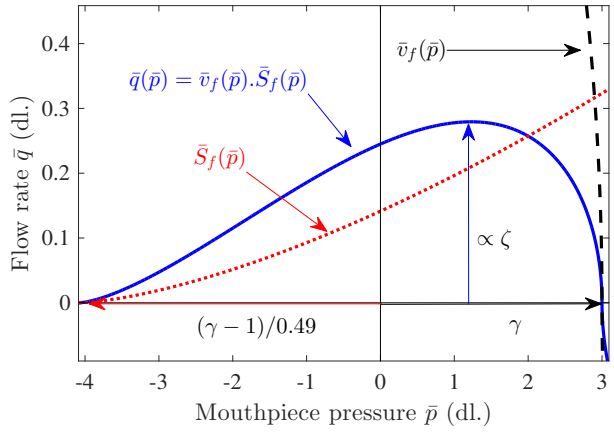

Figure 41: Dimensionless curves of the velocity, the reed opening area and the resulting volume flow rate, as a function of the pressure in the mouthpiece, for a quasistatic approximation of the lip-reed model with a dimensionless mouth pressure of $\gamma = 0.5$ and an embouchure parameter $\zeta = 0.4$.

then gives $\bar{y} \approx \gamma + (\frac{\omega_r}{\omega_0})^2 \bar{p}$ and, using equation (70), this gives the quasistatic approximation of the lip-reed channel opening:

$$\bar{S}_f \approx \zeta \mathcal{H}(\gamma + (\frac{\omega_r}{\omega_0})^2 \bar{p} - 1)(\gamma + (\frac{\omega_r}{\omega_0})^2 \bar{p} - 1)^\epsilon. \tag{75}$$

The frequency interval between the lip resonance frequency and the first resonance frequency of the resonator (ω_1) is much larger than the interval between the latter and the playing frequency (ω_0). With for example $\omega_r = 0.7\,\omega_1 \approx 0.7\,\omega_0$, the scaling parameter for $\bar{p}$ in equation (75) (using $\omega = \omega_0$) is $0.7^2 = 0.49$. This finally results in the nonlinear curve shown in figure 41, which is of similar shape as for the single-reed model, shown in figure 34. Though, the transition to the closed state is smoother, which is due to the opening section exponent ϵ.

Despite the similarity in shape and the similar influence of ζ for both models, the influence of the mouth pressure plays a quite different role here, which can be recognised from the fact that for the calculation of the reed opening section $\bar{S}_f(\bar{p})$, both γ and the 1 offset (representing the initial opening) are opposite in sign between lip-reed and single-reed models. For the lip-reed, a minimum pressure of $\gamma = 1$ is required for an initial opening between the lips and the mean lip-displacement is further proportional to γ, i.e. the nonlinear curve is widening with increasing γ. For the single-reed model however, the reed is ini-

tially open with no pressures involved and an increasing mouth pressure shifts the mean opening towards 0, resulting in an increasing shift of the nonlinear curve.

This different parameter influence has opposite consequences for the amplitude of oscillation and for the spectral predictions.

The intersection method stipulated by theorem 3 (which is illustrated for two particular parameter states with this model with the dotted curves in figure 43), predicts progressively increasing oscillation amplitudes for both the single-reed and lip-reed models, but there is no extinction predicted with the lip-reed model, as can be seen in respectively figures 35 and 42 (note that the displayed parameter ranges correspond to the ranges used for the evaluations in chapter 5).

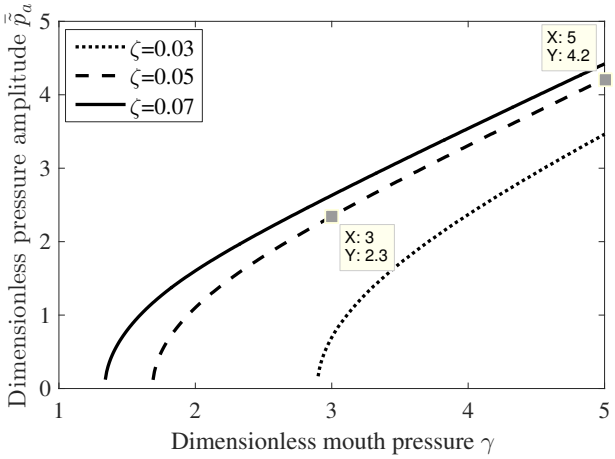

Figure 42: Evolutions of the estimated dimensionless pressure amplitude for three ζ values and γ ranging from the oscillation threshold until an arbitrary value. The two parameter sets presented in figure 43 are marked as data points.

Furthermore, as can be seen in figure 43, an increasing mouth pressure with the lip reed increases the normalised power introduced in the resonator (which is proportional to the integration of the gradient), as well as an increasing even flow component.

This suggests an opposite trend in terms of both the RMS of the normalised pressure wave $\hat{\tilde{p}}_{\mathrm{RMS}}$ and the RMS of the even harmonics normalised flow component $\hat{\tilde{q}}_{\mathrm{eRMS}}$ to that seen for the single-reed model. This is confirmed by

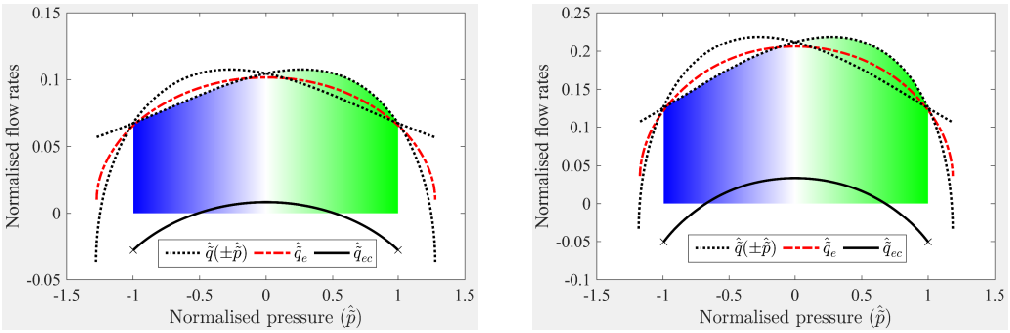

(a) $\zeta = 0.05$, $\gamma = 3$ (b) $\zeta = 0.05$, $\gamma = 5$

Figure 43: Nonlinear curves of the quasistatically approximated lip-reed excitation model for $\zeta = 0.05$ and two values of γ. The mean acoustic power estimation is indicated with a gradient (the amount of blue is to be subtracted from the amount of green); and the even component before and after the subtraction of the mean flow (respectively in dot-dashed red and solid black lines).

comparing the relevant curves for the single-reed model in figure 37 and for the lip-reed model in figure 44, where the latter results in progressive increases with γ.

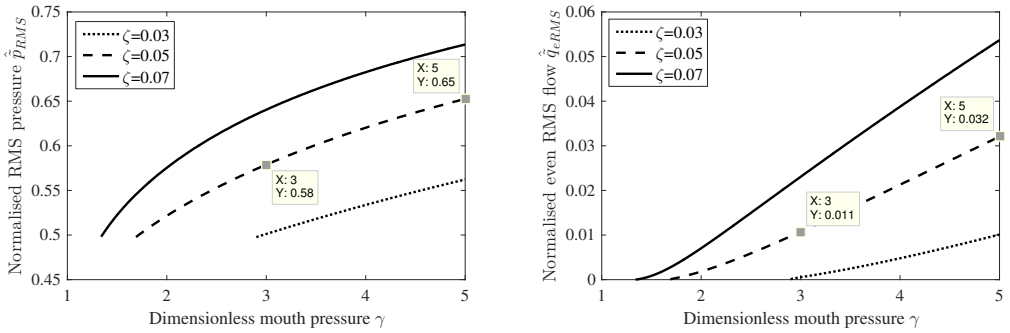

(a) (b)

Figure 44: Evolutions of the RMS of the normalised pressure wave $\hat{\tilde{p}}_{\text{RMS}}$ (a), and the RMS of the even harmonics normalised flow component $\hat{\tilde{q}}_{\text{eRMS}}$ (b), for three ζ values and γ ranging from the oscillation threshold until an arbitrary value. The two parameter sets presented in figure 43 are marked as data points.

Small-signal approximation

Another way to obtain useful clues regarding the properties of the self-sustained operation is to re-consider the model from scratch and to introduce other approximations, which are reasonable with respect to the operation. By neglecting the lip-beating and the nonlinear variation of the lip opening area, the model is

compatible with the generalised model used by Fletcher, who proposed a theory to obtain oscillation properties generated by "pressure-controlled valves" in gas flows (Fletcher, 1993). Very recently Velut extended this theory (Velut et al., 2017), but Fletcher's findings are sufficient for the current study.

Fletcher's approach was to express the force balance around the lip dynamics, consisting of the mass-spring-damper forces on the one hand and the acoustic force exerted by the resonator on the other hand. The latter is here expressed as an "acoustic stiffness" $K_a(\omega)$, a frequency dependent complex quantity that depends both on the resonator impedance and the lip-reed model parameters. In the frequency domain this gives:

$$-\left(\frac{\omega}{\omega_r}\right)^2 \bar{Y} + \frac{j\omega}{\omega_r Q_r}\bar{Y} + \bar{Y} = K_a(\omega)\bar{Y}, \tag{76}$$

where the parameter names are chosen to correspond with the current study and $\bar{Y}$ is the frequency domain response of the dimensionless reed displacement.

The general equation for K_a proposed in (Fletcher, 1993) also considers an acoustic impedance in front of the reed, which is left out here (by simply putting it to zero in Fletcher's equations). Furthermore, the equation is non-dimensionalised so as to match the dimensionless form used here, so that finally Fletcher's result reduces to:

$$K_a(\omega) = \frac{2\gamma}{\frac{\sqrt{2\gamma}}{\bar{Z}_t(\omega)\zeta} + 1 - \gamma}, \tag{77}$$

with $\bar{Z}_t = Z_t/Z_c$, the dimensionless input impedance of the resonator.

By then considering only the real part of each side of the equality expressed in (76), the expression reduces to:

$$\left(\frac{\omega}{\omega_r}\right)^2 = 1 - Re\left(K_a(\omega)\right), \tag{78}$$

whose solutions provide an indication of the self-sustained oscillation frequency ω_0.

Then, the imaginary part of equation (76) gives an indication of the total losses in the system and therefore can be used to verify if self-sustained oscillation is possible at the found frequency. Somewhat similar to theorem 1 in chapter (2) (but including the resonator impedance), this is the case when a "negative resistance" is present, i.e. if the following condition holds at $\omega = \omega_0$:

$$1 < \frac{Im\left(K_a(\omega)\right)\ \omega_r Q_r}{\omega}. \tag{79}$$

When satisfied, the negative resistance of the lip-reed model compensates for the dissipation (i.e. the acoustic losses) in the resonator. The term on the right of this equation is therefore referred to as the "dissipation ratio".

For both equation (78) and equation (79), it is not possible to find an analytical solution, as K_a depends on Z_t. Instead, a numerical calculation can be carried out, which can be graphically demonstrated, as shown in figure 45.

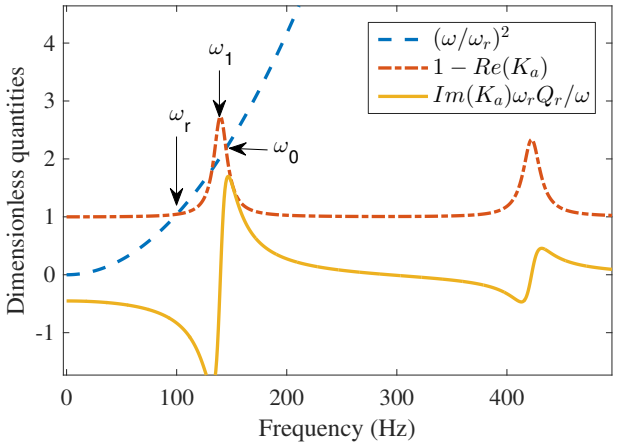

Figure 45: Graphical demonstration to provide the solutions of equation (78) (the intersections between the dashed blue and dot-dashed red curves) and to verify condition (79) (which holds when the solid yellow curve exceeds 1), for arbitrary lip-reed parameters.

The blue dashed curve corresponds to the left-hand side of equation (78) and is only related to the lip-resonance frequency, the red dash-dotted curve refers to the right-hand side of that equation and the solid yellow curve corresponds to equation (79). To obtain the resulting oscillation features for this case, first the intersections of the blue and red curves are studied, which reveals the oscillation frequency above a resonator resonance frequency ω_i (with $i \in \{1, 2, ...\}$).

Note that this can result in more than one "candidate" oscillation frequencies. Then, the imaginary component at these frequencies is verified. If a value above 1 is found, the oscillation condition is satisfied, and in the case of more than one candidate oscillation frequencies, the highest value indicates the chosen register and thereby the actual oscillation frequency ω_0.

This numerical procedure is repeated for the evaluated range of parameter values and the resulting predicted oscillation frequency evolutions (in Hertz $f_0 = \frac{\omega_0}{2\pi}$) are shown in figure 46, for three ζ values and γ progressions in (a) and for a lip-resonance frequency progression in (b).

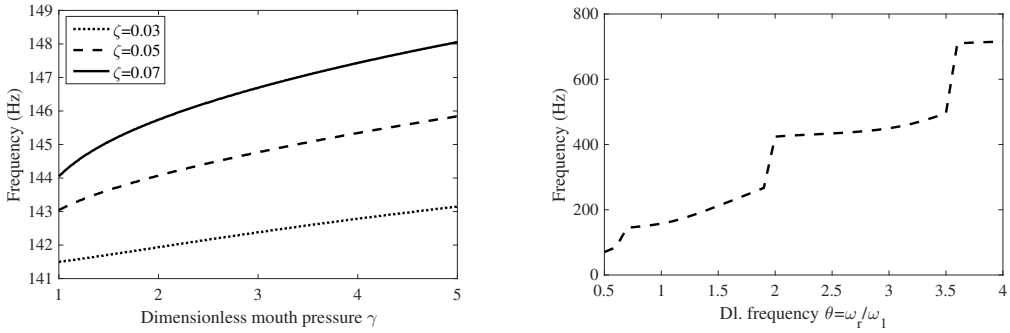

(a) (b)

Figure 46: Predicted oscillation frequency evolutions, for three ζ values and γ progressions (a), and for a dimensionless lip-resonance frequency θ progression (b).

Note that the latter is shown as a dimensionless frequency, relative to the frequency of the first tube resonance $\theta = \frac{\omega_r}{\omega_1}$.

It can be seen that ζ, γ, but particularly θ, are positively correlated to the playing frequency. For ζ and γ this is due to their decreasing influence on the real value of $K_a(\omega \approx \omega_0)$, and for all cases this can be understood from equation (78) and from figure 45. The increasing lip-resonance frequency also evokes register jumps, which are more clearly indicated by the dissipation ratio evolutions in figure 47 (plotted for the same parameter ranges).

It can be seen that the mouth pressure evaluations in figure 47 (a) all result in positive oscillation conditions (i.e. the curves all lie above 1), though for $\zeta = 0.03$ and $\gamma \approx 2.3$, the curve comes close to 1. For the lip-reed progression

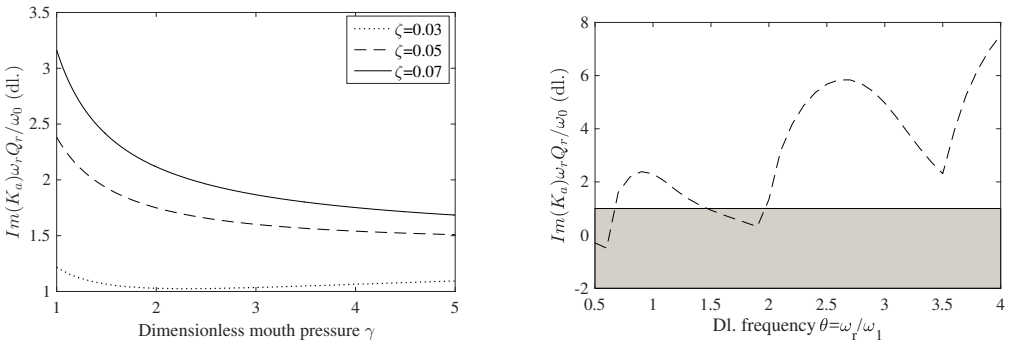

(a) (b)

Figure 47: The dissipation ratio , for three ζ values and γ progressions (a), and for a dimensionless lip-resonance frequency θ progression (b).

in figure 47 (b), it can be seen how the registers are selected and how the first register is surrounded by a prediction of a non-oscillatory state.

4.4 BOW-STRING INTERACTION MODEL

Given that the excitation of a hybrid wind instrument is performed by a computer, any excitation process that leads to self-sustained oscillations can be considered for implementation. A first thought was to implement existing physical excitation models of non-wind musical instruments. Knowing that both the excitation mechanism and the resonator are responsible for the characteristic sounds of each instrument, it can be anticipated that such a combination will produce a sound and functioning that contains a mixture of characteristics of the wind and non-wind instrument. Such features could most likely lead towards answers to the musical research question that is formulated in this dissertation.

A good starting point is to consider the excitation mechanism of bowed string instruments, as it is demonstrated that this class of typical self-sustained instruments has a closely analogous operation to wind-instruments.

4.4.1 *Common features of self-sustained instruments*

As McIntyre et al. (McIntyre et al., 1983) and later e.g. Ollivier et al. (Ollivier et al., 2004) have pointed out, there are significant common features in the fundamental physical functioning of instruments that produce self-sustained tones. They all consist of a resonator that is coupled to an excitation mechanism, with the resonator and excitation mechanism imposing respectively a linear and a nonlinear relationship between two physical quantities, so that the combined relationships can result in a self-sustained oscillation. As such, the sound production of a single-reed instrument can be compared to that of a bowed-string instrument; the resonator being respectively the vibrating air column and the string (when symmetrical and bowed exactly at its midpoint), the excitation mechanism being respectively the embouchure and the bow-string interaction, and the physical quantities being the pressure-air flow rate coupling and the bow-string velocity-force coupling.

This analogy inspired the idea of using the hybrid instrument to combine the bow-string interaction mechanism with an acoustic resonator. The computer allows a pressure and flow rate signal to be interpreted as if it were respectively the velocity and force between a bow and a string. The physical model discussed in this section only concerns physical units in the context of bowed strings (i.e. velocity and force), the switch to pressure and flow rate is made later in the evaluation in chapter 183.

4.4.2 *Physical model*

The study of the bowed string dates back to at least 1877, when Helmholtz discovered the typical triangular-shaped string motion (Helmholtz, 1877), which is still referred to as "Helmholtz motion". Figures 48 and 49 depict a diagram and a schematic demonstration of a string bowed at its midpoint. The key principle that enables an oscillatory energy transfer from the bow to the string, is

that the portion of the string that is in contact with the bow alternates between "sticking" and "slipping" phases. In the former case, its velocity equals that of the bow, while in the latter case, the string velocity is of equal amplitude but travels in the opposite direction. The corner or "kink" in the string travels back and forth, crossing the midpoint of the string vibration at the nut and at the bridge.

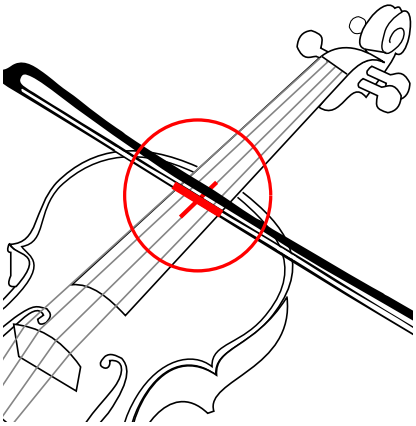

Figure 48: A bowed violin, with indication of the bow-string interaction location, on the middle of a string.

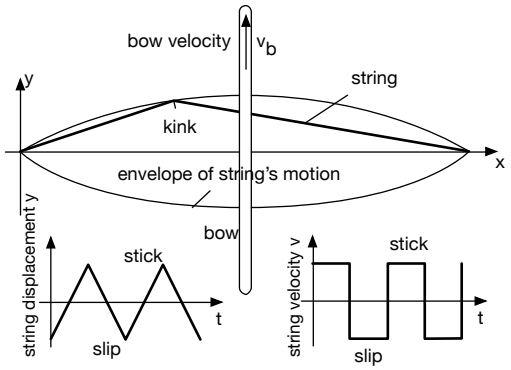

Figure 49: Schematic representation of the oscillations occurring when a string is bowed on its midpoint.

An aspect of the bow-string interaction that is not covered by the chosen model are the introduced noise pulses as the string periodically scrapes the bow hair during the slipping phase. This phenomenon introduces a particular periodical noise component that could be taken into account by using the phenomenological model proposed by Chafe (Chafe, 1990) (based on an analysis of recorded tones). While for the current study this aspect is left out for simplicity,

it may be of interest for later implementations, to achieve a more realistic sound quality.

HYPERBOLIC MODEL WITH ABSORBED TORSIONAL STRING WAVES In contrast to the single-reed case, several bow-string interaction models (hereafter referred to as "bow-string models") are currently in common usage, which is probably due to the empirical persistence of elementary models that allow mathematical simplicity and result in reasonably realistic sounds. For simplicity, it was initially decided to employ the "hyperbolic model" on the hybrid instrument, which employs a quasistatic but physically relevant stick-slip mechanism[2].

In this model, during the "sticking phase", the velocity difference between bow and string surface $\Delta v'(t)$ remains zero until the force $f(t)$ between those parts reaches a break-away "sticktion" force $f_b \mu_s$ (with f_b the bow force and μ_s the static friction coefficient), resulting in a velocity relation conditioned by a force threshold:

$$\Delta v' = 0 \quad \text{if} \quad f < f_b \mu_s. \tag{80}$$

During the "slipping phase", a kinetic "Coulomb" (viscous-less) friction with the Stribeck effect occurs as long as the bow and string differ in velocity, which results in a force relation conditioned by a velocity threshold:

$$f = sgn(\Delta v') f_b (\mu_d + \frac{(\mu_s - \mu_d) v_0}{|\Delta v'| + v_0}) \quad \text{if} \quad \Delta v' \neq 0, \tag{81}$$

where μ_d is the dynamic friction coefficient and v_0 is a characteristic velocity.

2 It should be noted that the hyperbolic model is somewhat outdated. Newer, more accurate models have been proposed more recently (Serafin, 2004; Smith and Woodhouse, 2000; Mansour et al., 2016), taking into account the thermal effects of rosin on the bow (designated by the term "tribology", which is the study of the interaction of surfaces in relative motion).

It has been reported that the quality of simulations is significantly improved by including the string rotations in this model (McIntyre et al., 1983). By defining $\Delta v(t) = v_b - v(t)$ as the difference between the bow and the string axis, the previous velocity difference can be expressed as :

$$\Delta v' = \Delta v - \frac{f}{2Z_R}, \tag{82}$$

where Z_R is the characteristic impedance for torsional waves. Note that these waves are assumed to be completely absorbed so that no reflections are considered. This modelling enables the sticking phase (equation (80)) to also be expressed as a force relation conditioned by a velocity threshold, which simplifies simulation.

It is worth noting that Weinreich and Caussé used a simplified formula to model the stick-slip phenomenon to evaluate their hybrid string instrument (Weinreich and Caussé, 1991). The formula was a reciprocal second order function, chosen for its simplicity and its resemblance to the nonlinear curve of the hyperbolic model; however, the parameters in this simplified formula are not in good agreement with the real physical model. Nevertheless, Weinreich's model was later adopted by Ollivier et al. to demonstrate the similarity between reed woodwinds and bowed-string instruments (Ollivier et al., 2004). Also Karkar continued using Weinreich's model, as it was a convenient formula to predict the oscillations in the steady state regime with a "continuation approach" (Karkar, 2012).

A DIMENSIONLESS AND REDUCED PARAMETER FORM Just as for the single-reed model, it is possible to rewrite the equations of this bow-string model using dimensionless quantities and with a reduced set of independent input parameters. The reduced and dimensionless form newly proposed here enables an interesting comparison with the single-reed model. By introducing the dimensionless force $\bar{f} = \frac{f}{2Z_c v_0}$ (where Z_c represents the characteristic impedance of the acoustic resonator, when implemented on the hybrid instrument)

and velocity $\bar{\Delta v} = \frac{\Delta v}{v_0}$ (with v_0 a characteristic velocity) and using equation (82), equations (80) and (81) can be rewritten and combined as:

$$\bar{f} = \begin{cases} \bar{f}_{\text{sl}} = sgn(\bar{\Delta v})\zeta_{\text{b}}(\delta + \frac{1-\delta}{|\bar{\Delta v} - \alpha\bar{f}|+1}) & \text{if } |\bar{\Delta v}| > \alpha\zeta_{\text{b}} \\ \bar{f}_{\text{st}} = \frac{\bar{\Delta v}}{\alpha} & \text{if } |\bar{\Delta v}| \leq \alpha\zeta_{\text{b}}, \end{cases} \tag{83}$$

where $\zeta_{\text{b}} = \bar{f}_{\text{b}}\mu_{\text{s}} = \frac{f_{\text{b}}\mu_{\text{s}}}{2Z_{\text{c}}v_0}$, $\delta = \frac{\mu_{\text{d}}}{\mu_{\text{s}}}$ and $\alpha = \frac{Z_{\text{c}}}{Z_{\text{R}}}$. This form shows that the parameter v_0 is solely controlling the amplitude of the oscillations (for a bowing force proportionally varying with v_0, i.e. for a constant $\bar{f}_{\text{b}}$). Due to the fact that μ_{s} and $\bar{f}_{\text{b}}$ play the same role (for constant δ), these parameters are merged into a global bow-force related parameter ζ_{b} (chosen in analogy to the embouchure parameter ζ). While there is still an $\alpha\bar{f}$ term in the equation of the slipping branch, it is small enough compared with $\bar{\Delta v}$ for typical bow-string model parameters so that ζ_{b} is almost directly proportionally controlling the excitation amplitude of that curve. While this term prevents the verification of the hysteretic condition with theorem 2, this condition can be verified after making the model explicit, which is carried out in the next subsection.

Also in analogy with the single-reed model, the dimensionless bowing velocity is introduced $\gamma_{\text{b}} = \frac{v_{\text{b}}}{v_0}$, so that $\bar{\Delta v}$=$\gamma_{\text{b}} - \bar{v}$, where $\bar{v} = \frac{v}{v_0}$ is the dimensionless velocity of the string axis.

Figure 50 shows the resulting characteristic nonlinear curve in the dimensionless $\{\bar{v}, \bar{f}\}$ coordinate system for a set of arbitrary typical parameters. The anti-symmetry around $\bar{v} = \gamma_{\text{b}}$ indicates that the model behaves analogously for up and down bowing (i.e. positive and negative bowing velocities). The linear part of the curve corresponds to the sticking state, where the constant torsional impedance is considered: $\bar{f}/\bar{v} = 1/\alpha$; and the hyperbolical part corresponds to the slipping state, whose decrement is proportional to $1/\delta$.

The two main, variable control parameters are the dimensionless bow velocity γ_{b} and bow force ζ_{b}, and typical parameter values are $v_0 \approx 0.2\,\text{m/s}$, $\delta \approx [3/8, 2/4]$, $\alpha \approx [0.26, 1]$, $\zeta_{\text{b}} \approx \frac{[10,50]}{\text{N}} f_{\text{b}}$, with $f_{\text{b}} \approx [0.15, 3]\text{N}$ and $\gamma_{\text{b}} \approx$

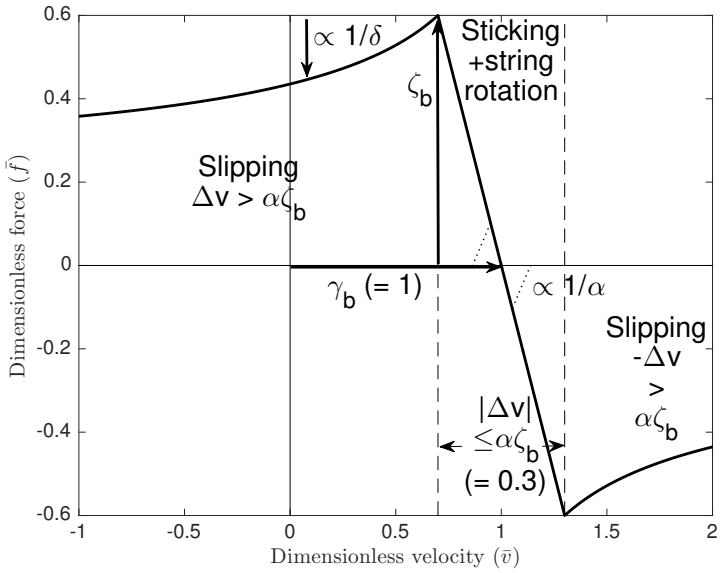

Figure 50: The characteristic nonlinear curve of the dimensionless bow-string model, with indication of the influence by its parameters.

$(5\,\mathrm{s/m})\,v_b$ with $v_b \approx [0.04, 3]\mathrm{m/s}$ (Pitteroff and Woodhouse, 1998; Askenfelt, 1989; McIntyre et al., 1983). However, these bow force and velocity ranges are based on low bow-bridge distances; much lighter forces (or higher bow velocities) are required when the middle of the string is bowed (McIntyre et al., 1983), which is a situation that is equivalent to a clarinet resonator.

4.4.3 *Making discrete and explicit*

In contrast to the two previous models there is no dynamic (i.e. time-dependent) component in this model. Hence, all variables are for the same time instance n, so that for simplicity, this sample index is left out in the equations. In a similar manner as for the single-reed model, the force exerted on the string induces an instantaneous change in velocity, proportional to the characteristic impedance of the string, so that: $\bar{v} = \bar{v}_h + \bar{f}$, where $\bar{v}_h (= \frac{v_h}{v_0})$ is the (dimensionless) "historical string velocity". The implicit equation that arises when inserting this expression into equation (83) (which was already implicit), can be made explicit analytically, which is another advantage of the hyperbolic model that has been demonstrated by Demoucron (2008). By firstly considering the $\bar{\Delta v} \geq 0$ domain,

the *sgn* operator can be dropped, therefore, the term $-\alpha\bar{f}$ can be brought out of the *abs* operator and thus, the *abs* operator itself can be dropped. Then, by writing the slipping phase equation as a second order function of $\bar{f}$, the calculation of one of its roots leads to the desired explicit equation (the second root does not correspond to a physical solution of the problem). Furthermore, given the symmetry of the model around $\Delta\bar{v} = 0$ (and thus also around $\Delta\bar{v}_h = 0$), the *abs* and *sgn* operators can be reintroduced to include the $\Delta\bar{v} < 0$ domain. Altogether this gives:

$$\bar{f} = \begin{cases} \bar{f}_{sl} = \frac{sgn(\Delta\bar{v}_h)}{2A}(B + |\Delta\bar{v}_h| + 1 - \sqrt{D}) & (\text{if } \diamond) \\ \bar{f}_{st} = \frac{\Delta\bar{v}_h}{A} & (\text{if } \circ), \end{cases} \tag{84}$$

where $A = 1 + \alpha$, $B = A\zeta_b\delta$, $D = (|\Delta\bar{v}_h| + 1 - B)^2 + 4(B - A\zeta_b)$ and $\Delta\bar{v}_h = \gamma_b - \bar{v}_h$. Condition $\diamond$ holds as long as $|\bar{f}_{sl}| \leq \zeta_b \,\&\, D > 0$ and condition $(\circ)$ holds as long as $|\bar{f}_{st}| \leq \zeta_b$. The potentially overlapping conditions show the possibility of a hysteretic behaviour between the stick and slip states (leading to a "dynamic excitation", as explained in subsection 2.2.2), which is the case when $\frac{d\bar{f}_{sl}(\Delta\bar{v}_h)}{d\Delta\bar{v}_h} < -1$ for any $\Delta\bar{v}_h \geq A\zeta_b$. This phenomenon is referred to as the Friedlander-Keller ambiguity and the conditions can also be demonstrated with a graphical method in the $\{\bar{v}, \bar{f}\}$ coordinate system (see e.g. (McIntyre et al., 1983)).

4.4.4 *Predicting the influence on the sound*

Given that the bow-string model is also a quasistatic simplification (just like the single-reed model presented earlier), it is possible to apply the theory to estimate the sound features of an arbitrary quasistatic excitation model (presented in chapter 2). Moreover, given that the single-reed's γ, ζ and the bow-string's γ_b, ζ_b parameters have a similar influence on their respective models, this may be expected to be reflected in the sound features.

While for the bow-string excitation model, following the oscillation condition theorem 1 (in chapter 2), the oscillation would simply occur from the moment that the static friction peak has been reached, i.e. from $\gamma_{bth} = \alpha\zeta_b$[3], a stable oscillation is only guaranteed when "the string velocity jumps returning to the bow are strong enough to cause release" (McIntyre et al., 1983). That is, the frictional force wave introduced during the slip state should be superior to the static friction peak. This has been first described by Schelleng (Schelleng, 1973), who derived a "maximum bowing force" (for a given bow velocity). When the condition is not satisfied, a raucous sound appears. For the current bow-string model, by supposing that the kinetic friction force is constant and fixed to $\delta\zeta_b$, an analytic expression that approximately indicates the non-raucous state can be derived:

$$\frac{\gamma_b}{\zeta_b} > \left(1 + \frac{\alpha}{2}(\alpha + 2\delta - 1) - \delta\right), \tag{85}$$

which will be referred to as the "raucous threshold". Just like Schelleng's formula (which corresponds to the case where $\alpha = 0$), this results in a linear relation between the bowing force ζ_b and velocity γ_b with respect to the raucous threshold value (as can be seen in figure 51), but here the non-infinite torsional impedance ($\alpha > 0$) raises the threshold.

As for the single-reed excitation, an analytic estimation of the steady state oscillation amplitude for the bow-string model is complicated, but for a lossless resonator the approximate amplitude can be found as:

$$\bar{v}_a = \frac{1}{2}\left(-b + \sqrt{b^2 + 2(\gamma_b - \alpha\zeta_b)}\right), \tag{86}$$

with $b = \alpha\delta\zeta_b - \gamma_b + \frac{1}{2}$. When $\gamma_b \gg \alpha\zeta_b$ (far above the oscillation threshold), $\gamma_b - \alpha\zeta_b \approx \frac{1}{2} - b$ so that the whole term under the root converges to $(1-b)^2$ and $\bar{v}_a \to \gamma_b - \alpha\delta\zeta_b$, which is similar to the single-reed case for high mouth pressures, but here an increasing dimensionless bow force slightly reduces the amplitude (as can be seen in figure 51). Formulations for a case with resonator

3 Note that this is not a realistic oscillation threshold due to the assumed constant torsional wave impedance.

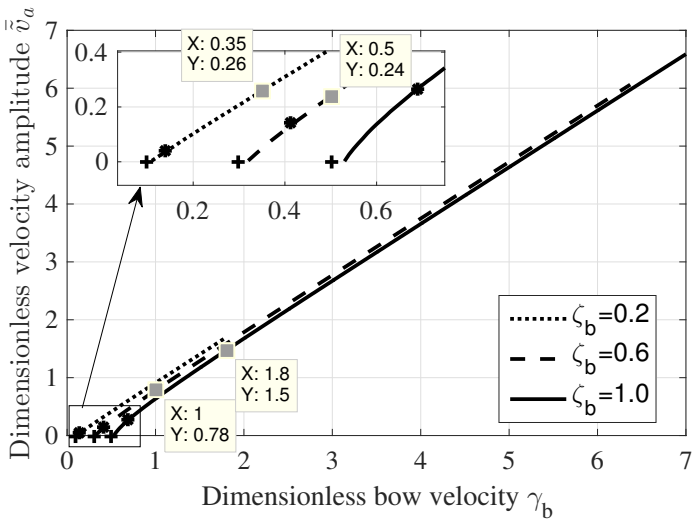

Figure 51: Evolutions of the estimated dimensionless velocity amplitude for three ζ_b values and γ_b ranging from the oscillation until the extinction threshold. The oscillation and raucous thresholds are indicated with respectively $+$ and $\bullet$ symbols.

losses would slightly reduce the amplitude and also cause extinction of the oscillation, which is attested to by the graphical (intersection) method. This method enabled the estimation of the amplitude velocities shown in figure 51.

As stated by theorems 4 and 5 (in section 2.3) the integration of the gradient under the excitation curves gives an estimate of the "spectral richness" and the even harmonics content is related to the even (symmetric) component of the excitation curve. Figures 52(a) to (d) show the nonlinear curves for four arbitrary sets of ζ_b and γ_b values, demonstrating the variety of sound features this excitation model is expected to produce.

A first general observation is that all of these states result in fairly similar nonlinear shapes, compared to the single-reed curves in figure 36. This suggests that the sound features are more progressively related to the excitation parameters. Additionally in comparison with the single-reed curves, it is remarkable that the bow-string oscillations appear to occur at a relatively high offset. This is due to the kinetic friction curve that only slowly descends (with decreasing velocity), while the single reed curve goes to zero from the moment the beating reed state is attained. Hence, even though the overall bow-string nonlinear curve is mainly asymmetrical in shape, there is a large amount of

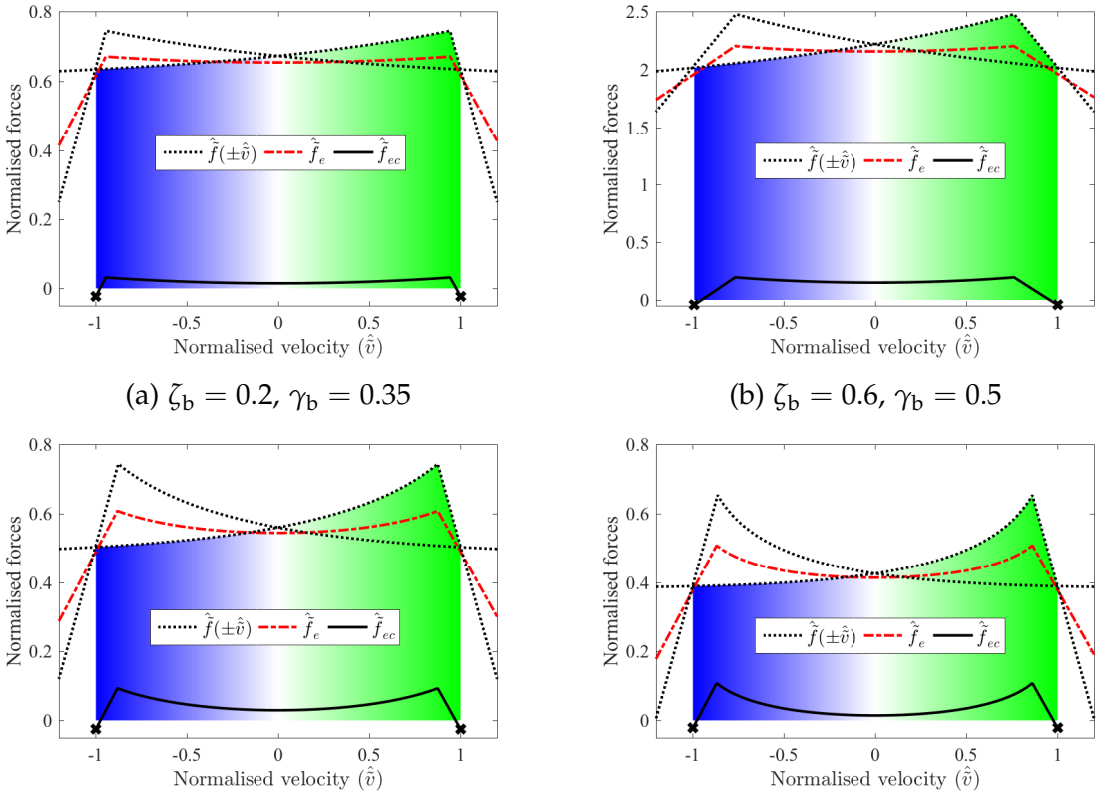

(a) $\zeta_b = 0.2$, $\gamma_b = 0.35$

(b) $\zeta_b = 0.6$, $\gamma_b = 0.5$

(c) $\zeta_b = 0.6$, $\gamma_b = 1.0$

(d) $\zeta_b = 1.0$, $\gamma_b = 1.8$

Figure 52: Nonlinear curves of the bow-string excitation model for four sets of parameters γ_b and ζ_b, with indication of the mean acoustic power estimation with a gradient (the amount of blue is to be subtracted from the amount of green); and the even component before and after the subtraction of the mean force (respectively in dot-dashed red and solid black lines).

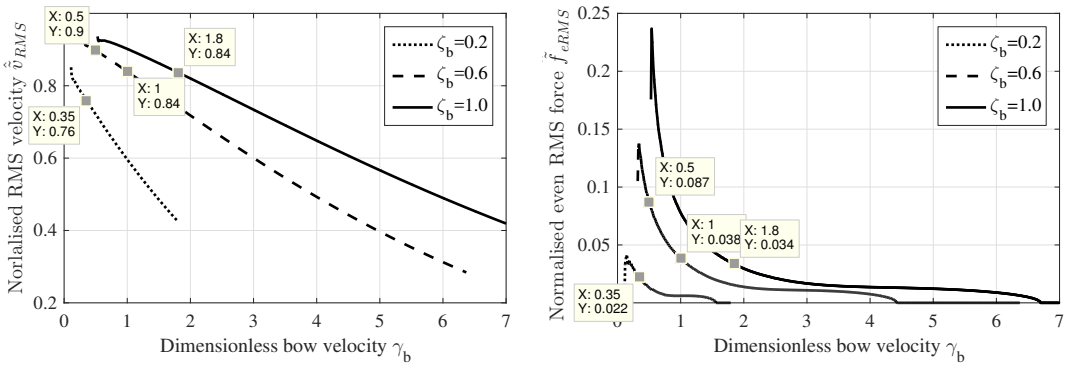

(a) (b)

Figure 53: Evolutions of the RMS of the normalised velocity $\hat{\hat{v}}_{\mathrm{RMS}}$ (a), and the RMS of the even harmonics normalised force component $\hat{\tilde{f}}_{\mathrm{eRMS}}$ (b), for three ζ_b values and γ_b ranging from the oscillation until the extinction threshold. The four parameter sets presented in figure 52 are marked as data points.

power that cancels itself out and the globally high normalised forces (compared to the normalised flow rates of the single-reed curves) result in a higher even harmonics component.

In the transition from (a) to (b) the ζ_b parameter is tripled, while γ_b is only moderately increased. This clearly raises both the acoustic power (i.e. the amount of green in the right upper dotted triangular zone) and the even amplitude (note the changed scaling). However, when then the bow velocity is increased more, the amplitude increases, but this also requires more energy, which is reflected in the decreasing normalised power (and accordingly the even amplitude is decreasing too).

In figure 53, the RMS of the normalised velocity $\hat{\hat{v}}_{\mathrm{RMS}}$ and of the normalised even force component $\hat{\tilde{f}}_{\mathrm{eRMS}}$, are plotted for three ζ_b values and γ_b ranging from the oscillation to the extinction threshold. The four discussed parameter states are indicated and the curves will be referred to in chapter 5, where the experimental evaluation of the hybrid instrument is discussed.

The earlier suggestion regarding the progressive evolutions is confirmed by these results. It is also interesting to note that near the oscillation threshold the even harmonics attain a peak value.

For increasing ζ_b, in contrast to the dimensionless amplitude that is slightly decreasing, both the normalised power and even amplitude are increasing, the latter being a similar behaviour as observed with the ζ parameter for the single-reed excitation.

Finally, it should be mentioned that the ζ_b range is chosen so as to meet a functional hybrid operation (see chapter 5). While the hysteretic case is not attained within this range, it is worth noting that the cyclic hysteresis effect causes the pitch to slightly decrease, which is known as the "pitch flattening effect" (McIntyre et al., 1983).

Note that for the implementation of the bow-string interaction model on the hybrid wind instrument, the dimensionless string velocity and force are simply interpreted as the dimensionless pressure and flow rate at the entrance of the resonator, so $\{\bar{v}, \bar{f}\}$ in the above theory is replaced by $\{\bar{p}, \bar{q}\}$. Accordingly, the characteristic velocity v_0, used to make the model dimensionless, is replaced by a characteristic pressure P_M around the desired pressure amplitude (in analogy with the other excitation models).

4.5 THE POLYNOMIAL MODEL

Given that the excitation of the hybrid wind instrument is achieved by executing programmed mathematical functions, it is possible to move away from any physical reality and program an arbitrary mathematical function that fulfils the requirements to establish self-sustained oscillations. This concept allows the study of the nature of excitation models by analytical decomposition and empirical evaluation. This is a convenient way to empirically study the independent influence of these sound properties, which is of interest both acoustically and musically (as discussed in section 1.2.1). Moreover, in view of the latter perspective, such excitations can be expected to provide easier access to a target timbre of choice, and to expand the timbre range towards potentially inspiring hybrid physical and synthetic sounds.

It appeared to be a reasonable choice to opt for a third order polynomial function $q(p)$. Such a function can be positively increasing around $p = 0$ and have three real solutions for $q(p) = q(-p)$, which matches the requirements that have been derived earlier in chapter 2.

The concept is somewhat similar to a well-established musical synthesis technique known as "waveshaping". With waveshaping, an input signal $x(t)$ is manipulated in the time domain with an arbitrary chosen nonlinear function: $y(t) = f(x(t))$ (also often a polynomial function), so that harmonics are introduced. However, while the excitation with self-sustained operations can be understood as a waveshape-like operation between the in- and out-going waves (thereby also introducing higher harmonics), it is substantially different, as the output is fed back to the input. Hence, the waveshaping theory is not relevant for this study and a different oscillatory behaviour can be expected.

4.5.1 *The model*

First, the flow rate is expressed as a generic polynomial third order function of the pressure:

$$q = ap^3 + bp^2 + cp + d \tag{87}$$

By now considering the theory of subsection 2.1.2 and sections 2.2 and 2.3, it can be shown that this function is a suitable excitation model and that it is possible to obtain a new set of parameters that are directly related to some sound properties. It would be ideal if the new parameter set took into account the influence of the frequency independent losses (i.e. the $(1 - \lambda)$ factor, introduced in chapter 2). However, this is mathematically very complicated and in practice these losses are relatively small, so that there is still a reasonable correlation with the sound features when these losses are neglected.

By defining the dimensionless pressure and flow rate similar to the previously discussed excitation models, by $\bar{p} = p/\alpha$ and $\bar{q} = qZ_c/\alpha$ (where α is an arbitrary parameter), the dimensionless form becomes:

$$\frac{\alpha\bar{q}}{Z_c} = a(\alpha\bar{p})^3 + b(\alpha\bar{p})^2 + c(\alpha\bar{p}) + d \tag{88}$$

Following theorem 6, which states that the mean flow can be neglected, the constant term d can be removed. After dividing through by α, the polynomial equation reduces to:

$$\frac{\bar{q}}{Z_c} = a\alpha^2\bar{p}^3 + b\alpha\bar{p}^2 + c\bar{p}. \tag{89}$$

From the oscillation condition stipulated by theorem 1, it can be concluded that, for the excitation to be unstable (which is the primary condition for self-sustained oscillations), the derivative of $\bar{q}$ at $\bar{p} = 0$ should be greater than the constant positive real factor $(1 - \lambda)$ $(\gtrsim 0)$. Evaluating $\bar{q}'(\bar{p} = 0) \geq (1 - \lambda)$, it is easy to show that this leads to the condition $c \geq (1 - \lambda)/Z_c \gtrsim 0$, i.e. c must be strictly positive.

Next, theorem 3 in section 2.3 states that a stable oscillation is obtained when the equality $\bar{q}(\bar{p}) = \bar{q}(-\bar{p})$ has a non-zero solution. Applying this equality to equation (89) results in $a\alpha^2\bar{p}^3 + c\bar{p} = 0$; which, apart from the trivial solution $\bar{p} = 0$, also has the amplitude of the steady state pressure wave as a solution: $\bar{p}_a = \sqrt{-c/(a\alpha^2)}$. By fixing this dimensionless amplitude to $\bar{p}_a = 1$, it follows that: $\alpha = \sqrt{-c/a}$, and given that c must be positive, a must be negative. Therefore, the α factor simply sets the amplitude of the dimensional system (in Pascals).

It is worth noting that this condition doesn't impose any requirements for the b coefficient. However, in practice this coefficient can make the system hysteretic (discussed later), it may evoke period-doubled bifurcations, or it can lead to undesirable instabilities when evaluated with the hybrid instrument.

Dividing equation (89) by c and defining $\zeta = cZ_c$, the equation can be rewritten as follows:

$$\bar{q} = \zeta(-\bar{p}^3 + \frac{b}{\sqrt{-ca}}\bar{p}^2 + \bar{p}), \tag{90}$$

which reveals that the ζ parameter directly controls the "amplitude of excitation". As explained in subsection 2.3.1, this parameter is inversely proportional to the attack time of emerging oscillations. Furthermore, by considering theorem 4 in section 2.3, it is straightforward to conclude that ζ controls the normalised power introduced by the excitation in the resonator, and therefore this parameter directly controls the brightness of the sound.

While theorem 5 enables the estimation of the level of even harmonics present in the sound, the a-priori unknown mean flow component (which should be subtracted, since it is inaudible) does not allow for the definition of an unambiguous parameter to provide linear and quantitatively known control for this polynomial model. However, by applying equations (10), it is straightforward to conclude that the odd and even harmonics are produced by respectively the odd and even powers of $\bar{p}$ (again, by not taking into account the acoustic losses). Therefore, the second power coefficient in this model can be expressed as a single new parameter: $\delta = \frac{b}{\sqrt{-ca}}$, which will be referred to as the "even amount parameter", so that the model equation finally reduces to:

$$\bar{q} = \zeta(-\bar{p}^3 + \delta\bar{p}^2 + \bar{p}). \tag{91}$$

It is easy to verify that using a negative δ factor is equivalent to using $-\bar{q}(-\bar{p})$ with the opposite (positive) δ, which produces the same oscillations due to the linearity of the resonator.

Using the condition expressed in theorem 2, the criterion for hysteresis can be evaluated, i.e. the model is non-hysteretic as long as $\bar{q}'(\bar{p}) \leq 1$ for any $\bar{p}$ involved in the oscillation. Applying this condition to the polynomial model yields:

$$\begin{aligned} \zeta(-3\bar{p}^2 + 2\delta\bar{p} + 1) &\leq 1 \\ \Leftrightarrow -3\bar{p}^2 + 2\delta\bar{p} + (1 - \frac{1}{\zeta}) &\leq 0 \end{aligned} \tag{92}$$

A first maximum gradient lies at $\bar{p} = 0$ and imposes the condition $\zeta < 1$. When $\zeta > 0.25$, the second maximum gradient lies between $0 < |\bar{p}| < 1$, so that equation (92) has no real solution, i.e. the discriminant has to be negative, or: $\delta^2 + 3(1 - \frac{1}{\zeta}) < 0$, imposing the condition $|\delta| < \sqrt{3(\frac{1}{\zeta} - 1)}$. Alternatively, when $\zeta \leq 0.25$, the second maximum gradient is found for $\bar{p} > 1$. The maximum gradient in the oscillation domain lies thus at $|\bar{p}| = 1$, so that the following condition applies: $|\delta| \leq \frac{1}{2\zeta} + 1$. For instance, with $\zeta = 0.5$, the excitation becomes hysteretic for $|\delta| > \sqrt{3} = 1.73$, while for $\zeta = 0.1$, that only occurs for $|\delta| > 6$.

It is worth mentioning that higher order polynomials can be used to excite the hybrid wind instrument. Using higher order polynomials would potentially give an even greater and more precise control of the sound properties. For example, it may be interesting to express any quasistatic excitation model as an approximate polynomial function, by applying a Taylor expansion; which could be a useful follow-up study.

4.5.2 *Making discrete and explicit*

The explicit equation for the polynomial excitation model can be found by solving the set of equations $\bar{p} = \bar{p}_\mathrm{h} + \bar{q}$ and equation (91), which leads to a third order equation of $\bar{q}$:

$$0 = \bar{q}^3 + \bar{q}^2 \underbrace{(3\bar{p}_\mathrm{h} - \delta)}_{\mathrm{r}} + \bar{q} \underbrace{(3\bar{p}_\mathrm{h}^2 - 2\delta\bar{p}_\mathrm{h} + \frac{1}{\zeta} - 1)}_{\mathrm{s}} + \underbrace{(\bar{p}_\mathrm{h}^3 - \delta\bar{p}_\mathrm{h}^2 - \bar{p}_\mathrm{h})}_{\mathrm{t}}. \tag{93}$$

This equation illustrates the existence of a hysteretic case, which occurs when it has more than one real root. As empirical evaluations revealed that this only occurs for parameter ranges exceeding the stable operational range, the hysteresis is not taken into account here and only the case for a single-real solution is considered. For this case, the determinant is written as:

$$D = (\sqrt{A^3 + B^2} - B)^{1/3}, \tag{94}$$

where

$$A = -r_f^2 + \frac{s}{3}, \tag{95}$$

$$B = r_f^3 - r_f\frac{s}{2} + \frac{t}{2} \tag{96}$$

and $r_f = \frac{r}{3}$ are introduced for notational and computational convenience. Finally, the explicit solution is found by:

$$\bar{q} = -r_f - \frac{A}{D} + D. \tag{97}$$

The computational protocol simply involves the successive calculation of r, s, t, r_f, A, B, D and finally $\bar{q}$.

4.5.3 *Predicting the influence on the sound*

The polynomial model is designed exactly with the goal of gaining independent control of the sound features. Therefore, one could think that the study to predict the sound features (introduced in section 2.3) is redundant for this model. Nevertheless, the theory is certainly meaningful, because the (frequency independent) acoustic losses have not been taken into account in the design of the model, while they are included in the sound prediction protocol (i.e. the virtual pressure and flow rate $\{\tilde{p}, \tilde{q}\}$ are used, rather than the real wave variables $\{p, q\}$). Furthermore, it is useful to obtain a more absolute estimation.

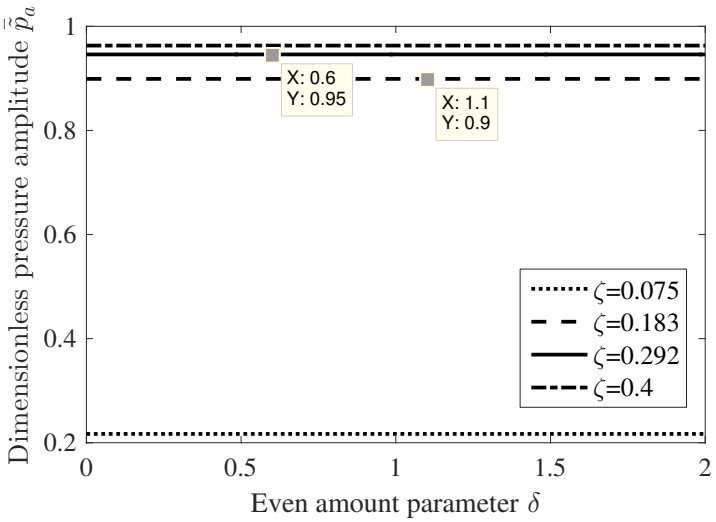

Figure 54: Evolutions of the estimated dimensionless pressure amplitude for four ζ values and θ ranging from 0 until 2.

The proposed parametrisation of the polynomial model lacks the concept of an oscillation threshold, as any given set of (non-zero) parameters $\{\alpha, \zeta, \theta\}$ results in an oscillatory state. While a decreasing ζ would lead to an extinction of the oscillation, it can be seen from equation (93) that the s term goes to infinity when ζ approaches 0, and while the α parameter could be used to initiate an oscillation, this parameter preserves the wave shape and therefore is not of great interest for evaluation.

For the evaluation of sustained oscillations, a set of four ζ values is chosen between 0.075 and 0.4, and increasing progressions of θ are applied from 0 to 2 (these ranges are determined from empirical experimental evaluations, which are further detailed in chapter 5).

Figure 54 shows the evolutions of the estimated pressure amplitudes, determined with the graphical intersection method (as explained in theorem 3 in section 2.3).

If there was total absence of frequency independent losses, this amplitude would remain constant at 1. As a consequence, taking into account these losses, more energy is required to maintain this amplitude. As can be seen from this figure, the lower the ζ value, the more the amplitude slightly decreases, until $\zeta \approx 0.075$, where a steep amplitude drop occurs.

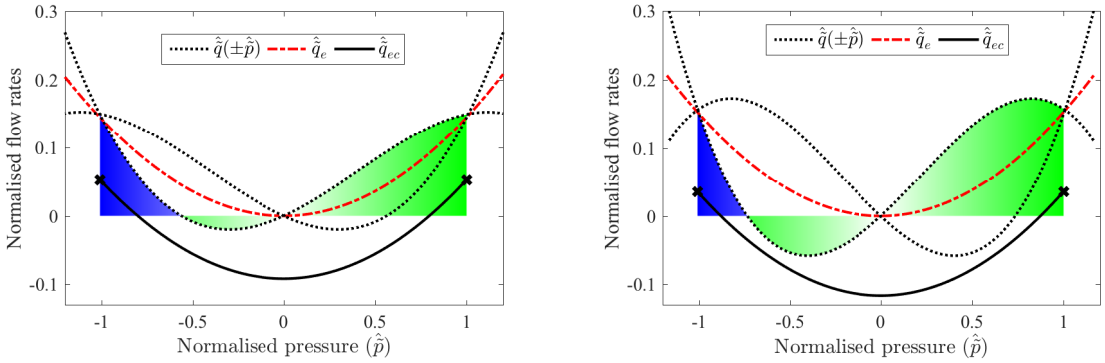

(a) $\zeta = 0.183$, $\delta = 1.1$ (b) $\zeta = 0.292$, $\delta = 0.6$

Figure 55: Nonlinear curves of the polynomial excitation model for two sets of parameters δ and ζ, with indication of the mean acoustic power estimation with a gradient (the amount of blue is to be subtracted from the amount of green); and the even component before and after the subtraction of the mean force (respectively in dot-dashed red and solid black lines).

Theorem 4 (in section 2.3) states that the integration of the gradient under the excitation curves gives an estimate of the "spectral richness" and theorem 5 states that the even harmonics content is related to the even (symmetric) component of the excitation curve, excluding the mean flow component. Figures 55(a) and (b) show the nonlinear curves for two arbitrary sets of ζ and δ values, demonstrating how each of the input parameters can affect the mentioned sound features.

Just like for the bow-string interaction curve, it is interesting to note that both curves are similar in shape (which is also the case for other parameter sets), so that a relatively progressive relation to the sound features can be expected.

The influence of the excitation parameters is relatively straightforward. Just like for the other excitation models, ζ directly influences the global flow rate which is therefore proportionally controlling the amount of positively introduced acoustic power. Meanwhile, the δ parameter determines the amplitude of the symmetrical component. Given that the transition from (a) to (b) involves a doubling of ζ and an almost halving of δ, it can be seen that the amplitude of the symmetrical component is almost equal.

In figure 56, the RMS values of the normalised pressure $\hat{\tilde{p}}_{\text{RMS}}$ and of the normalised even flow rate component $\hat{\tilde{q}}_{\text{eRMS}}$, are plotted for the mentioned para-

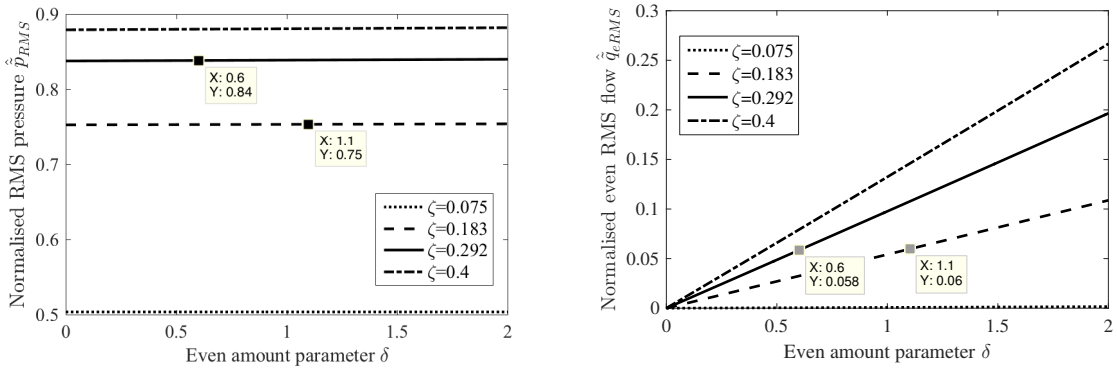

(a) (b)

Figure 56: Evolutions of the RMS of the normalised pressure $\hat{\tilde{p}}_{\text{RMS}}$ (a), and the RMS of the even harmonics normalised flow rate component $\hat{\tilde{q}}_{\text{eRMS}}$ (b), for four ζ values and δ ranging from 0 until 2. The two parameter sets presented in figure 55 are marked as data points.

meter ranges. The two discussed parameter states are indicated and the curves will be compared with the practical evaluations, discussed in chapter 5.

In (a), the normalised RMS pressures confirm that the ζ parameter controls the spectral richness. It is important to note that the earlier mentioned steep amplitude drop for $\zeta = 0.075$ also results in a stronger spectral deviation. That effect is also noted in (b), where the even component remains close to 0 for the whole range of δ. While δ does not affect the overall normalised RMS pressure, its influence for the higher three ζ values is clearly linearly related to the normalised even RMS flow rates.

4.6 SUMMARY

This chapter presented several "excitation models", which are physically based models whose role is to provide acoustic energy to the resonator. For the hybrid instrument, these models are executed on a computer. Therefore, first some computational considerations were made, dealing with the "delay-free loop" or "implicit equation" issue that arises with the simulation of physical models by a sequential operation. In order to cope with this issue, analytical explicit

expressions for the implicit representations were sought, which is a case-by-case task that was considered for each separate excitation model.

Four "excitation models" were presented. First a single-reed physical embouchure model was described, it was modelled as a classical single-degree-of-freedom (SDOF) mass-spring-damper (MSD) oscillating system that is forced by the pressure difference across the reed. This pressure difference, and the reed opening section, then determined the air flow rate that passes through the "reed channel". The dimensionless representation and the discretisation were drawn from the literature. Finally, relying on the theory of chapter 2, an estimation was made of the acoustic power that would be introduced in the resonator, as a function of the dimensionless mouth pressure γ and lip force ζ parameters. This estimation then led to a prediction of the oscillation threshold, the amplitude, the spectral richness and the amount of even harmonics present in the steady-state oscillations.

Next, a (brass-instrument-like) simple lip-reed model was presented. Like the single-reed model, it was also a SDOF MSD pressure-controlled valve, but the valve was of the "outward striking" type (i.e. an increasing mouth pressure tends to open the valve) and its resonance frequency lies below the playing frequency. Moreover, some additional features were introduced, such as a refined lip-collision model and a variable opening section, which both account for an improvement of the sound produced. While the theory to estimate the sound features was initially only derived for the case of quasistatic excitation models, it was shown that the acoustic power calculation for the case of dynamical models could be approximately reduced to an approach that allows the application of the quasistatic theory. Hence, also for this model, the amplitude, spectral richness and even harmonics predictions were made as a function of the most relevant parameters for the quasistatic approximation of this model: the dimensionless mouth pressure γ and lip force ζ. Meanwhile, using a sinusoidal signal approximation the theory by Fletcher was applied (Fletcher, 1993),

which allowed for oscillation threshold and fundamental frequency estimations for variations of γ, ζ, the lip resonance frequency θ and the quality factor Q_r.

By interpreting the pressure and flow rate at the entrance of the resonator as if it were respectively a string velocity and an introduced force to the string, it was explained that the hybrid wind instrument could be excited with the excitation mechanism of self-sustained string instruments, i.e. with a "bow-string interaction model". For this, a classical quasistatic "slip-stick" model was used. The slipping part was modelled by a hyperbolical curve, while for the sticking part the interaction was modelled by a constant impedance, induced by torsional string waves that are totally absorbed at the string ends. Also, a dimensionless reduced parameter form was proposed, which revealed interesting similarities with the single-reed model. These similarities were reflected in the obtained predictions of the amplitude, spectral richness and even harmonics curves, which were expressed as a function of the main control parameters: the dimensionless bowing velocity γ_b and bowing force ζ_b. Also the estimation of oscillation thresholds and "raucous thresholds" was obtained.

Finally, an arbitrary formula was considered as an excitation model. For this, a third order polynomial turned out to be an appropriate choice. Starting from a generic polynomial equation, the theorems stipulated in chapter 2 were applied so that a new form was obtained, whose parameters could be expected to independently control sound features such as the amplitude, the spectral richness and the amount of even harmonics. The application of the sound predicting theory confirmed the strong correlations.

5 IMPLEMENTATION AND EVALUATION

To evaluate the hybrid self-sustained operation, the loudspeaker-resonator system combined with the loudspeaker-compensating filters (described in chapter 3) is put in interaction with the theoretical excitation models laid out in chapter 4.

From the moment these components are active and interacting, a self-sustained operation will emerge if the excitation conditions are favourable. The hybrid results are compared with simulations of the entire instrument, where the tube resonator is also simulated.

All excitation models are evaluated with slowly varying input parameters to study the sustained operation, as well as with rapid "attack envelopes", enabling a characteristic transient sound to appear. These results are then studied by first observing snapshots of the mouthpiece pressure in both the time and frequency domains, and then focussing on a few typical "sound descriptors" to allow for a wider comparison. The descriptors are also compared with sound feature prediction curves, which were obtained for each excitation model in chapter 4.

5.1 COMPUTATIONAL AND SIMULATION ASPECTS

All the simulations and post-evaluations presented in this chapter were implemented in MATLAB and Simulink (see subsection B.3.1 for some examples), which are convenient platforms for both the real-time evaluation of physical models and the analysis of the obtained signals.

5.1.1 *Hybrid instrument computations*

For the evaluation of the hybrid instrument, a real-time computer was used, whose details and set-up are described in subsection B.2.1. This computer ensures that the total latency introduced by the analogue-to-digital and digital-to-analogue conversions and/or by the processing time is minimal, and well below the oscillation period of the appearing oscillations. In fact, the latency of the used computing system is just a single sample time (at a sampling rate of $f_s = 40$ kHz).

5.1.2 *Simulation of the excitation models*

For the simulation of the excitation models, their respective discretised models (laid out for each excitation model in chapter 4) were programmed with standard Simulink blocks; a straightforward task in most cases (for an example, see figures 84 and 85 in subsection B.3.1, which show the implementation of the single-reed model).

For the simulation of the dynamic reed with the particular discretisation scheme mentioned in section 4.2.2, a customised "S-function" block was employed (a Simulink-specific custom designed block in C++ code). Another S-function block was used for the discrete lip-reed dynamics (see section 4.3.2). This block is based on the same filter code as for the single-reed dynamics. The main difference is that the gradual lip-collision model is implemented as an additional "displacement-condition", which introduces nonlinearly variable filter coefficients. Both the bow-string interaction model and the polynomial model are entirely quasistatic (i.e. without dynamic components, see chapter 4). The former was implemented with Simulink blocks (using conditional blocks to switch between the slipping and sticking phases), while the latter was entirely programmed in a single S-function block.

It should be mentioned that the choice between Simulink blocks and C++ code does not influence the actual operation (when correctly implemented). Indeed, it is worth mentioning that a C++ code implementation is often easier for many models.

5.1.3 *Simulation of the entire instrument*

For the simulation of the entire instrument (hereafter simply referred to as "simulations"), each excitation model was coupled with a numerical simulation of the tube resonator. This resonator simulation was also carried out with Simulink, applying a fourth order Runge-Kutta solver and using the same sampling frequency as for the hybrid instrument ($f_s = 40$ kHz). The tube was simulated with a modal approximation (explained and calibrated in appendix-section A.4), calculated with a series of 14 "transfer function" blocks that operate as parallel bandpass filters (figure 86 in subsection B.3.1 partially shows this implementation). Each filter corresponds to a second order transfer function of equation (25) (see chapter 2). Even though the limited amount of modes truncates the spectrum of the produced signals, it is known that typically between 10 and 20 modes are necessary to ensure a coherent self-sustained operation, because either the cut-off frequency of the tone-hole lattice or the reed low-pass filter behaviour significantly reduces the importance of the higher frequency modes (Karkar et al., 2010). In this thesis, the reed resonance frequency is held constant at 2.5 kHz, so that the 14th mode of the chosen resonator — having a resonance frequency of about 3.8 kHz — is a reasonable truncation choice. This is also empirically confirmed by simulating the single-reed model (using parameter ranges used throughout the thesis) with higher numbers of modes. As can be noted from figure 83 (in appendix-section A.4), the modal approximation matches the measured input impedance of the resonator with high precision.

Hence, it can be concluded that the simulations correlate well with the functioning of the "ideal" hybrid instrument, which was identified in the require-

ments in subsection 1.4.3 as a target operation for the hybrid instrument. Therefore, the simulations enable a quantitative comparison with the hybrid system, which will be useful as a measure of accuracy and for identifying flaws in the hybrid system, with a focus on the intended self-sustained operation.

Given that the loudspeaker, including the associated compensation filters (see subsection 3.2.3), is the hybrid component that deviates the most from its simulated equivalent (i.e. from the ideal piston), most of the observed differences between the hybrid and the simulated results are due to the uncompensated loudspeaker effects.What to observe?

Figure 57 depicts a schematic representation of the hybrid and simulated evaluations, which are respectively indicated by blue and red arrows. (This colour index is maintained throughout this chapter.) The term "experimental results" is used to refer to both the simulated and hybrid results.

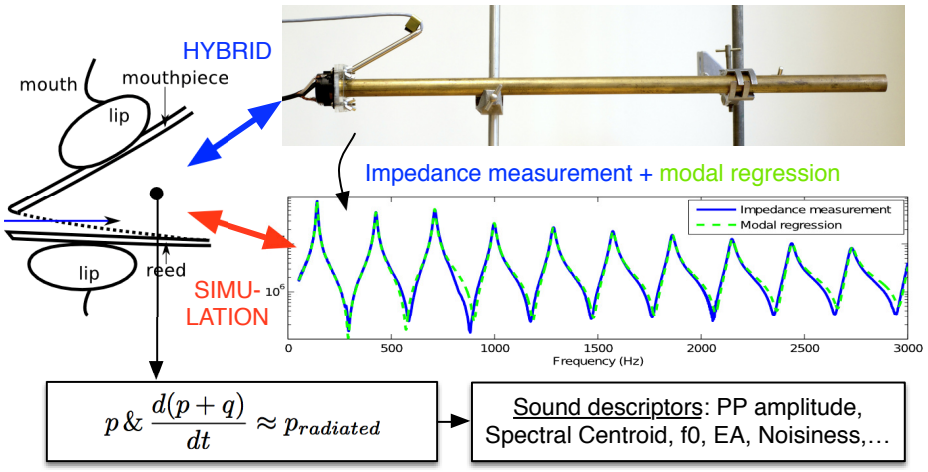

Figure 57: Schematic representation of the hybrid and simulated evaluation (with the example of a single-reed excitation).

The next question, which should be considered in the light of the main research questions, is which signals would be most suitable to observe?

5.1.4 *Selecting appropriate signals*

A straightforward choice of the signals that should be studied are the (dimensionless) pressure and flow rate at the entrance of the resonator, $\bar{p}$ and $\bar{q}$. These signals have the most direct relation to the physical functioning involved and are therefore particularly useful for studying and verifying the acoustic functioning of the instrument.

Another important focus is the sound perceived by a listener. Therefore, a signal related to the pressure waves radiated by the instrument is also calculated. A simplified, yet sufficiently relevant, "monopole" radiation model describes the radiated pressure as being proportional to the temporal derivative of the pressure waves propagating downstream in the resonator (i.e. $\bar{p}^+$) (see e.g. (Jacobsen, 2011)). Equation (9) in chapter 2 shows that this downstream dimensionless pressure corresponds to $\bar{p}^+ = (\bar{p} + \bar{q})/2$, so that the approximated external pressure can be written as:

$$\bar{p}_{\text{ext}} \propto \frac{\mathrm{d}(\bar{p} + \bar{q})}{\mathrm{d}t}. \tag{98}$$

To ensure a consistent comparison between the simulated and hybrid results, the spectral content of the signals obtained with the hybrid wind instrument in the frequency domain above the upper simulated mode should be ignored. Therefore, before studying the sound features, a steep (IIR, 33^{rd} order Butterworth) low-pass filter was applied on $\bar{p}_{\text{ext}}$, with a cut-off frequency of 4 kHz. This filter also prevents the amplification of high frequency noise that is amplified by the derivative.

5.1.5 *Sound descriptors*

To allow for a quantitative and useful comparison of hybrid and simulated sounds, so called "sound descriptors" were employed. These represent a stand-

ardised set of features that describe relational values derived from the spectral, temporal and harmonic representations of the sound. Sound descriptors can be meaningful characteristic features regarding both perception (to quantify the timbre and other sound features) and the instrument's acoustic functioning.

For the selection of descriptors, the work of Barthet — who extensively studied the timbre of the clarinet and its relation to the instrument's input parameters (Barthet et al., 2010; Barthet, 2009) — provides a useful starting point. Barthet's work resulted in the abstraction of a clarinet-related three-dimensional perceptive timbre space, based on the classification of a set of clarinet-synthesised sounds (using a realistic temporal mouth pressure envelope) by listeners. Then, an algorithmic procedure was used to demonstrate that these dimensions are well correlated to a selection of sound descriptors, in particular to the "(Logarithmic) Attack Time", the "Spectral Centroid" and the "Odd/Even harmonics Ratio" (OER).

However, Barthet only evaluated a single-reed excitation, and while he used a ζ range similar to the range used in the current study, he evaluated the γ parameter over a more narrow range, between 0.53 and 0.8 (see section 4.2 for an introduction to these parameters). Furthermore, for the current study it is also of interest to choose descriptors that are directly related to the curves obtained in chapter 4, which predict the sound features of each excitation model.

Therefore, the descriptors selected for evaluation in this thesis are the "Logarithmic Attack Time" (LAT), the "Harmonic Spectral Centroid" (HSC) and the "Even Amount" (EA)[1].

The LAT descriptor represents the logarithm (at a decimal base) of the time taken for the amplitude envelope to increase from 10% to 80% of the maximum amplitude value for the sound event (i.e. the amplitude of the steady-state regime when the excitation parameters are held constant).

1 The harmonic descriptors such as the HSC and the EA rely on a number of harmonic peaks in the spectrum. Here this number was set to 20 (both odd and even) harmonics, as above this value wrong peaks were sometimes identified.

The Spectral Centroid represents the frequency of the centre of the spectrum, using the amplitude weight of each frequency, and has a robust connection with the perceived impression of "brightness". Here the harmonic variant is opted for, which only takes into account the spectral content defined by a detected fundamental frequency and its multiples, though it should be mentioned that the HSC itself is not necessarily a multiple of the fundamental frequency. This choice is more convenient for the comparison of the hybrid instrument with the entirely simulated equivalent, given that other frequency components such as noise were filtered out. (The noise could be separately studied with the "Noisiness" (NN) descriptor.)

The Even Amount descriptor provides a dimensionless measure of the even harmonics' energy relative to the total energy of all the harmonics. The choice to opt for the EA rather than the OER descriptor is primarily motivated by the fact that the sound prediction theory also provides an estimation of the amount of even harmonics (see the relevant sections for each excitation model in chapter 4). Moreover, this choice turns out to be more suitable. Knowing that the OER descriptor is calculated as the ratio of odd and even harmonic amplitude components (i.e. the ratio of the "Odd Amount" and "Even Amount" descriptors), and given that the Odd Amount descriptor is empirically found to be well correlated with the Spectral Centroid, it can be concluded that the main component that differentiates the OER from the SC is the EA descriptor.

In addition, the fundamental frequency (f_0) and the Peak-to-Peak pressure (PP) evolutions are studied. Given the known typical progression of the PP mouthpiece pressure as a function of the mouth pressure progression (see e.g. (Atig et al., 2004)), the PP of $\bar{p}$ is calculated rather than $\bar{p}_{\text{ext}}$. Furthermore, the end of the attack time (EAT) is reported (for the single-reed model only), which is the time when the amplitude envelope reaches 80% of its maximum, relative to the start of blowing. In contrast to the LAT, this time span expresses the delay between the mouth pressure onset and the resulting sound onset, which is an important feature with respect to the timing of played notes. Finally the Spectral

Flux (SF) is measured in the attack transient of each sound (also only for the single-reed model). This descriptor is a measure of the degree of variation of the magnitude spectrum over time. It corresponds to the mean of the correlation coefficients between adjacent short-time spectra.

Peeters and Barthet provide precise mathematical definitions of all these descriptors (Barthet et al., 2010; Peeters et al., 2011), and the actual calculation of most of the descriptors was carried out using the MATIMBRE toolbox, a MATLAB program developed by Barthet (Barthet et al., 2010; Barthet, 2009). Only the Peak-to-Peak and Noisiness descriptors were programmed from scratch, based on the mathematical descriptions provided by (Peeters et al., 2011), and using pre-calculated features in the MATIMBRE toolbox.

5.2 PREPARING AND INTERPRETING THE EVALUATIONS

5.2.1 *Evaluation protocol and parameter ranges*

For the evaluation of the self-sustained operation, each excitation model was supplied with appropriate parameter values. It is possible to determine the range of parameter values by relying on existing theories. For instance the single-reed model is known to function within a typical parameter range, and in chapter 4 the sound feature estimations of other excitation models have indicated certain threshold values beyond which oscillation is not feasible. Empirical evaluations lead to certain threshold choices. It is also interesting for the sake of musicality to explore the effect of parameter values beyond the typical range.

Tables 2 to 5 show the evaluated parameter values for each excitation model. Many parameters were held constant as their variation is not of primary relevance or has little influence. Some parameters were evaluated for a discrete number of distinct values, which is notated as a set in curly brackets or using an indexed sequence (where $k \in \mathbb{N}$). Other parameters were evaluated over a continuous range, which is notated as a mathematical interval in square brack-

ets. More details on the parameter meanings and their respective excitation models can be found in chapter 4. The parameters values that were either used for the sustained or attack evaluation are indicated by the notation (S) or (A).

For the single-reed model, sustained sound evaluations were carried out for increasing γ values (over the ranges provided in table 2), repeated for four constant ζ values. The attack evaluations were performed over a reduced γ range as the extinction for the case of the sustained sounds is higher due to a hysteresis effect.

The self-sustained evaluation of the lip-reed model was carried out for two sets of varying parameters, which are indicated by the notations (S1) and (S2). For the first evaluation, the same protocol as for the single-reed evaluation was carried out, i.e. increasing γ values, repeated for constant ζ values and using a constant lip resonance frequency $\theta = \frac{\omega_r}{\omega_1} = 0.7$ (where $\omega_1 = 2\pi.140$ rad s^{-1} is the frequency of the first tube resonance). These parameters were also used for the attack evaluations (indicated with (A)). Then, these parameters were held constant at $\zeta = 0.05$ and $\gamma = 3$, and θ was progressively evaluated over the proposed range, and this was repeated for a set of Q_r values.

Just as for the single-reed evaluation, the sustained sounds of the bow-string interaction model were evaluated for increasing bow velocity γ_b, repeated for three constant bow forces ζ_b. The attack evaluation was performed over the same parameter ranges.

Finally, the sustained evaluation of the polynomial model was performed for four constant ζ values with increasing δ progressions. However, while the attack evaluation was performed for the same parameter ranges, the δ parameter cannot induce an oscillation onset, so in contrast to the other excitation models, the attack envelopes (whose shape is detailed in subsection 5.4) were applied to ζ (which does cross an oscillation threshold, i.e. when ζ lies below a certain threshold, no sound occurs).

Single-Reed	Sym-bol	Eval. values	Notes
"Global em-bouchure para-meter", related to the lip force.	ζ	$\{0.1, 0.2, \ldots 0.3, 0.35\}$	For real clarinets, this value is estimated to lie between 0.3 and 0.4 (Chaigne and Kergomard, 2013). However, empirical evaluations revealed an unstable state above 0.35.
Dimen-sionless mouth pressure	γ	(S) $[0.33, 2.4]$ (A) $\{0.45, (0.4 + \frac{k.(1.2-0.4)}{8})_{k=0}^{8}\}$	For $\gamma < 0.33$ theoretically no oscillatory would occur. But with the hybrid instrument this produces instabilities (see 5.5.1). The maximum values correspond to the extinction thresholds of the highest ζ value used. For the sustained sounds this is 2.4 and for the attack sounds 1.2.
Reed resonance frequency (including lip)	ω_r	2500 Hz	While this is relatively high compared to a real instrument, this close to quasistatic implementation is sufficient as a first investigation. It is reported that, to avoid pitch flattening, classical playing techniques involve reed resonance frequencies above 1500 Hz (Chaigne and Kergomard, 2013)
Quality factor of the lip dynamics	Q_r	5	The quality factor is typically assumed to be in the range $Q_r \approx [1, 4]$ (Avanzini and Van Walstijn, 2004; Dalmont et al., 2003; Silva et al., 2008), though it remains a relatively crude approximation. The used value is proposed by (Guillemain et al., 2005) and approximates a quasistatic (and still stable) implementation.
Beating pressure	P_M	100 Pa	Higher amplitudes (up to 800 Pa) resulted in similar results, but for high ζ, saturations easily occur. For real clarinets this lies between 4 kPa to 10 kPa (Ollivier, 2002). The maximum used here is much lower due to the hybrid instrument's amplitude limitations.

Table 2: Single-reed model parameter descriptions, evaluated values, and additional notes.

Lip-Reed	Symbol	Eval. values	Notes
"Global embouchure parameter", related to the lip force.	ζ	(S1,A) $\{0.03, ... 0.05, 0.07\}$	Realistic values for ζ are less well known than for the single-reed model. The values are based on empirical findings.
		(S2) 0.05	
Dimensionless mouth pressure	γ	(S1) $[1, 5]$	Below 1, no oscillation is possible, there is no extinction threshold but above 5 the sound does not change much in timbre.
		(A) $(1 + \frac{k.(5-1)}{8})_{k=0}^{8}$	
		(S2) 3	
Dimensionless lip resonance frequency (relative to ω_1)	θ	(S1,A) 0.7	This is based on empirical findings, but corresponds to typical values. This range covers three registers.
		(S2) $[0.5, 4]$	
Quality factor of the lip dynamics	Q_r	(S1,A) 3	As for the single-reed, real quality factor estimates are poor. The used values are of the same order as values proposed by other authors: 2.88 (Vergez and Rodet, 2000), 5 (Saneyoshi et al., 1987) and $2 \leq Q_r \leq 3$ (Keefe, 1992).
		(S2) $\{2, 3, 4\}$	
Beating pressure	P_M	50 Pa	This is much lower than for real brass instruments, which is due to the hybrid instrument's amplitude limitations.

Table 3: Lip-reed model parameter descriptions, evaluated values, and additional notes.

Bow-string interaction	Symbol	Eval. values	Notes
Dimensionless bow force	ζ_b	$\{0.2, 0.6, 1\}$	Based on empirical findings. While higher values can result in stable oscillations when γ_b is sufficiently high, the limit is eventually conditioned by the maximum amplitude (and therefore also by v_0).
Dimensionless bow velocity	γ_b	(S) $\zeta_b.[\alpha, 10.42]$ (A) $\zeta_b.(\alpha + \frac{k.(10.42-\alpha)}{8})_{k=0}^{8}$	The minimum value corresponds to the theoretical oscillation threshold (the peak of the nonlinear curve). The maximum value is based on a theoretical extinction threshold formula: $\gamma_{bth} = 4\zeta_b(1-\delta).(1-\beta)\beta^2/\frac{\omega_1}{a_1 Q_1}$ (Schelleng, 1973) (with $\frac{\omega_1}{a_1 Q_1} = 0.03$, an estimate of the dimensionless admittance of the first tube resonance mode).
The relative position of the bow on the string	β	0.5	The analogy with the clarinet imposes that the the string is bowed in the middle.
Torsional admittance relative to the characteristic string admittance $1/Z_{cs}$	$\alpha = \frac{Z_{cs}}{Z_R}$	0.5	Other values were also empirically evaluated (0.26 as proposed by (Schelleng, 1973) and 1), only minor influence was noted. This parameter also remains constant for real bowed strings.
Ratio of dynamic over static friction coefficients $\frac{\mu_d}{\mu_s}$	δ	0.375	Proposed by (McIntyre et al., 1983). Values between 0.4 and 0.5 were proposed by (Askenfelt, 1989). Other values were empirically evaluated, only minor influence was noted. This parameter also remains constant for real bowed strings.
Characteristic pressure	P_M	15 Pa	When exciting a wind instrument resonator, this parameter corresponds to a global pressure amplitude. This value was empirically found to result in a hybrid operation without saturations.

Table 4: Bow-string interaction model parameter descriptions, evaluated values, and additional notes.

Polynomial	Symbol	Eval. values	Notes
Excitation amplitude	ζ	(S) $(0.075+\frac{k.(0.4-0.075)}{3})_{k=0}^{3}$ (A) $(0.05+\frac{k.(0.4-0.075)}{3})_{k=0}^{3}$	The minimum values are empirically found oscillation thresholds for the hybrid instrument.
Even amount parameter	δ	(S) $[0, 2]$ (A) $\{0, 0.6, ... 1.2, 1.8\}$	Beyond the empirically found maxima, unstable regimes were obtained.
Pressure amplitude	α	100 Pa	Higher amplitudes resulted in similar results, but for high δ, saturations easily occur.

Table 5: Polynomial model parameter descriptions, evaluated values, and additional notes.

Where saturations are mentioned in the tables, this refers to the limitations imposed by different components of the hybrid instrument (discussed in section 3.3.2).

5.2.2 *General notes and observations*

Before moving on to the specific evaluations, a number of general facts and observations should be mentioned.

The hybrid sustained sound evaluation with the polynomial model was carried out at a later stage of the research. While generally good repeatability is noted (further discussed in section 5.5), at this later stage, the difference between the hybrid results and the simulations was found to be more significant. Given that all components have been thoroughly verified and no faults were found, the most likely cause of this difference is the loudspeaker, which is a relatively complex mechanical component whose deviations can result in subtle variations that are not easy to identify. From the empirical observations of the descriptor data presented below, it was concluded that the loudspeaker's characteristics were slightly changed due to ageing and/or occasional damage,

which is subsequently referred to as the "loudspeaker deterioration". The latter hypothesis relates to two known occurrences. First it was noticed that a part of the suspension became loose and had to be glued back, though the repair was done carefully and seemed successful. Another deterioration occurred later, a small particle became stuck between the voice coil and the gap surrounding the coil, it was successfully removed but it (indirectly) may have introduced damage to the coil. Brief attempts to re-calibrate the system, i.e. to find new parameters for the loudspeaker compensating filters, did not lead to satisfactory results, which suggests that the deterioration is nonlinear and cannot be compensated for with the linear compensation filters.

As a reference, to have an idea of the impact of the loudspeaker deterioration, the single-reed model is evaluated both before and after. For clarity, the second evaluation results are only shown for the HSC, the f_0 and the LAT descriptor. As mentioned, for the polynomial model, only data from the second hybrid evaluation is available. The hybrid evaluation after the loudspeaker deterioration is indicated by "Hybrid2" and green coloured curves are used to make the distinction, with the blue coloured curves belonging to the first hybrid evaluation.

The observed differences in the descriptors seem to indicate the presence of a slight phase shift close to the fundamental frequency of the produced tones. This reduces the overall accuracy of most descriptors, as this frequency range determines key features of the self-sustained operation. Due to this initial (yet hypothetical) phase shift, a downshift in fundamental frequency is caused, which affects other features. The consequences are further laid out throughout the descriptors discussion that will follow.

For each excitation model, the sound files of both the pressure signal at the resonator entrance and the calculated external pressure signal are available for download. There are separate DOI entries for each excitation model evaluation (which each include the sustained and attack evaluations). The corresponding DOI-URLs are given in table 6.

Excitation model	DOI-URL
Single-reed	http://dx.doi.org/10.21954/ou.rd.3848415
Lip-reed	http://dx.doi.org/10.21954/ou.rd.4587307
Bow-string interaction	http://dx.doi.org/10.21954/ou.rd.4587361
Polynomial model	http://dx.doi.org/10.21954/ou.rd.4587367
All evaluations	http://dx.doi.org/10.21954/ou.rd.c.3715489

Table 6: URLs to the download location of the sustained and attack sounds for each excitation model.

The evaluation order in each sound file is for ascending parameter values. For the sustained sounds, the ramped parameter (γ, γ_b or δ) is repeated for increasing values of ζ or ζ_b. The same order is maintained for the attack evaluation, except for the polynomial model, where both parameters are swapped.

Finally, it should be mentioned that due to the amount of data, not all descriptor comparisons are discussed. When the outcome was obvious, or the reason for a particular outcome was unknown, discussion is often omitted.

5.3 SELF-SUSTAINED OPERATION: SUSTAINED SOUNDS

5.3.1 *Recalling the theoretical sound feature estimations*

In order to verify the relevance of the experimental results, a comparison is made with the theoretical predictions of the sound features, which were obtained for each excitation model in subsections 4.2.3, 4.3.3, 4.4.4 and 4.5.3.

Some predictions are of direct quantitative relevance to the experimental results. Hence, to favour comparison efficiency, they are plotted along with the experimental descriptor results. The theoretical amplitudes (estimated with the "intersection method") are plotted with the experimental peak-to-peak amplitude descriptors in figure 62 and the fundamental frequency estimations are plotted with the according descriptor results, as shown in figure 64.

Meanwhile, figure 58 represents the "normalised RMS pressures". In subsection 2.3.2 it was explained how this notion is related to the spectral richness of the pressure waves. For the $\{\gamma, \zeta\}$ evaluation of the lip-reed model (figure 58 (LR1)), both the normalised RMS pressure and the "dissipation ratio" are copied from subsection 4.3.3 in the same plot here (corresponding to respectively the thick and thin curves), while for its $\{Q_r, \theta\}$ evaluation (figure 58 (LR2)), only the dissipation ratio is shown. These estimations are mainly related to the experimental Harmonic Spectral Centroid descriptors, discussed in subsection 5.3.5, but also reference is made from other descriptor discussions.

In figure 59 the "normalised even harmonic RMS flow rates" are presented. They were also obtained for each excitation model in chapter 4 (except for the lip-reed $\{Q_r, \theta\}$ evaluation), and are intended to provide an estimation of the amount of even harmonics that the excitation model produces when coupled to a clarinet-type resonator. Hence, they are related to the Even Amount descriptor findings presented in figure 65.

5.3.2 *Single oscillation periods*

Figure 60 shows single periods of the steady-state temporal dimensionless pressure waves $\bar{p}(t)$ produced by the hybrid and simulated instruments for constant input parameter states, along with their corresponding air flow signals $\tilde{\bar{q}}$ calculated by the excitation models. The parameter values — included on this figure — are based on average values of the previously mentioned parameter ranges for each excitation model, and hence, they result in a typical operational state.

GENERAL CONSIDERATIONS From an overall comparison of the hybrid and simulated signals it can be concluded that the amplitudes, wavelengths and wave shapes are in reasonable correspondence, in particular for the pressure waves. This conclusion can be drawn for the whole range of the sustained sound evaluations, although, a few notable deviations can be identified.

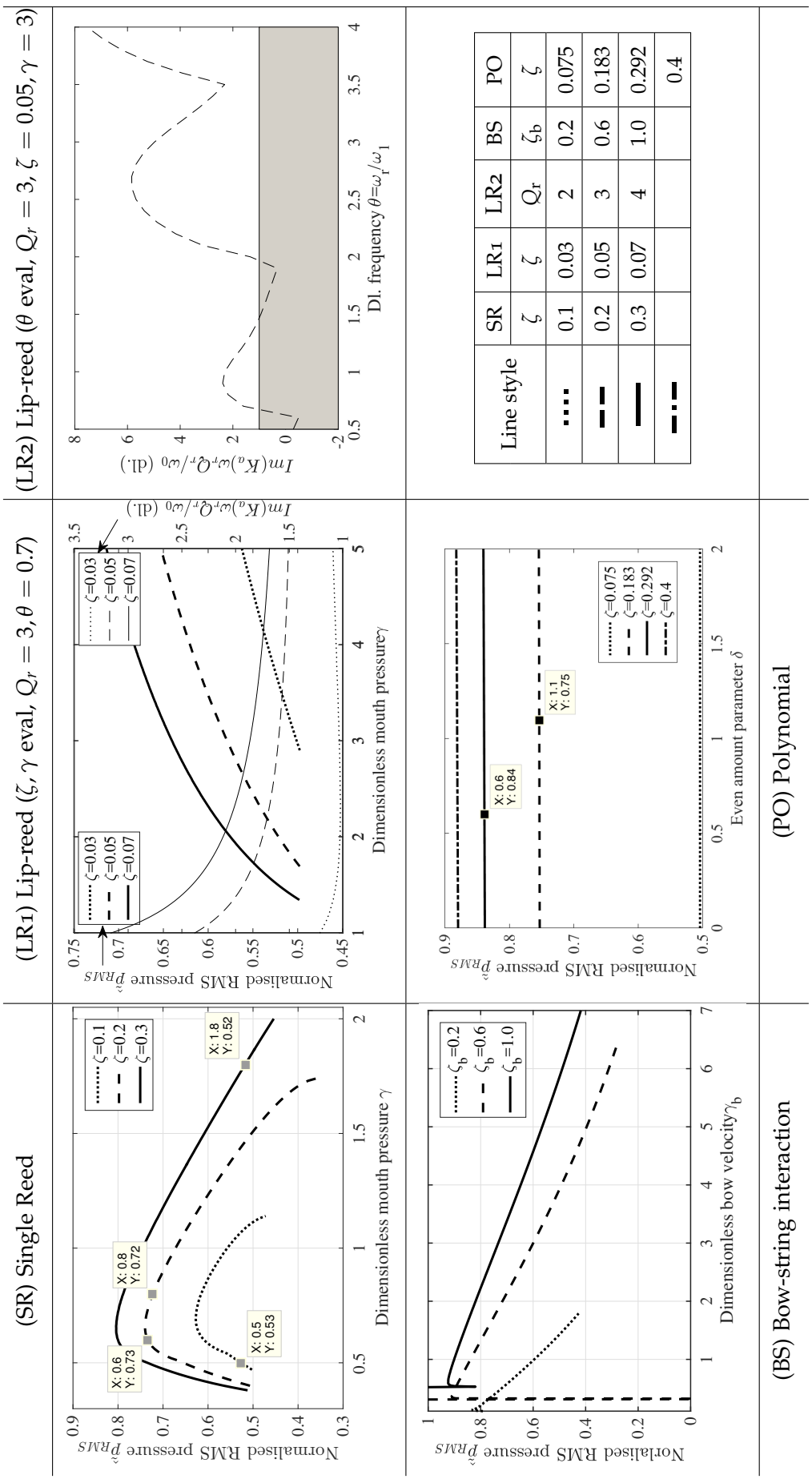

Line style	SR	LR1	LR2	BS	PO
	ζ	ζ	Q_r	ζ_b	ζ
····	0.1	0.03	2	0.2	0.075
– –	0.2	0.05	3	0.6	0.183
——	0.3	0.07	4	1.0	0.292
–·–					0.4

Figure 58: Sound predicting curves: Normalised RMS pressures $\hat{p}_{\text{RMS}}$.

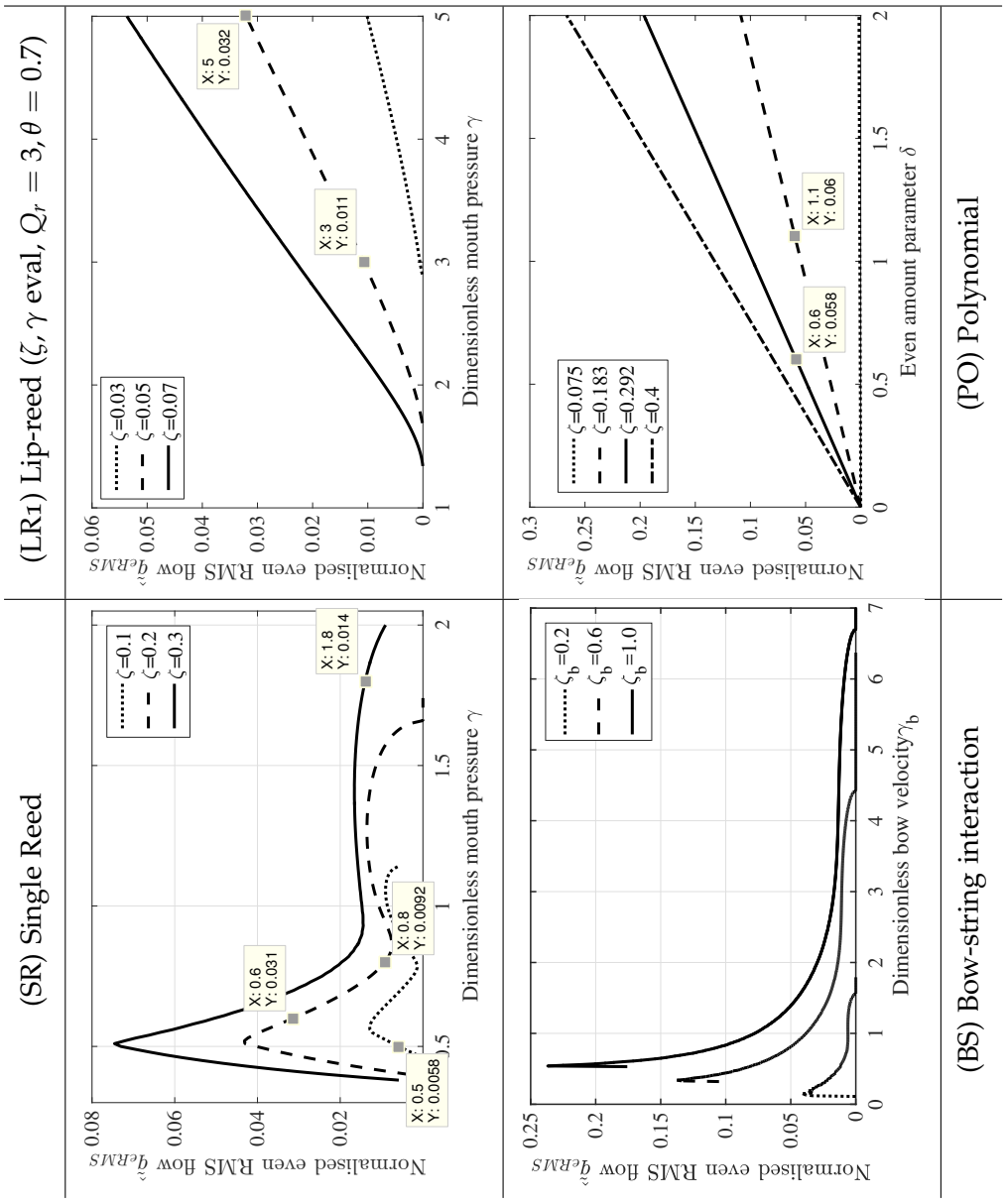

Figure 59: Sound predicting curves: Normalised even RMS flow rates $\hat{\tilde{q}}_{\text{eRMS}}$.

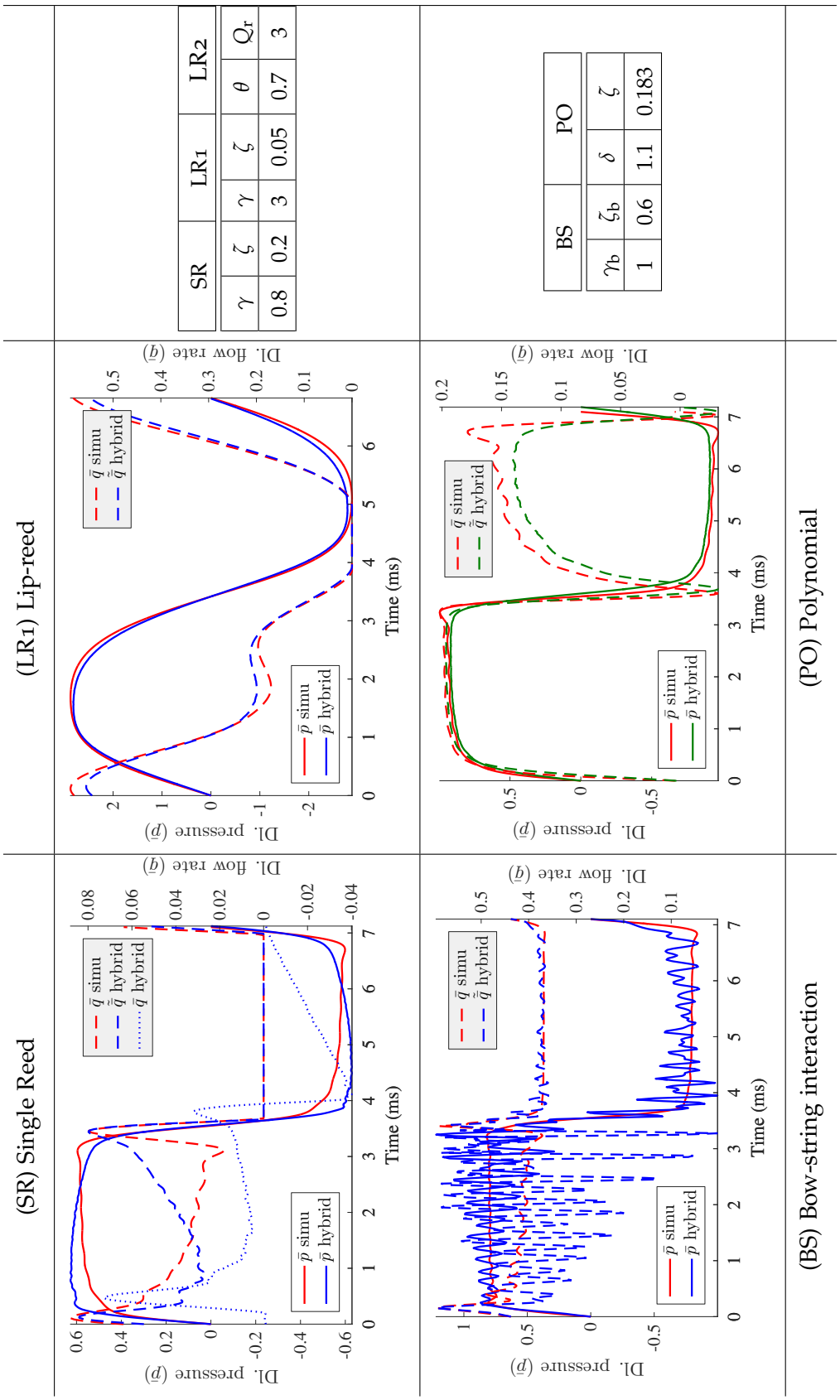

SR		LR1			LR2	
γ	ζ	γ	ζ	θ	Q_r	
0.8	0.2	3	0.05	0.7	3	

BS			PO	
γ_b	ζ_b	δ	ζ	
1	0.6	1.1	0.183	

Figure 60: Steady state temporal pressure wave at the resonator entrance for a selection of excitation parameters.

SINGLE-REED MODEL The simulated single-reed pressure and flow rate wave shapes (figure 60 (SR)) are somewhat asymmetrical from the hybrid waves, at the pressure extrema. This explains the phase difference in the spectra in the corresponding Fourier series in figure 61 (discussed in more detail later).

For the single-reed model, as well as the hybrid and simulated air flow signals, the measured air flow signal $\bar{q}$ is shown (determined from measurement of the loudspeaker membrane velocity with a laser Doppler vibrometer, along with an estimate of the membrane surface area S_d). As expected, this signal does not contain any mean flow given that the average membrane velocity is 0. However, it is interesting to note that there are significant deviations from the calculated flow rate. This is due to loudspeaker characteristics that are not fully compensated for by the feedforward and feedback filters discussed in chapter 3. A part of the effect appears to be (close to) a constant phase delay, as both flow rate peaks occur later in time. This is confirmed by the measurements carried out on the loudspeaker-tube system presented in subsection 3.3.3; while the $\tilde{Z}_t^*$ impedance curve reported in that section indeed reveals an increasing phase lag that resembles a constant phase delay, the $\tilde{Z}_{t(ss)}^*$ curve — calculated from the steady state oscillations presented here — shows an even greater constant phase delay, which is most likely due to a nonlinear loudspeaker effect.

Due to the complexity of the measurement set-up, and the unanticipated usefulness of the results, loudspeaker membrane velocity measurements were not carried out for the other excitation evaluations. However, given that the comparison of hybrid and simulated evaluations is characterised by broadly similar deviations for all excitation models, it is reasonable to assume that the difference between the calculated and real flow rate signals is mainly characterised by a similar phase deviation.

LIP-REED MODEL It can be seen that the waves generated from the lip-reed evaluation are more rounded in shape (figure 60 (LR1)), which is a direct consequence of the low-pass filtering effect of the relatively low lip resonance

frequency. A good correlation between simulated and hybrid results is noted for this model.

BOW-STRING MODEL Another notable deviation is observed for the bow-string interaction (figure 60 (BS)). At the pressure wave extrema, in comparison with the simulation results, the pressure and flow rate waves resulting from the hybrid operation exhibit an additional chaotic oscillation, which is perceived as a raucous sound. It should be mentioned that this phenomenon also occurs for the simulation, but the raucous behaviour appears below a much lower "raucous threshold" (given by equation (85), expressed as the ratio of bowing velocity over bowing force). While this chaotic instability is partly due to the characteristics of the excitation model (explained in section 4.4), it appears that the hybrid instrument's raucous threshold lies at a higher level, which is most likely due to a more general unstable behaviour of the hybrid instrument (further discussed in subsection 5.5.1). The more precise raucous thresholds are discussed later with the descriptor representation of the entire sustained sound evaluation.

POLYNOMIAL MODEL Similar to the single-reed and bow-string models, the polynomial model is a quasistatic excitation model and its produced pressure waves are essentially square-shaped. Unlike the single-reed model, the hybrid and simulated wave shapes are not asymmetrically related at the pressure extrema. This is related to the aforementioned loudspeaker deterioration and is further explained with the descriptor observations that will follow.

5.3.3 *Fourier series of the pressure periods*

Figure 61 shows the Fourier series corresponding to the steady-state pressure waves presented in figure 60. The magnitudes are represented in decibels of

the dimensionless pressures (i.e. 0 dB corresponds to $|\bar{p}| = 1$) and the phase responses are shown as relative to the phase of the first harmonic.

SINGLE-REED MODEL For the single-reed model (figure 61 (SR)), a very good overall match is observed between the hybrid operation and the simulation, particularly for the odd harmonics whose magnitudes differ by no more than 3 dB up to 3.5 kHz, while the first eight even harmonics resulting from the simulation are on average 3 dB louder. This level of agreement is obtained for all sounds obtained with the single-reed model within a parameter range that ensures a stable output (hereafter this notion is referred to as the "stable parameter domain"), $\gamma < \frac{3}{4}\gamma_{ex}$ (with γ_{ex} the extinction threshold) and $\zeta \geq 0.1$, where the steady oscillation state is not easily influenced by other parameters such as noise, the imperfect loudspeaker and its model. The relative phases of all harmonics remain fairly close (which is an expected outcome for at least the odd harmonics of a quasistatic excitation of a closed-open cylindrical resonator), and the previously mentioned asymmetrical difference between the wave shapes of the hybrid and simulated results is indeed explained by a phase difference, particularly present between 1 kHz and 3 kHz.

LIP-REED MODEL An interesting property of the lip-reed pressure wave is that the magnitudes of the harmonics (figure 61 (LR1)) decrease significantly faster with frequency than with the quasistatic excitation models. As a consequence, the magnitude from 1.7 kHz onwards goes below -70 dB so that the differences between the hybrid and simulated results are negligible.

BOW-STRING MODEL Examination of figure 61 (BS) reveals that, up to 2 kHz, the magnitudes of the odd harmonics corresponding to the hybrid and simulated bow-string evaluations are also in good agreement (and up to 1.5 kHz for the even harmonics). Above that, the harmonics corresponding to the hybrid operation are mostly higher in magnitude, which can be explained by the pres-

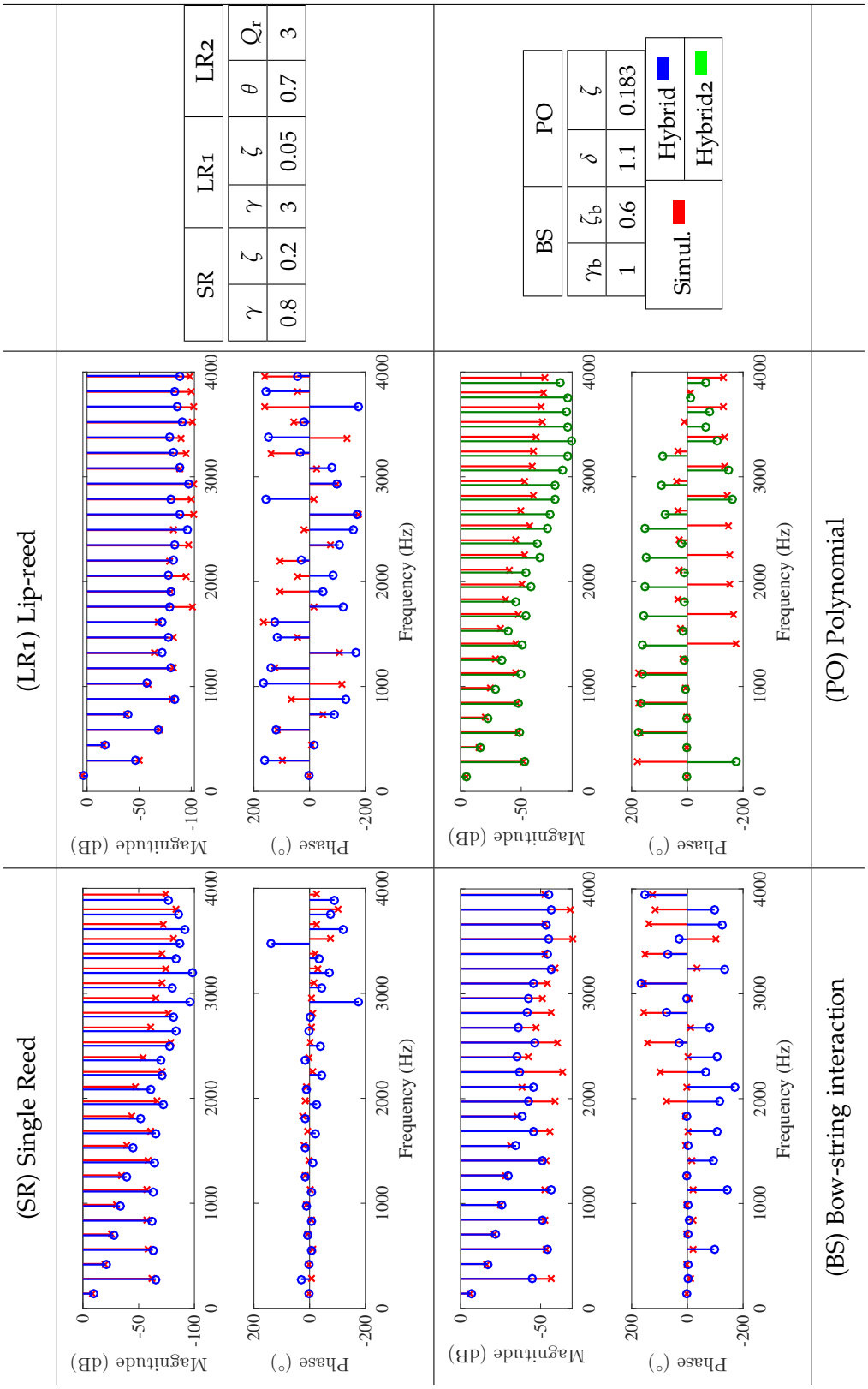

Figure 61: Fourier series of the steady state pressure wave at the resonator entrance (of the temporal signals in figure 60) for a selection of excitation parameters.

ence of the chaotic oscillations mentioned earlier. However, it should be noted that this additional component is not stationary in practice; i.e. in this Fourier series, although these oscillations appear in the harmonic series, in reality they represent a high frequency noise component, not bound to the harmonic series. These oscillations are also responsible for the large deviations in the relative phase response representation in that frequency range (note that the relative phases of the odd harmonics of the simulation remain close to zero up to 3.5 kHz).

POLYNOMIAL At lower frequencies, the magnitudes of the hybrid and simulated pressure waves generated with the polynomial model (figure 61 (PO)) are also in reasonable agreement. However, with increasing frequency, both the odd and even harmonics of the hybrid result progressively become smaller in magnitude in comparison with those arising from the simulation. This, and the slightly larger difference in fundamental frequency, can be explained by the loudspeaker deterioration, which is detailed later with the f_0 and HSC descriptors. It is interesting to note that the phase of the even harmonics for this model is almost opposite to that of the odd harmonics. This is due to the fact that the second order term of the polynomial curve has an inverted amplitude compared with the single-reed and bow-string models, which can be established from figures 36, 52 and 55 in chapter 4. While this does not have any audible influence with the cylindrical tube resonator, the sign of the even component is of importance when the excitation model is coupled to a resonator that excites both odd and even harmonics (such as a conical resonator for instance).

5.3.4 *Peak-to-peak descriptor*

Figure 62 shows the peak-to-peak amplitude descriptors (PP), calculated for the entire parameter ranges of all excitation models, evaluated for the sus-

tained sounds. Along with the hybrid and simulated results, the theoretical amplitudes are plotted. These amplitudes were graphically estimated with the "intersection method", and the curves are copied from the relevant figures (35, 42, 51 and 54) in chapter 4. For the single-reed and bow-string models (see figure 62 (SR and BS)) the oscillation thresholds are indicated with a + sign. For the bow-string interaction model, the "raucous thresholds" are also indicated (with large black dots).

GENERAL CONSIDERATIONS Both the simulated and hybrid results seem to correlate well with the theoretically predicted oscillation thresholds and amplitude progressions. Also the theoretical and experimental extinctions (where the amplitudes drop to zero with increasing γ and γ_b) coincide reasonably well. However, in some cases the theoretical extinction threshold (which only takes into account frequency independent losses in the resonator) is higher than the experimentally found extinction threshold. This can be explained by the frequency dependent part of the acoustic losses, which can be verified with the normalised RMS pressure estimations in figure 58. For these estimations, the pressure waves were assumed to be trapezoidal in shape (see figure 16) so that for $\hat{\tilde{p}}_{RMS} = 0.5$, the pressure wave becomes triangular in shape. For lower $\hat{\tilde{p}}_{RMS}$ values, the pressure maxima can no longer be reached so that extinction occurs, which explains how the frequency dependent losses can cause extinction. In order to address the oscillation condition for separate excitation models, further reference to figure 58 will be made.

Furthermore, the hybrid and simulated amplitude evolutions are in overall good agreement. However, a combination of high ζ and δ for the evaluation of the polynomial model (see figure 62 (PO)) or high ζ, γ and Q_r for the lip-reed model (see figure 62 (LR1 and LR2)), results in an excessive steepness of the nonlinear excitation curves leading to unstable states, particularly in the case of the hybrid evaluation (see section 5.5.1 for a general discussion on this issue). These states can be recognised by irregular amplitude descriptors, but

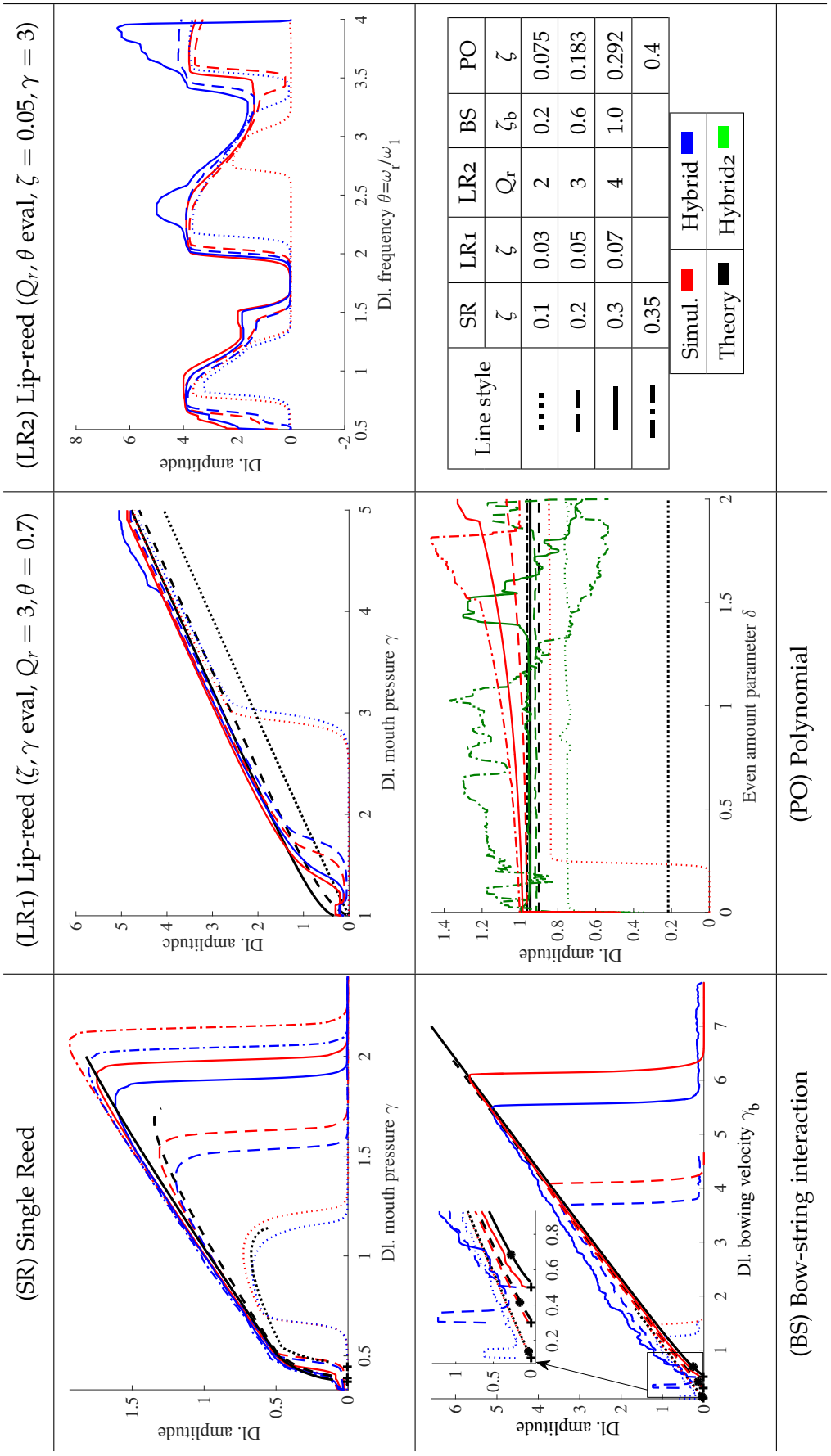

Figure 62: Peak-to-peak amplitude descriptors for the sustained sounds.

the noisiness descriptor (figure 66) represents an even better indicator of this issue.

The hybrid progressions generally reach extinction slightly earlier than the simulations, which could be explained by the fact that uncompensated loudspeaker effects (e.g. introducing the increasing phase lag noted in figure 27) can be interpreted as an increase in losses in the hybrid system.

SINGLE-REED MODEL According to the trapezoidal wave shape assumption, a somewhat contradictory single-reed occurrence can be observed. It can be noted that the experimental extinction thresholds in figure 62 (SR) correspond to $\hat{\tilde{p}}_{\mathrm{RMS}}$ values slightly below 0.5 (see figure 58 (SR)). This can be explained by the fact that the pressure waveform around this parameter state is closer to sinusoidal rather than trapezoidal or triangular, which somewhat invalidates the estimation theory.

LIP-REED MODEL In figure 62 (LR1), it can be seen that, in spite of the applied crude quasistatic assumption, the theoretical estimation of the amplitudes via the lip-reed model with the $\{\gamma, \zeta\}$ evaluation, turns out to be fairly coherent with the experimental results . Even the oscillation thresholds are predicted well.

Meanwhile, the "dissipation ratio" (shown in thin lines in figure 58 (LR1)), which should indicate the oscillation thresholds when above 1, only provides a coherent oscillation threshold estimation for $\zeta = 0.03$, where the ratio goes down to 1 at $\gamma = 2.5$. This could be explained by the fact that this prediction does not take into account the lip-beating, which might be of particular importance for high ζ and low γ. However, the usefulness of this predictor is clearly illustrated with the $\{Q_{\mathrm{r}}, \theta\}$ evaluation (figure 58 (LR2)), where the theoretically predicted oscillation condition is not satisfied for $\{Q_{\mathrm{r}} = 3, \theta = [1.5, 2]\}$, which is indeed reflected in the experiments. Finally, it should be noted that the register selection (clearly noted in the fundamental frequency leaps in figure 64

(LR2), which will be discussed later) is indeed coherently estimated by selecting the highest dissipation ratio (as explained in subsection 4.3.3).

As further noted from figure 62 (LR1 and LR2), the hybrid and simulated peak-to-peak amplitudes for all sustained lip-reed evaluations are in very good agreement, except for the mentioned unstable states.

BOW-STRING MODEL The theoretical and experimental bow-string extinctions show mismatches, in particular for $\zeta_b = 0.6$, where the theoretical extinction is almost twice as high (see figure 62 (BS)). As explained earlier, this can be explained by the frequency dependent losses in the resonator. Indeed, considering the bow-string model's normalised RMS pressure estimations in figure 58 (BS), it can be seen that for $\zeta_b = 0.6$ and $\gamma_b > 4$, the normalised amplitude $\hat{\tilde{p}}_{RMS} < 0.5$.

Comparing the hybrid and simulated results in figure 62 (BS), it is interesting to note that the former have a higher amplitude for low γ_b. This is an effect of the additional, raucous oscillations occurring at the pressure peaks (as could be noted from figure 60 (BS)). Observations of the pressure waves revealed that the hybrid amplitude in absence of these oscillations matches well to the simulations, even near the oscillation threshold.

POLYNOMIAL MODEL With the polynomial excitation model for $\zeta = 0.075$, the theory predicts a much lower amplitude than what is found experimentally (see figure 62 (PO)). However, as can be noted from figure 58 (PO), this ζ value results in $\hat{\tilde{p}}_{RMS} \approx 0.5$, which explains that the oscillation is near to extinction. The oscillation amplitude changes rapidly around this value, which explains the difference between experimental and predicted amplitudes.

For $\zeta = 0.4$, the hybrid evaluation produced a period doubling. While the chosen descriptors do not reveal this effect, it can be clearly heard in the sound examples. The period doubling phenomenon is further briefly discussed in section 5.5, but it is worth mentioning that the effect was not noted for the simu-

lated case, which may be an exceptional deviation that could be of interest from a musical point of view.

5.3.5 *Harmonic Spectral Centroid descriptor*

The Harmonic Spectral Centroid descriptors for the hybrid and simulated results are shown in figure 63.

GENERAL CONSIDERATIONS The "normalised RMS pressures" predictions of the quasistatic excitation models (figure 58 (SR, BS and PO)) give a useful indication of the related spectral centroids (figure 63 (SR, BS and PO)). Within the evaluated parameter domain of each excitation model, a reasonable direct proportionality can be noted, i.e. the shapes and relative distances of the predicted curves correlate reasonably well with the experimental results. Furthermore, the absolute interrelation between different excitation models is also respected to some extent.

For many parameter ranges with the single-reed and bow-string evaluations, a linear mapping can be made from the $\hat{\tilde{p}}_{\mathrm{RMS}} = [0.6, 0.8]$ range to a HSC range of $[500, 1000]$ Hz. For instance, this mapping is relevant with the single-reed model in the range $\{\gamma = [0.6, 1.2], \zeta = [0.2, 0.3]\}$, and with the bow-string model for all ζ_b values and γ_b somewhat higher than the oscillation threshold but below half the extinction value. Some non-matching ranges can be explained by the fact that the oscillation becomes sinusoidal instead of trapezoidal, as mentioned earlier. For the polynomial model (focussing on the simulations only, as the hybrid HSC results are affected by the loudspeaker deterioration) a linear mapping from $\hat{\tilde{p}}_{\mathrm{RMS}} = [0.52, 0.75]$ to a HSC range of $[500, 1000]$ Hz results in a good correlation for all parameter states.

The overall difference between the simulated and the hybrid evaluations does not exceed 10%.

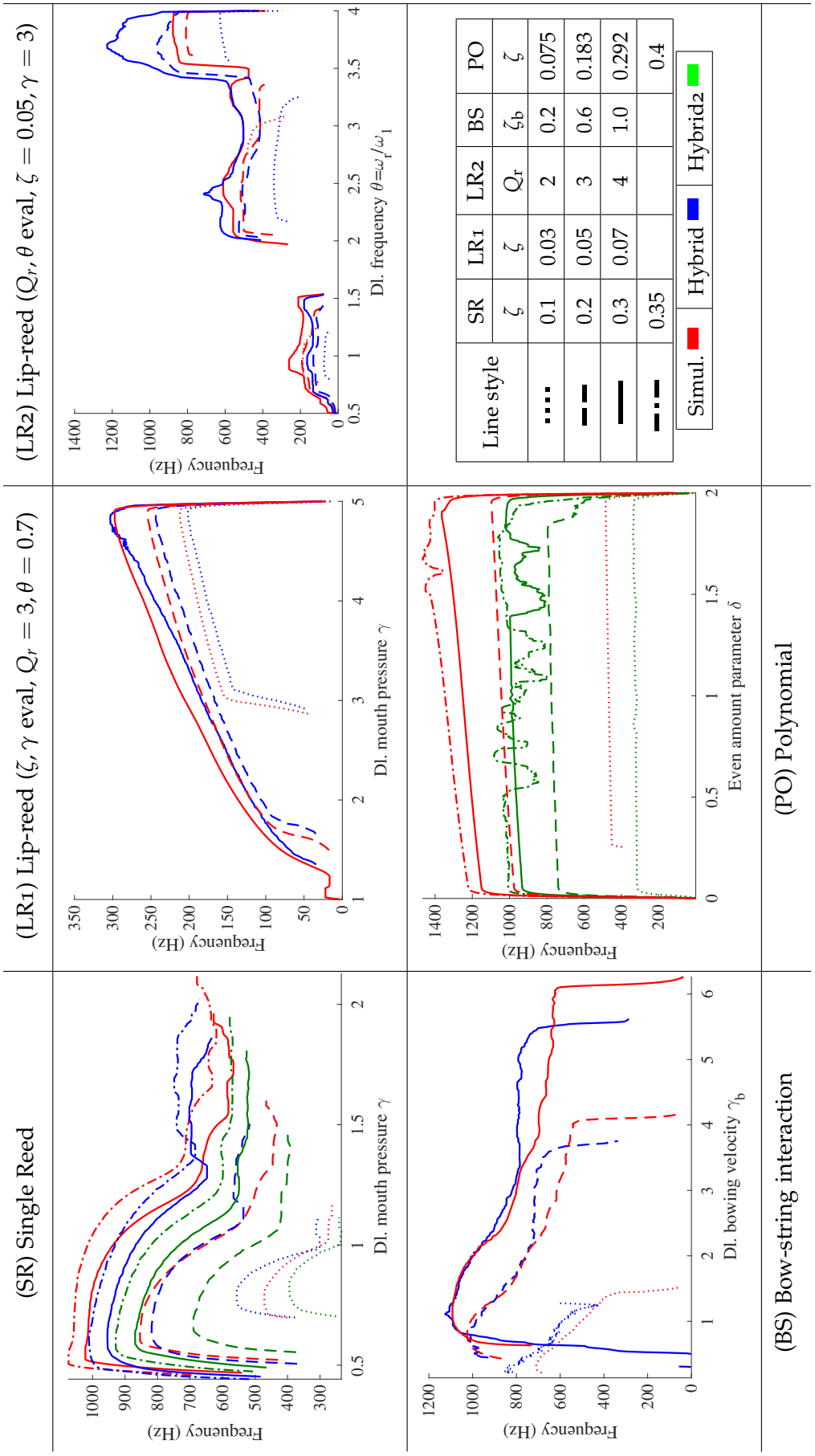

Figure 63: Harmonic Spectral Centroid descriptors for the sustained sounds.

SINGLE-REED MODEL It is worth mentioning that the findings with the single-reed excitation (figure 63 (SR)) are all in broad agreement with those of Almeida et al. (Almeida et al., 2013), who excited a real clarinet using a basic artificial mouth and then took a similar evaluation approach to that used in this study. However, the level of the agreement with Almeida's results is much smaller than the correlation between the hybrid and simulated results reported here. Hence, the similarity between Almeida's evaluation of a real clarinet and the results presented here only indicates that the single-reed model employed in this study reflects the behaviour of a real clarinet mouthpiece, played by an artificial mouth.

Nevertheless, as mentioned in subsection 1.4.3, and also stressed in another paper by Almeida (Almeida et al., 2010), such studies represent interesting potential for hybrid evaluation, for instance with more complex resonators.

Further in figure 63 (SR), for the single-reed excitation with $\zeta = 0.2$, the simulated and first (blue) hybrid curves are well-correlated. Higher ζ values (producing a richer sound) seem to increase the HSC of the simulated sounds slightly more. This can be partly explained in terms of the difference in fundamental frequency (shown in figure 64 (SR)). As noted in the characterisation of the hybrid system in chapter 3, in particular in the impedances presented in figure 27 in subsection 3.3.3, the modes of the resonator follow a positive inharmonicity (i.e. instead of being exact multiples of the frequency, the resonance frequencies shift upwards, e.g. $1275.3\,\text{Hz}/9 = 141.7\,\text{Hz} > 139.79\,\text{Hz}$). Provided the embouchure parameters remain unchanged, a higher fundamental frequency will lead the higher harmonics towards the tube's resonant peaks so that they are amplified, and hence the HSC increases. This is confirmed by the differences between the hybrid and simulated results in terms of both fundamental frequency and HSC. Nevertheless, the differences are relatively small and all progressions are similarly rapidly increasing after the note appearance, to then decrease until its extinction.

In contrast to the first hybrid evaluation, the loudspeaker deterioration resulted in a globally lower fundamental frequency in the second evaluations (the green curves), which in turn induces a lower HSC for the whole parameter range of the hybrid evaluation (see figures 63 (SR) and 64 (SR)). The second measurement lies between 8% to 20% lower.

LIP-REED MODEL The normalised RMS pressure curves (the thick lines in figure 58 (LR1), which are based on the quasistatic approximation of the lip-reed model) show a relative correlation with the HSC descriptor (figure 63 (LR1)). The quasistatic approximation used for this prediction is not relevant for the study of the variation of lip-reed dynamics, performed in the $\{Q_r, \theta\}$ evaluation. However, for that evaluation, the dissipation ratio (figure 58 (LR2)) seems to provide a reasonable correlation with the HSC descriptor (figure 63 (LR2)).

Like the peak-to-peak amplitudes, all simulated and hybrid lip-reed evaluations resulted in a good HSC descriptor agreement (see figure 63 (LR1 and LR2)).

It can be noticed that very low HSC values can be achieved, down to 100 Hz for a guaranteed oscillation condition. However, in contrast to the single-reed, where the reed resonance frequency can be very high and doesn't affect the oscillation so much, the lip-reed needs to be continuously "tuned" to the applied fingering. This represents a practical disadvantage that is of particular concern with a hybrid instrument. Indeed, while real brass players use the direct, acoustic feedback on the lips to find the right embouchure and obtain a targeted pitch, the playing control of the hybrid instrument normally lacks such a bi-directional interaction. Instead, to find the right pitch with the hybrid instrument, much slower feedback mechanisms are used, such as auditive feedback and/or based on the awareness of the applied fingering (where the latter can be understood as a form of cognitive feedback).

BOW-STRING MODEL Regarding the relationship between the HSC and the fundamental frequency (see respectively figures 63 (BS) and 64 (BS)), the bow-string interaction evaluations show a similar effect as for the single-reed evaluation.

With low γ_b, both hybrid and simulated HSC correlate positively with the fundamental frequency. For higher γ_b, the fundamental frequencies of the simulations decrease while they remain almost constant for the hybrid case. This, in turn, is reflected in the downwards diverging HSC of the simulation.

POLYNOMIAL MODEL For the polynomial model, as far as the theoretical estimation is concerned, the HSC is predicted to be independent of the even harmonics parameter δ (see figure 58 (PO)) . However, the experimental results indicate a slightly positive correlation with this parameter (see figure 63 (PO)). This can be explained by the fact that the theoretical prediction is based on the pressure signal at the resonator entrance, which is considered to only contain odd harmonics (see section 2.3). As indicated by equation (98), the radiated pressure also contains the even harmonics present in the flow rate signal $q(t)$, which therefore explains the positive correlation of δ and HSC.

As for the second hybrid evaluation of the single-reed, the fundamental frequencies and HSC of the hybrid polynomial model evaluation is globally lower than the HSC of the simulations (see figures 64 (PO) and 63 (PO)).

The fact that the HSCs resulting from the second measurement of the hybrid single-reed evaluations lies between 8% to 20% lower than the first evaluation suggests that the hybrid polynomial model's HSCs are decreased by similar percentages.

While the slightly decreasing fundamental frequency with δ tends to reduce the spectral richness, the variation is relatively small (compared to the other quasistatic evaluations), so that the opposing effect of the even harmonics is more important. This hypothesis is confirmed by observations of the "Odd

Spectral Centroid" descriptor (not shown here), which indeed slightly decreases with increasing δ.

Another interesting aspect of the polynomial model is that HSCs down to 350 Hz can be achieved, while the oscillation condition remains satisfied (even in combination with variable resonator conditions, i.e. while playing several notes on a clarinet resonator for instance). The obtained timbre is much more "rounded" than typical reed excitations, and therefore this excitation may enable interesting alternative musical expression possibilities. While the single-reed model with low ζ values can result in similar HSCs, the oscillation condition is much weaker and therefore cannot be easily applied to produce a melodic phrase for instance.

5.3.6 *Fundamental frequency*

All fundamental frequency progressions are represented in figure 64.

GENERAL CONSIDERATIONS There is a clearly different effect on the fundamental frequency between dynamic (the lip-reed) and (almost) quasistatic excitation models (the single-reed, bow-string and polynomial models).

For the lip-reed, the dynamics have a strong influence on the fundamental frequency, given that the lip resonance lies close to the playing frequency. Hence, the embouchure parameters have a much stronger effect on the pitch compared to the subtle effect of the resonator.

Close to the oscillation threshold, with a quasistatic excitation, the oscillation is close to sinusoidal and as such, relies almost solely on the first resonator mode, thereby determining its fundamental frequency. Further away from the oscillation threshold, the variation of the fundamental frequency is determined by the influence of higher resonator modes via the harmonics of the oscillation. This can be understood from the fact that the first few resonator modes are known to maintain the self-sustained oscillation (Dalmont et al., 1995); and

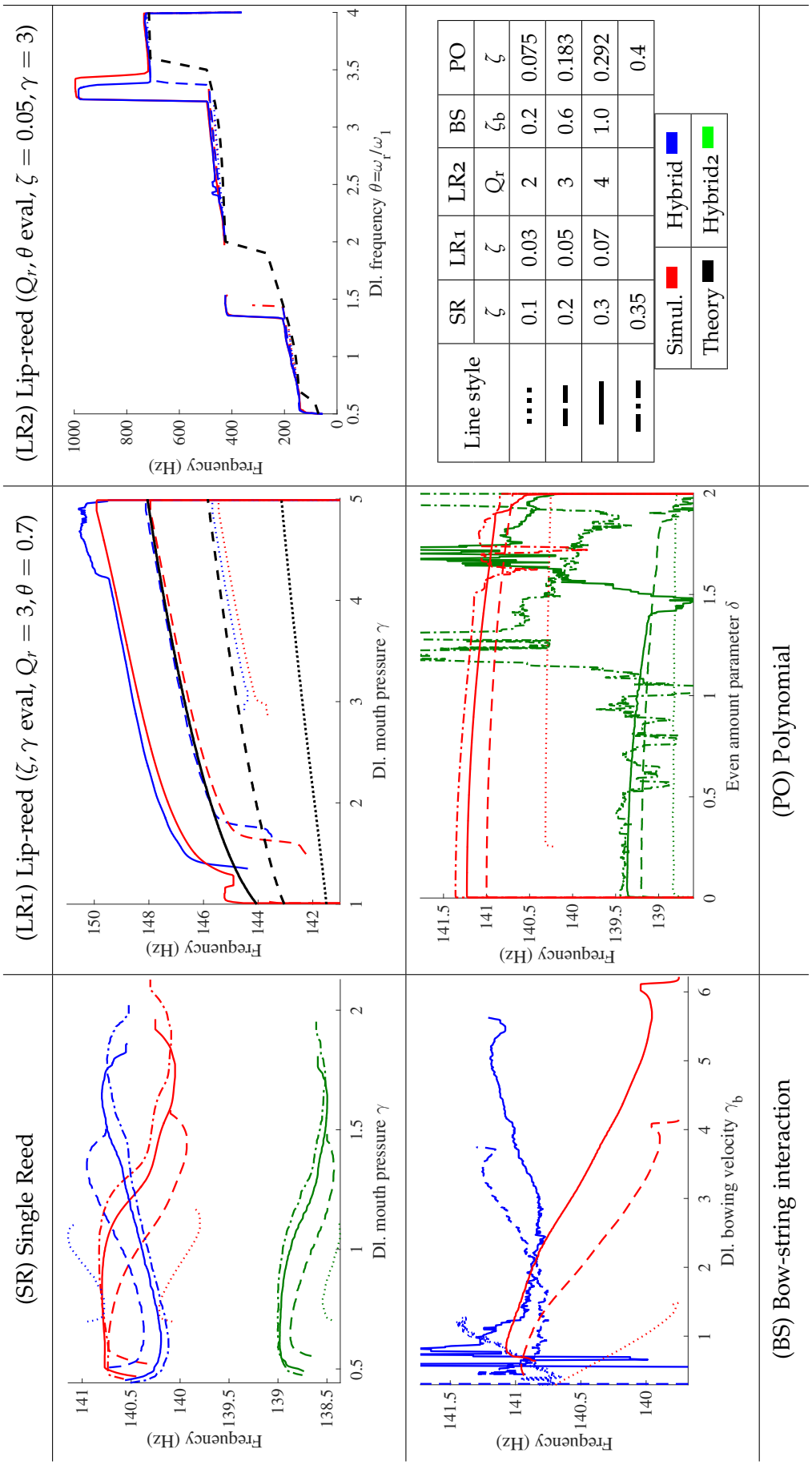

Figure 64: Fundamental frequency descriptors for the sustained sounds.

hence, the preferred oscillation frequency results from a weighting of these modes by the spectrum of the mouthpiece pressure. Therefore, the resonator's inharmonicity effect on the first modes should be considered[2]. As mentioned earlier, the tube impedance Z_t^* is positively inharmonic (as can be seen from the first five modes in figure 27).

Regarding the hybrid instrument, it should be first understood that the energy that sustains the oscillation comes from the frequencies where the phase response of the resonator impedance crosses zero. Hence, the observed phase decrease due to uncompensated (nonlinear) loudspeaker effects in $\widetilde{Z}_{t(ss)}$ in figure 27, indicates that during hybrid self-sustained operation, the resonator appears to be negatively inharmonic.

An interesting fact that applies to the quasistatic excitation models is that, as mentioned in the discussion on the HSC descriptor, the variation of the fundamental frequency in turn has an effect on the spectrum, given that the harmonics are weighted by the resonance frequencies of the resonator.

SINGLE-REED MODEL It is notable that the hybrid and simulated fundamental frequency curves have different trends (see figure 64 (SR)) which is not observed for the other descriptors. However all variations are small ($<$2 Hz or $<$25 cent) and are almost imperceptible.

Near the oscillation threshold, e.g. with $\zeta = 0.1$, the simulation starts at a fundamental frequency close to the first modal frequency of 139.8 Hz. However, the fundamental frequency of the first hybrid instrument evaluation (in blue) starts a few Hz above 139.8 Hz (the temperature used in the simulation matched that observed during the operation of the hybrid instrument). A possible reason for this initial pitch shift might be an imperfect compensation by the loudspeaker-correcting filter $\widetilde{H}_{LS}^{-1}$ which would introduce a slight phase shift for the first mode and as such a shift of the frequency at which instability occurs. This can

2 It is a well known theory that the inharmonicity causes the playing frequency to change with the brightness of the sound (see e.g. (Benade, 1990) and more recently developed analytical theories in (Coyle et al., 2014))

be verified from figure 27, where the phase response of the first mode of $\widetilde{Z}_t^*$ is indeed slightly shifted upwards in frequency from Z_t^* (by approximately 1 Hz, found by zooming).

At higher mouth pressures, the frequency variation can be explained by the resonator's inharmonicity, causing the fundamental frequency to generally follow the HSC (shown in figure 63 (SR)), which is indeed the case for the simulations in figure 64 (SR).

Meanwhile, for the case of the hybrid instrument, the negative inharmonicity indeed explains that the effect on f_0 for the first hybrid measurement is opposite to the simulated results (respectively the blue and red curves in figure 64 (SR)); and accordingly for the HSC descriptor (figure 63 (SR)).

In contrast, the fundamental frequency of the second hybrid evaluation (the green curves in figure 64 (SR)) starts somewhat lower, at about 138.4 Hz near the oscillation threshold, which globally shifts the f_0 downwards by about 2 Hz in comparison with the first hybrid evaluation. This is an effect of the phase lag introduced by the loudspeaker deterioration, which also turns the inharmonicity (considering the phase's zero crossings) positive again, thereby explaining the correlation with the simulation of the relative progressions.

LIP-REED MODEL The fundamental frequency for the case of the lip-reed excitation (see figure 64 (LR1 and LR2)) is clearly more variable and is mainly determined by the lip-resonance frequency θ (both enabling the selection of registers and controlling the playing frequency within the register), but also γ and ζ have a significant influence.

As predicted, the lower the lip-frequency below a resonance frequency of the tube, the closer the playing frequency approaches this modal frequency, though remaining always higher (which is valid with the "outward striking" lip-reed model used here). When the lip frequency is too distant from the modal frequency (i.e. below 0.5 or above 1.33 for the first register), extinction occurs or another register is selected.

From the good correlation between theory and experiments, for both $\{\gamma, \zeta\}$ and $\{Q_r, \theta\}$ evaluations, it can be concluded that the "small signal" assumption used in the prediction (i.e. subsection 4.3.3) is sufficiently valid to predict the fundamental frequency. The globally lower fundamental frequency estimation noted in the $\{\gamma, \zeta\}$ evaluation is due to the nonlinear stiffness increase during the lip-beating phase, which has been empirically confirmed with evaluations where the dynamical lip-reed parameters were held constant.

BOW-STRING MODEL The same conclusions as for the single-reed model (with the first hybrid evaluation) apply to the results with the bow-string interaction model.

POLYNOMIAL MODEL Unlike the single-reed and bow-string models, the simulation of the polynomial model does not result in a positive correlation between the HSC and the fundamental frequency (see respectively figures 63 (PO) and 64 (PO)), which is due to the earlier explained fact that the odd spectral centroid actually follows a progression that is opposite to the total HSC.

The hybrid results for this excitation model are comparable with the second evaluation with the single-reed model.

5.3.7 *Even Amount descriptor*

Figure 65 shows the Even Amount descriptors, calculated for all evaluations.

GENERAL CONSIDERATIONS It should be understood that, while a zero value for both the prediction (the "normalised even harmonic RMS flow rates" in figure 59) and the EA descriptor indicates that the signal only contains odd harmonics, there is an important scaling difference between both quantities. The prediction provides a quadratic mean estimation of the even harmonics wave component, relative to the total amplitude of the pressure at the reson-

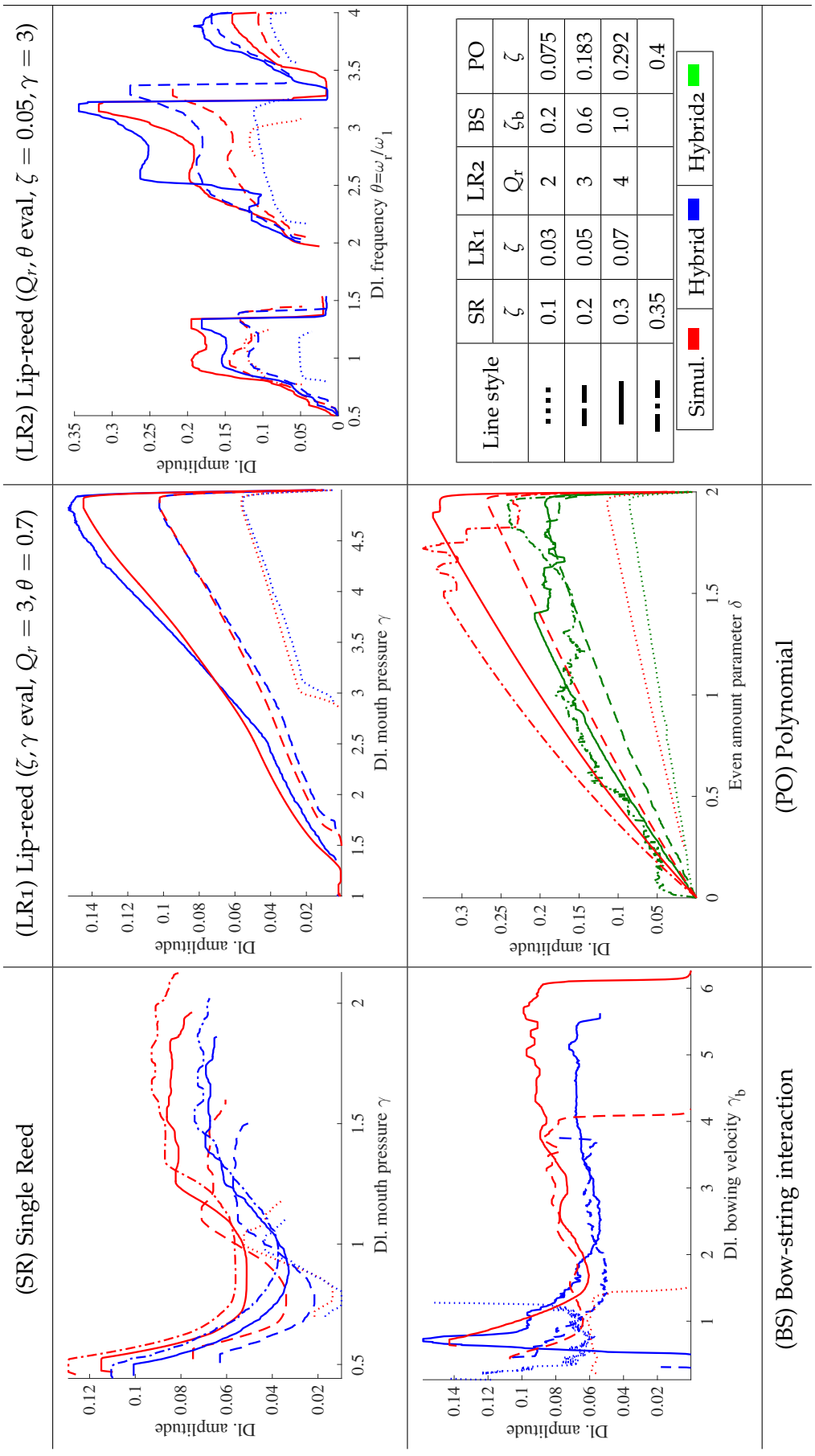

Figure 65: Even amount descriptors for the sustained sounds.

ator entrance. Conversely, the EA descriptor represents the energy ratio of the even over all harmonics, so that it is also influenced by the energy of the odd harmonics. Hence, in order to compare both features, the predicted normalised even RMS is to be interpreted relative to the total normalised RMS curves in figure 58.

Given the influence of the amount of odd harmonics on the EA descriptor, the hybrid-simulated relationship can be partly explained by the according conclusions made in the discussion on the HSC descriptor (see subsection 5.3.5 and figure 63). However, most hybrid evaluations with quasistatic excitation models globally result in slightly lower EA values (see figures 65 (SR, BS and PO)).

Another general observation is that a maximum EA of 0.2 could be obtained with the hybrid instrument.

SINGLE-REED MODEL Taking into account the mentioned influence of the odd harmonics in the EA descriptor, it can be understood that the EA descriptor changes more moderately for ζ variations and increases with γ, compared to the predictions (see figures 65 (SR) and 59 (SR)).

LIP-REED MODEL The theoretical prediction of the lip-reed model's EA (figure 59 (LR1)) is also in proportional agreement with the relevant experimental results (figure 65 (LR1)). Given that the EA descriptor results are less influenced by the resonator modes compared to the HSC descriptor, the lip-reed's EA results are of similar order as the other excitation models.

This descriptor seems to be highly influenced by the Q_r factor, though there are no theoretical estimations to explain this interesting observation.

BOW-STRING MODEL Similar conclusions as for the single-reed evaluation can be drawn regarding the relationship between theory and experiments.

Whereas the hybrid evaluations with other quasistatic excitation models result in lower EA values, with the bow-string model, as can be seen in figure 65

(BS), similar hybrid and simulated EA results are found with low γ_b (though the fluctuating curves attest to a low accuracy in this range).

POLYNOMIAL MODEL The conservation of the predicted linear progressions with the polynomial model attests for a particularly good correlation between the theory and the experiments (see figures 59 (PO) and 65 (PO)).

The potential of the polynomial model to obtain stable oscillations with high EA values, and to independently and precisely control this sound quality, down to an entirely odd spectrum (with $\delta = 0$) also provides an interesting potential for musical purposes.

5.3.8 *Noisiness descriptor*

Finally, the sustained sounds are analysed for the amount of noise by calculating the ratio of total spectral energy over the energy of all harmonic components, which is reported by the noisiness descriptors presented in figure 66.

It should be borne in mind that the ranges among the different excitation models vary greatly; e.g. the single-reed descriptor's noisiness range is more than 50 times smaller than the values that were obtained with the bow-string and polynomial models. For the latter models, this descriptor indicates where the oscillation becomes unstable, i.e. both due to the raucous character and due to the instability issue discussed in subsection 5.5.1.

5.4 SELF-SUSTAINED OPERATION: ATTACK SOUNDS

A second set of self-sustained evaluations is focussed on the study of attack transients. While clarinet players mostly initiate a note by tonguing, it is known that the tongue action mainly determines the timing of the initial transients (Li et al., 2016) rather than the attack time of the note onset. Hence, while the

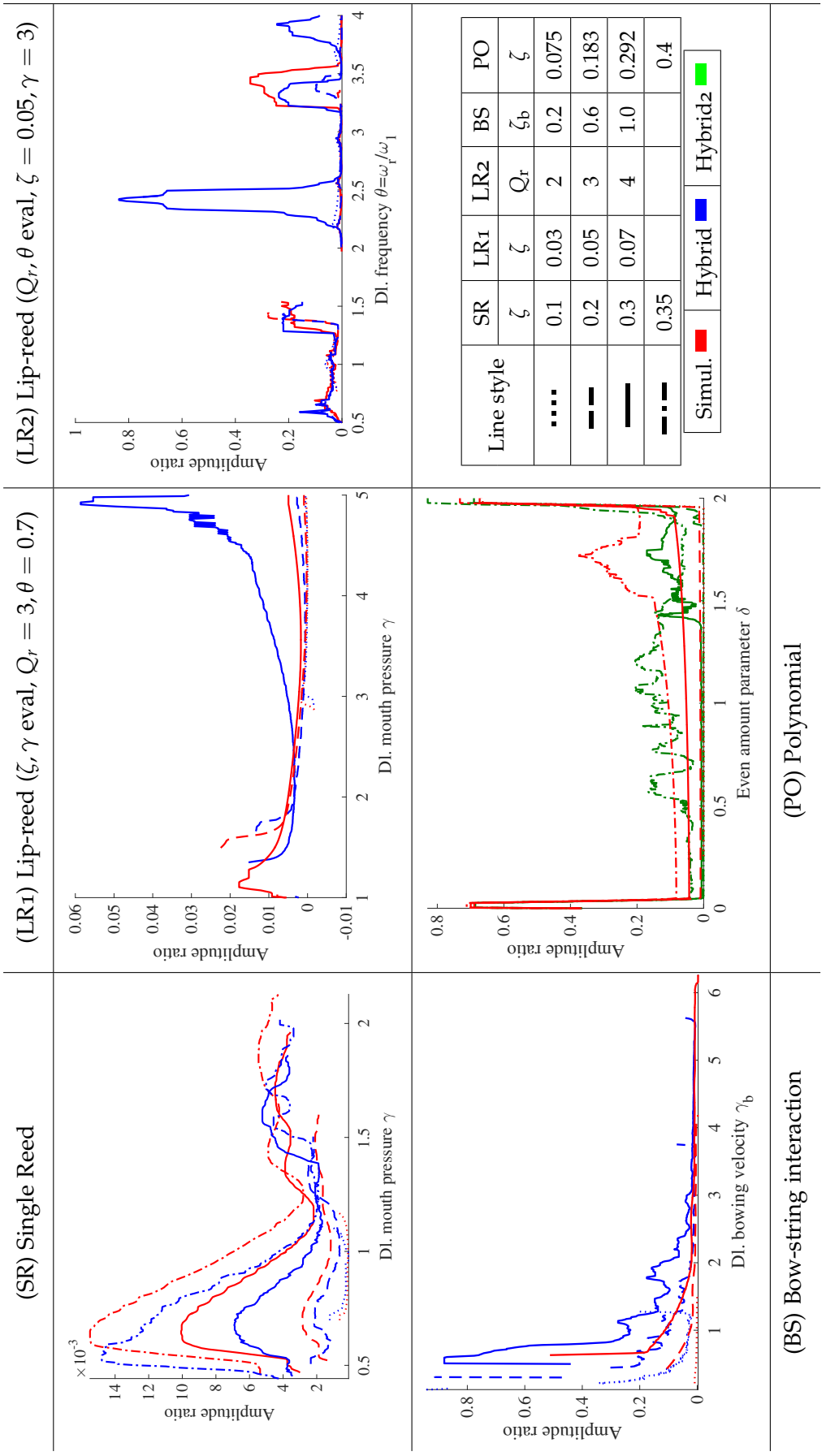

Figure 66: Noisiness descriptors for the sustained sounds.

applied single-reed model doesn't include the effect of the tongue, it is sufficient to apply a steep increase of the mouth pressure to imitate a tongue release. The same idea applies to the lip-reed model (with $Q_r = 3$ and $\theta = 0.7$) and analogously, attack envelopes of γ_b for the bow-string excitation were applied. However, for the polynomial model, the ζ parameter was used to generate attack transients, as the δ parameter does not cross an oscillation threshold.

These measurements were repeated for the same ζ and ζ_b values and, for the polynomial model, four constant δ values were chosen in the range used for the sustained sound evaluation (all values are provided in the tables in figures 67 to 68).

A number of constant values (ten γ values for the single-reed model, nine γ values for the lip-reed model, nine γ_b values for the bow-string model and four δ values for the polynomial model) between the parameter extrema stated in tables 2 to 5, were evaluated and the attack time measured.

These values were introduced using an "attack envelope" for the concerning excitation parameter. On the one hand, this is done to match real playing conditions, as even with a quick tongue release, the instrument is still gradually exposed to the mouth pressure. On the other hand, it turned out to be also required in order to obtain coherent results. Indeed, for most excitation models an (almost) instantaneous parameter onset resulted in chaotic attack times (sometimes faster, but sometimes much slower). Nevertheless, so as not to influence the attack time, the attack envelope's rise time must be shorter than the attack time. A rise time of 0.3 s appeared to be sufficient (shorter rise times did not influence the resulting attack time for the particular sets of ζ, ζ_b and δ). Any evaluations that did not result in a note onset were left out of the descriptor representation.

It should be mentioned that, like the sustained evaluation of the polynomial model, all attack evaluations with the bow-string, lip-reed and polynomial excitation models were evaluated in a later stage of the research and, hence, the loudspeaker deterioration influenced these results. In order to provide an idea

of the effect, the hybrid single-reed evaluation was also repeated and both evaluations (before and after the loudspeaker deterioration) are shown for the LAT descriptor. For this reason, and because of the noted high correlation between different attack-related descriptors, the overall evaluation of the attack measurements is kept brief. Apart from the Logarithmic Attack Time descriptors shown in figure 67, which are calculated for both hybrid and simulated instruments with all four excitation models, the End of Attack Time and Spectral Flux descriptors, shown in figure 68, are only represented for the single-reed evaluation.

5.4.1 *Logarithmic Attack Time descriptor*

SINGLE-REED MODEL For the single-reed excitation, it has been shown that the spectral centroid and the attack time of a note onset are inversely correlated features, which are mainly controlled by the embouchure parameter ζ (Barthet, 2009). This is clearly confirmed when comparing the LAT results in figure 67 (SR) with the HSC curves in figure 63 (SR) (over the common γ range from 0.4 to 1.2).

Nevertheless, it can be noted that for increasing ζ and notably considering the two highest ζ values, the LAT results are more "saturated" than the HSC. It can be said that the general effect of this saturation is partly due to the applied spectral truncation at 4 kHz (as explained in subsection 5.1.4), but it is also apparent that the attack time is more nonlinearly related to ζ than the spectral richness of the steady-state regime.

These findings on the attack time are also in good relative agreement with a recent study on the transients in a real clarinet (played with an artificial mouth). This study was conducted by Li et al. (Li et al., 2016), following a similar approach to Almeida (Almeida et al., 2013). However, as with the sustained sounds, the agreement between our and their findings is much smaller than the observed correlation between the simulated and hybrid results, so that

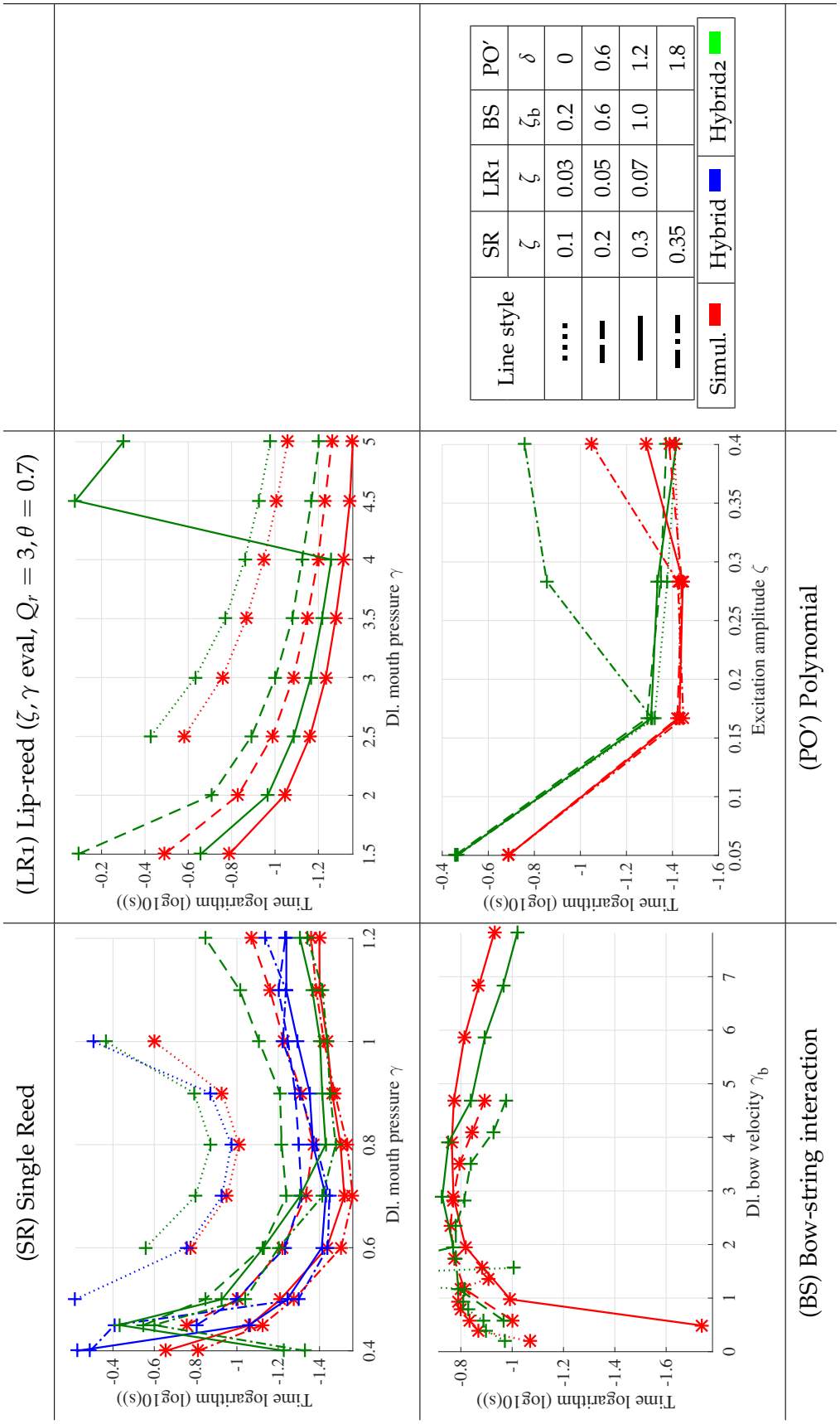

Figure 67: Logarithmic Attack descriptors for the attack sounds.

it is not possible to draw any further meaningful conclusions regarding their experiments. As mentioned in subsection 1.4.3, it is worth reminding here that the reproduction of rapid changes in mouth pressure is difficult to realise with a blowing machine (Ferrand and Vergez, 2010), so that such studies may well benefit from an evaluation with a hybrid instrument.

Furthermore, the correlation between the single-reed LAT and HSC simulation results with the first hybrid evaluation are of the same order of precision, but the systematic deviations don't follow the same trend. For instance, while the correlation is inverse, for $\zeta = 0.1$, both the hybrid HSC and LAT are higher than the simulations. Meanwhile, for $\zeta = 0.3$ and $\zeta = 0.35$, the LAT simulation and hybrid results match well for $\gamma \leq 0.6$, but diverge above. (The divergence is in the same direction, but the trend is somewhat opposite to that noted for the HSC.)

The second hybrid evaluation with the single-reed model resulted in slightly more hybrid-simulated deviating behaviour due to the loudspeaker deterioration (see the green curves in figure 67 (SR)). It is notable that for $\zeta \geq 0.3$, low mouth pressure onsets result in longer attack times than before the loudspeaker deterioration, while high mouth pressures result in the opposite effect. The fact that the correlation of the LAT and HSC of these results is weaker supports the hypothesis that the loudspeaker deterioration is nonlinear in nature.

LIP-REED MODEL Similar to the single-reed model, the results with the lip-reed are also inversely correlated to the HSC descriptor results (see figure 67 (LR1)). However, it is interesting to note that the lip-reed LAT values are of the same order as the quasistatic excitation models, while the HSC results were much lower.

BOW-STRING MODEL It is striking that the LAT descriptor results obtained with the bow-sting interaction are not inversely correlated to the HSC descriptor (see respectively figures 67 (BS) and 63 (BS)). Indeed, following a bow velocity

(γ_b) progression, the curves are actually positively correlated, and when γ_b is high, different bow-forces ζ_b also conserve this correlation. However, this is less the case around the oscillation threshold, where the HSC is peaking, while the LAT peaks (i.e. slowest attack times) lie in the middle of the oscillation and extinction thresholds. This is an interesting and different behaviour to the single-reed results, demonstrating the diversity that can be obtained with different excitation models, which are even only quasistatic.

A reasonable explanation of this difference can be gained by re-considering the sound-feature prediction theory, notably the acoustic power estimation curves in figures 17 and 52 in chapter 4. Indeed, given that the oscillation onset is an increasing amplitude from $\hat{\tilde{p}} = 0$ to the domain covered by the steady state, for the LAT descriptor it is of importance how the normalised power is distributed (from the centre to the sides). For the single-reed model, it can be verified that this distribution is correlated with the total normalised power in the steady-state oscillation, while for the bow-string model, the correlation is almost opposite.

It is known that the attack time of bowed strings can be much faster then the attack times obtained with reed instruments (McIntyre et al., 1983). The reason why the obtained attack times are of the same order for both excitation models is that the ζ_b parameter range that is used is much lower than for the case of real bowed-strings. The combination of a high bowing force and velocity leads to short attack times.

The overall agreement between the hybrid and simulated results is reasonable, although the hybrid results seem to be shifted upwards with respect to γ_b. However, the fact that these results are biased by the loudspeaker deterioration makes more detailed comparison irrelevant.

POLYNOMIAL MODEL As with the single-reed and lip-reed models, the polynomial model mainly shows an inverse correlation between the LAT and HSC descriptors. However, to compare those descriptors, the changed role of

ζ and δ should be considered. Hence, a correlation can be noted. Indeed, the HSC curves (in figure 63 (PO)) almost remain constant for δ variations, which is also the case for the LAT curves in figure 67 (PO') (given that the curves for several δ coincide).

The correlation is also mainly conserved for variation of the ζ parameter. However this is less the case for the simulation, where for $\zeta \geq 0.15$ the LAT stagnates at about -1.4, while the HSC is still increasing for these values, which might be due to similar reasons as for the noted saturation of the single-reed LAT descriptor.

5.4.2 *End of Attack Time and Spectral Flux descriptors*

Figure 68 shows the End of the Attack Time and Spectral Flux descriptors for the single-reed evaluation only. The EAT descriptor reveals the actual sound onsets, the time between the start of the input parameter envelope (which can be thought of as the start of a performer's action) and the instant the steady-state oscillation is reached. It can be noted that more important hybrid-simulation deviations occur than for the case of the LAT descriptor, in particular for low γ values. The additional delay in the simulations may be due to the absence of irregularities that may help stimulate the attack, such as noise (present in real wind instruments, due to the flow turbulence). This hypothesis is supported by the findings of an additional experiment: a repeated simulation with an added noise signal (of similar amplitude to the noise present with the hybrid instrument) resulted in a reduction of up to 30% in the EAT compared with the noiseless simulations, which partly confirms the assumption. Given the importance of timing, this aspect might be of consideration for reed instrument physical models. (It should be noted that the added noise did not significantly influence the LAT descriptor.)

The Spectral Flux curves show similar behaviour to the LAT curves of figure 67 (SR), but a main difference is the smaller descriptor variation with chan-

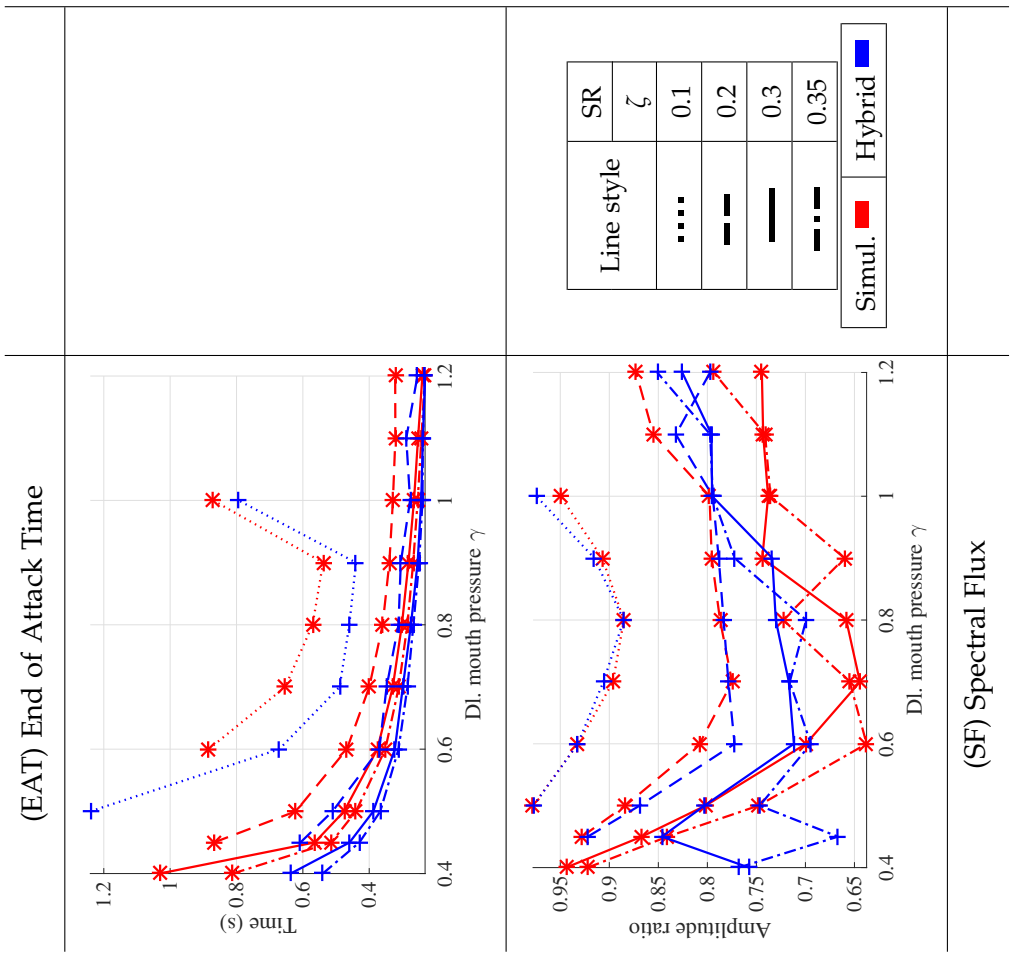

Figure 68: End of Attack Time and Spectral Flux descriptors calculated for the single-reed attack evaluations.

ging γ. Furthermore, this descriptor shows other particularities, such as the lower Spectral Flux values near the oscillation threshold. Similar conclusions can mostly be drawn for the other excitation models.

5.5 DISCUSSION AND CONCLUSIONS

5.5.1 *Comparisons within the obtained results*

THEORY VS. EXPERIMENTS While many simplifications were introduced when developing the theory to predict sound features of the steady-state oscillation regime, both amplitude and spectral based predictions showed valuable correlations with the related audio descriptors (both in a relative and an absolute sense). This suggests that the prediction theory can be helpful in the choice of particular quasistatic excitation models. Once the characteristic curve is presented, the theory and theorems presented in section 2.3 can be applied, in a similar fashion as was done for all presented excitation models in chapter 4. As demonstrated for the case of the lip-reed model, even dynamical models can be reduced to an approximate quasistatic case, still enabling good correlations with the sound features. However, those predictions cannot be used in absolute comparison with real quasistatic excitation models, in particular for the spectral features.

HYBRID VS. SIMULATION It is worth first commenting on the immediately apparent aural resemblance of the hybrid and simulated results across all excitation models (the only noticeable difference being the higher noise level of the hybrid sounds, caused by the derivative in (98), which is not an issue when listening to the direct performance of the hybrid instrument).

For both sustained and attack sounds, over most of the stable parameter domain, the difference for each descriptor curve between the simulated and the hybrid results is less than 5%, with the exception of the evaluations per-

formed after the loudspeaker deterioration, i.e. the second single-reed evaluation and the polynomial model evaluation. Another exception occurs when the extinction threshold is approached (occurring for the single-reed and bowstring models), as the sound changes rapidly towards this threshold and the threshold value itself appears to decrease with the noisiness of the sound. The increased noisiness in the measurements obtained with the hybrid instrument decreased the thresholds by about 8%.

While the parameter values were chosen over a range that mainly covers a stable domain, for certain extreme values undesirable instabilities could occur, which was found to always happen first with the hybrid instrument. The noisiness descriptor appears to be the best indicator for such instabilities, but the best distinction can be made aurally. The phenomenon occurred notably for high ζ or ζ_b values, but with the lip-reed high Q_r values also resulted in instabilities, particularly for the second and third register. This reduced stable range for the hybrid operation of the studied prototype imposes a limited timbre variety, representing restrictions to both the research tool and musical perspectives of this work (see section 1.4). The stability issue is related to a number of shortcomings mentioned in section 3.4. Particularly the increasing phase lag and the loudspeaker front-cavity modes measured in the hybrid system are responsible for unstable behaviour. In section 6.1, this issue is further investigated and an improved prototype is presented. Given the broadness of this topic, the issue is finally reviewed in subsection 7.1.1 in the general discussion in chapter 7.

Apart from the discussion around the loudspeaker deterioration, an aspect that has not been addressed so far is how well the hybrid instrument reproduces the same results upon repetition of the evaluations. The experiments have been repeated several times, with short and long interruptions and it can be concluded that a generally excellent repeatability is found with the hybrid instrument (which is why no error bars are used). However, the imperfect timing precision of the real-time computing system introduces a slight jitter (manifested as an additional noise signal, see appendix B). This slow irregular fluctu-

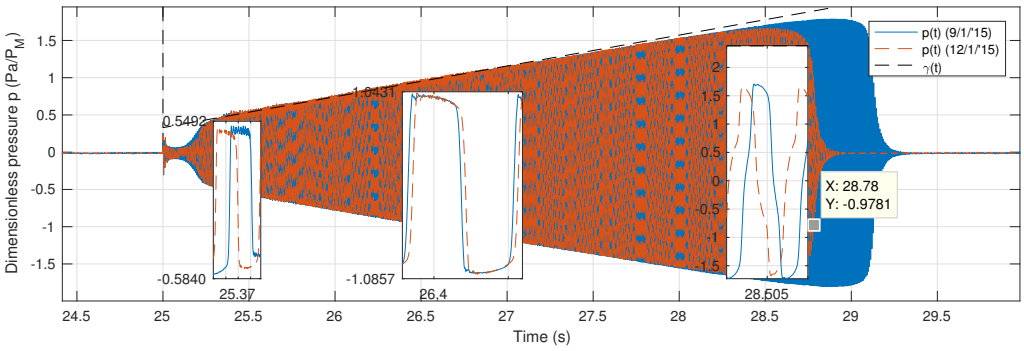

Figure 69: Temporal pressure signals obtained with a single-reed excitation model on the hybrid instrument at two distinct time instances, revealing a long-term non-repeatability.

ation is manifested as a long-term non-repeatability of the hybrid sounds. Nevertheless, the conclusions that have been drawn are all still applicable. Figure 69 shows two pressure signals measured with a three day gap in between. In this time, a sudden irregular change in jitter has occurred, leading to the noticeable non-repeatability effect. At 25.3 s, when p approaches γ, the steep part of the single-reed curve introduces some unstable behaviour, which appears more amplified for the first measured case (the solid blue signal) in comparison to the second (the dashed orange signal). The former also has a higher extinction threshold of about $\gamma_{\text{th}} = 2.04$, compared to the latter where $\gamma_{\text{th}} = 1.90$. The tube impedances including the loudspeaker and compensating filters ($\widetilde{Z}_{\text{t}}^{*}$) and related temporal signals were also measured at both instances, which did not show any significant differences, thereby confirming that the non-repeatability is not due to changes in the behaviours of any of those components.

It should be noted that the non-repeatability never exceeded the order of deviations demonstrated in this figure and all measurements reported above were carried out on the same day with no occurrence of such repeatability issues (apart from the mentioned "Hybrid2" measurements).

EXCITATION MODEL COMPARISON Comparing the descriptors and sounds produced across the different excitation models, it can be noted that the timbre range is fairly comparable for most excitation models, particularly for the quasi-

static models. As might be expected, the main reason for this is that a substantial part of the timbre is determined by the resonator, but there are also some excitation properties that are of consideration. A first limitation imposed by the hybrid excitation possibilities is the aforementioned instability issue. A second reason is related to the simplifications used for the basic physical excitation models; even though the operation of the single-reed and the bow-string interaction are fairly distinct physical phenomena, the fact that for both models a quasistatic approximation is used clearly results in resemblance of their timbres. That said, the manner in which parameters change the nonlinear excitation curve also influences the general perception of a model. Indeed, parameter transitions lead to distinct sound feature transitions, which in turn play an important role in defining the sound character. For instance, whereas a comparison with static parameters between the single-reed and the polynomial model does not suggest major differences, comparing those models with varying parameters clearly reveals the differences between these models. In the case of the single-reed model, an underlying physical model is perceived, while the polynomial model seems more artificial to the ear, which confirms the suggestions made in section 1.2.1 regarding physical versus non-physical systems.

5.5.2 *Unreported empirically obtained results*

OTHER PARAMETER VARIATIONS AND ATYPICAL STATES WITH MUSICAL POTENTIAL Most of the reported parameter ranges used for the evaluations were obtained after many empirical evaluations. While the most relevant variations are captured in the presented results, there were also a few particular states outside of the ranges used in the presented evaluations, which are worth mentioning.

As noted for the polynomial model, with $\zeta = 0.4$ a special phenomenon occurs, known as "period doubling". This particular excitation state enables the introduction of subharmonics, even in the absence of resonance modes of

the resonator at those frequencies. While not appearing in real single-reed instruments, the period doubling is found for the case of quasistatic theoretical models of the single-reed with $\zeta \geq 0.4$ (see e.g. (Taillard et al., 2010)).

A useful method to explain this phenomenon is with the graphical representation of the iterated maps theory, such as shown for the case of a quasistatic clarinet excitation with $\zeta = 0.4$ in figure 11 in chapter 2. In fact, when ζ is only slightly higher, it can be shown that the oscillation finally settles to two distinct iteration squares instead of a single square, which clarifies the period doubled appearance.

There is a wide range of literature covering this topic, focussing on theoretical developments (see e.g. (Feigenbaum, 1978; Collet and Eckmann, 1980; Taillard et al., 2010)), experimental observations on real instruments (Gibiat and Castellengo, 2000) and on hybrid constructions (Kitano et al., 1983; Maganza, 1985). Using physically based and abstract (i.e. a non-physically related mathematical formula) excitation models with his hybrid wind instrument set-up, Maganza has reported the appearance of a series of period doubling "bifurcations", eventually leading to a chaotic oscillation state (Maganza et al., 1986).

While this phenomenon has interesting potential regarding the musical perspectives, a thorough investigation lies outside the scope of this thesis, but it can be confirmed that the hybrid instrument investigated here is capable of producing period-doubled oscillations. As well as being possible to produce such oscillations with the polynomial model, with the bow-string model several period doublings could be obtained, when setting $\alpha = 1$ and for $\zeta_b \geq 8$. With the single-reed model, the required condition to obtain period doublings is $\zeta \geq 0.4$. Hence, those states could not be obtained with this prototype, given that such high ζ values result in the appearance of instabilities.

Furthermore, with the bow-string model with $\alpha = 1$, for ζ_b values up to 4, the sound was less raucous. When setting $\alpha = 0.26$ (as proposed by (Schelleng, 1973)), a more raucous, slightly more crackling and nasal sound was obtained. Also $\delta = 0.75$ was verified, which required high ζ_b and γ_b values to obtain

an oscillatory state. However, the simulation produced mainly squeaks and the hybrid instrument produced a chaotic instability with little variation, likely of poor musical interest.

Variation of other parameters (other than those evaluated in the thesis) and other parameter ranges with the lip-reed model did not result in significantly different timbres.

Another noteworthy finding occurs when the hybrid instrument is driven with (too) high amplitudes. While the correlation with the simulations decreases, the increasing saturation also introduces a particular character, which may be of interest to composers or musicians. In fact, such deviations represent a particular character of the hybrid instrument. This effect could be obtained by increasing the P_M (for the single-reed and lip-reed models), v_0 (for the bow-string model) or α (for the polynomial model) parameter.

DEVIATING MODELS A few deviations from the presented excitation models were also verified with simulations and/or hybrid evaluation. While many of the experiments were not intended, due to a wrong implementation of the theory, others were implemented to try out a different physical model or to obtain a certain effect.

Hence, the previously mentioned amplitude saturation effect could also be obtained purposefully by adapting the programmed model. This can result in even more extreme saturations, as the excitation model could be designed so that (in theory) the amplitude would never stop expanding; that is, when the excitation model has an initial instability, as mentioned in theorem 1, but lacks the presence of a fixed amplitude, as described by theorem 3. This results in a continuously growing oscillation amplitude, until the limit of the loudspeaker is reached (note that this could also be the limit of either the amplifier or the microphone when other components are used). The effect could be obtained for example by omitting the Heaviside function in the single-reed excitation model (i.e. in equation (52)), which resulted in a very rich spectrum of odd harmonics

with a partly synthetic and partly acoustic character that might be of musical interest.

Other deviating models were empirically found. This resulted in effects such as larger frequency shifts than reported earlier (with a quasistatic model) or fast alternations of the sound features by driving excitation parameters with low frequency oscillators (LFOs).

Finally, many ideas for various excitation models and techniques are reported for future evaluation in the perspectives section of chapter 7.

5.5.3 *Perceptual considerations*

In the present study, the focus lies on the spectrum of the steady-state oscillation of the hybrid instrument. However, it is known that the characteristic sound of self-sustained instruments is determined to a large extent by the transient behaviour (see e.g. (Deutsch, 1999)). Therefore it is important to bear in mind that excitation models with similar steady-state spectra may differ in character when more extensive transient evaluations and analyses are performed.

While the descriptors all relate to perceptual features, it is not straightforward to draw direct conclusions with regard to the "perceivable distance" when comparing the descriptor results. Moreover, while the descriptors represent a quantitative kind of perception space, musical sound events are not so easy to categorise. There are complex interrelations between features and even these are often not fixed, as there are high level psycho-acoustic aspects that come into play. Therefore, it was preferable to restrain the study to the descriptor set used here, which is also based on perceptually and musically relevant features. A qualitative musical evaluation is kept as a future study, which should be carried out by taking into account the preferences of human listeners and involve musicians to play the instrument (see section 7.2).

5.6 SUMMARY

In this chapter, the functioning of the hybrid instrument whose development was described in chapter 3 has been evaluated by introducing the four excitation models described in chapter 4: the single-reed model, the lip-reed model, the bow-string interaction model and the polynomial model. The performance of the prototype hybrid instrument has been assessed via comparison with simulations.

First a few computational aspects were discussed, explaining the implementation in MATLAB, Simulink and C++. Then, appropriate signals for consideration were selected (the pressure at the resonator entrance and an approximation of the radiated pressure), the notion of audio descriptors was introduced and a selection of suitable descriptors was made.

The applied parameter ranges for each excitation model were provided in a set of tables. These values were derived from both theory and empirical findings.

Some general observations were made, regarding the appearance of a loudspeaker deterioration which affected a number of evaluations, and referring to the sound files of all evaluations.

First an evaluation of sustained sounds was performed, by slowly varying one parameter: the mouthpiece pressure γ for the single-reed and lip-reed models, the bow speed γ_b for the bow-string interaction model and the even harmonics amount parameter δ for the polynomial model. The lip-reed was also evaluated for lip-resonance frequency θ progressions. This was repeated for a set of constant values of a second parameter, respectively the global embouchure parameter ζ, the bow force ζ_b, the excitation amplitude ζ and the quality factor Q_r.

After studying an isolated pressure wave for each excitation model, for sets of typical parameters, the sounds obtained over the evaluated parameter range was studied with the following descriptors: the Peak-to-Peak pressure amp-

litude (PP), the Harmonic Spectral Centroid (HSC), the Fundamental frequency (f_0), the Even Amount (EA) and the Noisiness (NN).

Sound prediction curves (estimating both amplitude and spectral related features) obtained for each excitation model in chapter 4 showed valuable correlations with the related audio descriptors, both in a relative and an absolute sense.

The hybrid and simulated descriptor curves are generally in good agreement which was also confirmed by aural judgement, demonstrating the successful implementation of the hybrid system. In particular, the descriptors show similar progressions, indicating that the excitation models and their control maintains their effect, and characteristic values such as the beating pressure and the oscillation thresholds are approximately the same in both the hybrid and simulated curves. The fundamental frequency progressions showed particular differences, which were identified as an effect of the increasing phase lag reported in subsection 3.3.3 and which in turn influenced other descriptors such as the HSC. Nevertheless, the effect remained small.

The lip-reed model was the only non-quasistatic model (i.e. where dynamics play an important role). This was reflected in the sound and descriptor outcomes, e.g. by generally much lower HSC values.

Next a brief study on the evaluation of attack transients was carried out, investigating the same excitation parameters and studying the logarithmic attack time descriptor (LAT). The single-reed LAT values showed an inverse correlation with the HSC progressions, which was also found to be the case for the lip-reed and polynomial models. However, it was notable that for the bow-string model this relation was almost opposite.

The end-of-attack time (EAT) and spectral flux (SF) were only investigated as part of the single-reed evaluation, revealing good correlation with the LAT descriptor but also that the hybrid instrument showed shorter EAT.

Finally a general comparison of the results was made, some unreported empirically obtained outcomes were presented, and some perceptual considerations were discussed.

6 FURTHER DEVELOPMENTS

In contrast to the other chapters, the sections in this chapter are unrelated. Each section discusses a particular further development to the hybrid instrument. First, in section 6.1, the instability issue is investigated and appropriate measures are taken for the design of an improved prototype. Then, the implementation of the hybrid principle on a real clarinet resonator is briefly described in section 6.2. Finally, section 6.3 describes the implementation and evaluation of some control and effect possibilities.

6.1 IMPROVING THE STABILITY WITH A CENTRED AND SECOND MICROPHONE

As mentioned in section 3.4 and noted throughout chapter 5 (particularly discussed in subsection 5.5.1), the normal operation of the hybrid instrument that has been studied so far (from here on referred to as the "initial prototype") is limited by an "instability issue" when certain excitation models with particular parameter values are evaluated. The study described in this section focusses on this particular issue.

In subsection 6.1.1, the functioning of the initial prototype hybrid instrument is briefly reviewed (a detailed description is given in chapter 3), and an explanation is given as to how unstable behaviour can appear with this prototype. Then, in subsection 6.1.2, the development and evaluation of an improved prototype is laid out.

6.1.1 *The initial prototype and its instabilities*

Set-up using a single microphone

The design of the initial prototype and the excitation models have been discussed in detail in respectively chapters 3 and 4. To help understand the instability issue, the main concept is revisited here. The complete set-up is shown schematically in figure 70. The prototype features a loudspeaker and a single microphone, both positioned at the entrance of the tube. Given that the loudspeaker's membrane velocity is transformed by the driver's dynamics (which can be modelled as a mass-spring-damper system), a feedback and feedforward filter are implemented on the computing system to account for the loudspeaker's response. Details of the filters are reported in chapter 3. Here, both filters are included in the block entitled "Filters accounting for the loudspeaker" in figure 70.

The pressure signal captured by the microphone is sent to the computing system which introduces input-to-output (I/O) latency. For the case of the computing system used for the initial prototype, the latency is 20 µs, corresponding to 1 sample ($N = 1$) at a sampling rate of $f_s = 50\,\text{kHz}$. The dimensionless pressure signal is sent to both the feedback filter and the excitation model. For the latter, the (equally delayed) dimensionless flow rate signal is subtracted, in order to obtain the required (dimensionless) "historical pressure" $\bar{\tilde{p}}_h = \bar{p}(z^{-1}) - \bar{\tilde{q}}(z^{-1})$. As well as using the tilde sign for the flow rate calculated by the excitation model, in this chapter the tilde is also used for the approximate historical pressure supplied to the excitation model.

For a coherent hybrid operation, the flow rate generated by the loudspeaker should be as close as possible to the flow rate calculated by the excitation model and then sent to the feedforward filter, so that $\bar{q} \approx \bar{\tilde{q}}$; and the latency should be as small as possible so that $\bar{\tilde{p}}_h \approx \bar{p} - \bar{\tilde{q}}$.

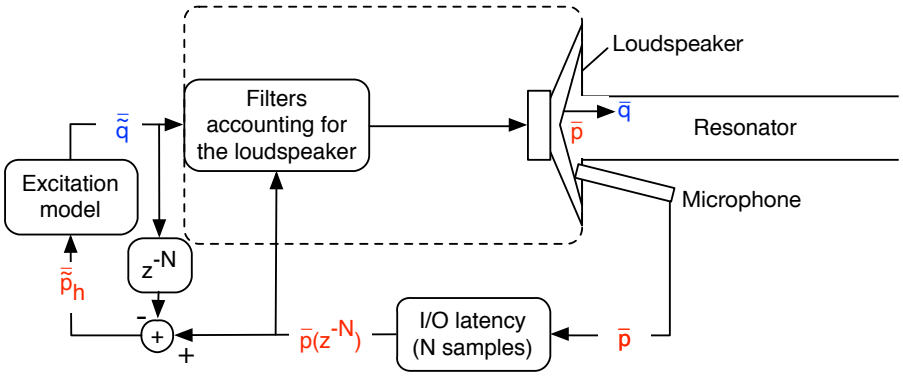

Figure 70: Schematic diagram of the initial prototype, using a single microphone to supply a pressure signal to the excitation model. The pressure is delayed by the input-to-output latency of the computer.

Observed instabilities with a single-reed excitation model

THE SINGLE REED EXCITATION MODEL By introducing a single-reed excitation model to the set-up (its detailed description can be found in section 4.2), hybrid self-sustained clarinet sounds can be produced. The resulting nonlinear curve, relating the outputted flow rate as a function of the pressure in the mouthpiece $\bar{q}(\bar{p})$, is represented as a dashed curve in figure 71 (note that for convenience of the further development, the quasistatic implementation is considered, which assumes the reed to be mass and friction-less).

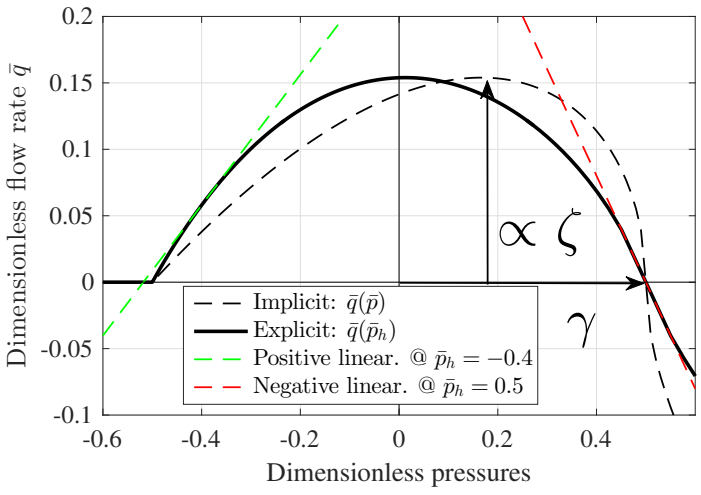

Figure 71: Characteristic nonlinear curves associated with the functioning of the embouchure. The dashed curve corresponds to the implicit equation $\bar{q}(\bar{p})$ and the solid curve to the explicit equation $\bar{q}(\bar{p}_h)$. γ represents the dimensionless mouth pressure and ζ is a global "embouchure parameter".

γ represents the dimensionless mouth pressure and shifts the curve along the horizontal axis, and ζ is a generalised "embouchure parameter", which controls the vertical scaling of the nonlinear curve.

Given that the flow rate instantaneously influences the pressure at the entrance of the tube, $\bar{p}$ is also an instantaneous function of $\bar{q}$ (as explained in section 4.1). Hence, for a numerical sequential simulation, it is not possible to directly use the implicit equation $\bar{q}(\bar{p})$ to obtain the flow rate from a measured pressure value. Therefore, the so-called "historical pressure" is used, which excludes the instantaneous pressure contribution resulting from the entering flow rate: $\bar{p}_\mathrm{h} = \bar{p} - \bar{q}$. As explained in section 4.2, using an approach proposed by van Walstijn (van Walstijn, 2002) and Guillemain et al. (Guillemain et al., 2005), an explicit equation $\bar{q}(\bar{p}_\mathrm{h})$ is derived (see equation (64) in subsection 4.2.2), whose (quasistatically approximated) curve is represented as a solid line in figure 71.

OBSERVED INSTABILITIES Although a stable and musically relevant self-sustained operation was obtained for a range of ζ values, when $\zeta \geq 0.35$ an unstable behaviour appeared. Figure 72 shows the (steady state) pressure wave generated using the single-reed excitation model with $\zeta = 0.35$ and $\gamma = 0.5$. As can be seen, a high frequency oscillation appears when the mouthpiece pressure is around $\bar{p} \approx \gamma = 0.5$, which rapidly increases in amplitude with increasing ζ. Looking up this pressure value on the nonlinear curve in figure 71 leads to the

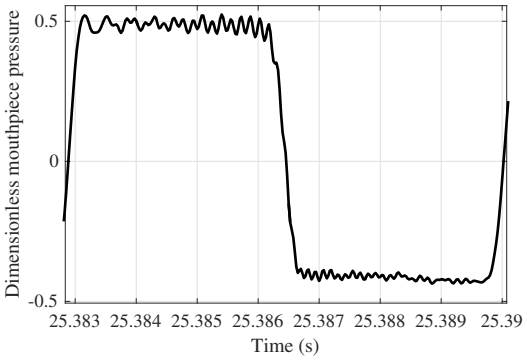

Figure 72: Pressure wave of a self-sustained oscillation produced with the initial prototype (with applied parameters $\zeta = 0.35$ and $\gamma = 0.5$), demonstrating the appearance of a high frequency oscillation.

hypothesis that the system becomes unstable when a strong negative gradient is encountered on the curve.

Stability analysis of a linearised system: study of the open-loop

While it is not straightforward to derive theoretical stability criteria in a nonlinear system[1], it is possible to linearise the nonlinear curve at an arbitrary point so that a locally valid linear stability study can be carried out. Considering the nonlinear single-reed curve, it can be seen that a positive and a negative linearisation is possible, as is shown by respectively the green and red dashed lines in figure 71.

A typical stability study in such a system involves considering the Bode plot of the "open-loop", i.e. the system contained between the signals $\bar{\tilde{q}}$ and $\bar{\tilde{p}}_h$, including the filters, the coupled loudspeaker-resonator system, the microphone and the calculation of $\bar{\tilde{p}}_h$. In the frequency domain, this system is represented by the transfer function $\bar{\tilde{P}}_h / \bar{\tilde{Q}}$ and its Bode plot (obtained by supplying a sine-swept signal $\bar{\tilde{q}}$ while recording $\bar{\tilde{p}}_h$) is shown in figure 73. It is worth noting that this transfer function is related to $\widetilde{Z}_t$, the input impedance including the loudspeaker and compensating filters (earlier reported in subsection 3.3.3). The relationship is as follows: $\frac{\bar{\tilde{P}}_h}{\bar{\tilde{Q}}} = \frac{\bar{\tilde{P}} - \bar{\tilde{Q}}}{\bar{\tilde{Q}}} = \widetilde{Z}_t - 1$ (note that $\widetilde{Z}_t$ is complex).

The gain margins are the complement (i.e. the inverse) of the gains at the $0°$ and $-180°$ phase transitions, respectively corresponding to the positive and negative linearisation of the excitation curve (indicated in respectively green and red in figure 73). The stability criterion stipulates that, at frequencies for which the gain multiplied by the slope of the linearised excitation curve surpasses 1 (or 0 dB), the system is unstable.

While the low frequency positive instabilities at the resonator's resonance frequencies enable the desired instability that leads to the self-sustained operation, also a few prominent negative instabilities at high frequency can be noted. These instabilities are normally not present in the case of an entirely acoustic

1 This could be done with energy methods however, see e.g. (Falaize et al., 2015).

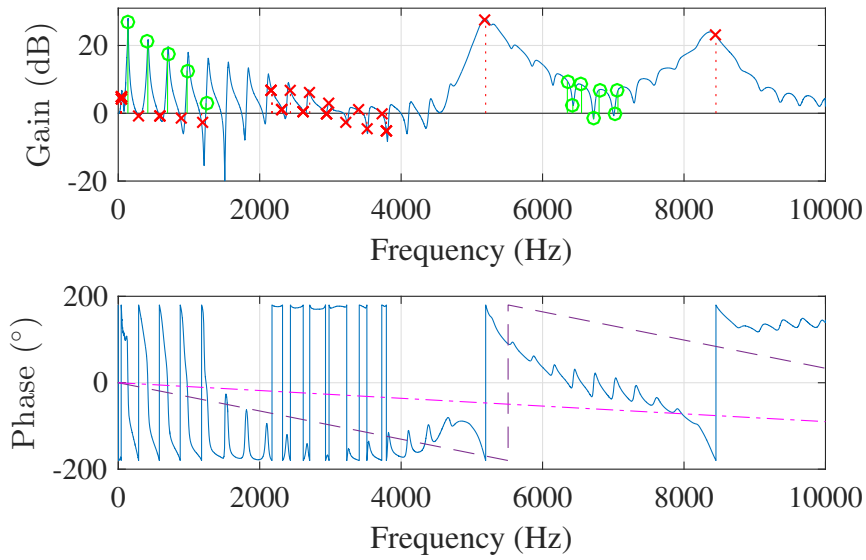

Figure 73: Open-loop stability study: Bode plot of the ratio $\bar{\tilde{P}}_h/\bar{\tilde{Q}}$ for the initial prototype; with indication of the $0°$ and $-180°$ gain margins. The magenta dot-dashed and purple dashed lines represent the phase response corresponding to the I/O latency of respectively the initial and improved prototype's computing systems.

instrument whose open-loop phase response remains in the $[90°, -90]$ range. Moreover, it is somewhat surprising, as normally the excitation can only add energy to the resonator when it is acting as a "negative resistance" (McIntyre et al., 1983).

In subsection 3.4.3, more precisely with figure 31, it was revealed that the high gains at these frequencies result from non-planar (transverse) vibration modes in the small cavity in front of the loudspeaker, which has a diameter that is about 2.7 times the diameter of the tube. Meanwhile, the observed increasing phase lag has multiple causes such as the I/O latency and loudspeaker effects that cannot be compensated for with filters, which was discussed in subsection 3.4.1. The group-delay corresponding to the I/O latency of the initial and the improved prototype's computing systems (the latter is discussed in the next subsection) is shown in figure 73 by respectively magenta dot-dashed and purple dashed lines.

It can be concluded that during hybrid self-sustained operation, when $\bar{p} \approx \gamma$, high pitched oscillations can occur. Given the nonlinear variation of the excita-

tion, this unintended instability is not just a high pitched squeak (such as in the case of a typical audio feedback or "Larsen" effect), but rather a raucous sound with chaotically introduced high frequency oscillations.

6.1.2 *The improved prototype*

In order to improve the stability, a new prototype with a modified set-up has been constructed. For this prototype, the digital real-time audio platform "Bela" is used. The details of this system are provided in subsection B.2.2. While the total latency is about 4.5 times larger than the previous computing system (the effect on the phase can be seen when comparing the relevant phase responses in figure 73), this is still a fraction of the latency of generic souncards and a technique is put in place to compensate for the latency.

Furthermore, given the microphone positioning requirement (detailed later) and due to material availability limitations, different microphones to that used for the initial prototype were employed. The Knowles EK-26899-P03 microphone turned out to be an appropriate choice (see section A.1 for technical details). However, it should be mentioned that this microphone has a less flat frequency response.

Accounting for the instabilities

By introducing a second microphone a distance $c.\Delta t$ along the tube (where c is the speed of sound), the I/O latency can be accounted for. (This approach is related to that of Guicking (Guicking and Karcher, 1984), who used two microphones to modify the reflection coefficient.) It should be noted that this is of importance, particularly given that the Bela platform has a larger input-to-output latency than the previous system, which had a latency of only 20 µs. However, migration to a new system was necessary, as the previous system did not support the now required multiple audio inputs. Figure 74 shows a schematic diagram explaining this concept by considering the pressure as subdivided

into forward and backward travelling waves, respectively represented by $\bar{p}^+$ and $\bar{p}^-$.

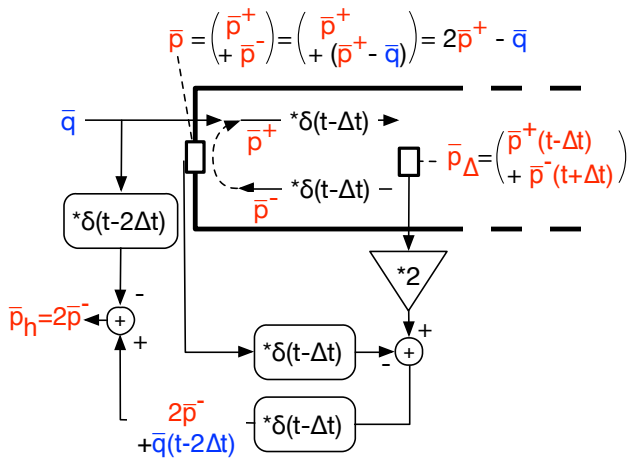

Figure 74: Schematic diagram describing how the historical pressure $\bar{p}_\mathrm{h}$ can be obtained from two pressures $\bar{p}$ and $\bar{p}_\Delta$. $\bar{p}$ is measured at the (closed) tube entrance and $\bar{p}_\Delta$ at a distance $d = c.\Delta t$ from the entrance.

Hence, taking into account the closed boundary condition, from the pressure signal at the first microphone one can derive (see also equation (9) in subsection 2.1.1):

$$\bar{p} = \bar{p}^+ + \bar{p}^- = \bar{p}^+ + (\bar{p}^+ - \bar{q}) = 2\bar{p}^+ - \bar{q} \;\Rightarrow\; \bar{p}^+ = \frac{\bar{p} + \bar{q}}{2}. \tag{99}$$

As such, the pressure at the second microphone position can be expressed as:

$$\bar{p}_\Delta = \bar{p}^+(t - \Delta t) + \bar{p}^-(t + \Delta t) = \frac{\bar{p}(t - \Delta t) + \bar{q}(t - \Delta t)}{2} + \bar{p}^-(t + \Delta t). \tag{100}$$

Finally, the historical pressure can be obtained from delayed measurements from both microphones and a delayed flow rate signal:

$$\bar{p}_\mathrm{h} = 2\bar{p}^- = 2\bar{p}_\Delta(t - \Delta t) - \bar{p}(t - 2\Delta t) + \bar{q}(t - 2\Delta t). \tag{101}$$

This principle is then applied in the final implementation (schematically represented in figure 75). The distance of the two microphones is chosen so as to correspond to the I/O latency: $d = c.\Delta t = c.N/f_\mathrm{s}$.

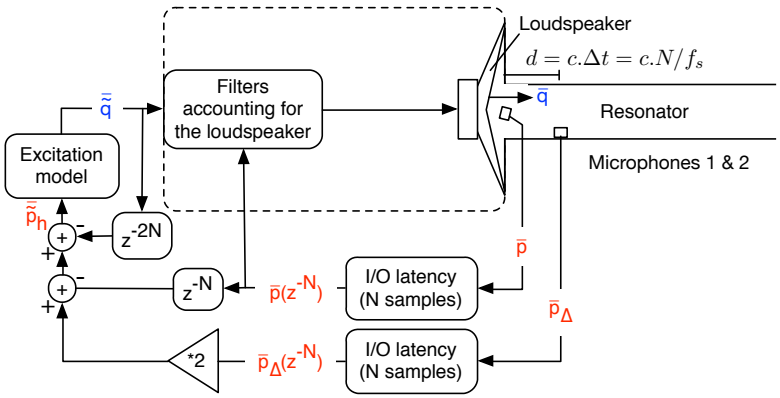

Figure 75: Schematic outline of the implementation of the new prototype, using two microphones to obtain $\tilde{\bar{p}}_h \approx \bar{p}_h (= \bar{p} - \bar{q})$, which is an approximation that is free of I/O latency.

It is worth mentioning that this method doesn't affect the precision of the final $\tilde{\bar{p}}_h$ calculation in theory, given that the first microphone is positioned at the closed boundary of the tube, where all of its acoustic longitudinal modes have a pressure antinode. Instead, the precision is equal to the single-microphone technique for frequencies that have a pressure node at the second microphone position and an increased precision is achieved for frequencies where both microphones are located at a pressure antinode.

It should be noted that this latency compensation concept assumes that the acoustic wave propagation between the two microphones is lossless. Hence, the relevance of the concept is only guaranteed when the two microphones are reasonably close to each other, i.e. when the latency is small.

A second improvement simply involves the repositioning of the first microphone to the centre of the loudspeaker cavity, so that the pressure antinodes of the first non-planar vibration modes are avoided.

Presentation of the improved prototype

Figure 76 shows the improved prototype set-up. As can be seen, the prototype is also equipped with two dial-buttons, enabling real-time control of the excitation parameters.

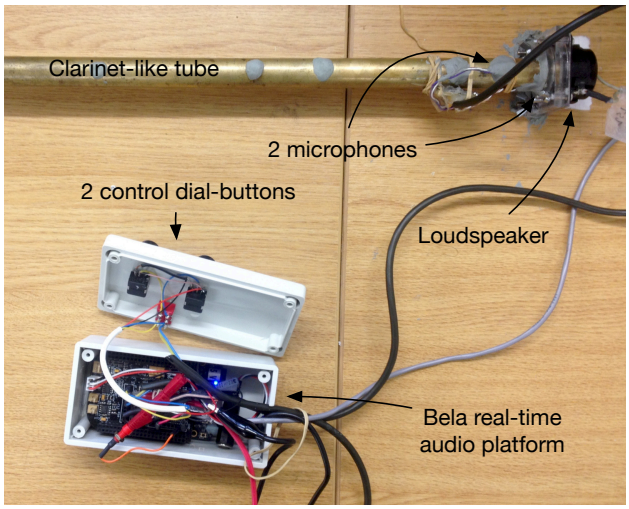

Figure 76: Picture of the improved prototype set-up, with indication of the components.

Study of the open-loop

Figure 77 shows the transfer function $\tilde{\bar{P}}_h/\tilde{\bar{Q}}$, for the new prototype. As can

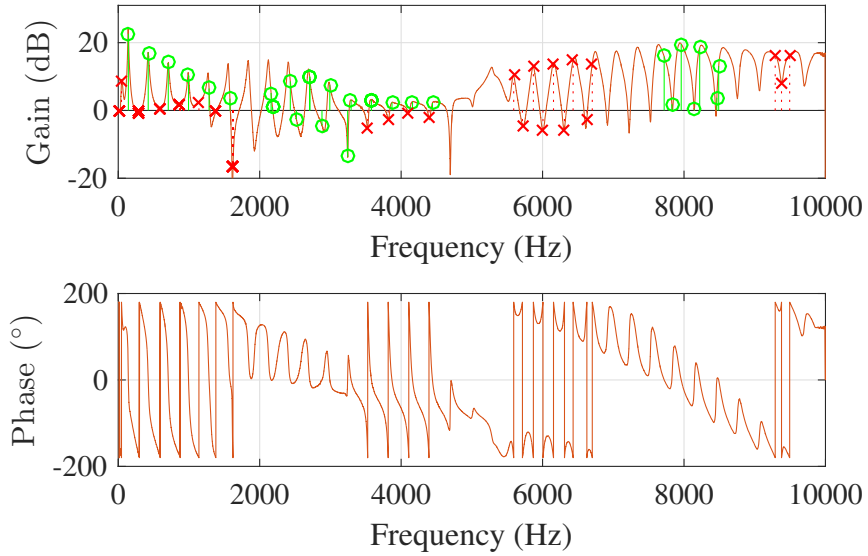

Figure 77: Open-loop stability study: Bode plot of the ratio $\tilde{\bar{P}}_h/\tilde{\bar{Q}}$ for the improved prototype; with indication of the $0°$ and $-180°$ gain margins.

be seen, the high frequency gain peaks caused by the non-planar modes have disappeared and the phase lag is reduced so that, all together, the gain margins are increased and the system remains stable, even in regions where the gradient of the nonlinear curve is steep. Nevertheless, it can be noted that there is still a phase lag, which is mainly due to an uncompensated loudspeaker effect (see

3.4.1), but it could be that the nonlinear frequency response of the microphone (see section A.1) also contributes to this effect.

However, it should be noted that in comparison with figure 73 the lower frequency response (around 2 kHz) has also slightly changed. By studying the influence of separate components, it has been shown that this is a result of the two-microphone concept, combined with the loudspeaker front cavity, which introduces a small phase shift compared with a directly terminated tube. This conclusion was made after verifying many possible causes. For instance, a measurement with a directly terminated tube was carried out, feeding a sine sweep signal at the other end of the tube while measuring the pressure signals with the two microphones. This enabled it to be demonstrated that the re-calculation of the pressure at the tube entrance (using equation (101) with an added $\bar{q}(t)$ term) resulted in a close agreement to the directly measured pressure at the entrance by the first microphone. Meanwhile, for the case where the loudspeaker was used to terminate the tube, a significant phase lag could be noted around the low frequency range under consideration.

Self-sustained operation

An evaluation of the improved prototype was carried out, using the single-reed excitation model with the same parameter values. The resulting pressure wave, represented in figure 78, is indeed free of high frequency noise. The system remains stable for ζ values up to 0.7, a wider timbre domain can be reached and an evaluation with a real clarinet resonator results in musically relevant sounds (see section 6.2).

This opened up the possibility of studying the particular phenomenon of "period doubling bifurcations", which is a form of multiphonic where subharmonic frequencies are introduced and which is only manifested for $\zeta \geq 0.4$ with the single-reed excitation model (the period doubling phenomenon was briefly discussed in section 5.5).

However, it is important to note that the wave is less square in nature than that produced by the initial prototype (see figure 72) and that resulting from simulations. This is most likely due to the change in the lower frequency region of the open-loop transfer function.

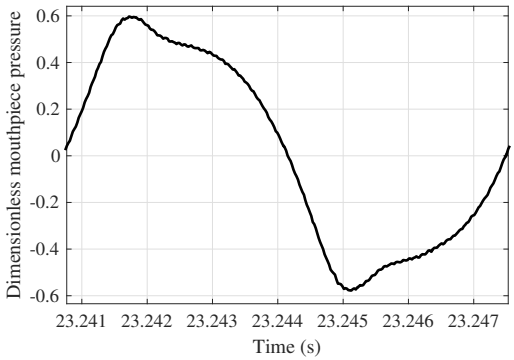

Figure 78: Pressure wave of a self-sustained oscillation produced with the improved prototype (with a single-reed embouchure model with parameters $\zeta = 0.35$ and $\gamma = 0.5$). No high frequency noise is present, but the wave is less square in nature.

6.2 IMPLEMENTATION ON A CLARINET-RESONATOR

Given that the hybrid instrument's operating principle is almost entirely independent of the acoustic resonator, it requires very little work to replace the tube with another resonator, such as that of an existing reed instrument. This is successfully confirmed by empirical tests with a clarinet resonator. To this end, a new mechanical adaptor piece was designed, enabling the loudspeaker to be mounted on the clarinet, while conserving its internal cross-sectional area S_t. This latter point is important, as the cross-sectional area affects the characteristic input impedance ($Z_c = \frac{\rho c}{S_t}$). This value is used in the excitation simulation, more precisely, to re-dimensionalise the dimensionless flow rate calculated by the excitation model (see subsection 4.2.1). Nevertheless, it only involves a small change, given that the inner diameter of the clarinet that was used is 14.3 mm, while the tube had an inner diameter of 15.0 mm.

A video of the empirical evaluation, carried out with the initial prototype and the single-reed excitation model, can be found here: http://dx.doi.org/10.21954/ou.rd.3848115. As can be verified, the sound is more "clarinet-like" than the single-reed evaluations obtained with the tube resonator (a selection of sounds, originating from the evaluation with a single-reed model (discussed in chapter 5) can be found here: http://dx.doi.org/10.21954/ou.rd.3848415).

Figure 79 shows a spectrogram of the radiated sound produced in the evaluation with the clarinet resonator. It should be mentioned that the conditions, the set-up and the recording equipment were not intended for research use (using a mobile phone, next to a reflecting wall,...). Therefore, only relative conclusions can be drawn from the spectrogram, and the most relevant are spectral comparisons between the notes.

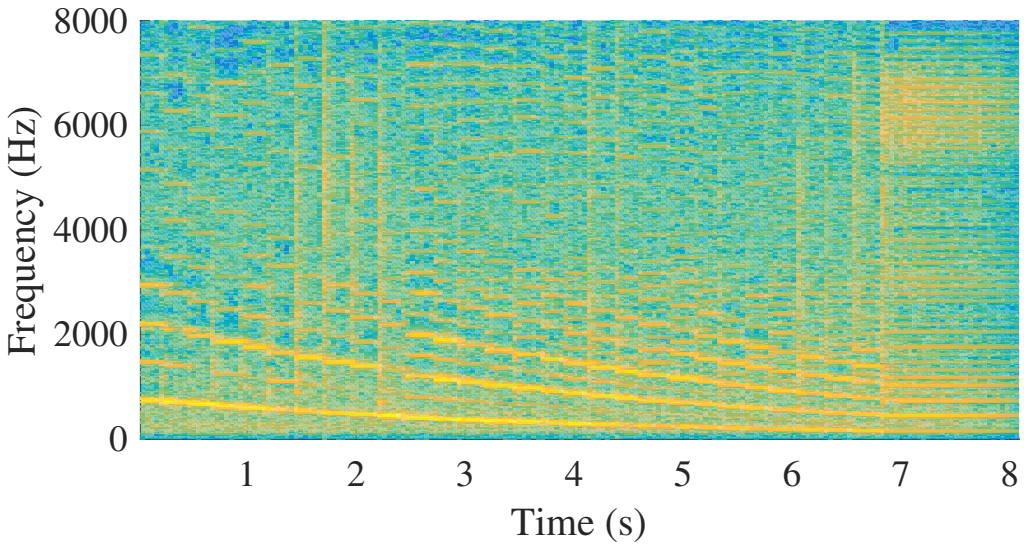

Figure 79: Spectrogram of the radiated sound by the clarinet resonator while playing two chromatic scales downwards.

It can be seen and heard that a fairly good note-range of 2 octaves is covered and that the notes all sound reasonably similar in timbre, which confirms that the loudspeaker is reasonably well compensated for over a broad frequency range. Furthermore, it can be seen that the first two (odd) harmonics are clearly present for the whole note range. A much higher number of harmonics are present, but the overall spectrum appears to be low-pass filtered above about

3 kHz. It is worth noting that the spectrally rich events at some note onsets (for example around 2 s) represent the sound of the keys being operated. The key noise is relatively loud in comparison with the produced notes as the self-sustained operation of the hybrid clarinet operates at a down-scaled amplitude (see subsection 7.1.1 for further discussion on this). As can be heard, and seen on the spectrogram, the last note (around 7 s) is affected by high pitched oscillations, caused by the instability issue mentioned in section 3.4 and compensated for in section 6.1.

It can be perceived that the instrument is slightly mistuned (i.e. the higher notes are somewhat too low in pitch). This could be either due to uncompensated increasing (loudspeaker) phase lag (see subsection 3.3.3 or figure 73 in this chapter) or due to the crudely estimated effect of the missing "reed-induced flow" (or both). The alternating reed induced flow component is generated by the movement of the reed, which acts as a "membrane" and pulls and pushes the air that is in contact with it. As it introduces a virtual length correction, it is taken into account by reed instrument manufacturers by shortening the resonator, e.g. by up to 10 cm for a clarinet (Dalmont et al., 1995). For the hybrid instrument, since the employed single-reed model (and the other excitation models) does not take into account this flow component, the clarinet resonator is increased in length again by using a 10 cm long adaptor to the loudspeaker. Hence, it is possible that this physical length correction is overestimated. An alternative would be to include a reed-induced flow model in the mouthpiece simulation, see for example (Avanzini and Van Walstijn, 2004).

Similar results were obtained with the improved prototype in combination with the clarinet resonator, and the improved stability also applied to the entire playable note range. Furthermore, it was observed that the sensitivity for instability and the magnitude of the related undesired squeaks is dependent on the played note. This can be explained by the fact that certain notes have high frequency longitudinal vibration modes that stimulate the undesirable

non-planar waves in the loudspeaker cavity, while for other notes this situation does not occur.

From the musical perspective, a logical next step is to explore sound manipulation options with the hybrid instrument and to consider useful control possibilities to enable a musical interaction with the instrument. Some brief investigations of these are presented in the next section.

6.3 CONTROL AND EFFECTS

This section groups together a few extensions supporting the musical potential of the hybrid instrument. It should be mentioned that these extensions were only briefly tested. Their usefulness in a research context will be relevant when it comes to qualitative evaluation with performers and/or composers.

The first two subsections discuss some control possibilities, with the development of a mouthpiece controller and parameter mapping strategies. The following subsection presents a vibrato sound effect obtained with a parallel operation in the hybrid feedback loop.

6.3.1 *Development of a mouthpiece controller*

For a hybrid instrument to be adequately employable in a musical performance, it is important to provide and maximise expressive control possibilities available to a player. As for many wind instruments both hands are already used to obtain a desired note by manipulating the resonator, it is an appropriate choice to re-introduce the mouth as a means of controlling the excitation properties. Another motivation for this choice is that it enables an existing wind instrument player to conserve their embouchure expertise (to a certain extent). This is an important advantage for new musical instrument designs, given that the conservation of expertise is a research-worthy proposition for tackling the

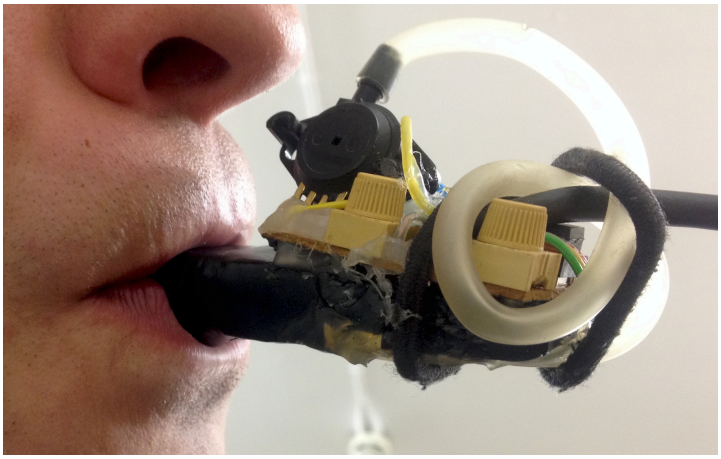

Figure 80: The prototype mouthpiece controller.

ongoing problem concerning poor employment prospects after the introduction of new (electronic) instruments.

First, some ready-made mouth-controllers were considered for use with the hybrid instrument. However, few controllers are sold as a separate tool that provides both mouth air pressure and lip force measurements. A large variety of "breath controllers" exists, but typically these are only equipped with a pressure sensor (such as the Yamaha BC series). While TEControl provides two "breath and bite" controllers (e.g. the BBC2), they only feature a USB output with MIDI encoded data, which is not straightforward for implementation on the real-time computing system.

Alternatively, there are complete "wind controllers", which do provide both pressure and force measurements. However, they too are not suitable for controlling the hybrid instrument excitation, given the redundant instrument body (hosting keys and synthesis electronics) and, similar to the TEControl controller, due to the difficulty accessing analogue sensor signals. Currently available wind controllers are, for example, the AKAI EWI series, the Yamaha WX series, the Softwind Synthophone and the recently introduced Roland AE-10 aerophone.

It was therefore decided to develop a custom-made mouth controller. Figure 80 depicts the designed prototype mouthpiece controller. It is equipped with a Freescale MPX12GP pressure sensor, measuring the air pressure in the

mouth via a small tube. Meanwhile, the lip-force is captured with a Honeywell FSS020WNSX load cell. Both of these sensors can capture realistic physical embouchure states, i.e. pressures of up to 10 kPa and forces of up to 10 N. Two INA125 instrumentation amplifier ICs provide amplification and an offset to obtain a voltage range suitable for the computing system's acquisition interface.

It should be mentioned that the controller cannot be used with the initial prototype, given that multiple simultaneous data acquisition is not supported by that computing system. However, it can be employed with the improved prototype.

6.3.2 *Mapping control parameters to the excitation model*

An important element for consideration, both in terms of obtaining a realistic operation and providing alternative musical expressions, is how the excitation model's input parameters are related to the musician's control commands (i.e. their physical gestures). This provides a strong motivation for considering parameter "mapping" strategies.

A parameter mapping is a function that states how the raw input data from the controller (e.g. the mouth controller) is related to the parameters of a given excitation model.

While Hunt et al. argue that a complex and combinational mapping of electronic musical instruments is preferred for an expressive "instrument-like" behaviour (Hunt et al., 2002), their view disregards the sound generation by physical modelling, which inherently **is** instrument-like when conserving the one-to-one natural mapping. This is, for instance, emphasised by Smith, who states that virtual instruments (physical models simulating real instruments) "contrast with "abstract" and "recording-based" synthesis algorithms that are capable of high quality sound synthesis, but which lack the intuitive and expressive control-response of model-based synthesis." (Smith, 2005).

Nevertheless, given that the wind-instrument physical excitation models employed in this thesis (i.e. the single-reed and lip-reed models) have been re-expressed in dimensionless and reduced parameter forms, a simple mapping is required. This mapping can be obtained from the dimensionless parameter definitions in respectively subsections 4.2.1 and 4.3.1, leading to:

$$\begin{aligned} P_{\mathrm{M}} &= \frac{H_0 k - f_{\mathrm{l}}}{S_{\mathrm{r}}} = c_1(c_2 - f_{\mathrm{l}}) \\ \gamma &= \frac{p_{\mathrm{m}}}{P_{\mathrm{M}}} \\ \zeta &= Z_{\mathrm{c}} w \sqrt{\frac{2(H_0 - f_{\mathrm{l}}/k)}{\rho k}} = c_3 \sqrt{c_4 - f_{\mathrm{l}}} \end{aligned} \tag{102}$$

where p_{m} is the dimensional mouth pressure and f_{l} the lip force, both captured by the mouth controller. H_0 is the initial reed opening without the presence of the mouth, and k, S_{r}, Z_{c}, w and ρ are earlier defined dimensional parameters. For use with arbitrary mouthpiece parameters, the form with the constants $c_{i=1\ldots4}$ can be implemented. This way, the controller sensor ranges can be matched to the γ, ζ and P_{M} parameter ranges specified in tables 2 and 3, which are convenient for an optimal hybrid operation. Doing this results in a realistic mouthpiece simulation, except for P_{M}, as realistic beating pressures surpass the amplitude capacity of the hybrid instrument (i.e. c_1 would need to be about ten times smaller than a realistic value, in order to avoid saturations).

It should be mentioned that the reed resonance frequency and quality factor are two unknown parameters. It might be possible to use an advanced mouthpiece model to find an approximate mapping between the lip force and the resonance frequency. However, the quality factor is mainly dependent on embouchure features that are not captured with the provided sensors. In any case, the constant average values proposed in the tables can be provisionally used.

Alternatively, from the point of view of exploring different musical expression possibilities, less realistic or arbitrary parameter mappings can be chosen. This can be useful to accentuate certain timbres, e.g. focussing on the period

doubling appearance (mentioned in chapter 5), which only appears over a narrow excitation parameter range. Moreover, nonlinear and dynamic mappings can be implemented, using for instance techniques such as wave-shaping, derivation, integration, low-frequency-oscillators (LFOs),...

6.3.3 *Vibrato*

While in this thesis the focus is on the design of nonlinear excitation models, the hybrid set-up is perfectly capable of allowing one to (simultaneously) perform active control operations. For an advanced active control implementation on a wind instrument, the work by Meurisse can be consulted (Meurisse, 2014). Here, a simple "vibrato" application is presented to provide a preliminary demonstration of active control as a "side-chain" application to the excitation model.

In contrast to advanced active control applications, the proposed vibrato effect is not "aware" of the resonator's status (i.e. the resonator's impedance), resulting in a crude implementation, but with the advantage of being almost note-independent.

One way to understand the applied concept is by considering it as an addition of a virtual volume positioned at the entrance of the resonator. This volume behaves as an acoustic compliance, which can be simulated by introducing a flow rate signal proportional to the derivative of the measured pressure at the resonator entrance (see e.g. (Chaigne and Kergomard, 2013)). Given that the virtual volume induces a "length correction" of the resonator, the pitch will decrease. In order to obtain the targeted vibrato effect, the volume's parameters can be controlled with a LFO, which ultimately leads to the following controller expression:

$$C_{\text{vib}} = \frac{a_{\text{vib}} \left(\sin(2\pi f_{\text{vib}} t) - 1\right)}{Z_c} s. \tag{103}$$

a_{vib} and f_{vib} refer to, respectively, the amplitude and frequency of the vibrato effect and s is the Laplace transform of the derivative. The amplitude is related to the "depth", i.e. the approximate frequency span of the fundamental frequency fluctuation. Mathematically, the amplitude sets the time added to the period of oscillation; thus, the vibrato depth is proportional to the fundamental frequency of the played note. While this note-dependency is inevitable with a resonator-independent implementation, in practice the effect sounds sufficiently homogeneous over the entire clarinet scale.

Another inconvenience is that this technique does not allow one to shift the frequency upwards, given that a positive C_{vib} (which would require a "negative volume") leads to an unstable system (hence the -1 term in equation (103)). This means that the vibrato will occur around a mean frequency slightly below the fundamental frequency of the note played without vibrato. However, it should be noted that this mean frequency flattening also occurs when producing a vibrato effect with the mouth on a single-reed mouthpiece.

Empirical evaluations demonstrated that maximum amplitudes of $a_{\text{vib}} = 20\,\mu\text{s}$ could be used (above that, undesirable instabilities occurred), resulting in vibrato depths of about $\pm 0.5\,\text{Hz}$ and $\pm 3.5\,\text{Hz}$ for fundamental frequencies of respectively 140 Hz and 320 Hz, i.e. corresponding to vibrato depths of respectively ± 6 cents and ± 19 cents.

6.4 SUMMARY

This chapter discussed a number of discrete further developments to the hybrid instrument.

First, the instability issue noted in the earlier chapters was investigated. It was demonstrated that the behaviour of the initial prototype hybrid wind instrument (using the single-reed excitation model as an example) could become unstable when the nonlinear curve of the excitation model had regions with strong negative gradients.

A linearised "open-loop"study of the $\bar{\bar{P}}_h/\bar{\bar{Q}}$ transfer function Bode plot revealed that this was due to low gain margins. The high frequency gain peaks appeared to result from non-planar air vibration modes in the front-loudspeaker cavity, which could be avoided by repositioning the microphone at the centre of the loudspeaker cavity. Meanwhile, the inverted ($-180°$) phase state was caused by various phase lag sources, including the input-to-output latency of the computing system. This could be accounted for by introducing a second microphone a distance $c.\Delta t$ along the tube.

These changes were implemented in a new prototype, which used the "Bela" real-time audio platform. Despite the higher input-to-output latency, this computing system featured several analogue inputs so that the two-microphone method could compensate for this delay. The new prototype's open-loop study revealed improved gain margins, but at the expense of a modified lower frequency response.

Evaluation with the single-reed model resulted in more stable but less coherent (i.e. less square-shaped) sounds, enabling a larger variety of musical sounds and opening up the study of the period doubling phenomenon.

Next, the successful development of the hybrid instrument was assessed by considering it in relation to a real wind instrument. To this end, the prototype system was empirically tested by connecting it to a real clarinet resonator, resulting in more realistic clarinet sounds than achieved with the cylindrical tube resonator. Both the sound produced and the associated spectrogram were reported to demonstrate a fairly consistent timbre over 2 octaves.

Another development concerned the introduction of control and effects to the hybrid wind instrument. A mouth controller was designed, featuring two sensors to capture both the mouth pressure and the lip force. Mapping strategies were then proposed to relate the controller output to the excitation model's input parameters. It was concluded that a "physical" mapping is an appropriate choice in the first instance, while other mappings could be of interest for explor-

ing particular timbres and functionalities, which supports the musical potential of the hybrid instrument.

Finally, the successful implementation of a vibrato effect was discussed. This effect demonstrated the possibility of applying an active control application in parallel to the hybrid functionality. The effect was obtained by introducing a controller that adds a size-fluctuating "virtual volume" to the entrance of the resonator.

7

GENERAL DISCUSSION, CONCLUSIONS AND PERSPECTIVES

This last chapter first discusses a number of aspects that are of key importance to the thesis. A number of unrealistic aspects observed in the hybrid instrument's behaviour are reviewed. Then, in order to check the overall work for consistency, the research questions and requirements defined in the introductory chapter are reassessed.

Following this, a wide variety of perspectives is presented, bringing together various new ideas to further the development and evaluation of the hybrid instrument.

7.1 GENERAL DISCUSSION

7.1.1 *Unrealistic hybrid aspects*

The performance of the current hybrid instrument prototype is not fully realistic in several different aspects. The following paragraphs consider a number of ways in which its behaviour does not reflect the functioning of real acoustic wind instruments. (While also of minor concern, the list does not include the inconsistent slight repeatability issue, discussed in section 5.5.)

DYNAMIC RANGE For the imaginary case of a resonator with an infinite linear acoustic response (which is assumed in the simulations), arbitrarily small or large self-sustained amplitudes can be produced. However, this does not apply to the case of the hybrid instrument, whose dynamic range is limited by noise and saturation thresholds introduced by the equipment.

For example, it is found that self-sustained operations with amplitudes below about 10 Pa are difficult to realise on the prototype hybrid instrument, which is due to noise starting to dominate the sound.

Meanwhile, as mentioned in section 3.3.2, the maximum dynamic level of the hybrid instrument (with a reasonably linear loudspeaker operation) is determined by the power rating of the loudspeaker. Unlike the minimum dynamic performance, the maximum level is not only determined by the pressure amplitude, but also by the spectral richness of the sound. This is explained by the fact that the feedforward (i.e. the flow rate related) component of the coil current is proportional to the derivative of the flow rate signal.

In order to inspect the evaluations in this regard, their dimensional peak-to-peak amplitude has to be considered first. This can be obtained by multiplying the dimensionless amplitudes by the relevant amplitude parameter of the excitation model. The following constant amplitudes were used in the reported evaluations: $P_M = 100\,\text{Pa}$ for the single-reed model, $P_M = 50\,\text{Pa}$ for the lip-reed model, $v_0 = 15\,\text{Pa}$ for the bow-string model and $\alpha = 100\,\text{Pa}$ for the polynomial model.

Comparing for instance the simulations of the single-reed and bow-string excitation models, it can be noted that a similar spectral richness (indicated by equal harmonic spectral centroid values of HSC = 1000 Hz) was found at respective parameter states of $\{\zeta = 0.35, \gamma = 0.75\}$ and $\{\zeta_b = 1, \gamma_b = 2\}$. If attention is now turned to the hybrid operation, while the same HSC for the bow-string evaluation was found, the single-reed HSC turned out to be only 940 Hz. Taking into account the amplitude parameters, the dimensional amplitudes at these instances were 70 Pa for the single-reed and 28 Pa for the bow-string result, which indeed suggests that the loudspeaker's operation during the hybrid single-reed evaluation was slightly saturated at this state. This assumption is also supported by the fact that lower ζ values resulted in better correlations between hybrid and simulated results.

The hypothesis is also supported by the findings for the lip-reed evaluation. In fact, with this model, amplitudes up to 300 Pa could be reached with the hybrid HSC remaining close to the simulations (i.e. no saturation occurred). This can be explained by the fact that the HSC value of 300 Hz is relatively low compared with the HSC's obtained with the single-reed, bow-string and polynomial quasi-static excitation models. As a result, a lower coil-current is required with the lip-reed model. Despite all of this, the overall brightness performance of the hybrid instrument is still much lower than typical brightness values found for real clarinets evaluations (see e.g. (Almeida et al., 2013; Li et al., 2016)).

It should be mentioned that the derivative of the flow rate also increases with the pitch of the played note. A quantitative investigation on that effect is yet to be carried out, but it can be expected that the dynamic range of higher notes will be even more constrained.

Additionally, in section 3.3.2, it was noted that the range over which the hybrid instrument produces stable sounds lies well below the pressure amplitudes found in real wind instruments, which tend to range from 1 kPa to 8 kPa (Fuks and Sundberg, 1996). The evaluated wind instrument excitations are "scaled down" in amplitude (by using much smaller P_M values than are realistic). Consequently, the current hybrid instrument prototype cannot be used to investigate the nonlinear sound propagation within the resonator that can occur at large amplitudes in real wind instruments, particularly for narrow and long ducts.

Another consequence of the reduced dynamic range is in terms of perception. Indeed, while the same waveforms may be produced at lower amplitude, the human ear does not behave linearly with respect to amplitude (which is related to the notion of loudness), resulting in a change of the perceived timbre. An empirical experiment was carried out where the hybrid performance (using a real clarinet resonator) was amplified with an additional (external) loudspeaker. Informal evaluations by a few musicians revealed that this not only resulted in

more realistic perceived timbres, it also improved the musician's immersion with their playing performance.

ABSENT MEAN FLOW COMPONENT In chapter 2, theorem 6 stated that the mean air flow passing through a real wind instrument when it is played has a negligible influence on the oscillating behaviour; this was informed by the literature (see e.g. (Rienstra and Hirschberg, 2013; da Silva et al., 2010)). While this statement is valid to the first degree, the flow component can have a perceptible influence in certain cases. Given that the hybrid instrument filters out this part of the spectrum (with no DC flow generated by the loudspeaker), this represents another unrealistic property of the hybrid instrument.

For instance during transient oscillations, in a real instrument, there is a volume flow component that changes at a frequency far below the loudspeaker resonance frequency. Given that this flow is not produced with the hybrid instrument, the transients will not be perfectly reproduced. This limitation was also acknowledged by Almeida, as he reported in his work on a simplified hybrid wind instrument set-up with a loudspeaker (Almeida et al., 2010). In contrast, the sustained operation does not include sub-fundamental frequency components (apart from the mean flow), which suggests that the hybrid sustained operation is likely to be more truthful. This is indeed supported by aural comparison of the hybrid and simulated results, where the attack sounds appear to diverge more than the sustained sounds.

THE INSTABILITY OF THE HYBRID INSTRUMENT A cross-cutting topic in this thesis is the instability of the hybrid instrument.

In section 3.4, an increasing phase lag and high frequency gain peaks were reported in the measurement of the impedance curve of the resonator including the loudspeaker and compensating filters. These issues were caused by uncompensated loudspeaker effects and transversal resonant modes in the loudspeaker front cavity.

In section 5.5, some unstable occurrences were observed, which appeared to be best indicated by the noisiness descriptor. It was concluded that the unstable behaviour of the studied hybrid wind instrument imposed a limitation on the variety of the timbres that could be produced, representing restrictions both in its usage as a research tool and its musical potential. However, throughout chapter 5, there was no ground to identify the phase lag issue as one of the reasons for the unstable behaviour. Instead, the issue was identified as the primary reason for the variation in fundamental frequency from the expected value and consequentially for the associated shift in the harmonic spectral centroid.

In the following chapter, in section 6.1, a focussed study on the stability issue led to in the hypothesis that it arises due to a combination of the high frequency gain peaks, the phase lag issue and a steep nonlinear excitation curve. The hypothesis was confirmed by the design of an improved prototype where the phase lag introduced by the computing system's latency was compensated for by the addition of a second microphone. Meanwhile, the gain peaks were reduced by repositioning the first microphone at the centre of the loudspeaker. While the stability was improved, the oscillations produced with the improved prototype hybrid instrument seemed to show greater divergence from the simulations than the initial prototype. For future realisations it may be worth reconsidering some of the prevention strategies noted in section 3.4.

Finally, it is interesting to note that the (earlier mentioned) restriction on dynamic level occurs in similar conditions as the appearance of instabilities. Indeed, a steep nonlinear excitation curve usually produces high HSC values, which should lead both to increasing saturation and greater likelihood of instability. However, surprisingly it was noted that the coincidental surpassing of the maximum dynamic level and the instability condition does not necessarily lead in (strong) unstable behaviour, i.e. it appeared that the occurrence of saturation increased the instability threshold. This interesting observation may be related to the fact that the steep nonlinearity implies high flow rate derivatives, which cannot be realised with the loudspeaker at high dynamic levels.

FUNDAMENTAL FREQUENCY DEVIATIONS AND CONSEQUENCES The fundamental frequencies obtained for the hybrid evaluations with the quasistatic excitation models have been found; in general, to differ from these obtained via the simulations. This effect has been shown to be due to the phase lag issue. In turn, the fundamental frequency deviation results in variation from the expected values for other sound features, such as the spectral centroid.

CONCLUDING REMARK Particularly from the "research tool" perspective, it is important to note that even though the obtained accuracy of the hybrid instrument is reasonably good, the concept of accuracy is not "one-dimensional". That is, certain features may be independent of the current hybrid instrument's shortcomings (e.g. a study on the mean air flow), while others are highly dependent on them (e.g. a study focussed on the influence of the fundamental frequency). Nevertheless, certain acoustic self-sustained properties in wind instruments are very suitable for investigation with the current hybrid instrument prototype, particularly those properties that are not influenced by the shortcomings presented in section 3.4.

7.1.2 *Reviewing the "research tool" and musical motivations*

In order to confirm that the presented work has remained in line with the intended goals, it is relevant to reconsider the motivations (see section 1.2). These motivations were formalised in the research questions and the derived requirements laid out in subsection 1.4.3. While two distinct research questions were stipulated (one regarding the hybrid instrument as a new musical instrument and the other regarding the usage as a tool for wind instrument research), the requirements demonstrated that both viewpoints shared many common initial targets.

For convenience, the requirements are briefly repeated here:

- Diversity (in terms of the perceptible variety of the sound)

- Precision, in terms of:
  - the sound control (regardless of parameter mapping strategies).
  - the accuracy of the sound control in relation to predictions and simulations.
- Repeatability, i.e. repeated progressions of the excitation model's input parameters should result in repeated sound features (if hysteresis effects are avoided before the repetition).
- Musically relevant atypical behaviour, typical to the hybrid operation.

These requirements support the general aim of ensuring a hybrid functioning that is as close as possible to that of an ideal hybrid instrument. This target and the separate requirements have been guiding factors throughout the development, excitation design and evaluation stages.

In the development phase (including the further investigation of the stability issue in section 6.1), the main focus was to obtain a "hybrid impedance" as close as possible to the measured input impedance of the resonator. The close impedance agreements revealed in figure 27 confirm that this was successfully achieved for the first five resonant modes of the prototype hybrid instrument. Given that those modes are of greatest importance for the self-sustained operation, this indicates that the hybrid operation will behave similar to predictions and simulations, which clearly supports the accuracy requirement. Furthermore, the close to harmonic reconstruction of the input impedance also ensures that the sounds produced by the hybrid instrument are spanned over a wide spectral variety, which is in support of the diversity requirement. This, combined with the fact that an excellent repeatability was found also favours a precise control of the sound of the hybrid instrument. However, it should be said that those impedance measurements only concern low amplitude measurements, therefore, conclusions with regard to the dynamic range cannot be made yet.

The choice of evaluating two wind instrument excitation models was motivated by both research questions, whereas the implementations of the bow-string interaction and polynomial excitation models were mainly with a view to exploring further musical potential. For all four excitation models, the sound prediction theory provided understanding of how certain sound features are related to the excitation models and their parameters. Therefore, the theory represents a helpful tool for inspecting the variety of sounds that can be produced as a function of the excitation model and its parameter values, and which parameter states are likely to give precisely tunable timbres. Moreover, given that this theory can also predict extreme states (e.g. high amplitudes or spectral features) it may also be useful for identifying when atypical behaviour is likely to occur.

The hybrid evaluations were studied with sound descriptors to enable quantitative and perception relevant comparisons with theoretical predictions and with simulations. Given the accuracy of the resonator simulation, the simulated results were used as a reference, representing the ideal hybrid functioning, allowing the precision along with the atypical behaviour of the real hybrid instrument to be evaluated, which turned out to be reasonably precise within the evaluated parameter ranges for all excitation models. Also a generally good repeatability was confirmed in these evaluations. Meanwhile, comparison between different excitation models was of interest in terms of the diversity requirement. While it was observed that some audio descriptors describe a similar range among distinct excitation models, the particular progressions can make one model distinct from another model, which can also be interpreted as a wide perceptible variety.

The further investigations concerning player control, mapping strategies and effects are mainly relevant from the musical performance perspective. The player control and mapping strategies allow one to select or accentuate certain parameter ranges and enable a suitable gesture control, which is useful for maximising the range of timbre variations with regard to the practical use of the

instrument, or to ensure that only precise and/or repeatable ranges are given attention. Alternatively, mappings can also be designed to focus on atypical behaviour of the hybrid instrument.

For future research, there remains common ground between both research questions. For instance, in both cases it would be appropriate to study the behaviour of the hybrid instrument with conventional wind instrument resonators for various notes. However, the increased functionality achieved during this study, culminating in the improved prototype of the hybrid instrument, increasingly enables development and evaluation strategies independently focussed on one of the research questions. This is demonstrated by the ideas for future investigation, presented in the next section. For instance from the musical point of view, it would be interesting to initiate a qualitative evaluation with human participants, including exploring more excitation possibilities. Also, the ideal hybrid instrument does not necessarily represent the target hybrid operation for musical use. Indeed, it is likely that certain deviations from the ideal operation do not represent a problem in that respect. Indeed, it may even be desirable that the hybrid instrument does not produce the same sounds as an entirely simulated instrument, in a similar way to it being preferable to use a non-ideal amplifier with an electric guitar. The non-ideal behaviour imposes part of the particular character of the total instrument. However, for the hybrid instrument to be a useful research tool, the ideal hybrid operation target should be maintained.

7.2 PERSPECTIVES AND RECOMMENDATIONS

In this section, some ideas for future hybrid wind instrument investigations, developments and evaluations are proposed.

7.2.1 *The hybrid resonator*

LOUDSPEAKERS AND OTHER ACTUATORS There are good reasons to carry out further investigations regarding the hybrid instrument's actuation. The loudspeaker in the prototype presented in this study has proven to provide a reasonably good operation, but it has been shown that this component is still responsible for the principal shortcomings of the hybrid instrument.

To extend the dynamic range, a more powerful loudspeaker would be desirable. As mentioned in section 3.3.2, the optimal loudspeaker design is not available as an off-the-shelf product. Instead, such a design could be realised via customisation of an existing loudspeaker, for instance by replacing the voice coil with a higher power rating coil. This would increase the total mass of the moving parts of the loudspeaker, but therefore removes the need for adding more mass to the membrane to lower the loudspeaker's resonance frequency.

While the use of alternative loudspeaker technologies has been considered, it may be helpful to review the available loudspeaker types with the present results and shortcomings in mind. Dynamic loudspeakers were found to offer the best power ratings for the required operation, but it could be that certain loudspeaker technologies offer better linearity, so that the increasing phase lag issue could be avoided.

Finally, it may be worth considering the use of other aeroacoustic actuation possibilities. Earlier studies have reported on the employment of an electrovalve with a "supercritical" set-up (i.e. using an air supply of much greater pressure than the pressure at the output) to drive a hybrid wind instrument (see (Buys and Vergez, 2012)). However, compared with the current hybrid instrument's performance, the results were much less close to the ideal hybrid behaviour (although the electrovalve system did provide a greater dynamic level). This was mainly due to the mechanical friction of the valve components.

It is worth noting the possibility of a subcritical set-up with an electronic valve mechanism. Hence, a mouth pressure equivalent supply pressure could

be chosen, which would result in a reed-equivalent valve displacement. A related idea is to equip a real reed with a piezo-electric actuator to realise a particularly relevant subcritical valve actuation.

MICROPHONES The microphone used in the initial prototype hybrid instrument was largely satisfactory in terms of acoustic requirements. However, its rather large size made it impractical for the centrally located position in the improved prototype hybrid instrument discussed in section 6.1. Another motivation for looking for alternative microphone options could be the relatively high cost.

However, it is not straightforward to find a low-cost microphone that can withstand the high pressures generated in wind instrument resonators (even the reduced dynamic levels experienced with the current hybrid prototype appear to be challenging in that regard). While currently unsuitable, it may be that future MEMS microphone realisations (i.e. piezo-based or dynamic miniature microphones) will provide good candidates. Early research results seem to confirm this perspective (see e.g. (Horng et al., 2010)).

ELECTRONIC SYSTEMS Some alternative electronic systems used in the realisations of related hybrid and augmented instruments are discussed in section B.1. In particular computing performance is continuously improving and it is more than likely that even faster, more compact and cheaper systems than the ones used in the current research will soon become available. Nevertheless, there are few real world applications which have ultra-low latency requirements, which explains why typical everyday computing systems remain unsuitable for hybrid instrument implementations. Such requirements are mainly driven by industrial control system applications, which have been key in contributing to the development of real-time computing solutions. Such solutions include the Xenomai platform used in this study (see section B.2) and digital signal processing (DSP) interfaces for instance.

As demonstrated in earlier work, the excitation can also be realised with analogue electronic circuitry (Kitano et al., 1983; Maganza, 1985; Weinreich and Caussé, 1986; Grand, 1994; Grand et al., 1997; Almeida et al., 2010). While this option is much more restrictive (given that electronic components cannot model any desirable operation), it has the advantage that virtually no latency is present. Moreover, from the musical perspective, it is likely that certain imperfect analogue behaviour is reflected in the sound. This could produce musically desirable variations, similar to the often preferred analogue electronic musical systems. Furthermore, as for the amplification of the electric guitar, electronic vacuum tubes could be used for the excitation, which may introduce a characteristic nonlinear behaviour with musically expressive potential.

GENERAL SET-UP It is also worth considering (slightly) alternative hybrid wind instrument set-ups.

For instance, it may be advantageous to additionally make use of a real-time measurement of the loudspeaker's membrane displacement during the hybrid operation. This could for instance be applied in the context of an active control application to modify the acoustic impedance at the diaphragm of the loudspeaker (Boulandet et al., 2012). While Boulandet et al's set-up allows simulation of "open pipe" conditions at the loudspeaker position, it should be mentioned that this extreme case is only achievable within a narrow frequency range. Indeed, as stipulated in subsection 1.4.2, the target operation remains close to the functioning with an uncompensated loudspeaker. Hence, the passive presence of the loudspeaker only allows for an open pipe simulation close to its resonance frequency. Dr Sami Karkar confirmed this conclusion and proposed considering a hybrid set-up with an actual opening at the resonator entrance, along with a loudspeaker (personal communication, 23 November 2016). Provided that the flow rate at the resonator entrance can be measured in real-time (rather than the pressure for this case), such a set-up would enable the simulation of open-entrance wind instruments such as flutes and (flue pipe)

organs. However, this approach does not allow the computing system to select either the closed or open resonator situation, which would be a convenient feature for musical purposes.

Regarding the two-microphone set-up discussed in subsection 6.1.2, the low-frequency deviation could be possibly avoided by designing an appropriate filter to compensate for the loudspeaker cavity.

SIMULATION OF THE ENTIRE HYBRID SET-UP In order to study the influence of transducers and of other elements that are not intended to affect the principal functionality of the hybrid instrument, the option of simulating the whole hybrid system (including the transducers and compensating filters) could be investigated. Such configurations could be simulated with Port-Hamiltonian Systems (PHS) and/or other frameworks (e.g. COMSOL).

7.2.2 *Excitation models*

Another possible future development of the hybrid instrument prototype concerns the exploration of various excitation models and techniques.

PHYSICALLY BASED EXCITATION Physical models that are closely related to the currently used single-reed and lip-reed models (such as double-reed (Guillemain, 2004)) are easy to implement. In addition, the implementation of a free-reed model could be tried, which is rarely applied for self-sustained oscillations. Also the recorder's excitation mechanism could be considered. The latter would either require the open-entrance pipe situation as discussed in the previous section, or it may be possible to switch the physical (Kirchhoff) variables, i.e. to interpret the microphone's pressure measurement as a flow rate signal and vice-versa for the signal sent to the loudspeaker.

Furthermore, some more advanced physical excitation models could be considered. This is of interest from the point of view of obtaining more realistic and

more "physical" sounds. For instance, the bow-string and single-reed excitation models studied in this thesis were both approximated using a quasi-static assumption. However, it is likely that more advanced physical models may result in quite different timbres for both excitation types.

More sophisticated single-reed models could, for example, include the flow that is induced by the reed movement (Dalmont et al., 1995), or more realistic reed geometries and physics (Avanzini and Van Walstijn, 2004). As well as an improved realism, such additional inclusions might lead to a flow signal that is easier to produce by the loudspeaker (given that the loudspeaker cannot easily reproduce the abrupt flow variations imposed by the sudden and discontinuous reed beating with the current single-reed model).

A more advanced bow-string interaction model is proposed by Smith and Woodhouse (Smith and Woodhouse, 2000), where the thermal effect of rosin is taken into account. Meanwhile, the addition of pulsed noise to simulate the structural irregularities during the bow-string's slipping phase or the turbulent air injection of flow-based excitation models could introduce another element of realism (Chafe, 1990).

Regarding the lip-reed model, more dimensional models could be considered (see e.g. (Adachi and Sato, 1996)), but it may also be possible to add another filter to simulate the nonlinear propagation of air waves in the resonator (see e.g. (Msallam et al., 2000) where this is taken into account for the case of an entirely simulated brass instrument).

NON-PHYSICALLY BASED EXCITATION To fully explore the musical potential of the hybrid approach (as discussed in section 1.2.1), more non-physically based models (such as the polynomial model) could be combined with an acoustic resonator using the prototype set-up.

For example, tools intended for other audio purposes could be considered, such as a limiter or compressor, which also introduce controlled nonlinearities.

It may be of further interest to introduce a delay corresponding to the oscillation period (provided this period is known in advance). This could, for example, be useful to introduce effects that otherwise require anti-causal operations (for instance, to compensate for the increasing phase lag introduced by the loudspeaker).

A challenging yet promising idea would be to consider excitation model design strategies that are guided by a target (steady-state) external pressure spectrum. This could be achieved by deconvolution of that spectrum with the resonator impedance and further inverse operations to finally obtain (pointers towards) formulations of an excitation model. Such a study may be informed by the harmonic balance or related techniques (see e.g. (Gilbert et al., 1989; Karkar et al., 2012)). A related approach has been investigated by Drioli et al., who aimed for the design of a "generalised musical-tone generator" using neural network identification techniques to identify both the excitation model and suitable parameters (Drioli and Rocchesso, 1997).

SOLUTIONS TO THE IMPLICIT EQUATION ISSUE AND NUMERICAL STABILITY Each model requires discretisation, which forms an important constraint for numerical simulations in general. For many excitation models it is not possible to analytically obtain an explicit solution, which may then necessitate the employment of complicated and computationally heavy algorithms (see section 4.1). The "K-method" appears to be a reasonably good technique for the digitalisation of such excitation models (Borin et al., 2000). However, overall it can be concluded that even if the theoretical model is known, it is not guaranteed that it is ready for use with the hybrid instrument.

As mentioned in subsection 4.1.1, globally energy balanced numerical schemes could be used, so that numerical stability is guaranteed, also under highly nonlinear conditions (Bilbao, 2009b; Desvages and Bilbao, 2016). This technique may prove useful for the simulation of more complex excitation models.

7.2.3 *Other additions*

As illustrated as a further development in subsection 6.3.3, it is possible to simultaneously perform active control operations while the hybrid instrument is operating. This represents an interesting new focus for detailed investigation, both in terms of musical potential and usage as a research tool.

A related idea is the application of an arbitrary filter to the signal sent to the loudspeaker, and the simultaneous application of its inverse filter to the microphone signal (provided both filters are causal). Given that the resonator is linear with respect to the amplitude (to a good extent), from the excitation model's perspective these filters cancel each other out, so that the operation is identical to the situation without filters. However, from the perspective of the resonator, the signals are filtered. Hence, this technique opens up the possibility of applying "equalisation" and other linear (and causally invertible) filter operations to the sound produced by the hybrid instrument, without affecting the underlying oscillation mechanism. However, it should be borne in mind that this idea is only possible in practice when the filters do not significantly affect the principal frequency components that are of key importance to the self-sustained oscillation mechanism. This concept may, for instance, be of interest for investigating the earlier proposed idea: for the perceptive simulation of the nonlinear propagation of air waves in the resonator.

In addition to the mouthpiece controller introduced in section 6.3, various other sensors could be introduced. For instance, the motion of the instrument body could be measured with incorporated sensors or simple foot pedals could be used.

7.2.4 *Further evaluations and uses*

MUSICAL MOTIVATION The hybrid operation can certainly produce unique sounds with interesting musical potential, i.e. sounds that are not produced by

full simulations. In this view, the reported saturation effects or appearances of certain noises could be explored for instance.

Meanwhile, many sounds are (almost) equally produced by simulation. It is still of interest to study such features, but it is important to note that the simulation already represents a good method for their (initial) evaluation. This approach has the advantage of bypassing the hybrid instrument's technical complications. The simulated evaluation provides a good indication of the musical suitability, which could then be verified using the hybrid instrument.

This is of general interest for the initial evaluation of various excitation models and specific oscillation phenomena. One example is the observed period doubling phenomenon (reported in section 5.5), demonstrating how atypical behaviour can enlarge the musical expression domain. In line with Maganza's evaluation focus (see (Maganza, 1985)), it would be interesting to examine this phenomenon in more detail, verifying the occurrence of further period doubling "branches" and chaotic states.

As proposed in the introduction, it would be useful to conduct a qualitative evaluation with musicians and/or listeners regarding the musical potential of the hybrid instrument. This could be carried out with a real clarinet resonator as well as with other wind instrument resonators. Furthermore, it would be useful to employ the newly developed mouthpiece controller discussed in section 6.3. To evaluate perceptive features, a (parallel) psycho-acoustic test can be envisaged, comparing the hybrid instrument with real and/or simulated instruments.

It is also conceivable that the hybrid instrument could be a component of a larger (i.e. "intelligent") musical system, where the resonator fingering could also be automatised for example.

RESEARCH TOOL EVALUATION As questioned earlier, it could be investigated whether the absence of the mean air flow through the instrument adversely affects the sound produced. This could be addressed by, for example,

injecting a separate mean flow component via a capillary tube connected to the entrance of the instrument. This injection technique could be further expanded to introduce other chemical gas compositions, and the influence of the temperature and humidity could also be verified. It is known that these gas properties play a role when wind instruments are blown by human players (Rienstra and Hirschberg, 2013), and an evaluation with a hybrid instrument would enable a precise experimental verification.

It is worth noting that, while the dynamic range of the hybrid instrument is restricted, it is nevertheless possible to simulate a small range of realistic wind instrument excitation situations. For example, it would be possible to use a realistic beating pressure (P_{M}) in combination with a γ value just above the oscillation threshold, resulting in a low amplitude oscillation, which can be realised with the hybrid instrument.

The evaluation carried out in this thesis has mainly focussed on the sustained operation of the hybrid instrument. However, it is known that the perception of transient behaviour is of vital importance in defining an instrument's character. An interesting perspective would be to perform a detailed study of how the transients are produced by the hybrid instrument, and then compare those findings with simulations and a real instrument's behaviour.

OTHER PURPOSES In addition to the uses for the hybrid instrument that have already been discussed, some alternative applications were raised in the introductory chapter.

For instance, Dr Henri Boutin stressed the potential of the hybrid wind instrument concept for application to historical wind instruments that are no longer allowed to be sounded by human players (personal communication, 25 November 2016), which was already mentioned in subsection 1.4.3 as a potential of hybrid instruments.

Meanwhile, the possibility of (partly) automatising the excitation control could have potential use in an educational context, allowing students to sep-

arately train their fingering. The reduced dynamic range could also represent a desirable feature, for instance in environments where the maximum sound level is restricted. This perspective is supported by Yamaha, who are developing a "Silent instrument" series.

Finally, in agreement with the "research tool" aspect, the hybrid instrument can also be useful as a tool for wind instrument makers. Indeed, the implementation of sophisticated physical embouchure models leads to a good relationship with real mouthpiece constructions. By comparing a hybrid evaluation with various embouchure properties and geometries, this can then inform the design of a given mouthpiece component.

7.3 SUMMARY

In the first section of the current chapter, the work presented in this thesis was reviewed. This was done by considering together all unrealistic hybrid aspects (with respect to real wind instruments) noted throughout the thesis: the restricted dynamic range, the absence of the mean flow component, unstable hybrid behaviour and fundamental frequency deviations. A concluding remark was made on the ambiguous notion of the "accuracy" of the hybrid instrument. Then, the initial research questions and the associated requirements were reassessed, verifying that their focus was maintained throughout the development, excitation model design and evaluation stages.

The second section of the chapter presented a wide variety of perspectives and recommendations, focussing on separate parts and possible functionalities of the hybrid instrument. The suggestions were mainly ideas of the present author, although where relevant they were informed by literature. For the further development of the instrument, ideas for alternative loudspeakers, other actuators, microphones, electronic systems (digital and analogue) and general set-up considerations were made. Then, for the design of further excitation models, the implementations of alternative and more advanced physical and non-physical

models were suggested and a generic solution for the implicit equation issue was proposed. Furthermore, the addition of simultaneous active control possibilities, an equalisation implementation, and a few ideas for sensor systems were proposed. Finally, some ideas for further evaluations and uses were presented, covering musical, "research tool" and other perspectives.

Part III

APPENDIX

The last part of this dissertation comprises two appendixes. The first appendix includes information on measurement equipment, preparations and regression techniques. It also reports on two measurements and on the associated loudspeaker-tube parameter identification. The second appendix discusses the real-time computing systems employed in this thesis, preceded by a brief literature review on related systems. Also some examples of code and programs are provided.

A

MEASUREMENT AND REGRESSION

The main practical measurement equipment, techniques and protocols that have been applied in this study are laid out in this appendix, including a report on the measurement of the coupled loudspeaker-tube system and the parameter identification using the models provided in chapter 3.

A.1 MEASUREMENT EQUIPMENT

In this section, the equipment used to make the measurements to characterise the loudspeaker and the resonator are reported. For details on the mouthpiece controller (comprising the load cell and pressure sensor), subsection 6.3.1 should be consulted. Meanwhile, more details on the computing systems are discussed in the next appendix, in chapter B.

A.1.1 *Microphones*

The microphone used in the initial prototype (generally used in this thesis, except for the piece of work involving the improved prototype, discussed in section 6.1) is a 1/4 ″ Brüel & Kjær (B&K) microphone type 4187 (equivalent to the more common type 4135) with a B&K microphone preamplifier type 2633. This microphone has a sensitivity of $-48\,\mathrm{dB}$ re. $1\,\mathrm{V\,Pa^{-1}}$ ($4\,\mathrm{mV\,Pa^{-1}}$), which is relatively low, but sufficient to capture the lowest amplitude pressure waves in the resonator. An excellently linear frequency response is reported in the datasheet, with sensitivity deviations of maximum 1 dB for frequencies between 10 Hz to 20 kHz. The 3% Total Harmonic Distortion (THD) limit, giving an indication

of the maximum achievable linear dynamic pressure measurement, is high at 164 dB (3170 Pa) and the lower threshold of the dynamic range is limited by the (A-weighted) noise level of 39 dB (1.8 mPa). Both thresholds largely exceed both the amplitude range used for the characterisation measurements and the operational range of the hybrid instrument.

For the improved prototype, two Knowles microphones of type EK-26899-P03 were used. These are small (4 mm $\times$ 5.6 mm $\times$ 2.2 mm) relatively low cost microphones offering a high dynamic range (which is a rare combination). The sensitivity of -71 dB re. 1 V Pa^{-1} (0.28 mV Pa^{-1}) still enables a reasonable accuracy in the context of the hybrid instrument's operation, given that signals largely exceed the (A-weighted) noise level, found at 40 dB (2.0 mPa). The frequency response of these microphones is slightly less flat than that of the B&K microphone. The sensitivity increases with frequency, culminating at 10 kHz with -68.5 dB, and while this magnitude deviation is not an issue for the hybrid operation, the associated phase deviation is not provided and is potentially of greater concern. A characterisation of this microphone model with respect to this matter may be a useful future investigation. Using the "extended dynamic range circuit" with a supply voltage of 10 V, as proposed by the manufacturer, the dynamic range of the microphones can be fully exploited. The 10% THD limit lies at 154 dB (1002 Pa), which still exceeds the useful pressure range for the current hybrid wind instrument prototypes.

A.1.2 *Amplifiers*

Throughout the entire thesis, the loudspeaker is powered using a Cambridge Audio type A1 amplifier, providing 30 W of maximum continuous power. The frequency response of this amplifier was measured and the gain and phase were found to deviate by less than ± 0.42 dBV and ± 0.1 rad respectively, in a frequency band far greater than the hybrid operation.

Initially, a B&K amplifier type 2706 amplifier was tested, which had a slightly flatter frequency response. However, it was suspected that this amplifier did not sufficiently reject power line noises.

A.1.3 *Vibrometer and data acquisition*

For the measurement of the loudspeaker membrane velocity, a Polytec Laser Doppler vibrometer was employed, consisting of a PSV-400 scanning head, a junction box, an OFV-5000 vibrometer controller and a data management system to conduct the acquisition and store the measurements. This system allowed for the additional measurements of the voltages originating from the amplifier input and output and from the microphone. By carrying out all measurements with the same acquisition card, synchronisation of all measurement data was guaranteed.

In earlier measurements sessions than the ones reported in section A.4, an additional USB acquisition card was used, and the data of the real-time computing system was also considered for use as "measurement data". However, the combination of measurement data originating from different acquisition equipment consistently resulted in synchronisation issues, which demonstrated the importance of using a single measurement system.

A.2 MEASUREMENT PREPARATIONS

A.2.1 *Precautions*

A typical issue when dealing with electrical measurements is related to grounding. This issue can greatly affect accuracy and introduce (fluctuating) bias signals when not properly considered. The problem can occur when the electrical supply of a signal source is "distantly related" to the electrical supply of the ac-

quisition equipment. A detailed description of the issue lies outside the scope of this thesis, but a suitable National Instruments guide provides a clear explanation and useful practical guidelines (National-Instruments, 2016). All signal sources used in this thesis were "floating" (i.e. all of the output leads were independent of the electrical ground), which allowed for an appropriate use of a "referenced single-ended" (RSE) configuration. In this configuration, the floating ground and signal outputs of the source are connected to the respective inputs of the acquisition card (set to RSE mode) without additional wiring or resistors.

A major cause of failures and malfunctions in today's electrical components and systems is "electrostatic damage" (ESD). This can occur when an electrostatic loaded body makes contact with a vulnerable contact of a component. To cope with this issue, whenever possible, contacts and leads of components were not touched and for the assembly of sensitive electronic components (e.g. the Knowles microphones) an antistatic wrist strap was worn to direct any static charges to ground.

Finally, given that the measurement set-up is relatively complex, involving a large amount of equipment and wiring, the measurement set-up was built up step-by-step with intermediate test measurements. This approach enables rapid identification of the cause of faults in the system. It was particularly helpful following problems originating from the vibrometer system, whose acquisition inputs turned out to substantially decrease in impedance when powered off (thereby affecting the measurement of signal sources that were still connected to these inputs).

A.2.2 *Calibration*

Some of the equipment that was used required calibration in order to obtain coherent absolute measurements. Both microphones could be calibrated using a B&K "pistonphone", which provides a pressure signal of known dynamic level.

The amplifier could be calibrated by measuring its input and output voltages while supplying a sine signal to the input. During this calibration, care was taken to suppress noise, by applying an averaging filter, which could be carried out using an oscilloscope.

A.3 NONLINEAR CURVE FITTING BY REGRESSION

In order to characterise a physical system, a suitable physical model and appropriate measurement data can be matched, resulting in the retrieval of approximate physical parameter values for the system. This can be done using curve fitting methods, which attempt to match the measurement data with curves obtained with the model. A widely used nonlinear curve fitting method, that is appropriate for all measurements carried out in this thesis, is the regression with a "least-squares" approach[1]. This involves the calculation of the sum of squares

$$S = \sum_{i=1}^{m} (y_i - f(x_i, \beta))^2 \tag{104}$$

where (x_i, y_i) are measured data points (e.g. the pressure and flow rate amplitudes at a certain frequency), $f(x_i, \beta)$ is the physical model's function (e.g. a modal impedance model), and β is a vector containing the model's parameter values (e.g. the modal frequencies, quality factors and amplitudes).

The minimum value of S is obtained when the gradient of this equation (with respect to β) is zero. Hence, a preparatory step is to theoretically obtain all gradient equations (each parameter leads to a gradient equation); this theoretical development is not further described here. Once the gradient equations are known, the regression procedure can start. An initial parameter vector β_0, contains an "initial guess" of the parameter values (note that this guess should be reasonably close for the regression to converge). In the next step, a slightly di-

1 Note that alternatively the very recently appeared technique using recursive parallel filters by Maestre et al. could be employed (Maestre et al., 2017).

verging parameter vector β_1 is evaluated, which allows the gradient equations to be solved. In turn, these equations indicate whether the new parameters were improved. Finally, the iteratively repeated execution of these steps leads to the numerical approximation of the parameter values.

This regression technique is entirely performed by the MATLAB `lsqcurvefit` function which takes (x_i, y_i), $f(x_i, \beta)$ and β_0 as input parameters and returns an estimated parameter vector β. Depending on the intended use, it is important to make decisions regarding the data to use. For instance, when the parameters are to be used to simulate the resonance modes of the resonator for simulation of the self-sustained operation, it is important that the model matches the measurements closely around the resonant peaks (particularly of the lower resonance modes). Given that both the measured data and the physical model can diverge at frequencies far away from these resonant peaks (e.g. at frequencies far below the first resonance), it is of interest to exclude this frequency range from the regression. In addition, it is important to select an appropriate function in this regard. For instance, to obtain a good regression around the impedance peaks, an optimal regression is obtained by using the impedance expression and not the related admittance (which would accentuate the antiresonances).

Apart from the modal resonator estimation, regressions were also used in the characterisation of the loudspeaker, and for finding optimal parameter values for the lead-lag filter, all discussed in the next section.

A.4 MEASUREMENTS AND IDENTIFICATION OF LOUDSPEAKER AND TUBE PARAMETERS

In a first approach, the loudspeaker and tube were individually measured and characterised. For the loudspeaker's parameter identification, Klippel's method can be used (Klippel and Seidel, 2001). However, it was found that all measurements could actually be performed on the assembled loudspeaker-tube system. Using its associated coupled model, a method related to the one proposed by

Klippel could then be used, enabling the estimation of both loudspeaker and resonator parameters. This assembled approach allows an even more direct and complete parameter identification. It also has the advantage of comprising in-situ measurements so that the parameter values fully correspond with the hybrid instrument application. The adapted version of Klippel's method involves two measurements (described in A.4.1 and A.4.2) and four least square linear regressions. The regressions were carried out on the frequency domain representations of the measured data and enabled retrieval of both the loudspeaker and resonator parameters. In theory it should even be possible to characterise the entire system with a single measurement. However, this would require a nonintrusive electrical current measurement of reasonable precision, which is difficult to realise with practically available current sensors, in particular due to the precision requirement. (This was empirically confirmed with a Hall Effect-based current sensor).

For reference, all of the obtained loudspeaker parameters and lead-lag filter coefficients are shown in table 1 in subsection 3.3.3.

A.4.1 *Measurement 1*

For the first measurement, a resistor with resistance R_s was placed in series with the loudspeaker and a sine wave signal with an amplitude of 0.3 V was supplied, swept in frequency from 0 kHz to 1 kHz over 20 s. This amplitude is of the same order as the hybrid signals encountered in this study, and covers about half of the loudspeaker's linear dynamic range. The voltages across both the resistor and the loudspeaker were measured so that the current (and thus the speaker's electrical input impedance) could be derived, as in equation (37). To ensure a good precision for both voltage measurements, R_s was chosen to be of the same order as the DC voice coil resistance, with its precise value determined using an ohm-meter. The loudspeaker's membrane velocity was measured synchronously using the laser-Doppler-vibrometer (see section A.1). The meas-

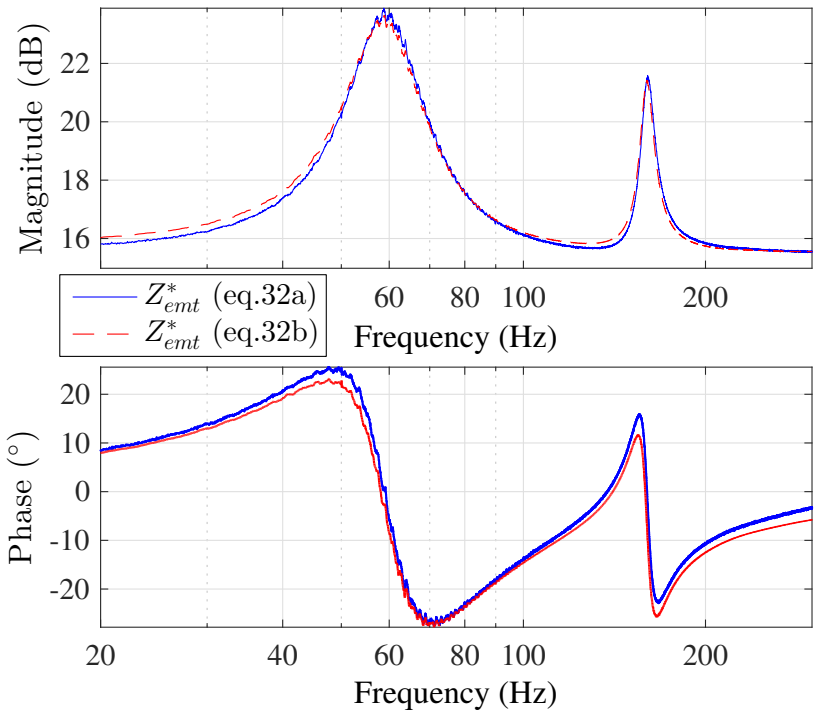

Figure 81: Regression of the electrical loudspeaker input impedance $Z^*_{e(mt)}$ using equations (105a) and (105b).

ured values were then inserted into the following two alternative expressions for the impedance:

$$Z^*_{e(mt)} = \frac{V^*}{I^*} \tag{105a}$$

$$Z^*_{e(mt)} = \frac{Z_e\ V^*}{V^* - Bl\ \dot{X}^*}, \tag{105b}$$

where the asterisks refer to measured quantities.

A regression using both expressions resulted in a good match, as can be seen in figure 81, enabling the retrieval of precise electrical loudspeaker parameters Bl and R_e.

It should be noted that the observed phase lag in the impedance obtained with equation (105b) increases with frequency and isn't taken into account by the used model. In subsection 3.3.3 it is reported that, unlike the loudspeaker's model, its input to output phase response indeed increases more and more with frequency (possible causes for that are given in subsection 3.4.1). Given that the velocity measurement is used in equation (105b), the phase lag is reflected in

the measurement with that equation. Hence, for a correct parameter estimation with the used loudspeaker model, the regression is applied from 20 Hz to 300 Hz only.

A.4.2 *Measurement 2*

In the second measurement, the series resistance was left out so that the low amplifier output impedance and, consequently, the loudspeaker's Q_{ts}-factor were maintained. Here, the supplied sine wave signal was swept from 0 kHz to 5 kHz over 55 seconds for both a 0.3 V and a 0.6 V amplitude, in order to observe possible nonlinear effects. The amplifier's input voltage was captured, together with the membrane velocity and the pressure in front of it. The amplifier gain was derived before the measurement, so that the voltage V delivered by the amplifier could be obtained.

Identification of the loudspeaker's mechanical parameters

The measurements were then inserted into equation (38), so that a regression with:

$$1/Z^*_{\mathrm{m(et)}} = \frac{1}{Z_{\widetilde{\mathrm{m(e)}}} + S_{\mathrm{d}}\,\frac{P^*}{\dot{X}^*}} \tag{106a}$$

$$1/Z^*_{\mathrm{m(et)}} = \frac{Z_{\mathrm{e}}\,\dot{X}^*}{V^*\,Bl}, \tag{106b}$$

using the expression for $Z_{\widetilde{\mathrm{m(e)}}}$ in (30), revealed all mechanical loudspeaker parameters (note that the inverse impedances are needed for optimal conversion, as explained in section A.3).

The regressed curves (presented in figure 82) show a good correlation. At higher frequencies the same increasing phase lag behaviour is observed, but it is interesting to note that the measurement with the 0.6 V input signal is less affected. The 20 Hz to 1000 Hz frequency range is chosen for the parameter

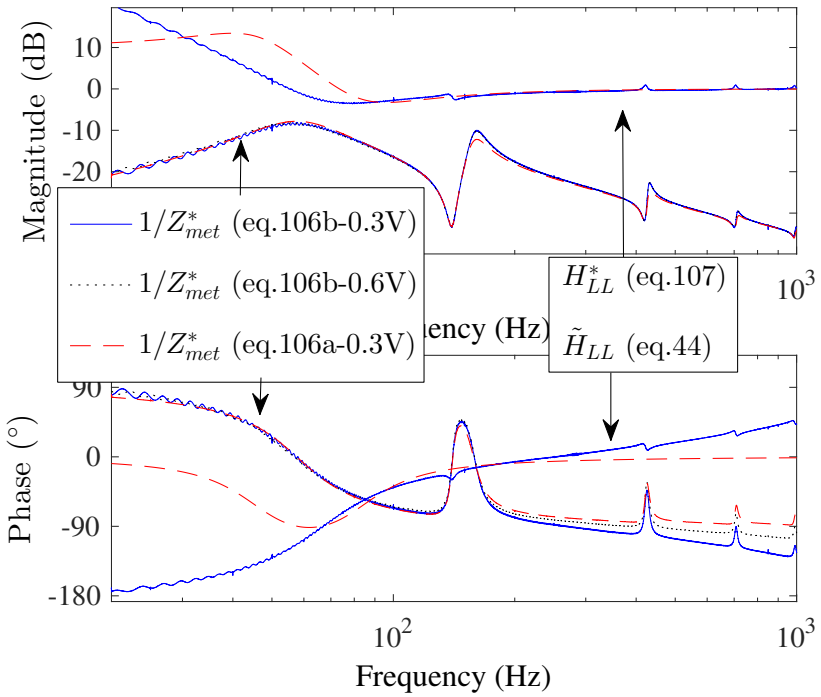

Figure 82: A regression of two mechanical loudspeaker reciprocal impedances $1/Z^*_{\mathrm{m(et)}}$, obtained by equation (106a) (for a 0.3 V amplitude) and equation (106b) (for 0.3 V and 0.6 V amplitudes) and a regression of $\hat{Q}/Q^*$ (including the H_{LL} compensator transfer function).

estimation, as it corresponds with the spectral domain that is of importance to the self-sustained operation with an excitation model.

Identification of the lead-lag filter coefficients

The same measurement data can be used to find appropriate coefficients for the lead-lag compensator H_{LL}. The targeted range for this filter is between the loudspeaker resonance frequency and the frequency where the effect of the loudspeaker's damping and stiffness becomes negligible, i.e. 80 Hz to 300 Hz for the current set-up.

Using the obtained electrical and mechanical loudspeaker parameters and the measured pressure signal P^*, the signal $\widehat{Q}^*$ can be derived by inversely applying the feedback and feedforward filters to the measured amplifier output

voltage V^*. A regression using the lead-lag equation (44) was applied on the ratio between this input and output:

$$H^*_{\mathrm{LL}}(f = [80, 300]) = \frac{\widehat{Q^*}}{S_\mathrm{d}\ \dot{X}^*}, \tag{107}$$

which is also shown in figure 82, revealing an effective loudspeaker resonance compensation above $\omega_{\mathrm{LS}} (= 2\pi \times 67.4\,\mathrm{rad\,s^{-1}})$.

Identification of the modal tube coefficients

This measurement data and the S_d value (obtained via the first regression) also enabled the measurement of the input impedance of the resonator:

$$Z^*_\mathrm{t} = \frac{P*}{\dot{X} * S_\mathrm{d}}.$$

Figure 83 shows the magnitude and phase of this impedance (solid line), along with a modal approximation (dashed line), which is derived from the measured impedance by regression, using equation (25) (thereby revealing the modal parameter values). The resonance frequencies of the regression are found with a ± 2 cent precision and, over a large range around the resonances, the magnitude does not deviate by more than ± 0.3 dB from the measurement.

This method is compared with other acoustic input impedance measurement techniques (e.g. with the "capillary tube method" (Sharp et al., 2011)) and is found to provide a measurement with the closest match to a theoretically obtained curve, except in terms of the phase at frequencies greater than 2 kHz, where the phase-lag issue arises (which is why the measurement with the 0.6 V signal is used here). Nevertheless, the regression can be focussed on the magnitude response for that frequency range, resulting in a corrected phase. Moreover, the phase response at such high frequencies doesn't affect self-sustained oscillations at the tube's first register note. As such, using a frequency range of 20 Hz to 4050 Hz, the parameters of 14 modes are identified. A

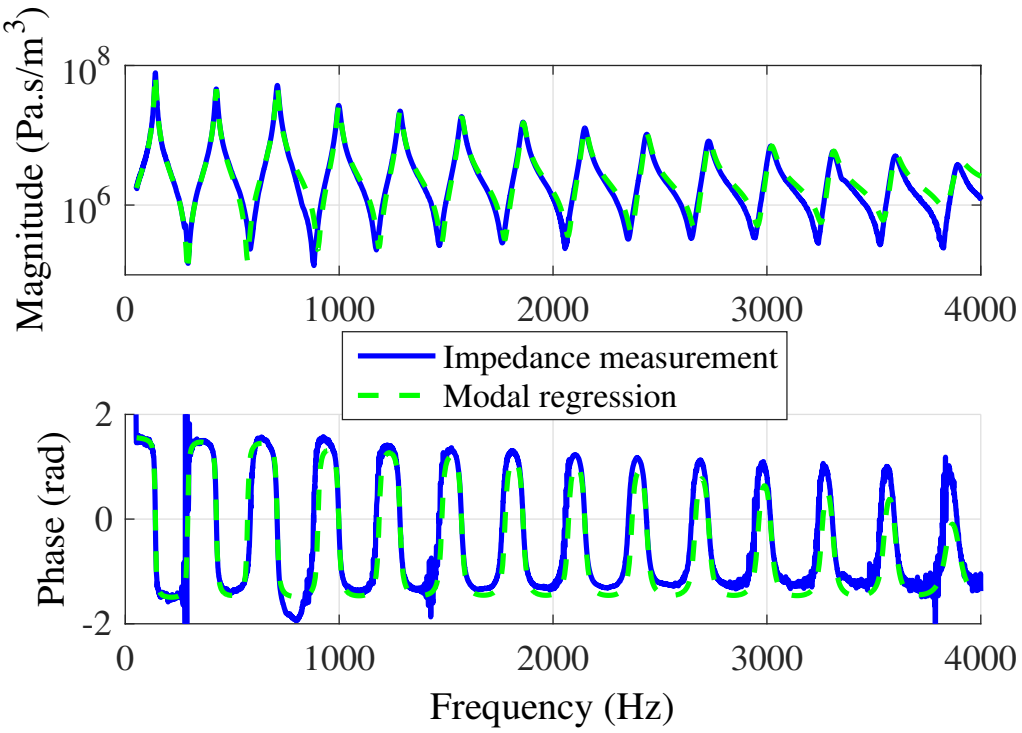

Figure 83: Fourteen first modes of the measured tube impedance Z_t^* (solid line) and its modal regression using equation (25) (dashed line).

detailed view on the first five impedance peaks is given in figure 27 in subsection 3.3.3.

B

COMPUTING SYSTEMS AND PROGRAMS

B.1 DIGITAL AND ANALOGUE ELECTRONIC SYSTEMS USED IN EARLIER HYBRID INSTRUMENTS

An important component of hybrid musical instruments is the electronic system that must acquire, process and deliver signals within specific time constraints, determined by the target operation. This section reviews a number of electronic systems reported in the literature. When provided, the characteristics that are relevant to the current study are mentioned.

Analogue systems, although benefiting from fast response times, often lack in control precision or flexibility. However, the studies of Kitano et al. (1983), Grand et al. (Grand, 1994; Grand et al., 1997), Almeida et al. (2010) and (partly) Maganza (1985) and Weinreich and Caussé (1986) allowed the use of simplified excitation models, which could be realised with a few simple (nonlinear) electronic components.

In contrast, digital systems are appealing for their flexible and precise control options, but many fall short when it comes to timing requirements. Moreover, the processing power imposes a maximum sampling frequency, which limits the usable frequency range.

A non-negligible difference between active control and hybrid applications with regard to the restricted frequency bandwidth is that, with the former, the instrument can still produce frequencies exceeding the bandwidth, while with hybrid instruments, the bandwidth fully dictates the spectrum of the sound produced by the instrument. Early digital solutions were based on specialised analogue-to-digital (A/D) and digital-to-analogue (D/A) converters and fast Digital Signal Processing (DSP) integrated circuits that could be programmed

in low-level programming languages or in C. Such solutions were, for example, employed by Guérard et al. (Guerard and Boutillon, 1996; Guérard, 1998), Weinreich et al. (Weinreich and Caussé, 1991) (mentioning a "computer" with a sampling rate of 125 kHz), Boutin (2011) and Berdahl (2009), with various levels of system performance. Hanagud and Griffin (1998) initially used a DSP board and a PC, and later they used a system housed in a "portable box" (without mentioning further technical details). Maganza also evaluated his hybrid wind instrument with a digitally implemented excitation model, using IRCAM's 4C computer, which was specially developed for such applications, featuring a total input-to-output delay of 100 µs (Maganza, 1985; Maganza et al., 1986). This computer was also used by Weinreich, as reported in earlier work on his hybrid string instrument (Weinreich and Caussé, 1986).

Vergez and the current author have previously used a dSpace "DS1006" digital interface, which can be programmed in Simulink, offering flexible and graphical programming benefits (Buys and Vergez, 2012). This system could run at a maximum sampling rate of 50 kHz with a total latency of only 20 µs, corresponding to a single sample delay. Disadvantages of the dSpace system are the considerable price and its relatively large size, in comparison with the compact DSP interfaces for instance.

More recently, musical active control projects have been reported which use standard PCs, optimised with a real-time framework such as *Xenomai* or *RTAI*. These systems enabled similar performances to the dSpace interface, with total latencies down to 24 µs at sampling frequencies around 40 kHz (Dozio and Mantegazza, 2007; Lee et al., 2008; Berdahl, 2009; Benacchio et al., 2013; Meurisse et al., 2013). While more complex operations increase the delay time slightly, excitation models are relatively simple operations, so that this approach was chosen for the development of the hybrid instrument presented in this thesis.

B.2 THE REAL-TIME COMPUTING SYSTEMS EMPLOYED IN THE CURRENT WORK

The hybrid operation requires a "real-time" feedback-loop that includes a numerical interface. For both prototype hybrid instruments described in this dissertation, general purpose computing systems were configured in order to meet the real-time requirement.

A typical computer operating system rapidly alternates between the execution of various processes (both user-defined and background tasks such as verifying e-mails, or making a cursor blink on the screen), so that their occurrence appears to be simultaneous. However, within small time scales, the process alternations become clear. Everyday computing applications can be interrupted in this way, but the short waiting periods prove to be problematic for applications with fast and almost instant processing requirements.

The solution chosen for the hybrid wind instrument implementation in the current work involves the recompilation of a Linux kernel on general purpose computer architecture, which is covered by the *Xenomai* framework[1] . This framework makes changes in the priority handling of a Linux distribution, allowing the attribution of 100% priority to user defined processes. That is to say, when a program is compiled from C++ code that includes specific Xenomai code, its execution gains full priority over all processes; this is also referred to as a "hard real-time" process. Meanwhile, a fast acquisition interface guarantees equally fast analogue signal to data conversion and vice versa.

B.2.1 *A PC-based system*

The first Xenomai implementation, used for the development and evaluation of the initial prototype (used throughout this thesis, apart from in section 6.1), was carried out on a Pentium 4 desktop computer. While being a relatively old

1 http://www.xenomai.org

computer, its processor only contains a single core, which is known to provide better co-operation with the Xenomai platform. Furthermore, given that the set-up of the Xenomai system is not always straightforward, it was decided to choose the set-up to be as close as possible to the successful Xenomai set-up by Benacchio et al., who also used a Pentium 4 computer (Benacchio et al., 2013).

This system includes special drivers (by the "Analogy" software project), which enable uninterrupted access to a National Instruments 6281 (M series) 16-bit acquisition card that provides analogue inputs and outputs. To enable the co-operation with the Xenomai functionality, specific Analogy driver-code is added to the processes that require "hard real-time" data input and output handling.

In order to introduce these specific commands into the C++ code that is generated from a Simulink program, the work by Benacchio et al. is relied on, who created a patch-file that makes the necessary modifications to the C++ code (Benacchio et al., 2013). In this way, the system can be used with a minimum sampling time (without overruns) of $T = 25\,\mu s$, corresponding to a sampling rate of f_s =40 kHz (sufficient for capturing the frequencies produced by the instrument).

The analogue inputs are sampled with an A/D converter while calculated digital output data is simultaneously sent to the D/A converter (shown in the global block diagram in figure 19). In this process, some signal transformations occur. While the A/D converter contains an anti-aliasing low-pass filter and introduces quantisation noise, the D/A converter also involves a low-pass "reconstruction filter". However, given that a high sampling rate and bit depth are used, the effect of these transformations is negligible for the frequency and amplitude range of interest in this study, so that only the introduced latency is taken into account in the general computing system transfer function $H_{cptr}(z)$. For the PC-based system, as there are no sources of latency other than the A/D and D/A conversion itself, the total latency is restricted to a single sample only, so that:

$$H_{\text{cptr}}(z) = z^{-1}. \tag{108}$$

It should be mentioned that the real-time computing system was still affected by an imperfect timing issue, which introduced a slight "jitter" (i.e. small fluctuations of the acquisition punctuality, which is manifested as an additional noise signal). The mean time deviation (around $\pm 3\,\mu s$), and therefore the amplitude of the noise, was found to change over longer periods (hours or days). A hypothesis for the cause of this issue is that the clock signal used for the Simulink code is independent from the acquisition card's clock, when ideally they should be co-operating. In chapter 5, the issue was identified as the reason for a long-term non-repeatability effect, causing deviations of the hybrid sounds.

Another drawback of this system is that it only supports a single input and output to be used.

B.2.2 *Bela, a BeagleBone Black based system*

Relatively recently, with the purpose of fast-interacting audio computing in mind, Andrew McPherson et al. at Queen Mary University designed "Bela", a system based around the BeagleBone Black embedded small computer (McPherson and Zappi, 2015). The BeagleBone Black is equipped with a Linux distribution which therefore supports a Xenomai implementation. McPherson et al. specifically designed an additional acquisition board (a "cape") for the hard real-time audio purpose, supporting 8 analogue inputs and outputs.

The support of several audio inputs has been the main reason for the choice of this platform for use in the improved prototype discussed in section 6.1, as that prototype requires an input for each of the two microphones.

Bela's minimum total I/O latency is Δt =90.7 µs, with $N = 4$ (i.e. the minimum I/O sample delay) and $f_s = 44.1\,\text{kHz}$. Hence, for this system the computing system transfer function is:

$$H_{\text{cptr}}(z) = z^{-4}. \tag{109}$$

While this system introduces a greater input-to-output latency then the PC-based Xenomai system discussed in subsection B.2.1, as explained in section 6.1, the 2 microphone technique compensates for this delay.

Another advantage of the Bela system is that its compactness makes the entire hybrid wind instrument easily transportable.

While the system does not support the use of Simulink, the hybrid wind instrument's computing operations (the excitation models and the loudspeaker-compensating filters) are relatively simple to implement in C++ code, which also provides superior performance compared with Simulink-generated C++ code.

B.3 SELECTED PROGRAMS

B.3.1 *Principal programs for the hybrid and simulated evaluations with the PC-system*

The MATLAB code displayed in code listing 1 shows the main contents of the `hybrid_wind.m` file, which governs the evaluation procedure for the hybrid instrument and for the simulations. A detailed explanation is not provided, but it can be verified that the code handles functions as discussed in this dissertation.

Listing 1: "hybrid_wind.m" — MATLAB code for the global self-sustained evaluations.

```
% Script for the hybrid wind instrument
% version 1.3


clc
clearvars
close all
```

```
%% %!set the instrument mode and the desired excitation model:

instrument_mode = 'simulation';
%instrument_mode = 'hybrid';

%Main excitation models %!select
%excitation_model = 'single_reed';
excitation_model = 'lip_reed';
%excitation_model = 'bowed_string_hyperbolic';
%excitation_model = 'polynomial';

% Solver
Ts = 25e-6; %(s) solver period
fs = 1/Ts;  %(Hz) sampling frequency for solver
runtime = 5; %(s)

%Resonator Parameters:
rho = 1.204; %(kg/m^3) air volumetric mass
c = 344; %(m/s) the speed of sound (21.5 C)
% Tube characteristic impedance :
a = 14.2e-3/2  % (m) tube cross sectional radius: 14.2e-3/2; %real
    clarinet: 15.0e-3/2 %! set!
St = a^2 *pi; % (m^2) tube cross sectional area
Zc = rho*c/St;

%Excitation model:
% Execute script containing the excitation model variables and
    vectors:
run(excitation_model)
```

```
if strcmp(instrument_mode,'simulation')
    % Load the modal resonator parameters:
    load('../../../Data/Characterising/Calculated/Impedances/Modal
        coefficients/modal_coeff_vibro_pt1-2.mat','modal_coeff');
    an = modal_coeff(:,1);
    wn = modal_coeff(:,2);
    Qn = modal_coeff(:,3);

elseif strcmp(instrument_mode,'hybrid')
    temp = 22.6; %!set
    %Amplifier parameters:
    maxlinevoltage=0.447;
    maxoutputvoltage = 5;
    %! Perform an amplifier gain calibration first. Put the found
        factor here:
    amp_gain_factor =   0.73316;%last calibration:%23/9/2016
    % Microphone, loudspeaker and amplifier parameters
    micpreampsensitivity =  -0.0025726 % (V/Pa) the minus sign is to
         correct for the inverted output.
    %Loudspeaker Parameters:
    % load LS estimated parameters for the loudspeaker compensating
        filters:
    load('../../../Data/Characterising/Calculated/LS Parameter
        estimation/Estimated_LS_parameters_vibro_pt1-2.mat')

        %Calculate lead-lag discrete filter variables:
    HLL_c = tf([1 LLwresn/LLQnd LLwresn^2],[1 LLwresd/LLQnd LLwresd
        ^2]);
    HLL_d = c2d(HLL_c,Ts);
```

```
end

%% Runtime & post procedures:

if strcmp(instrument_mode,'simulation')
    % Launch the simulation with these parameters :
    sim(['simu_wind_' excitation_model '.mdl']);
    p_dl = p_dl.signals.values;
    q_dl = q_dl.signals.values;
    %zeta_vect_simu = zeta_vect_simu.signals.values;
    %gamma_vect_simu = gamma_vect_simu.signals.values;
    % Save all acquisition parameters & results:
    timevect = (0:Ts:runtime)';
    plotlinespecs = '--r';
    save(['Acquisition_parameters_and_results_simulation_'
        excitation_model]);
elseif strcmp(instrument_mode,'hybrid')
    %activate driver (actually needed just once, but does no harm
        executing each time...)
    unix('echo xenomai | sudo -S /usr/xenomai/sbin/analogy_config
        analogy0 analogy_ni_pcimio 0x4,0');
    %run the calibration program:
    unix('./calib_micoffset -time 3');
    load('calib_micoffset.mat');
    voltsin_calib = rt_yout(:,2); ampin_volts_calib = rt_yout(:,3);
    micoffset_V=mean(voltsin_calib);
    %build the c code:
    rtwbuild(['hybrid_wind_' excitation_model])
    %run the xenomai patch:
```

```
    unix(['echo xenomai | sudo -S ./moulinette.sh hybrid_wind_'
        excitation_model]);
    %execute the program:
    unix(['echo xenomai | sudo -S ./hybrid_wind_' excitation_model '
         -time ' num2str(runtime)]);
    %load the results and put it into appropriate vectors:
    load(['hybrid_wind_' excitation_model '.mat'])
    timevect = rt_tout(:,1);
    p_dl = rt_yout(:,1);
    q_dl = rt_yout(:,2);
    ampin_volts = rt_yout(:,3);
    nclipped=sum(abs(ampin_volts)-maxoutputvoltage>=0);
    if nclipped>0
        warning('AMPLIFIER SIGNAL HAS CLIPPED %d TIMES!',nclipped)
        figure,
        plot(timevect,ampin_volts)
    end
    clear rt_yout rt_tout;
    plotlinespecs = '-b';
    save(['Acquisition_parameters_and_results_hybrid_'
        excitation_model]);
end
```

On line 34 the excitation parameter values and vectors are prepared. If the simulation mode is set, the `sim` command on line 66 starts the calculation of the Simulink patch. If the hybrid mode is set, the commands between line 76 and 85 prepare the C++ code from the hybrid instrument's Simulink patch. On line 85, the Xenomai patch is applied on the C++ code and the program is compiled, using the `moulinette.sh` script. Finally, the real-time program is launched with a unix command on line 88.

Figure 84 presents the relevant Simulink patch for the simulation. The red block represents the excitation model (in this case the single-reed model), whose content is detailed in figure 85. While the magenta blocks handle the excitation input parameters, the blue blocks store the generated pressure and flow rate signals. Furthermore, the orange blocks handle the conversion between dimensionless and dimensional physical variables. Finally, the yellow block contains the modal resonator simulation, whose contents are partly shown in figure 86 (for the first two modes).

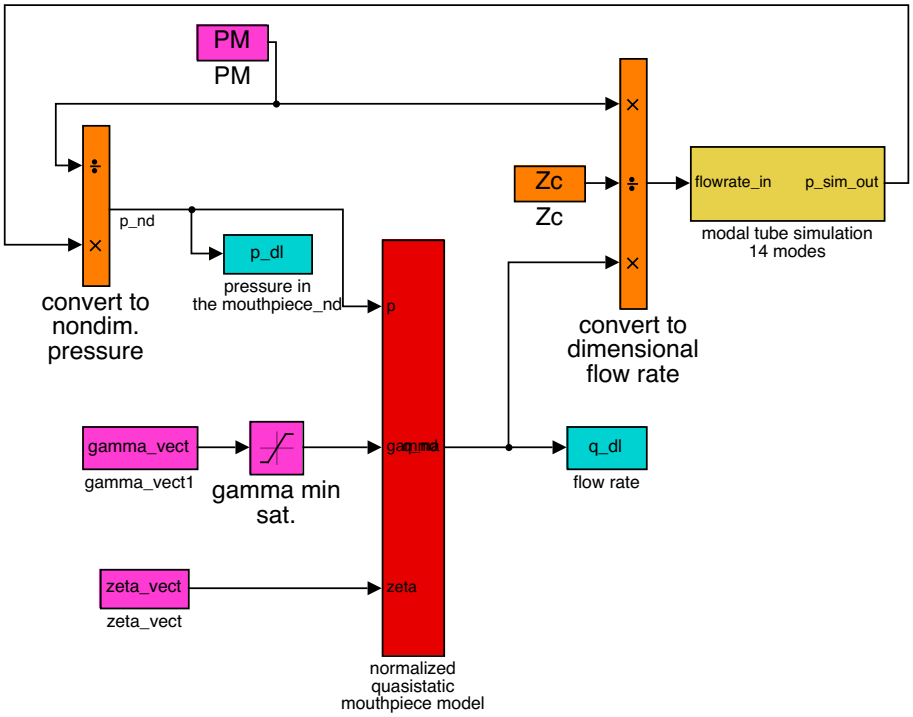

Figure 84: Main Simulink patch for the simulated evaluations. The red block contains the excitation model, the orange blocks handle the dimension(less) conversion and the yellow block contains the modal tube simulation.

The Simulink patch for the hybrid instrument (not shown) is fairly similar. Instead of a resonator block, it contains input and output ports, which enable access to the acquisition card.

These and more hybrid and simulated evaluation programs are available for download on the following webpage: http://dx.doi.org/10.21954/ou.rd.4753465.

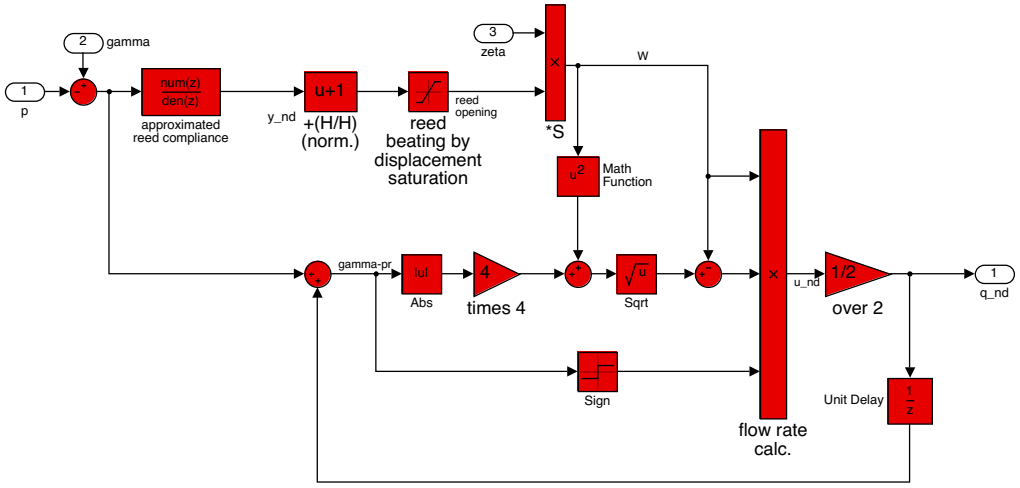

Figure 85: Simulink patch for the single-reed excitation (the content of the red block in figure 84). The patch corresponds to the calculations detailed in subsection 4.2.2.

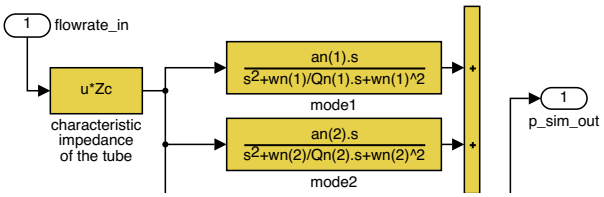

Figure 86: A part of the Simulink patch for the modal resonator simulation (the content of the yellow block in figure 84). The shown part corresponds to the calculations of the first two modes, as calculated by equation (25) in section 2.4.

B.3.2 *Main programs for the hybrid evaluation on Bela*

The C++ code developed for execution on the Bela platform is partly similar to the MATLAB code presented above. Additionally, the Simulink patches are transformed into C++ code. All hybrid evaluation code for execution on the Bela platform can be downloaded from the following web location: `http://dx.doi.org/10.21954/ou.rd.4753471`. Here, only the arbitrary example of the bow-string interaction model is given in listing 2 (copied from the file). As with the MATLAB example, only a few explanations are given below the code.

Listing 2: "BowStringInteraction.cpp" — C++ code for simulation of the bow-string interaction excitation model on the Bela platform.

```
/*
 *
 * Bow-string interaction model. The classical quasi-static "hyperbolic"
     model by Woodhouse, but proposed in a new dimensionless form.
 *
 * Kurijn 04/2016
 *
 *
 */

#include "BowStringInteraction.h"

#include "../include/Utilities.h"
#include <cmath>
#include <stdio.h>
#include <cstdlib>

// Excitation control types:
#define PT 1 //excitation through potentiometers
#define MC 2 //excitation through mouthcontroller
#define CV 3 //excitation with constants value
#define SC 4 //excitation with scores
#define EXCITATION_CONTROLLER MC    // Set to PT / MC / CV / SC

BowStringInteraction::BowStringInteraction()    {
    beta = 0.5;
    mu_d=0.3;
    mu_s=0.8;
    delta=mu_d/mu_s;
    alpha=0.5;//Schelleng: lies in between 0.26 and 1.

    gammab=1;
    zetab=0.2;
    _f = 0.0;
```

```
    _slipping = false;

    v0_cte = 400;
    v0 = v0_cte;

    //Define the excitation control scores:
    int numcycles = 3;
    float runtime = 15;
    float zetab_min = 0.2;
    float zetab_max = 1.0;
    zetab_score.setCteStepEnvs(numcycles, runtime, zetab_min, zetab_max);

    float minmult = alpha;
    float Y0t2Zcstring = 0.03;//based on 1st mode: 1/(an(1)*Qn(1)/wn(1));
    float maxmult = 3*(1-delta)*(1-beta)*powf(beta,2)/Y0t2Zcstring;
    gammab_score.setProgresSawToothEnvs(numcycles, runtime, zetab_min,
        zetab_max, minmult, maxmult);
}

void BowStringInteraction::mouthcontroller(float control_0_smooth, float
    C0in_offset, float control_1_smooth, float C1in_offset) {
    gammab = map(control_0_smooth, C0in_offset, .65f, 0.0f, 7.0f); // 1st
        controller for the bow velocity
    zetab = map(control_1_smooth, C1in_offset, .8f, 0.0, 1.4f); // 2nd
        controller for the bowing force
    v0 = map(control_1_smooth, C1in_offset, .8f, v0_cte, 0.0f); // Lip
        force -> PM
}

float BowStringInteraction::update(float Vh, float control_0_smooth, float
    C0in_offset, float control_1_smooth, float C1in_offset)      {

    // Map controllers to parameter ranges
    #if EXCITATION_CONTROLLER == PT
```

```
// Using the potentiometers:
gammab = map(control_0_smooth, 0, 1, 1.0f/3.0f, 4.2f); // 1st
    controller for the mouth pressure
zetab = map(control_1_smooth, 0, 1, 0, 0.8); // 2nd controller for the
    lip force

#elif EXCITATION_CONTROLLER == MC
mouthcontroller(control_0_smooth, C0in_offset, control_1_smooth,
    C1in_offset);

#elif EXCITATION_CONTROLLER == CV
// Using cte. values
gammab = 0.5;
zetab = 0.15f;

#elif EXCITATION_CONTROLLER == SC
// Using a score
gammab = gammab_score.update();
//excitation.zeta = 0.6f;
zetab = zetab_score.update();

#endif

// dimensionless mouth pressure minus dimensionless historical pressure
static float _deltavh; _deltavh = gammab-Vh/v0;
static float A; A = alpha+1.0f;
static float B; B = A*zetab*delta;
static float abs_vh_p_1; abs_vh_p_1 = fabs(_deltavh)+1;
static float D; D=powf((abs_vh_p_1-B),2.0f) + 4*(B-A*zetab);

static float fstick; fstick = _deltavh/A;
static float fslip; fslip = ((0.0 < _deltavh) - (_deltavh < 0.0)) * (
    abs_vh_p_1+B-sqrtf(D)) / (2*A);
```

```
    if(_slipping) // If previously slipping, determine if still slipping:
        _slipping = fabs(fstick)>zetab;
    else // If previously sticking, determine if now slipping starts.
        _slipping = fabs(fslip)<=zetab && D>0.0f;

    // Set output force to slipping / sticking accordinly
    if(_slipping)
        _f = fslip;
    else
        _f = fstick;

    //Return bow-string force:
    return (_f*v0/Zc);
}
```

In contrast to the PC-based system, this code enables the input of control data, originating from the mouth controller (using the specifically dedicated `mouthcontroller` function starting on line 52) or from dial buttons. Preprocessor directives (the commands preceded by a # sign) are used in the code to enable a user-defined choice between excitation control options, which will be processed before the compilation of the program.

The actual stick-slip calculation of the model is processed in the `update` function, starting on line 58. As can be seen, the physical simulation process is captured between lines 82 and 101, which involves relatively few calculations.

BIBLIOGRAPHY

Adachi, S. and M.-a. Sato

1995. Time-domain simulation of sound production in the brass instrument. *J. Acoust. Soc. Am.*, 97(June):3850. (Cited on pages xxiv, 143, 144, 145, and 147.)

Adachi, S. and M.-a. Sato

1996. Trumpet sound simulation using a two-dimensional lip vibration model. *J. Acoust. Soc. Am.*, 99(2):1200. (Cited on page 278.)

Almeida, A., D. George, J. Smith, and J. Wolfe

2013. The clarinet: how blowing pressure, lip force, lip position and reed "hardness" affect pitch, sound level, and spectrum. *J. Acoust. Soc. Am.*, 134(3):2247–55. (Cited on pages 7, 213, 226, and 267.)

Almeida, A., M. Laruaz, and J.-P. Dalmont

2010. Attack transients in a loudspeaker / resonator coupled system. In *Proc. 20th Int. Congr. Acoust. ICA 2010*, number August, Pp. 1–4. (Cited on pages 11, 21, 30, 41, 213, 268, 276, and 299.)

Askenfelt, A.

1989. Measurement of the bowing parameters in violin playing. II: Bow-bridge distance, dynamic range, and limits of bow force. *J. Acoust. Soc. Amer.*, 86(2):503–516. (Cited on pages 165 and 194.)

Atig, M., J.-P. Dalmont, and J. Gilbert

2004. Saturation mechanism in clarinet-like instruments, the effect of the localised non-linear losses. *Appl. Acoust.*, 65(12):1133–1154. (Cited on pages 52 and 189.)

Atkinson, K. E.

1991. An introduction to numerical analysis. 1989. *New York*, 528. (Cited on page 128.)

Avanzini, F.

2001. *Computational issues in physically-based sound models*. PhD thesis, Università degli Studi di Padova. (Cited on page 34.)

Avanzini, F. and M. Van Walstijn

2004. Modelling the mechanical response of the Reed-mouthpiece-lip system of a clarinet. Part I. A one-dimensional distributed model. *Acta Acust united Ac*, 90(3):537–547. (Cited on pages 11, 131, 192, 256, and 278.)

Backus, J.

1977. Multiphonic tones in the woodwind instruments. *J. Acoust. Soc. Am.*, 62(S1):543. (Cited on page 7.)

Baines, A.

1993. Brass Instruments: Their History and Development. (Cited on page 143.)

Barthet, M.

2009. *De l'interprète à l'auditeur: une analyse acoustique et perceptive du timbre musical*. PhD thesis, Université de la Méditerranée Aix-Marseille II. (Cited on pages 188, 190, and 226.)

Barthet, M., P. Guillemain, R. Kronland-Martinet, and S. Ystad

2005. On the relative influence of even and odd harmonics in clarinet timbre. In *Proc. Int. Comp. Music Conf (ICMC 2005), Barcelona, Spain*, Pp. 351–354. (Cited on page 74.)

Barthet, M., P. Guillemain, R. Kronland-Martinet, and S. Ystad

2010. From Clarinet Control to Timbre Perception. *Acta Acust united Ac*, 96(4):678–689. (Cited on pages 188 and 190.)

Barthet, M., P. Guillemain, R. Kronland-martinet, and S. Ystad

2011. The way timbre shapes musical preference : a clarinet performance case study. In *Proc. Perform. Stud. Netw. Int. Conf.*, volume 2011, Pp. 1–44. (Cited on page 7.)

Benacchio, S.

2015. *Contrôle actif modal appliqué aux instruments de musique à cordes*. PhD thesis, Université Pierre et Marie Curie - Paris VI. (Cited on page 29.)

Benacchio, S., B. Chomette, and A. Mamou-mani

2015. Mode tuning of a simplified string instrument using time-dimensionless state-derivative control. *J. Sound Vib.*, 334:178–189. (Cited on page 29.)

Benacchio, S., B. Chomette, A. Mamou-Mani, and F. Ollivier

2016. Modal PD state active control applied to a simplified string instrument. *J. Vib. Control*. (Cited on page 29.)

Benacchio, S., R. Piéchaud, and A. Mamou-Mani

2013. Active Control of String Instruments using Xenomai. In *15th Real Time Linux Work.* (Cited on pages 300 and 302.)

Benade, A. H.

1988. The clarinet spectrum: Theory and experiment. *J. Acoust. Soc. Am.*, 83(1):292. (Cited on page 69.)

Benade, A. H.

1990. *Fundamentals of Musical Acoustics*, second edition. Courier Dover Publications. (Cited on page 218.)

Beranek, L. L.

1954. *Acoustics*, McGraw-Hill electrical and electronic engineering series. McGraw-Hill. (Cited on page 95.)

Berdahl, E.

2009. *Applications of Feedback Control to Musical Instrument Design*. PhD thesis,

Stanford University (CCRMA), Stanford University. (Cited on pages 27, 35, 37, and 300.)

Berdahl, E., G. Niemeyer, and J. O. Smith

2009. Using Haptics to Assist Performers in Making Gestures to a Musical Instrument. *Proc. Int. Conf. New Interfaces Music. Expr.*, Pp. 177–182. (Cited on pages 13 and 32.)

Bernoulli, D.

1764. *Recherches physiques mécaniques et analytiques: sur le son et sur le tons des tuyaux d'orgues différemment construits*, number 74. A. Forni. (Cited on page 53.)

Besnainou, C.

1995. Modal stimulation: a sound synthesis new approach. In *Proc. Int. Symp. Music. Acoust.*, Pp. 434–438. (Cited on page 26.)

Besnainou, C.

1999. Transforming the voice of musical instruments by active control of the sound radiation. In *INTER-NOISE NOISE-CON Congr. Conf. Proc.*, volume 1999, Pp. 1317–1321. Institute of Noise Control Engineering. (Cited on page 26.)

Bilbao, S.

2009a. Direct simulation of reed wind instruments. *Comput. Music J.*, 33(4):43–55. (Cited on pages 126 and 133.)

Bilbao, S.

2009b. *Numerical Sound Synthesis: Finite Difference Schemes and Simulation in Musical Acoustics*. John Wiley & Sons. (Cited on pages 126 and 279.)

Bilbao, S. D.

2003. Wave and scattering methods for the numerical integration of partial differential equations. (Cited on page 126.)

Blades, J.

1992. *Percussion instruments and their history*. Bold Strummer Limited. (Cited on page 12.)

Blauert, J. and P. Laws

1978. Group delay distortions in electroacoustical systems. *J. Acoust. Soc. Am.*, 63(5):1478–1483. (Cited on page 118.)

Borin, G., G. De Poli, and D. Rocchesso

2000. Elimination of Delay-Free Loops in Discrete-Time Models of Nonlinear Acoustic Systems. 8(5):597–605. (Cited on pages 128, 136, and 279.)

Boulandet, R., H. Lissek, and E. Rivet

2012. Advanced control for modifying the acoustic impedance at the diaphragm of a loudspeaker. In *Acoust. 2012*, number April, Pp. 3981–3986. (Cited on page 276.)

Boutillon, X. and J. Guérard

1995. Hybrid Synthesis. In *proc. ISMA 95*, Pp. 439–445, Dourdan. (Cited on pages 23, 29, and 34.)

Boutin, H.

2011. *Méthodes de contrôle actif d'instruments de musique. Cas de la lame de xylophone et du violon*. PhD thesis, Université Pierre et Marie Curie. (Cited on pages 27, 35, and 300.)

Bromage, S., M. Campbell, and J. Gilbert

2010. Open areas of vibrating lips in trombone playing. *Acta Acust united Ac*, 96:603–613. (Cited on pages 146, 148, and 149.)

Buys, K. and C. Vergez

2012. A hybrid reed instrument: an acoustical resonator with a numerically simulated mouthpiece. In *Proc. Acoust. 2012*, Nantes. (Cited on pages 22, 29, 274, and 300.)

Campbell, D. M.

1999. Nonlinear dynamics of musical reed and brass wind instruments. (Cited on pages 11, 143, and 146.)

Campbell, M.

2004. Brass Instruments As We Know Them Today. *Acta Acust united Ac*, 90:600–610. (Cited on page 64.)

Chafe, C.

1990. Pulsed noise in self-sustained oscillations of musical instruments. In *Int. Conf. Acoust. Speech, Signal Process.* (Cited on pages 131, 161, and 278.)

Chaigne, A. and J. Kergomard

2013. *Acoustique des instruments de musique (2e édition revue et augmentée)*. Belin. (Cited on pages 13, 57, 70, 76, 78, 83, 109, 139, 192, and 261.)

Chapman, P.

1998. Thermal simulation of loudspeakers. *Audio Eng. Soc. Conv. 104*. (Cited on page 109.)

Chatziioannou, V. and M. Van Walstijn

2012. Estimation of clarinet reed parameters by inverse modelling. *Acta Acust. united with Acust.*, 98(4):629–639. (Cited on pages 132, 133, and 136.)

Chen, F.-C. and G. Weinreich

1996. Nature of the lip reed. *J. Acoust. Soc. Am.*, 99(2):1227. (Cited on pages 26 and 145.)

Collet, P. and J.-P. Eckmann

1980. *Iterated maps on the interval as dynamical systems*, volume 1. Boston: Birkhauser. (Cited on pages 18 and 236.)

Cook, P. R.

2001. Principles for designing computer music controllers. In *Proc. New Interfaces Music. Expr. Conf.* (Cited on pages 9 and 42.)

Cook, P. R.

2004. Remutualizing the Musical Instrument: Co-design of Synthesis Algorithms and Controllers. *J. New Music Res.*, 33(3):315–320. (Cited on page 16.)

Copley, D. C. and W. J. Strong

1996. A stroboscopic study of lip vibrations in a trombone. *J. Acoust. Soc. Am.*, 99(2):1219–1226. (Cited on page 148.)

Coyle, W. L., J. Kergomard, and P. Guillemain

2014. Clarinet playing frequency predictions: Comparison between analytic and numerical simulations. *J. Acoust. Soc. Am.*, 135(4):2184–2184. (Cited on pages 82 and 218.)

da Silva, A. R., G. P. Scavone, and A. Lenzi

2010. Numerical investigation of the mean flow effect on the acoustic reflection at the open end of clarinet-like instruments. *Acta Acust. united with Acust.*, 96(5):959–966. (Cited on page 268.)

Dalmont, J., B. Gazengel, J. Gilbert, and J. Kergomard

1995. Some aspects of tuning and clean intonation in reed instruments. *Appl. Acoust.*, 46(1):19–60. (Cited on pages 216, 256, and 278.)

Dalmont, J.-P., J. Gilbert, J. Kergomard, and S. Ollivier

2005. An analytical prediction of the oscillation and extinction thresholds of a clarinet. *J. Acoust. Soc. Am.*, 118(5):3294–3305. (Cited on pages 11 and 139.)

Dalmont, J.-P., J. Gilbert, and S. Ollivier

2003. Nonlinear characteristics of single-reed instruments: Quasistatic volume flow and reed opening measurements. *J. Acoust. Soc. Am.*, 114(4):2253–2262. (Cited on pages 132, 135, and 192.)

Dalmont, J.-P., C. J. Nederveen, V. Dubos, S. Ollivier, V. Méserette, and E. te Sligte

2002. Experimental Determination of the Equivalent Circuit of an Open Side

Hole: Linear and Non Linear Behaviour. *Acta Acust united Ac*, 88:9. (Cited on page 11.)

De Poli, G. and D. Rocchesso

1998. Physically based sound modelling. *Organised Sound*, 3(1):61–76. (Cited on pages 8, 14, and 33.)

Demoucron, M.

2008. *On the control of virtual violins: Physical modelling and control of bowed strings instruments*. PhD thesis. (Cited on page 165.)

Desvages, C. and S. Bilbao

2016. *Two-polarisation physical model of bowed strings with nonlinear contact and friction forces, and application to gesture-based sound synthesis*, volume 6. (Cited on pages 126 and 279.)

Deutsch, D.

1999. *The psychology of music*, volume 2nd. Academic Press. (Cited on pages 7 and 238.)

Donovan, L. B. and A. McPherson

2015. Active control of a string instrument bridge using the posicast technique. In *Audio Eng. Soc. Conv. 138*. Audio Engineering Society. (Cited on page 29.)

Dozio, L. and P. Mantegazza

2007. General-purpose processors for active vibro-acoustic control: Discussion and experiences. *Control Eng. Pract.*, 15(2):163–176. (Cited on page 300.)

Drioli, C. and D. Rocchesso

1997. A generalized musical-tone generator with application to sound compression and synthesis. In *Acoust. Speech, Signal Process. 1997. ICASSP-97., 1997 IEEE Int. Conf.*, volume 1, Pp. 431–434. IEEE. (Cited on page 279.)

Eisenmann, R.

1893. Musical instrument. (Cited on page 23.)

Elliott, S. J. and P. A. Nelson

1985. The application of adaptive filtering to the active control of sound and vibration, ISVR, Univ. Southampton. Technical report. (Cited on pages 25 and 26.)

Facchinetti, M. L., X. Boutillon, and A. Constantinescu

2003. Numerical and experimental modal analysis of the reed and pipe of a clarinet. *J. Acoust. Soc. Am.*, 113(5):2874. (Cited on page 11.)

Falaize, A., N. Lopes, T. Hélie, and D. Matignon

2015. Energy-balanced models for acoustic and audio systems : a port-Hamiltonian approach. In *DAFx 2015 - Proc. 18th Int. Conf. Digit. Audio Eff.* (Cited on pages 126 and 247.)

Feigenbaum, M. J.

1978. Quantitative Universaility for a Class of Nonlinear Transformations. *J. Stat. Phys.*, 19(1):25–52. (Cited on page 236.)

Ferrand, D. and C. Vergez

2010. High-Precision Regulation of a Pressure Controlled Artificial Mouth: The Case of Recorder-Like Musical Instruments. *Acta Acust united Ac*, 26. (Cited on pages 10, 40, 41, and 228.)

Fletcher, N. H.

1979a. Air Flow and Sound Generation in Musical Wind Instruments. *Annu. Rev. Fluid Mech.*, 11(1):123–146. (Cited on page 131.)

Fletcher, N. H.

1979b. Excitation Mechanisms in Woodwind and Brass Instruments. *Acta Acust united Ac*, 43(1):63–72. (Cited on pages 57 and 144.)

Fletcher, N. H.

1993. Autonomous vibration of simple pressure-controlled valves in gas flows. *J. Acoust. Soc. Am.*, 93(April):2172. (Cited on pages 131, 156, and 180.)

Fletcher, N. H. and T. Rossing

2012. *The physics of musical instruments*. Springer Science & Business Media. (Cited on page 13.)

Fuks, L. and J. Sundberg

1996. Blowing pressures in reed woodwind instruments. *Quart. Prog. Status Rep., Speech Music Hear.*, 37(3):41–56. (Cited on pages 112 and 267.)

Gibiat, V. and M. Castellengo

2000. Period doubling occurences in wind instruments musical performance. *Acustica*, 86(4):746–754. (Cited on pages 7 and 236.)

Gilbert, J., J. Kergomard, and E. Ngoya

1989. Calculation of the steady-state oscillations of a clarinet using the harmonic balance technique. *J. Acoust. Soc. Am.*, 86(1):35–41. (Cited on pages 70 and 279.)

Giordano, B. and S. McAdams

2010. Sound Source Mechanics and Musical Timbre Perception: Evidence From Previous Studies. *JSTOR*, 28(2):155–168. (Cited on page 7.)

Grand, N.

1994. *Etude du seuil d'oscillation des systèmes acoustiques non-linéaires de type instrument à vent*. PhD thesis, Université Paris 7. (Cited on pages 21, 29, 276, and 299.)

Grand, N., J. Gilbert, and F. Lalo

1997. Oscillation threshold of woodwind instruments. *Acta Acust united Ac*, 83(1):137–151. (Cited on pages 21, 139, 276, and 299.)

Guérard, J.

1998. *Modélisation numérique et simulation expérimentale de systèmes acoustiques - Application aux instruments de musique*. PhD thesis, Université Pierre et Marie Curie - Paris VI. (Cited on pages 23, 26, 34, 38, 102, and 300.)

Guerard, J. and X. Boutillon

1996. Bowing Virtual Strings. In *Proc. Acoust. Speech, Signal Process. 1996. Conf. Proceedings., 1996 IEEE Int. Conf. - Vol. 03*, ICASSP '96, Pp. 1755–1758, Washington DC, USA. IEEE Computer Society. (Cited on pages 23, 34, 38, and 300.)

Guérard, J. and X. Boutillon

1998. Real-time wave separation in a cylindrical pipe with applications to reflectometry, echo-cancellation, and a hybrid musical instrument. In *Proc. 16th ICA 98*, number 1, Pp. 2261–2262. (Cited on pages 26 and 29.)

Guicking, D. and K. Karcher

1984. Active Impedance Control for One-Dimensional Sound. *J. Vib. Acoust. Stress. Reliab. Des.*, 106(July 1984):393–396. (Cited on page 249.)

Guillemain, P.

2004. A digital synthesis model of double-reed wind instruments. *EURASIP J. Appl. Signal Processing*, 2004(ii):990–1000. (Cited on page 277.)

Guillemain, P., J. Kergomard, and T. Voinier

2005. Real-time synthesis of clarinet-like instruments using digital impedance models. *J. Acoust. Soc. Am.*, 118(1):483–494. (Cited on pages 134, 136, 192, and 246.)

Guillemain, P., C. Vergez, D. Ferrand, and A. Farcy

2010. An instrumented saxophone mouthpiece and its use to understand how an experienced musician plays. *Acta Acust united Ac*, 4:622–634. (Cited on page 7.)

Hanagud, S. and S. Griffin

1998. Active Structural Control for a Smart Guitar. In *Fourth Eur. Conf. Smart Struct. Mater.* (Cited on pages 28, 30, and 300.)

Harrison, R., S. Bilbao, and J. Perry

2015. An Algorithm for a Valved Brass Instrument Synthesis Environment us-

ing Finite-Difference Time-Domain Methods with Performance Optimisation. *Proc. 18th Int. Conf. Digit. Audio Eff.*, (1):1–8. (Cited on page 126.)

Heet, G. S.

1978. String instrument vibration initiator and sustainer. (Cited on page 23.)

Helmholtz, H.

1877. *On the Sensations of Tone*. translated by A. J. Ellis (reprinted by Dover, New York, 1954). (Cited on pages 144 and 160.)

Hiller, L. and P. Ruiz

1971. Synthesizing musical sounds by solving the wave equation for vibrating objects: Part 1. *J. Audio Eng. Soc.*, 19(6):462–470. (Cited on page 15.)

Hirschberg, A.

1995. Aero-acoustics of wind instruments. In *Mech. Music. Instruments*, A. Hirschberg, J. Kergomard, and G. Weinreich, eds. Wien: Springer. (Cited on pages 94, 131, and 133.)

Horng, R.-H., K.-F. Chen, Y.-C. Tsai, C.-Y. Suen, and C.-C. Chang

2010. Fabrication of a dual-planar-coil dynamic microphone by MEMS techniques. *J. Micromechanics Microengineering*, 20:065004. (Cited on page 275.)

Hunt, A., M. M. Wanderley, and M. Paradis

2002. The Importance of Parameter Mapping in Electronic Instrument Design. *Proc. 2002 Conf. New Interfaces Music. Expr.*, 32(4):149–154. (Cited on page 259.)

Jacobsen, F.

2011. Propagation of sound waves in ducts. *Lect. notes*, (31260). (Cited on pages 74 and 187.)

Jenkins, T. S.

2004. *Free jazz and free improvisation: an encyclopedia*, volume 1. Greenwood Publishing Group. (Cited on page 39.)

Karkar, S.

2012. *Méthodes numériques pour les systèmes dynamiques non linéaires. Application aux instruments de musique auto-oscillants*. PhD thesis, Université d'Aix-Marseille. (Cited on page 163.)

Karkar, S., B. Cochelin, and C. Vergez

2012. A high-order , purely frequency based harmonic balance formulation for continuation of periodic solutions : the case of non polynomial nonlinearities. *J. Sound Vib.*, 4:968–977. (Cited on pages 70 and 279.)

Karkar, S., C. Vergez, and B. Cochelin

2010. Toward the systematic investigation of periodic solutions in single reed woodwind instruments. In *ISMA ICA*, number August, Pp. 25–31. (Cited on page 185.)

Karplus, K. and A. Strong

1983. Digital synthesis of plucked-string and drum timbres. *Comput. Music J.*, Pp. 43–55. (Cited on page 15.)

Keefe, D. H.

1992. Physical modeling of wind instruments. *Comput. Music J.*, 16(4):57–73. (Cited on page 193.)

Kergomard, J.

1995. Elementary considerations on reed-instruments oscillations. In *Mech. Music. instruments*, chapter 6. Wien: Springer. (Cited on pages 58, 68, 132, and 134.)

Kergomard, J., S. Ollivier, and J. Gilbert

2000. Calculation of the Spectrum of Self-Sustained Oscillators Using a Variable Truncation Method : Application to Cylindrical Reed Instruments. *Acta Acust united Ac*, 86(June 1999):685–703. (Cited on pages 70 and 132.)

Kitano, M., T. Yabuzaki, and T. Ogawa

1983. Chaos and Period-Doubling Bifurcation in a Simple Acoustic System. *Phys. Rev. Lett.* (Cited on pages 18, 236, 276, and 299.)

Klippel, W. and U. Seidel

2001. Fast and accurate measurement of linear transducer parameters. *Prepr. Eng. Soc.*, Pp. 1–7. (Cited on page 292.)

Kowal, P., D. Sharp, and S. Taherzadeh

2014. Comparison of perceived sound qualities of five clarinets of different makes. In *Int. Symp. Music. Acoust.* (Cited on page 11.)

Krefeld, V. and M. Waisvisz

1990. The Hand in the Web: An Interview with Michel Waisvisz. *Comput. Music J.*, 14(2):28–33. (Cited on page 9.)

Lee, N., E. Berdahl, G. Niemeyer, and J. Smith III

2008. Practical implementation of low-latency DSP for feedback control of sound. In *Proc. Acoust.*, volume 8. (Cited on page 300.)

Li, W., A. Almeida, J. Smith, and J. Wolfe

2016. The effect of blowing pressure, lip force and tonguing on transients: A study using a clarinet-playing machine. *J. Acoust. Soc. Am.*, 140(2):1089–1100. (Cited on pages 223, 226, and 267.)

Lopes, N. and T. Hélie

2016. Energy Balanced Model of a Jet Interacting With a Brass Player's Lip. *Acta Acust. united with Acust.*, 102(1):141–154. (Cited on page 126.)

Lueg, P.

1936. Process of silencing sound oscillations. (Cited on page 25.)

Maestre, E., J. O. Smith, and G. P. Scavone

2017. Analysis-Synthesis of Saxophone Input Impedances via Recursive Parallel Filters. In *ISMA 2017, Int. Symp. Music Acoust.*, volume 1, Pp. 1–4. (Cited on page 291.)

Maganza, C.

1985. *Excitations non linéaire d'un conduit acoustique cylindrique. Observations de doublements de période précédant un comportant chaotique. Application à la Clarinette*. PhD thesis, Université du Maine. (Cited on pages 8, 19, 29, 34, 46, 236, 276, 281, 299, and 300.)

Maganza, C., R. Caussé, and F. Laloë

1986. Bifurcation, Period Doublings and Chaos in Clarinetlike Systems. *Europhys. Lett.*, 1(6):295–302. (Cited on pages 7, 19, 62, 236, and 300.)

Mansour, H., J. Woodhouse, and G. P. Scavone

2016. Enhanced Wave-Based Modelling of Musical Strings. Part 2: Bowed Strings. *Acta Acust. united with Acust.*, 102(6):1094–1107. (Cited on page 162.)

McGinnis, C. S. and C. Gallagher

1941. The Mode of Vibration of a Clarinet Reed. *J. Acoust. Soc. Am.*, 12(4):529–531. (Cited on page 10.)

McIntyre, M. E., R. T. Schumacher, and J. Woodhouse

1983. On the oscillations of musical instruments. *J. Acoust. Soc. Amer.*, 74(5):1325–1345. (Cited on pages 7, 11, 13, 52, 55, 60, 62, 75, 160, 163, 165, 166, 167, 171, 194, 229, and 248.)

McPherson, A.

2010. The Magnetic Resonator Piano: Electronic Augmentation of an Acoustic Grand Piano. *J. New Music Res.*, 39(3):189–202. (Cited on page 27.)

McPherson, A. and V. Zappi

2015. An environment for submillisecond-latency audio and sensor processing on BeagleBone Black. In *Audio Eng. Soc. Conv. 138*. Audio Engineering Society. (Cited on page 303.)

Messner, W. C., M. D. Bedillion, L. Xia, and D. C. Karns

2007. Lead and lag compensators with complex poles and zeros: De-

sign formulas for modeling and loop shaping. *IEEE Control Syst. Mag.*, 27(February):44–54. (Cited on page 104.)

Meurisse, T.

2014. *Contrôle actif appliqué aux instruments de musique à vent*. PhD thesis, Université Pierre et Marie Curie - Paris VI. (Cited on pages 29, 35, 37, and 261.)

Meurisse, T., A. Mamou-Mani, R. Caussé, B. Chomette, and D. B. Sharp

2014. Simulations of Modal Active Control Applied to the Self-Sustained Oscillations of the Clarinet. *Acta Acust united Ac*, 100(6):1149–1161. (Cited on page 29.)

Meurisse, T., A. Mamou-Mani, R. Caussé, B. Sluchin, and D. Sharp

2016. An active mute for the trombone. *J Acoust Soc Am.* (Cited on page 29.)

Meurisse, T., A. Mamou-Mani, C. R., and D. D. Sharp

2013. Simulations of Modal Active Control Applied to the Self-Sustained Oscillations of the Clarinet. In *Proc. SMAC 2013*, Stockholm, Sweden. (Cited on page 300.)

Michon, R. and J. O. I. I. I. Smith

2014. A Hybrid Guitar Physical Model Controller : The BladeAxe. In *ICMC Int. Comput. Music Conf.*, number September, Pp. 573–579. (Cited on page 30.)

Mills, P. G. L. U. o. E. and M. O. J. U. o. E. Hawksford

1989. Distortion reduction in moving-coil loudspeaker systems using current-drive technology. *J. Audio Eng. Soc.*, 37(3):20. (Cited on page 119.)

Msallam, R., S. Dequidt, R. Causse, and S. Tassart

2000. Physical Model of the Trombone Including Nonlinear Effects. Application to the Sound Synthesis of Loud Tones. *Acta Acust united Ac*, 86:725–736. (Cited on pages 147 and 278.)

Muñoz Arancón, A., B. Gazengel, J.-P. Dalmont, and E. Conan

2016. Estimation of saxophone reed parameters during playing. *J. Acoust. Soc. Am.*, 139(5):2754–2765. (Cited on page 133.)

Mudd, T., P. Mulholland, and S. Holland

2015. Investigating the effects of introducing nonlinear dynamical processes into digital musical interfaces. (Cited on page 43.)

Müller, G. and W. Lauterborn

1996. The Bowed String as a Nonlinear Dynamical System. *Acustica*, 82(t 996):657–664. (Cited on page 23.)

National-Instruments

2016. Grounding Considerations for Improved Measurements. (Cited on page 290.)

Nelson, P. A. and S. J. Elliott

1991. *Active control of sound*. Academic press. (Cited on page 25.)

Ollivier, S.

2002. *Contribution à l'étude des oscillations des instruments à vent à anche simple*. PhD thesis, Université du Maine. (Cited on pages 132 and 192.)

Ollivier, S., J. P. Dalmont, and J. Kergomard

2004. Idealized models of reed Woodwinds. Part I: Analogy with the bowed string. *Acta Acust united Ac*, 90(6):1192–1203. (Cited on pages 62, 160, and 163.)

Olson, H. F. and E. G. May

1953. Electronic sound absorber. *J. Acoust. Soc. Am.*, 25(6):1130–1136. (Cited on page 25.)

Onozawa, N. and K. Fujita

2006. Hybrid wind instrument selectively producing acoustic tones and electric tones and electronic system used therein. (Cited on pages 16 and 30.)

Osborne, G. T. and A. A. Hoover

1999. Sustainer for a musical instrument. (Cited on page 23.)

Paddison, M. and I. Deliège

2010. *Contemporary music: theoretical and philosophical perspectives*. Ashgate Publishing, Ltd. (Cited on page 39.)

Papoulis, A.

1977. *Signal Analysis*, volume 31. (Cited on page 116.)

Peeters, G., B. L. Giordano, P. Susini, N. Misdariis, and S. McAdams

2011. The Timbre Toolbox: Extracting audio descriptors from musical signals. *J. Acoust. Soc. Amer.*, 130(5):2902–2916. (Cited on page 190.)

Pickett, P. B. and W. R. Saunders

1998. *An Investigation of Active Tonal Spectrum Control as Applied to the Modern Trumpet*. PhD thesis, Virginia Polytechnic Institute and State University. (Cited on pages 26 and 37.)

Pierce, A. D.

1989. *Acoustics: An Introduction to Its Physical Principles and Applications*. Acoustical Society of America. (Cited on page 95.)

Pitteroff, R. and J. Woodhouse

1998. Mechanics of the contact area between a violin bow and a string. Part I: Reflection and transmission behaviour. *Acta Acust united Ac*, 84(3):543–562. (Cited on page 165.)

Polack, J.

1987. Reflection function of a plane sound wave in a cylindrical tube. *Rev. Phys. Appliquée*, 22(5):331–337. (Cited on page 70.)

Preumont, A.

2011. *Vibration control of active structures: an introduction*, vol. 179. edition. Springer. (Cited on pages 28, 35, and 37.)

Rabenstein, R., S. Petrausch, A. Sarti, G. De Sanctis, C. Erkut, and M. Karjalainen

2007. Blocked-based physical modeling for digital sound synthesis. *IEEE Signal Process. Mag.*, 24(2):42–54. (Cited on pages 126 and 127.)

Raes, G.-W.

2015. <Hybr>. (Cited on page 30.)

Raman, C. V.

1918. On the mechanical theory of the vibrations of bowed strings and of musical instruments of the violin family, with experimental verification of the results. *Indian Assoc. Cultiv. Sci. Bull*, 15:1–158. (Cited on page 61.)

Rienstra, S. and A. Hirschberg

2013. *An Introduction to Acoustics*, volume 20. Eindhoven University of Technology. (Cited on pages 11, 84, 268, and 282.)

Rodet, X. and P. Depalle

1990. Modèles de Signaux et Modèles Physiques d'Instruments. In *Proc. Colloq. Modèles Phys. Création Music. Ordinateur, Grenoble*, Pp. 351–370. (Cited on page 148.)

Russ, M.

2004. *Sound synthesis and sampling*. Taylor & Francis. (Cited on page 15.)

Sagers, J. D., T. W. Leishman, and J. D. Blotter

2013. An extended lumped-element model and parameter estimation technique to predict loudspeaker responses with possible surround-dip effects. *J. Acoust. Soc. Am.*, 134(5):3580–93. (Cited on page 120.)

Saneyoshi, J., H. Teramura, and S. Yoshikawa

1987. Feedback oscillations in reed woodwind and brasswind instruments. *Acta Acust united Ac*, 62(3):194–210. (Cited on page 193.)

Scavone, G.

2003. The Pipe: explorations with breath control. *Proc. 2003 Conf. New interfaces Music. Expr.*, Pp. 15–18. (Cited on page 16.)

Schelleng, J. C.

1973. The bowed string and the player. *J. Acoust. Soc. Am.*, 53(1):26. (Cited on pages 59, 167, 194, and 236.)

Schumacher, R. T.

1978. Self-Sustained Oscillations of the Clarinet: An Integral Equation Approach. *Acustica*, 40:298–308. (Cited on page 70.)

Schumacher, R. T.

1979. Ab initio calculations of the oscillations of a clarinet. *J. Acoust. Soc. Am.*, 65(S1):S73. (Cited on page 19.)

Serafin, S.

2004. *The Sound of Friction: Real-Time Models, Playability and Musical Applications*. PhD thesis. (Cited on page 162.)

Sharp, D. B., A. Mamou-Mani, and M. Van Walstijn

2011. A Single Microphone Capillary-Based System for Measuring the Complex Input Impedance of Musical Wind Instruments. *Acta Acust united Ac*, 97(5):819–829. (Cited on page 297.)

Sharp, D. B., H. A. K. Wright, and W. Ring

2003. An acoustical investigation into the effect of the crook profile on the sound produced by the bassoon. *Acta Acust united Ac*, 89(1):137–144. (Cited on page 11.)

Silva, F., J. Kergomard, C. Vergez, and J. Gilbert

2008. Interaction of reed and acoustic resonator in clarinetlike systems. *J. Acoust. Soc. Am.*, 124(5):3284–3295. (Cited on pages 84, 134, and 192.)

Slawson, W.

1985. *Sound Color*. University of California Press. (Cited on page 6.)

Slovenian Academy of Sciences

1997. Early Music. *Science (80-.).*, 276(5310):203 – 205. (Cited on page 12.)

Small, R. H.

1972. Direct Radiator Loudspeaker System Analysis. *J. Audio Eng. Soc*, 20(5):383–395. (Cited on pages 95 and 97.)

Smith, J. H. and J. Woodhouse

2000. The tribology of rosin. *J. Mech. Phys. Solids*, 48:1633–1681. (Cited on pages 162 and 278.)

Smith, J. O.

1986. Efficient simulation of the reed-bore and bow-string mechanisms. In *Proc. Int. Comput. Music Conf.*, Pp. 275–280, The Hague, Netherlands. (Cited on page 128.)

Smith, J. O.

2005. A history of ideas leading to virtual acoustic musical instruments. In *Appl. Signal Process. to Audio Acoust. 2005. IEEE Work.*, Pp. 299–306. IEEE. (Cited on page 259.)

Smith III, J. O.

2006. A basic introduction to digital waveguide synthesis (for the technically inclined). *Cent. Comput. Res. Music Acoust. (CCRMA), Stanford Univ. http//c-crma. stanford. edu/~ jos/swgt*. (Cited on page 15.)

Strong, W. J.

1990. Computer simulation of a trumpet. *J. Acoust. Soc. Am.*, 87(S1):S138–S138. (Cited on page 148.)

Taillard, P.-A., J. Kergomard, and F. Laloë

2010. Iterated maps for clarinet-like systems. *Nonlinear Dyn.*, 62(1-2):253–271. (Cited on pages 7, 55, 60, 62, 66, and 236.)

Thompson, S. C.

1979. The effect of the reed resonance on woodwind tone production. *J. Acoust. Soc. Am.*, 66(5). (Cited on page 7.)

van Walstijn, M.

2002. Discrete-Time Modelling of Brass and Woodwind Instruments with Application to Musical Sound Synthesis. *PhD Thesis*, (January 2002). (Cited on pages 136, 151, and 246.)

Van Walstijn, M. and F. Avanzini

2007. Modelling the mechanical response of the reed-mouthpiece-lip system of a clarinet. Part II: A lumped model approximation. *Acta Acust. united with Acust.*, 93(3):435–446. (Cited on page 132.)

Van Walstijn, M. and G. D. Sanctis

2014. Adaptive calibration of a three-microphone system for acoustic waveguide characterization under time-varying conditions. 917. (Cited on page 37.)

Velut, L., C. Vergez, J. Gilbert, and M. Djahanbani

2017. How Well Can Linear Stability Analysis Predict the Behaviour of an Outward-Striking Valve Brass Instrument Model? *Acta Acust. united with Acust.*, 103(1):132–148. (Cited on page 156.)

Vergez, C. and X. Rodet

2000. Dynamic systems and physical models of trumpet-like instruments. Analytical study and asymptotical properties. *Acta Acust united Ac*, 86:147–162. (Cited on pages 143, 146, 147, and 193.)

Weinreich, G. and R. Caussé

1986. Digital and analog bows: Hybrid mechanical-electrical systems. In *ICASSP*, Pp. 1297–1299. (Cited on pages 23, 29, 36, 276, 299, and 300.)

Weinreich, G. and R. Caussé

1991. Elementary stability considerations for bowed-string motion. *J. Acoust. Soc. Amer.*, 89(2):887–895. (Cited on pages 23, 36, 163, and 300.)

Wilson, T. A. and G. S. Beavers

1974. Operating modes of the clarinet. *J. Acoust. Soc. Am.*, 56:653–658. (Cited on pages 10, 41, 131, 132, 133, and 134.)

Wishart, T.

1996. *On sonic art*. Psychology Press. (Cited on page 39.)

Wolfe, J. and A. Tarnopolsky

2003. Some effects of the player's vocal tract and tongue on wind instrument sound. *Stock. Music Acoust. Conf.*, 2003(Smac 03):307–310. (Cited on page 7.)

Worman, W. E.

1971. Self-Sustained Nonlinear Oscillations of Medium Amplitude in Clarinet-Like Systems. (Cited on page 69.)

COLOPHON

This document was typeset using the typographical look-and-feel `classicthesis` developed by André Miede. The style was inspired by Robert Bringhurst's seminal book on typography *"The Elements of Typographic Style"*. `classicthesis` is available for both LaTeX and LyX:

http://code.google.com/p/classicthesis/

Happy users of `classicthesis` usually send a real postcard to the author, a collection of postcards received so far is featured at:

http://postcards.miede.de/

Final Version as of February 15, 2018 (`classicthesis` version 4.1).